Haemodynamic Causes of Abdominal Aortic Aneurysm Growth

Christophe Emmanuel SARRAN

Doctor of Philosophy

University of Dundee

March 2012

Contents

Appendix: Programs and Functions

I would like to thank Dr. Graeme HOUSTON for initiating this work and supporting me throughout my studies;

I would like to thank my principal supervisor, Prof. Alan VARDY, for his constant support and valued counsel;

My thanks also go to the other members of my supervisory team, and in particular Drs. Jenny WOOF, Ian MACKIE and Peter ROSS and Mr. Robin HOOD.

I am particularly thankful for the help and advice received from Mr. Gareth GRIFFITHS and Drs. Tish LAING-MORTON and Simon OGSTON who have reviewed draft parts of the thesis.

I gratefully acknowledge the financial support of Tayside Flow Technologies, the National Health Service Tayside, the University of Dundee, the Met Office and the Bancroft Clark Charitable Trust.

Thankfulness and gratefulness do not begin to describe what I feel for my wife, Helen, for her patience, support and love over many years:

I love you, Helen.

DECLARATION

I, Christophe SARRAN, am the sole author of this thesis; that, unless otherwise stated, all references cited have been consulted by me; that the work of which the thesis is a record has been done by me, and that it has not been previously accepted for a higher degree.

Signature:

STATEMENT

I confirm that the conditions of the relevant Ordinance and Regulations have been fulfilled.

Signature:

Summary

Abdominal aortic aneurysms affect approximately 5% of the population over 65 years of age. It is thought that rapidly growing aneurysms are at greater risk of rupture. It is therefore important to understand what the causes of aneurysm growth are and whether these are different from the causes of rupture. In particular, blood flow is believed to influence the rate of aneurysm growth. The 1-dimensional method of characteristics offers a means of simulating the haemodynamics in the arterial network. Its major advantage over 3-dimensional models is that extensive parts of the vascular network can be simulated. The influence of vessel characteristics on other parts of the network can then be examined. The method of characteristics has been adapted to build a computer program that simulates the flow of incompressible fluids in elastic pipes. The program is used in the first part of the thesis to demonstrate that changes in arteries far from the aorta influences the haemodynamics within the aorta. In the second part of the thesis, a retrospective population-based statistical study is carried out of clinical and geometric factors of abdominal aortic aneurysms. Clinical measurements have been collected from patients records at Ninewells Hospital, Dundee. To strengthen the analysis of these measurements, a novel approach to include measured parameters into multiple linear regressions has been developed using a kernel smoother. The results suggest that aneurysm diameter remains a significant predictor of abdominal aortic aneurysm growth and the rate of growth is influenced by several geometric characteristics of the abdominal aorta. If the haemodynamics influence aneurysm growth rate, the conclusions suggest that 3-dimensional computational fluid dynamics models would help to study the influence of aneurysm geometry on the blood flow dynamics.

Source: Sherrington 1946.

Portrait of Jean Fernel, in the Medicina, 1554.

Chapter 1

Introduction

1.1 Abdominal Aortic Aneurysms

The first notice of aortic aneurysm was made by Jean Fernel, and also described at the same time by Vesalius, and was published in Medicina in 1555 (Gibson 1898). An aneurysm consists of damage to the wall of a blood vessel and an increase in the vessel's size. When left untreated, the aneurysm ruptures, with an overall fatality rate of 80% (Blanchard 1999; Wilmink and Quick 1998).

The abdominal aorta lies from the diaphragm to the aorta-iliac bifurcation where it separates into two iliac arteries that supply the legs. It is an artery of the elastic category, also referred to as a conductance artery. Arteries are composed of three layers or tunicae. The innermost layer is the tunica intima consisting of a single layer of endothelial cells 0.2 to 0.5 μm thick in contact with the blood stream. In addition, the intima of the aorta may contain a subendothelial layer that includes smooth muscle cells. The tunica media, middle layer, alternates smooth muscle cells and collagen with sheets of elastin to make 20 to 70 concentric musculo-elastic layers in the aorta, each 5 to 15 μm thick (Humphrey 2002; Wolinsky and Glagov 1967). The smooth muscle cells, collagenous fibrils and elastin laminae are usually oriented circumferentially which is expected to regulate the distensibility of the aorta. The outermost layer of the aorta, about 10% of the wall thickness, is the tunica adventitia, a sheath of

collagen containing the vasculature of the aortic wall, the vasa vasorum. Whereas the thoracic aorta has a vasa vasorum that penetrates deep into the media, the abdominal aorta's vasa vasorum is limited to the adventitia with no vessels supplying the media (Dollar 1994).

It is suggested that damage to the intima by inflammation or impairment of the endothelium by atherosclerotic plaque (Crawford et al 2003) is the precursor to abdominal aortic aneurysms. Elastin has a Young's modulus of ~500 kPa while that of collagen is ~500 MPa (Rutten 1998). The load bearing elastin in the aorta is not replaced when damaged so that destruction of elastin and damage to the media cause the much stiffer collagen to become the main load bearer (MacSweeney et al 1994). Furthermore, while elastin is an elastic material, collagen is visco-elastic and will deform over time (Caro et al 1978). The media of the abdominal aorta has fewer musculo-elastic layers than other sections of the aorta, and hence less elastin content, making the abdominal aorta more sensitive to elastin degradation; this may explain that 95% of aortic aneurysms occur in the infra-renal aorta (Kent and Boyce 1994).

Remodelling of the collagen due to the extra load it has to bear increases the size of the aorta (Crawford et al 2003; MacSweeney et al 1994). The precise causes for the onset and growth of aneurysm are unclear (Faxon et al 2004). The vessel ruptures when its diameter is so large and its wall so thin that it cannot bear the load any longer (Kent and Boyce 1994).

It is estimated that 5% of the population has or will have an abdominal aortic aneurysm (see Table 1.1.1). A greater proportion of men (6%) than women (2%) will develop aneurysms. Screening studies have measured a prevalence of abdominal aortic aneurysm up to 14.2% for men (Wanhainen et al 2001) and up to 5.9% for women (Newman et al 2001). There are geographical variations in these epidemiologic figures. While Scandinavia and the United States of America are particularly affected, Benelux is less so, and a screening study in Japan did not reveal a single aneurysm (Wilmink and Quick 1998). In the United Kingdom variations in prevalence also appear to exist, with measurements for men from 2.9% in Liverpool (Loh et al 1989) to 8.4% (Smith et al 1993) in Birmingham. The largest population-based screening study is the Multicentre Aneurysm Screening Study in the south of England (Scott 2002) with in excess of 27 000 men and measured a prevalence of 4.9%.

There are indications that a proportion of the population may be genetically predisposed to aneurysm and so to some extent the disease is heritable (Kuivaniemi et al 2003; Cannon Albright et al 2003; Salo et al 1999). For example mutations of the COL3A1 gene affect the structure of type III collagen and is thought to weaken the arterial wall (MacSweeney et al 1994; Henney et al 1993); in addition it is suggested that genetic polymorphisms of tissue inhibitors of metalloproteinases and matrix metalloproteinases may be linked to aneurysm (Ogata et al 2005). However, no single gene has yet been clearly associated with abdominal aortic aneurysm (Sandford et al 2007). The recent possibilities of

Table 1.1.1. Prevalence of abdominal aortic aneurysm in the United Kingdom and worldwide from screening, for men (♂) and women (♀). Included are studies with at least the 65 to 74 year age group and an aneurysm diameter minimum criterion between 29 and 35 mm. Estimated totals are from meta-analysis of tabulated prevalence studies where numbers are known.

Location	Study	Numbers		Prevalence (%)		
		♂	♀	♂	♀	♂ and ♀
United Kingdom						
Edinburgh	Lee et al 1997 *	1156				2.9
Birmingham	Smith et al 1993	2669		8.4		
Chichester	Scott et al 1995	2342	3052	7.6	1.3	4.0
Croydon	Jones et al 1996	203		5		
Huntingdon	Wilmink and Quick 1998	7493		5.2		
Liverpool	Loh et al 1989	657		2.9		
Northumberland	Holdsworth 1994	628		6.7		
Oxford	Collin et al 1988	426		5.4		
Southern England	Scott 2002	27147		4.9		
Estimated Totals for the United Kingdom:		*41565*	*3052*	*5.3*	*1.3*	*3.8*
Rest of the World						
Belgium (Liege)	Vazquez et al 1998	727		3.8		
Denmark (Viborg)	Lindholt et al 2006	4852		4		
Italy (Genoa)	Simoni et al 1995 * **	741	860	8.8	0.6	4.4
Italy (Asola)	Settembrini et al 1992 *	648				3.1
Netherlands (Rotterdam)	Pleumeekers et al 1995	2217	3066	4.1	0.7	2.1
Norway (Tromso)	Singh et al 2001	2962	3424	8.9	2.2	5.3
Norway (Oslo)	Krohn et al 1992	500		8.2		
Sweden (Norsjo)	Wanhainen et al 2001	248	256	14.2	3.1	8.6
Australia (Freemantle)	Nicholls et al 1992 *	654	571	4.7	0.4	2.7
Japan	Takei et al 1995 **	348				0
United States of America	Newman et al 2001	1953	2781	12.9	5.9	8.8
Western Australia	Jamrozik et al 2000	12203		7.2		
Estimated Totals for the World:		*68622*	*14010*	*6*	*2*	*5*

Sources: * Cornuz et al 2004; ** Wilmink and Quick 1998.

genome-wide analyses might soon provide an answer to genetic predisposition (Kuivaniemi et al 2006; Tilson and Ro 2006).

"*The outlook in aortic aneurysm is always serious, and the prognosis is usually therefore somewhat grave.*" Gibson (1898) further assesses that "*the subject of treatment, it must be confessed, is somewhat discouraging.*" By the beginning of the 20th century, treatment consisted of encouraging the coagulation of the blood in the aneurysm. This was achieved partly by reducing the blood pressure through enforcing complete rest and a diet of starvation, and extracting 100 mL or so of blood when necessary. Remedies such as iodide of potassium and nitro-glycerine could be used. Clotting of the blood was also achieved by electrolysis and the introduction of metallic wire or horse hair in the aneurysm.

In 1951 in Paris the first successful graft replacement of an abdominal aortic aneurysm was performed by Dubost (1952) (Cannon et al 1963). Mortality rates from surgery were immediately much lower than that from aneurysm rupture and elective surgical repair of aortic aneurysms became possible. By the start of the 21st century the mortality rate from elective aneurysm repair can be as low as 2% to 3% (Kent et al 1994b). For each patient it is essential to assess both the probabilities of mortality from aneurysm rupture and from elective surgery (Brewster et al 2003; Hallett 2000). The most used criterion for estimating the probability of rupture is aneurysm diameter although alternatives based on diameter are frequently advocated such as the ratios of the aneurysm diameter to the supraceliac aorta diameter and to the aneurysm length (Blanchard 1999; Ouriel et al 1992). For aneurysms in the 40 to 50 mm range (see Table 1.1.2) the

probability of rupture (up to 0.05 for 1 year, equal to 5% risk per year) can exceed the mortality rate of elective surgery (0.02 to 0.03). Even with a probability of rupture of 0.005 per year (0.5% risk per year), a patient with a remaining 10 year life-expectancy will have a probability of rupture of 0.05 in those 10 years (5% risk of rupture). Katz et al (1992) estimated that elective surgery should be offered to some patients with aneurysms as small as 43 mm in diameter.

Table 1.1.2. Probabilities of rupture for different ranges of abdominal aortic aneurysm diameters.

Aneurysm Diameter (mm)	Probability of Rupture (per year)
less than 40	0
40 to 50	0.005 to 0.05
50 to 60	0.03 to 0.15
60 to 70	0.1 to 0.2
70 to 80	0.2 to 0.4
more than 80	0.3 to 0.5

Source: Brewster et al 2003.

Currently, patients with abdominal aortic aneurysm larger than 55 mm in diameter are recommended elective surgery (Brewster et al 2003). Many aneurysms larger than 55 mm however never rupture (Lederle et al 2002) while some smaller aneurysms do rupture (10% of ruptured abdominal aortic aneurysms were smaller than 50 mm in a study by Nicholls et al 1998). The United Kingdom Small Aneurysm Trial investigated the benefits of operating on small aneurysms 40 mm to 55 mm in diameter (Powell et al 1998). The trial returned a "*neutral result*" whereby the 527 patients that were not operated on had a similar mortality over 6 to 8 years as the 563 patients that underwent elective surgical aneurysm repair (Brady et al 2002; Powell 1999). Although there is no evidence that surgery improves survival, nor is there any evidence to

the contrary (Pretre and Turina 1998). It should be expected that the survival rate of patients operated on is worse immediately after surgery, but then drops less rapidly than that of patients with aneurysms (McCleary and Mahomed 1999). The survival curves published in 2002 (Brady et al) seem to follow this expectation even though the difference between mortalities is not statistically significant (with a 95% confidence): the survival curves cross each other after about 3 years and thereafter the gap between them appears to be ever widening.

It is important to estimate the probability of rupture for the individual patient, and it is essential to determine the probability of mortality from surgery, which can be as low as 0.02 (2% risk) but higher than 0.4 (40% risk) for some (Kleinstreuer and Li 2006; Brewster et al 2003). For small abdominal aortic aneurysms, diameter is not a suitable criterion to differentiate the probabilities of rupture for individual patients. The first recommendation of Brewster et al (2003) is that "*the arbitrary setting of a single threshold diameter for elective AAA* [Abdominal Aortic Aneurysm] *repair applicable to all patients is not appropriate, as the decision for repair must be individualized in each case*". Although it was suggested that the United Kingdom Small Aneurysm Trial looks at aneurysm growth rate as a predictive factor of rupture (Brown and Powell 1999), results concentrated on the link between growth and the increase in rupture probability due to the increase in size: however, no direct link between rate of growth and probability of rupture appears to have been made (Brady et al 2004). This implies that predicting risk of rupture by using the growth rate may

not be justified. The work accounted for in the following chapters is concerned with the rate of aneurysm growth rather than the probability or risk of rupture. It is thought that an improved understanding of the factors that accelerate abdominal aortic aneurysm growth will help in differentiating the risks incurred by patients (Thompson et al 2002; Vardulaki et al 1998; Schewe et al 1994) and so improve patient selection for repair.

1.2 Aneurysm Growth

While it is conceivable that aneurysm rupture can be explained by purely mechanical causes, it is clear that aneurysm growth is caused by biochemical effects, namely elastin degradation and collagen remodelling. However, the processes of elastin degradation and collagen remodelling may themselves be caused in part by haemodynamic phenomena within the aneurysm.

The association of aortic wall inflammation with abdominal aneurysms (Swedenborg and Eriksson 2006; Treska et al 1999; Freestone et al 1995) is a clear indication of the involvement of biochemical factors such as homocysteine (Halazun et al 2007) and macrophage migration inhibitory factor (Pan et al 2003) in aneurysm growth. This has led to the trial of possible pharmacological treatment of aneurysms, for example using doxycycline to reduce the rate of aneurysm growth (Baxter et al 2002; Mosorin et al 2001; Baxter 2001; Gadowski et al 1994). Furthermore, the aneurysmal aorta will itself produce chemicals that can be measured in the blood, such as interleukin-6 which concentrations have been found proportional to the aneurysm surface area (Dawson et al 2007). On

the one hand some chemicals in the blood cause the growth of the aneurysm, on the other hand the existence of an aneurysm causes higher concentrations of other chemicals (Satoh et al 2010; Golledge et al 2007; Satta et al 1995).

Atherosclerosis is the most important contributor to inflammatory vascular disease, which, through changes to the endothelium damages the tunicae intima (Libby et al 2011; Libby 2002). Lipids, and in particular Low-Density Lipoprotein (LDL), are associated with inflammation, atherosclerosis and the formation of plaque (Aikawa et al 2002; Kinlay et al 2001; Libby et al 2000). Several studies have found that greater thickness of the intima and media is associated with lower wall shear stress of the blood in the lumen of the carotid artery (Kornet et al 1998) and the femoral artery (Kornet et al 1999); greater intima-media thicknesses have also been related to higher systolic and diastolic pressure (Augst et al 2007). While low wall shear stress may contribute to plaque formation, high wall shear stress may be associated with plaque rupture (Groen et al 2007) though this association may be confounded by other biochemical effects localised to where higher wall shear stress is likely (Segers et al 2007). Wall shear stress throughout the arterial network can now be estimated with 3-dimensional medical imaging and the use of computational fluid dynamics (Hoskins and Hardman 2009; Stroev et al 2007).

Blood pressure and blood flow in the artery may also be associated with arterial damage and in particular with arterial wall remodelling. It is suggested that a progressive increase in pulmonary artery diameter is associated with hypertension in the vessel, though the statistical correlation is missing

(Boerrigter et al 2010). Furthermore, it was demonstrated by in vivo experiments that exposing the wall of an artery to high blood flow causes holes in the internal elastic lamina leading to remodelling of the intima through elongation and dilatation (Masuda et al 1999). Other biomechanical processes of the arterial wall, such as smooth muscle tone adaptation (Fridez et al 2001), are caused by high blood pressure. It has also been recently demonstrated in vitro that, at higher pressures, a pulsed flow can cause the progressive expansion of an elastic vessel through mechanical processes alone (Duclaux et al 2010; Lasheras 2010).

Other haemodynamic factors such as peripheral vascular disease are possibly linked to aneurysm growth. The aneurysm geometry and size itself have been correlated to growth. Growth rate has been linked to maximum diameter with correlation coefficient $r = 0.59$ (Wilson et al 1999) and regression coefficients of 0.22 yr^{-1} 95% Confidence Interval (CI) [0.15;0.28] yr^{-1} (Lindholt et al 1998) and 0.129 yr^{-1} 95% CI [0.105;0.153] yr^{-1} (Brady et al 2004) have been measured. No study has yet found a link between aneurysm growth and blood pressure (Vega de Ceniga et al 2006; Wilson et al 1999; Chang et al 1997) and measurements of regression coefficients yielded 95% CI [-0.02;0.03] mm/yr/mmHg for diastolic pressure (Lindholt et al 1998), [-0.006;0.003] mm/yr/mmHg and [-0.007;0.003] mm/yr/mmHg for systolic pressure (Brady et al 2004). Occlusion of the lower limb arteries have been linked to aneurysm growth by measuring the regression coefficient for the Ankle-Brachial Pressure Index (ABPI): coefficients of 1.0

mm/yr 95% CI [0.4;1.7] mm/yr and 1.1 mm/yr 95% CI [0.5;1.7] mm/yr were obtained by Brady et al (2004).

A note must be made of the size of the regression coefficients measured for aneurysm diameter and ABPI. The coefficient for diameter of 0.22 yr^{-1} means that for every extra 10 mm in diameter there is a predicted extra 2 mm/yr in the rate of aneurysm growth: this is useful because over the range of possible aneurysm diameters the extra growth rates are clinically relevant and this will influence how the aneurysm is managed. The coefficient for ABPI of 1 mm/yr means that for every extra 0.1 unit of the index there is a predicted extra 0.1 mm/yr in the rate of growth: over the range of possible ABPI [0;~1] the extra growth rates are very small and unlikely to be clinically relevant.

Tobacco consumption is associated with the rate of aneurysm growth (Lindholt et al 2001; Wilmink et al 1999): linear regression coefficients of 0.025 mm/yr/(µg/L) for levels of S-cotinine and 0.22 mm/yr/(µg/L) for levels of P-elastase have been found (Lindholt et al 2003); however, another study failed to link plasma cotinine with growth with a 95% CI [-0.014;0.086] mm/yr/ln(µg/L) (Brady et al 2004). This illustrates the difficulty in obtaining clear results using statistical analyses. Attempts have also been made to link cholesterol levels with rates of aneurysm growth by linear regression (Chang et al 1997). No link was found, with Brady et al (2004) measuring regression coefficients 95% CI [-0.092;0.133] mm/yr/(mmol/L) and [-0.058;0.175] mm/yr/(mmol/L) for total cholesterol, and [-0.13;0.85] mm/yr/(mmol/L) and [-0.28;0.80] mm/yr/(mmol/L) for High Density Lipoprotein (HDL) cholesterol.

As commented by Doyle et al (2011), there are many contributory factors to the risk of aneurysm rupture, many of which are difficult to estimate. Small aneurysms are known to rupture and larger ones may never rupture, nevertheless probability of rupture increases with size. The rate of aneurysm growth becomes an important factor in deciding when to operate and the frequency of visits for surveillance. A model of abdominal aortic aneurysm growth was developed based on an assumption of the relationship between wall stress and expansion rate using the finite element method with medical imaging to obtain aneurysm geometries (Helderman et al 2008). This numerical method combined with statistical methods was recently used by Helderman et al (2010) to calculate rate of aneurysm growth for 11 patients with validation measurements of diameter over a 30 month period: it was found that local anatomy from medical imaging contributed 62% to the aneurysm growth rate and other risk factors 38%.

1.3 Research Aims

It is suggested here, in section 1.2, that abdominal aortic aneurysm growth is caused by a combination of biochemical and mechanical effects, both being wholly or partially linked to the haemodynamics local to the aneurysm. It is unclear what the links are between the local haemodynamics and different characteristics of the arterial network. The aim of the work presented here is to determine the links between haemodynamic conditions in the arterial network and the rate of abdominal aortic aneurysm growth.

Chapter 2 describes how changes in characteristics at different parts of the arterial system might influence the haemodynamics within the abdominal aorta. The blood flow dynamics within the human arterial network have been simulated using a 1-dimensional computational model. The influence of changes of characteristics of the arterial network on the blood flow dynamics throughout the network have been studied by comparing the results from simulations using a 'normal' healthy model, an aged model with more rigid arteries, and three different types of vascular prostheses.

Chapter 3 examines how clinical factors related to blood flow dynamics, including measurements of AAA size, are statistically linked to the rate of AAA growth. The hypothesis is that changes in the condition of the cardio-vascular system over the period of AAA growth might affect the growth rate. The parameters analysed have been AAA diameter, blood pressure and pulse rate, the Ankle-Brachial Pressure Index (ABPI) and levels of urea and creatinine (linked to haemodynamics by their indication of kidney function) and cholesterol. To this end, a method to analyse time-line data comprehensively has been developed in order to estimate the clinical factors from patients' historic medical records at times when measurements are not being taken and with appropriate weighting functions.

Chapter 4 extends the statistical analysis to include geometric factors of AAA obtained from medical imaging. The geometric factors provide a description of the shape of the vessel lumen along the length of the abdominal aorta, and in addition a description of the aortic centreline and hence its tortuosity.

The intention of the work presented here is to determine whether factors that might affect the haemodynamics within the abdominal aorta are linked to AAA growth. Determining how these haemodynamic factors then influence the biochemistry of the aortic wall (e.g. atherosclerosis) which in turn is linked to AAA growth is outside the scope of this thesis.

Chapter 2

Simulations

2.1 The Use of Computational Simulation Methods

Even when a hypothesis is accepted statistically, the process does not provide a reason for the correlation between the measurements analysed. For example, a statistical link between hypertension and the rate of aneurysm growth does not indicate whether hypertension is causing the growth, or the growth is causing the hypertension, or both are caused by another phenomenon not included in the analysis. Indeed, there are other factors likely to influence aneurysm growth such as smoking, connective tissue disorder, etc. Even then, to gain an understanding of the causal effects between parameters in an aneurysmal aorta, and in the vascular system in general, the field of fluid mechanics offers a range of analytical and experimental tools (Chung 2002; Ku 1997; Skalak et al 1989).

A key characteristic of the flow of blood in arteries is its pulsatile nature; an early study of oscillatory flow in an elastic vessel is Witzig's 1914 thesis on incompressible fluid flow dynamics in elastic pipes. The behaviour of pulsatile flow in a vessel depends on the Womersley number, of Womersley (1957) who developed and applied elastic tube theory to flow in arteries. The Womersley number defines the radial distribution of velocities in a vessel, the mathematical solution for velocity requiring the use of Bessel functions J_n (c.f. Watson 1944). This analytical approach is useful for simple geometries as it provides a most robust analysis, e.g. to examine the effect of taper on flow characteristics

(Belardinelli and Cavalcanti 1992). Yet it relies on approximations which may or may not represent real arteries (Mirsky 1967), and once the problems for which solutions are sought deviate from the simplest of specifications it is no longer efficient to develop purely analytical solutions.

Physical experiments provide the flexibility of examining the flow characteristics in model arteries with complex geometries, and model specifications can be controlled (Chaudhuri et al 2004; Peattie et al 2004; Egelhoff et al 1999). Recently, with advances in non-invasive measurement technologies of the arterial system in vivo, such as with Computed Tomography (CT), precise physical models of individual patients' aortas have become possible (Kato et al 2001; Lermusiaux et al 2001). However, physical experiments can be expensive because of the equipment and materials required, invasive measurements can affect the flow being studied and non-invasive techniques are not always suitable.

To determine how differences in arterial characteristics far from the abdominal aorta may affect the flow characteristics within the infra-renal aorta, an efficient numerical simulation method is required to model extensive parts of the arterial network.

Computers offer a means of simulating physical experiments using only the electronic equipment available. Statistical modelling of blood flow on computers can be achieved with Monte Carlo simulations that are achieved by reproducing a population with known characteristics distributions given

correlations of principal components obtained from measurements (Burnette 1996), but this does not simulate the haemodynamics. Computational Fluid Dynamics (CFD) modelling of the arterial flow is a means of applying the underlying mathematical theory of fluid dynamics in a numerical volume broken down into small cells, so as to simulate the blood flow and, when required, the movement of the arterial walls (Steinman et al 2003).

CFD is used to simulate the haemodynamics of abdominal aortic aneurysms by building simple models in 2D (2 dimensions) (Finol and Amon 2001) or 3D (3 dimensions). Studies normally use a physiological transient wave form, but some approximate to steady flow and rigid arterial walls to examine the characteristics at peak flow (Ekaterinaris et al 2006). Ranges of different aneurysm shapes can be studied using simple models, with and without fluid-structure interaction, to determine for example arterial wall stresses (Scotti et al 2005; Finol et al 2003). As with physical experiments, non-invasive scanning technology such as CT allows the development of patient-specific numerical models (Hammer et al 2009; Yamamoto et al 2006; Steinman et al 2003). Several computer simulations of the haemodynamics of abdominal aortic aneurysms have been carried out using patient-specific arterial geometries with pulsatile flow, and some with fluid-structure interaction, thus allowing the artery to expand with the fluid pressure (Papaharilaou et al 2007; Leung et al 2006; Wolters et al 2005; Finol and Amon 2003; Di Martino et al 2001). Figure 2.1.1 illustrates one of the 3D computational models of a patient's aortic aneurysm described in this thesis.

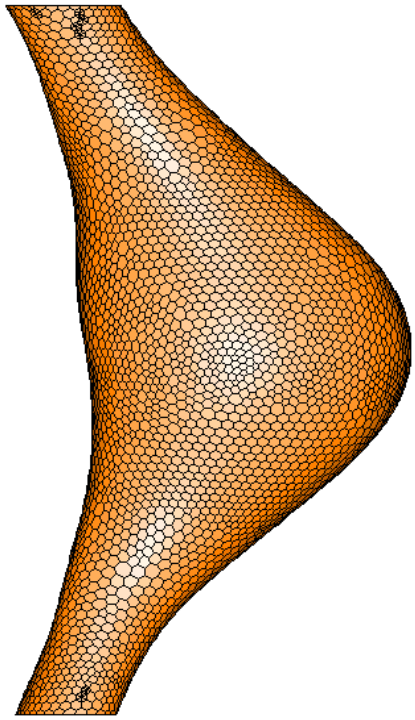

Figure 2.1.1. Computer model of a patient's abdominal aortic aneurysm at Ninewells Hospital, Dundee, with polygonal cells using Star-CD (CD Adapco, London).

Assumptions are made for such patient-specific models, because while the arterial geometry is measured non-invasively, little is known of the elasticity of the patient's vessel wall. Bergel (1961) has measured the static and dynamic elastic properties of the arterial wall and techniques have been developed to assess elasticity from medical imaging (Kanai et al 2003). Values for the elastic modulus of arteries can also be found in a review by Hoskins (2007). Using such measurements, it is possible to allow for compliant arteries in experiments (Deters et al 1986) and to examine differences in results between rigid and compliant models (Pedrizzetti et al 2002; Liepsch and Moravec 1984). Models are often simplified in one respect or another according to what specifically is being researched, for instance with the use of constant flow (Doorly et al 2002) or of simple 2D geometries (Marques et al 2003). An assumption that is usually

made is that blood in large arteries is Newtonian. This is not strictly the case and assessments of the flow differences when using non-Newtonian fluid properties have been made (Leuprecht and Perktold 2001).

The pulsatile flow of blood can be considered with 1D (1 dimension) wave propagation models (Cox 1969). Flow can be simulated by discretising the hyperbolic equations that govern the flow and finding a solution using the method of characteristics (Sherwin et al 2003; Versteeg and Malalasekera 1995; Parker and Jones 1990; Shapiro 1953). A 1D model was chosen instead of 3D for the analysis described in this chapter because it allows blood flow through an extensive part of the vascular network to be simulated with ease and, using the method developed here, with no numerical iterations.

1D simulations of the haemodynamics in extensive parts of the arterial network can be carried out using the method of characteristics. Avolio (1980) published physiological data for 128 segments of the arterial tree, from the aorta to the tibial arteries. Using this, he carried out 1D computer simulations to examine pressure and flow pulse shapes (Karamanoglu et al 1994). Anliker et al (1971) judge that an advantage "*is that the method of characteristics includes automatically the effects of reflections and makes it possible to account for the variations in cross-sectional area with distance and pressure and for the convection of the signal by the flow*". Wang and Parker (2004) used the method of characteristics to research the effects of occlusion and changes in peripheral resistance on pressure and velocity waveforms, and observed that "*the complex pattern of wave propagation in the large arteries may be the most important determinant of arterial haemodynamics*".

Several studies have used 1D modelling to help inform clinicians, e.g. for planning bypass operations (Schulz et al 1997; Suda et al 1993; Stergiopulos et al 1991).

Some of the effects of different arterial characteristics on wave propagation can be determined analytically (Atabek 1968; Atabek and Lew 1966). However, physical experiments are carried out to verify the properties derived from theory (Horsten et al 1989; Gerrard 1985; Ling and Atabek 1972). Repeated wave reflections (Berger et al 1993) contribute to the pulse shape and play a physiological role: Berger et al (1995) examined power dissipation in the arterial system and suggest that "*the presence of wave reflections leads directly to a reduction of oscillatory power and an increase in the efficiency of power dissipation*".

Analyses using linear models describe the space and time distribution of pressure and velocity well (Skalak 1972), but need assumptions to linearise the equations. In a 1D model, approximations have to be made for the arterial geometry, in particular for curved vessels and bifurcations (Lou and Yang 1992); this may result in errors concerning for example the predicted locations of atherosclerosis.

1D models of the arterial network allow physiological parameters at different locations in the vascular network to influence the simulated haemodynamics within the aorta. These numerical experiments help to provide an understanding of the possible causal relationships between haemodynamics and specific vascular diseases, in particular abdominal aortic aneurysm. 1D

simulations could help with studying the changes in physiology that led to markedly detrimental pressures and flows in the aneurysm described by Cooney (1976), with a tenfold rise in pressure between resting and exercise conditions.

2.2 1D Method

The aim of the use of 1D numerical simulation methods is to determine what the effects on the haemodynamics are of altering the properties of the arterial network. For the purpose of the interpretation of results by radiologists, surgeons and medical engineers, a space-time formulation was chosen for the 1D model. Furthermore, instead of using a system of governing equations in terms of area-velocity variables (Sherwin et al 2003), a system using pressure and flow rate was adopted because of the discretisation method developed here. This discretisation procedure relies on properties of the variables at changes in vascular cross-sectional area, provides an efficient way of solving the model and enables the simulation of applied changes in time of the cross-sectional area.

Measurements were taken of a patient's artery sizes and clinically relevant alterations were examined by simulating the placing of vascular prostheses. The study of the arterial system using the 1D method described here required the development of a computer program that allowed the building of 1D models of the arterial network and the simulation of pulsatile blood flow in the vessels. Analysis of a patient's radiography was also necessary to describe the arteries

geometrically, which allowed the reporting of some network characteristics through analytical means. The main limitation of the 1D method is that none of the detail of the haemodynamics in the vessel will be simulated as this requires 3D models. However, the 1D method was chosen because of allowing the simulation of extensive parts of the arterial network and the computation of pressure, flow rate and mean velocity of the blood throughout that network. Both the mathematical development of the computer program Art 2 (written by Sarran for this thesis) and the clinical methods used to build the patient specific model are described here.

For a pipe in which cross-sectional area can vary with time as well as distance, a control volume can be defined to enclose a section of size Δx of the pipe and within which the pipe is allowed to expand (c.f. Vardy 1990). Effectively, the control volume encloses not only the fluid domain in the pipe, but also the pipe wall and its surroundings. The fluid in the control volume has density ρ, pressure P and mean velocity u, and the pipe within the control volume has mean cross-sectional area a. Figure 2.2.1 (a) represents the pipe with the fluid flow into the control volume from which the net flow can be derived as $-\rho\frac{\partial(au)}{\partial x}\Delta x$. The rate of change of mass of the fluid in the control volume $\frac{d}{dt}(\rho a\Delta x)$ is exactly balanced by the flux into the volume so as to form the equation of continuity (mass-conservation equation) (Batchelor 1967):

$$\frac{d}{dt}(\rho a\Delta x) = -\rho\frac{\partial(au)}{\partial x}\Delta x \qquad \text{Equation 2.2.1}$$

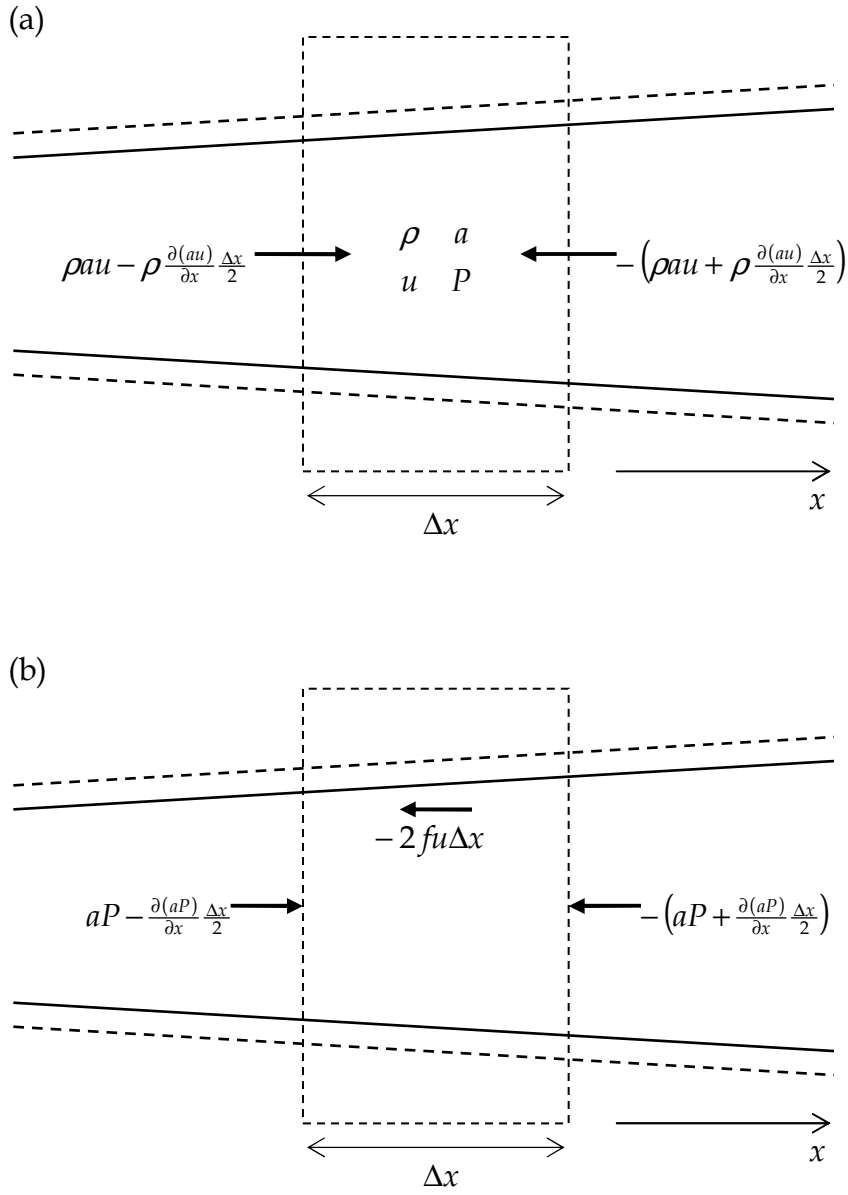

Figure 2.2.1. Pipe (solid lines) with cross-sectional area varying with time (dashed lines) and distance x, with a control volume of size Δx showing (a) the flow into the control volume and (b) the forces acting on the control volume (2nd order forces not represented).

The rate of change of momentum of a fluid is governed by the body and surface forces acting on it. For the motion of blood in the cardiovascular system, body forces due to corporeal movement are neglected because of their complexity. The gravitational force may be included, but for the purpose of this study it is neglected because the direction of the acceleration from gravity depends on the patient's position which is not an object of this analysis. Figure 2.2.1 (b) represents the pipe with the forces acting on the control volume, namely the net force $-\frac{\partial(aP)}{\partial x}\Delta x$ due to the pressure gradient and the friction force $-2fu\Delta x$ due to viscosity. The rate of change of momentum of the fluid in the control volume $\frac{d}{dt}(\rho au\Delta x)$ is balanced by the forces acting on the fluid to form the equation of motion:

$$\frac{d}{dt}(\rho au\Delta x) = -\frac{\partial(aP)}{\partial x}\Delta x - 2fu\Delta x \qquad \text{Equ. 2.2.2}$$

Blood is an incompressible fluid so its density ρ remains constant. The phase velocity c for blood in an artery ($c \sim 10\,\mathrm{m/s}$) is therefore dependent on the compliance of the vessel wall which allows changes in the cross-sectional area of the vessel dependent on the internal fluid pressure P. For an elastic vessel with rigidity K defined by $\frac{dP}{K} = \frac{da}{a}$ and with cross-sectional area a allowed to change with time due to elasticity, the equation of continuity (Equation 2.2.1) becomes:

$$\frac{a}{K}\frac{\partial P}{\partial t} + \frac{au}{K}\frac{\partial P}{\partial x} + \frac{\partial(au)}{\partial x} = 0 \qquad \text{Equ. 2.2.3}$$

The flow rate $Q = au$ and the pressure P are quantities that are constant across step changes in space of the cross-sectional area. Using Q and P, the equations of continuity and motion become, respectively:

$$\begin{cases} \frac{a}{K}\frac{\partial P}{\partial t} + \frac{Q}{K}\frac{\partial P}{\partial x} + \frac{\partial Q}{\partial x} = 0 \\ \rho\frac{\partial Q}{\partial t} + \frac{\rho Q}{a}\frac{\partial Q}{\partial x} + a\frac{\partial P}{\partial x} + \frac{2fQ}{a} = 0 \end{cases} \qquad \text{Equ. 2.2.4}$$

A linear combination of the governing equations in Equation 2.2.4 leads to:

$$\frac{a}{K}\frac{dP}{dt} + \lambda\rho\frac{dQ}{dt} + \frac{2\lambda fQ}{a} = 0 \quad \text{if } \lambda = \pm\frac{1}{\sqrt{K\rho}} \qquad \text{Equ. 2.2.5}$$

From this the characteristic equations (Douglas et al 2001) are derived for the 1D flow of an incompressible fluid in an elastic vessel:

$$\begin{cases} \frac{dP}{dt} + \frac{\rho c}{a}\frac{dQ}{dt} + \frac{2cfQ}{a^2} = 0 & \text{if } \frac{dx}{dt} = u + c \\ \frac{dP}{dt} - \frac{\rho c}{a}\frac{dQ}{dt} - \frac{2cfQ}{a^2} = 0 & \text{if } \frac{dx}{dt} = u - c \end{cases} \qquad \text{Equ. 2.2.6}$$

Where c is the wave speed defined by Equation 2.2.7:

$$c \equiv \sqrt{\frac{K}{\rho}} \qquad \text{Equ. 2.2.7}$$

The friction factor f is defined by considering Poiseuille flow and using the Navier-Stokes equation of motion to derive the flow rate given a pressure gradient in a pipe of radius R under steady flow conditions:

$$Q = -\frac{\pi R^4}{8\mu}\frac{dP}{dx} \qquad \text{Equ. 2.2.8}$$

Rearranging and substituting Q and $a = \pi R^2$, the friction factor is defined by Equation 2.2.9:

$$f = 4\pi\mu \qquad \text{Equ. 2.2.9}$$

While it is an approximation, the factor $f = 4\pi\mu$ does not depend on any of the variables P, Q, u or a and is constant as long as the viscosity μ is constant.

While the phase velocity c is of the order of 10 m/s, the velocity u of blood in the arterial system is of the order of 0.1 m/s. It is therefore assumed that $c >> |u|$. This simplifies the characteristic equations so that they apply to the characteristic lines depicted in Figure 2.2.2. The pressure P_A and flow rate Q_A at point A are related to the pressures and flow rates P_L, P_R, Q_L and Q_R at the points L and R because (Nassiet et al 1994):

$$\lim_{\Delta t \to 0} \frac{P_A - P_L}{\Delta t} = \frac{dP}{dt} \text{ and } \lim_{\Delta t \to 0} \frac{Q_A - Q_L}{\Delta t} = \frac{dQ}{dt} \text{ along } (LA) \text{ defined by } \frac{dx}{dt} = +c$$

$$\lim_{\Delta t \to 0} \frac{P_A - P_R}{\Delta t} = \frac{dP}{dt} \text{ and } \lim_{\Delta t \to 0} \frac{Q_A - Q_R}{\Delta t} = \frac{dQ}{dt} \text{ along } (RA) \text{ defined by } \frac{dx}{dt} = -c$$

Averages of the flow rate $\frac{Q_A + Q_L}{2}$ and $\frac{Q_A + Q_R}{2}$ are used along $]LA[$ and $]RA[$, respectively, to have constant friction terms, such that Equation 2.2.10 are characteristic equations along $]LA[$ and $]RA[$:

$$\begin{cases} P_A - P_L + \frac{\rho c_L}{a_L}(Q_A - Q_L) + \frac{c_L f_L \Delta t}{a_L^2}(Q_A + Q_L) = 0 \\ P_A - P_R - \frac{\rho c_R}{a_R}(Q_A - Q_R) - \frac{c_R f_R \Delta t}{a_R^2}(Q_A + Q_R) = 0 \end{cases} \qquad \text{Equ. 2.2.10}$$

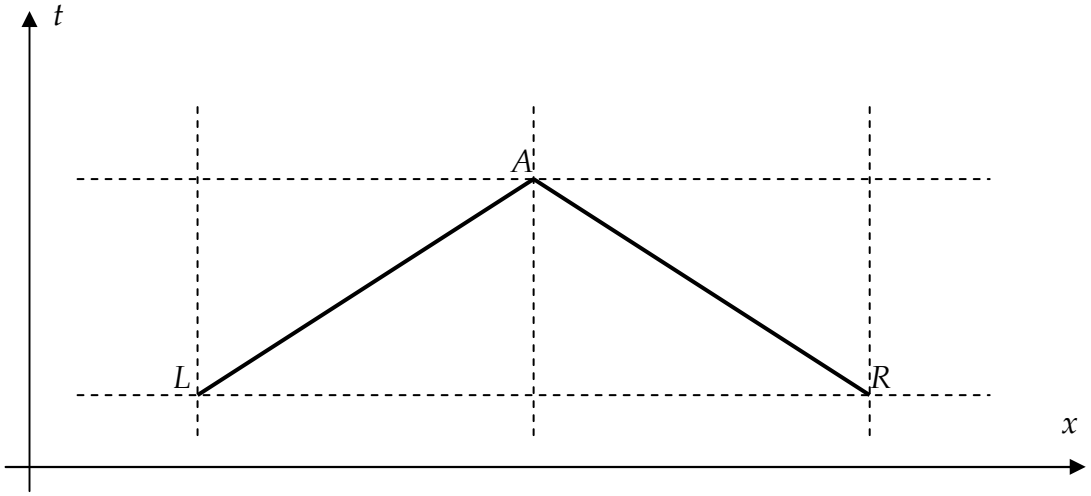

Figure 2.2.2. Characteristic lines (LA) and (RA) of gradients $\dot{x} = +c$ and $\dot{x} = -c$, respectively, linking the point $A(x_A; t_A)$ to points $L(x_A - \Delta x; t_A - \Delta t)$ and $R(x_A + \Delta x; t_A - \Delta t)$ at either side and at the previous time step.

The constants c_L, a_L and f_L are the parameters of the vessel between L and A, and c_R, a_R and f_R are those between R and A.

The characteristic equations provide a means of simulating blood flow in numerical 1D models of arteries. In such models, pressure P_A and flow rate Q_A at most grid points A can be solved from the solution for the previous time step, or from specified initial conditions if it is the first time step, using Equation 2.2.11:

$$\begin{pmatrix} 1 & \frac{\rho c_L}{a_L} + \frac{c_L f_L \Delta t}{a_L^2} \\ 1 & -\frac{\rho c_R}{a_R} - \frac{c_R f_R \Delta t}{a_R^2} \end{pmatrix} \begin{pmatrix} P_A \\ Q_A \end{pmatrix} = \begin{pmatrix} P_L + \left(\frac{\rho c_L}{a_L} - \frac{c_L f_L \Delta t}{a_L^2} \right) Q_L \\ P_R - \left(\frac{\rho c_R}{a_R} - \frac{c_R f_R \Delta t}{a_R^2} \right) Q_R \end{pmatrix} \qquad \text{Equ. 2.2.11}$$

The boundaries of the vascular network are the ends of vessels that are not connected to any other. At vessel ends only one characteristic equation applies so that a boundary condition has to be specified. Pressure P or flow rate Q is

specified, or a given function between pressure and flow rate such as for a resistive boundary.

If the boundary condition is a given pressure P_A, Equation 2.2.12 provides a solution for flow rate Q_A:

$$Q_A = \left[P_A - P_R + \left(\frac{\rho c_R}{a_R} - \frac{c_R f_R \Delta t}{a_R^2} \right) Q_R \right] \left(\frac{\rho c_R}{a_R} + \frac{c_R f_R \Delta t}{a_R^2} \right)^{-1}$$

left-hand-side boundaries Equ. 2.2.12a

$$Q_A = \left[P_L - P_A + \left(\frac{\rho c_L}{a_L} - \frac{c_L f_L \Delta t}{a_L^2} \right) Q_L \right] \left(\frac{\rho c_L}{a_L} + \frac{c_L f_L \Delta t}{a_L^2} \right)^{-1}$$

right-hand-side boundaries Equ. 2.2.12b

If the boundary condition is a given flow rate Q_A, Equation 2.2.13 provides a solution for pressure P_A:

$$P_A = P_R + \frac{\rho c_R}{a_R}(Q_A - Q_R) + \frac{c_R f_R \Delta t}{a_R^2}(Q_A + Q_R)$$

left-hand-side boundaries Equ. 2.2.13a

$$P_A = P_L - \frac{\rho c_L}{a_L}(Q_A - Q_L) - \frac{c_L f_L \Delta t}{a_L^2}(Q_A + Q_L)$$

right-hand-side boundaries Equ. 2.2.13b

A resistance boundary is where at the end of a vessel, the greater the velocity of the fluid exiting the vessel the greater the pressure, such that the resistance κ provides a second equation (Equation 2.2.14) in addition to the single characteristic equation. At a right-hand-side boundary, for example, a resistance condition leads to:

$$P_A - \frac{\kappa}{a_L} Q_A = 0 \qquad \text{Equ. 2.2.14}$$

and

$$\begin{pmatrix} 1 & \frac{\rho c_L}{a_L} + \frac{c_L f_L \Delta t}{a_L^2} \\ 1 & -\frac{\kappa}{a_L} \end{pmatrix} \begin{pmatrix} P_A \\ Q_A \end{pmatrix} = \begin{pmatrix} P_L + \left(\frac{\rho c_L}{a_L} - \frac{c_L f_L \Delta t}{a_L^2} \right) Q_L \\ 0 \end{pmatrix} \qquad \text{Equ. 2.2.15}$$

There is a vessel only to one side of a grid point at boundaries and there are vessels connected to two sides of most other grid points. At bifurcations, the grid point is connected to the ends of three vessels. This requires solving a system of three characteristic equations. While pressure is the same in the three vessels at the bifurcation, flow rate is split such that the sum of the flow rates in two vessels is equal to that of the remaining vessel to satisfy continuity. This means obtaining solutions for three unknowns P_A, Q_A and $Q_{A'}$ from the three characteristic equations for the characteristic lines (LA), (RA) and $(R'A)$ where $R'(x_A + \Delta x; t_A - \Delta t)$ is in a grid representing a different vessel to that of R. At the bifurcation, the flow rate is Q_A in the R-vessel, and $Q_{A'}$ in the R'-vessel, such that the flow rate in the L-vessel is $Q_A + Q_{A'}$. The pressure P_A and flow rates Q_A and $Q_{A'}$ are found by solving Equation 2.2.16:

$$\begin{pmatrix} 1 & \frac{\rho c_L}{a_L}+\frac{c_L f_L \Delta t}{a_L^2} & \frac{\rho c_L}{a_L}+\frac{c_L f_L \Delta t}{a_L^2} \\ 1 & -\frac{\rho c_R}{a_R}-\frac{c_R f_R \Delta t}{a_R^2} & 0 \\ 1 & 0 & -\frac{\rho c_{R'}}{a_{R'}}-\frac{c_{R'} f_{R'} \Delta t}{a_{R'}^2} \end{pmatrix} \begin{pmatrix} P_A \\ Q_A \\ Q_{A'} \end{pmatrix} = \begin{pmatrix} P_L+\left(\frac{\rho c_L}{a_L}-\frac{c_L f_L \Delta t}{a_L^2}\right)Q_L \\ P_R-\left(\frac{\rho c_R}{a_R}-\frac{c_R f_R \Delta t}{a_R^2}\right)Q_R \\ P_{R'}-\left(\frac{\rho c_{R'}}{a_{R'}}-\frac{c_{R'} f_{R'} \Delta t}{a_{R'}^2}\right)Q_{R'} \end{pmatrix}$$

Equ. 2.2.16

In principle there is no limit to the number of interconnected vessels and to the number of characteristic equations to be solved; however it is usually easier numerically to solve these as several bifurcations connected to each other. For example, trifurcations (a grid point at the junction of 4 vessels) can be solved as two bifurcations separate only by a small distance Δx. In vascular applications only bifurcations and trifurcations are present. For this study of the abdominal aorta the only trifurcation is the junction of the renal arteries with the aorta which is solved as two bifurcations.

Specifying constant vessel characteristics such as cross-sectional area a in the areas between grid points is a new approach to using characteristic equations in 1D models. By considering flow rate instead of velocity it has been possible to allow for changes in cross-sectional area along the vessel to affect velocity. The velocity at one side of a grid point is different to that at the other side if the cross-sectional areas on each side are different:

$$\left(\lim_{x\to x_A^-} u=\frac{Q_A}{a_L}\right)\neq\left(\lim_{x\to x_A^+} u=\frac{Q_A}{a_R}\right) \quad \text{if } a_L \neq a_R \qquad \text{Equ. 2.2.17}$$

Changes in cross-sectional area with time can be seen as affecting pressure in a similar way. The change in pressure given a change in cross-sectional area is driven by the bulk modulus B defined by $\frac{dP}{B} = \frac{d\rho}{\rho} = -\frac{da}{a}$ (Young 1992). If pressures at L and R are defined by Equation 2.2.18 and if the cross-sectional areas are specified by Equation 2.2.19, then a small instantaneous change in cross-sectional area from a_L to a'_L and from a_R to a'_R means a change in pressure given by Equation 2.2.20.

$$\begin{cases} \lim\limits_{t\to(t_A-\Delta t)^-} P|_{x_A-\Delta x} = P_L \\ \lim\limits_{t\to(t_A-\Delta t)^-} P|_{x_A+\Delta x} = P_R \end{cases} \quad \text{and} \quad \begin{cases} \lim\limits_{t\to(t_A-\Delta t)^+} P|_{x_A-\Delta x} = P'_L \\ \lim\limits_{t\to(t_A-\Delta t)^+} P|_{x_A+\Delta x} = P'_R \end{cases} \qquad \text{Equ. 2.2.18}$$

$$a'_L \text{ if } \begin{cases} x \in]x_A-\Delta x; x_A[\\ t \in]t_A-\Delta t; t_A[\end{cases} \quad \text{and} \quad a'_R \text{ if } \begin{cases} x \in]x_A; x_A+\Delta x[\\ t \in]t_A-\Delta t; t_A[\end{cases} \qquad \text{Equ. 2.2.19a}$$

$$a_L \text{ if } \begin{cases} x \in]x_A-\Delta x; x_A[\\ t \in]t_A-2\Delta t; t_A-\Delta t[\end{cases} \quad \text{and} \quad a_R \text{ if } \begin{cases} x \in]x_A; x_A+\Delta x[\\ t \in]t_A-2\Delta t; t_A-\Delta t[\end{cases} \qquad \text{Equ. 2.2.19b}$$

$$\frac{P'_L - P_L}{B} = -\frac{a'_L - a_L}{a_L} \quad \text{and} \quad \frac{P'_R - P_R}{B} = -\frac{a'_R - a_R}{a_R} \qquad \text{Equ. 2.2.20}$$

By substitution the characteristic equations become:

$$\begin{pmatrix} 1 & \frac{\rho c_L}{a_L} + \frac{c_L f_L \Delta t}{a_L^2} \\ 1 & -\frac{\rho c_R}{a_R} - \frac{c_R f_R \Delta t}{a_R^2} \end{pmatrix} \begin{pmatrix} P_A \\ Q_A \end{pmatrix} = \begin{pmatrix} P_L + \left(\frac{\rho c_L}{a_L} - \frac{c_L f_L \Delta t}{a_L^2} \right) Q_L - B \frac{a'_L - a_L}{a_L} \\ P_R - \left(\frac{\rho c_R}{a_R} - \frac{c_R f_R \Delta t}{a_R^2} \right) Q_R - B \frac{a'_R - a_R}{a_R} \end{pmatrix} \qquad \text{Equ. 2.2.21}$$

Characteristic equations have been used before to describe the 1D fluid dynamics of blood flow in the arterial network (Jones 1985; Ghiassy 1982). The equations, valid on the characteristic lines, provide a means of finding solutions

to fluid flow in pipe networks by computer simulation, as long as the assumptions made hold, namely that the phase velocity c is much greater than the blood velocity $|u|$ and that changes in cross-sectional area are small. Setting a constant time step Δt, computational grids representing portions of the arterial system have been generated using Matlab version 6.1.0.450 release 12.1 (Mathworks Inc., Natick), the spacing Δx between grid points being determined by the local phase velocity c, ensuring all points have been connected by characteristic lines (the programs, geogen.m and bcgen.m, can be found in the Appendix). The program Art 2 has been written in Matlab to simulate the flow of blood in the 1D models of the arterial network using the method of characteristics (c.f. art2.m with test.m, lhsb.m, rhsb.m, bif.m, bifb.m and point.m in the Appendix).

2.3 Application to the Arterial Network

The ways in which changes in the arterial network affect the pressure and flow characteristics at different locations in the network can be examined using the 1D numerical simulation tool Art 2. The geometric characteristics of the vascular network have been obtained from a patient's scan, a numerical model has been built and haemodynamic flow in the model has been simulated. The arterial wall rigidity in the model has then been changed to simulate vascular prostheses of different types, grafts and stents. The flow characteristics in the modified models could then be compared with those of the original model,

hence providing knowledge about the influence of the changes on the haemodynamics.

The Radiology department at Ninewells Hospital, Dundee, provided a CT (Computed Tomography) scan of a patient's abdomen and lower limbs from which an anonymised arterial network was characterised. Two scan images for a single patient were provided, namely (i) a coronal section of the abdomen and lower limbs showing the main configuration of the arterial network, in particular the abdominal aorta at the level of the renal arteries and the bifurcation of the distal end of the abdominal aorta with the two common iliac arteries and (ii) a lateral view showing the angles at which the configurations of arteries lie. The latter was necessary to resolve the positions of anterior branches such as the superior mesenteric artery (Figure 2.3.1 and Figure 2.3.2). The graphical representation of the network analysed from the images is shown in Figure 2.3.3. Measurements of the lengths of the arterial sections and of their diameters at regular intervals (~10 mm) along each section have been made using Matlab. The cross-sectional areas were estimated from the diameters. The measured artery lengths and cross-sectional areas are listed in Table 2.3.1. The diameter measurement error is estimated from the CT image pixel size $\sigma_r = 1.4\,\text{mm}$.

How well the haemodynamic pulse is transmitted through the network can be assessed at the bifurcations from the rigidities and the measured cross-sectional areas of the vessels (Wang and Parker 2004). The rigidities were derived from

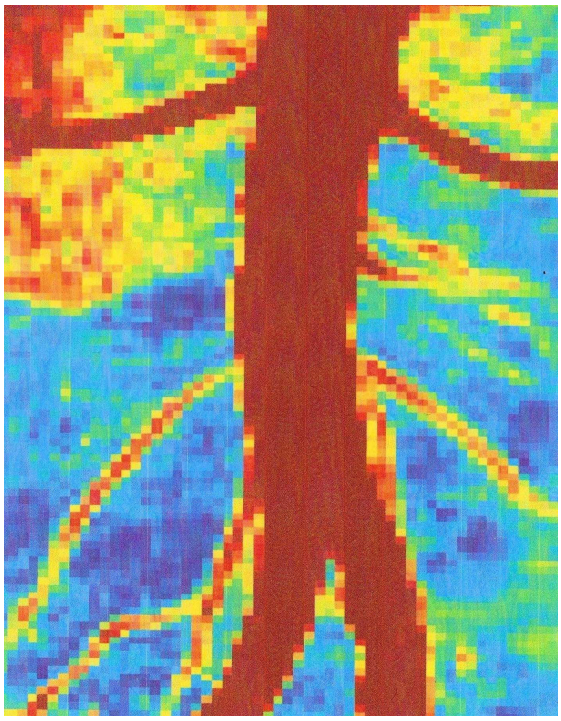

Figure 2.3.1. Colour-enhanced part of the coronal CT image showing the infra-renal abdominal aorta. Individual image pixels can be seen.

published wave speed values that are assumed constant for each vessel and that are themselves based on values of Young's modulus and wall thickness (Westerhof et al 1969). For instance, the assumed rigidity of the thoracic aorta is 19.2 kN/m^2 derived from a wave speed of 4.28 m/s based on a Young's modulus of 0.4 MPa and a wall thickness of 1.00 mm; the rigidity of the internal iliac arteries is 109 kN/m^2 based on a wave speed of 10.21 m/s implied by a Young's modulus of 1.6 MPa and a wall thickness of 0.40 mm. These values are within the ranges described by Hoskins (2007). For waves travelling from the proximal vessel to the two distal vessels, a bifurcation is said to be well matched when the transmission coefficient is $E = 1$, implying that the pressure wave is perfectly transmitted through the bifurcation with no reflection. A well

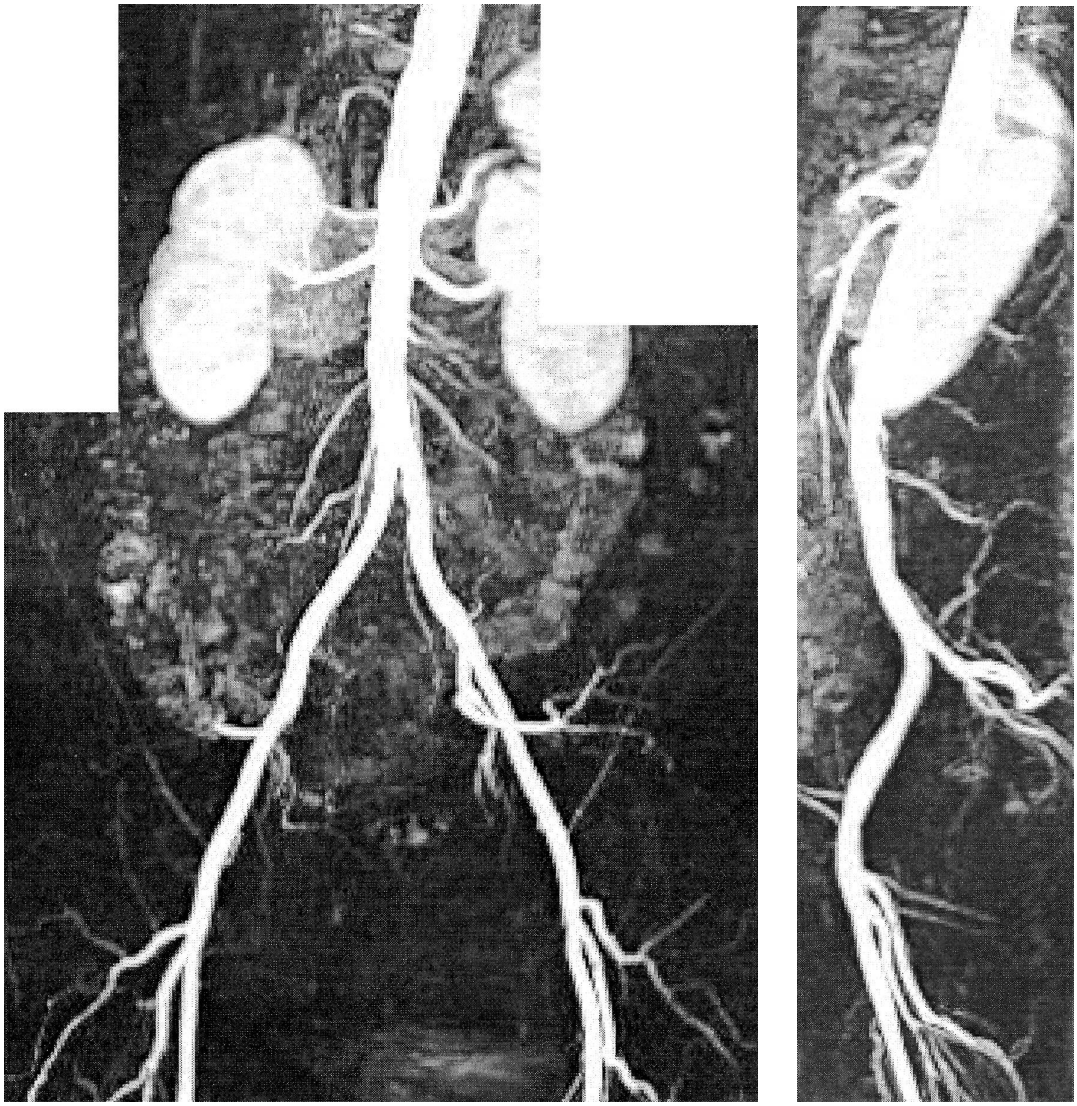

Figure 2.3.2. Coronal (left) and lateral (right) CT images of a patient's abdomen and lower limbs at the Radiology department, Ninewells Hospital, Dundee; the main features are the abdominal aorta with the renal arteries leading to the kidneys (top of coronal image), the aorto-iliac bifurcation (centre), the iliac arteries (lower half) and circumflex and femoral arteries (bottom).

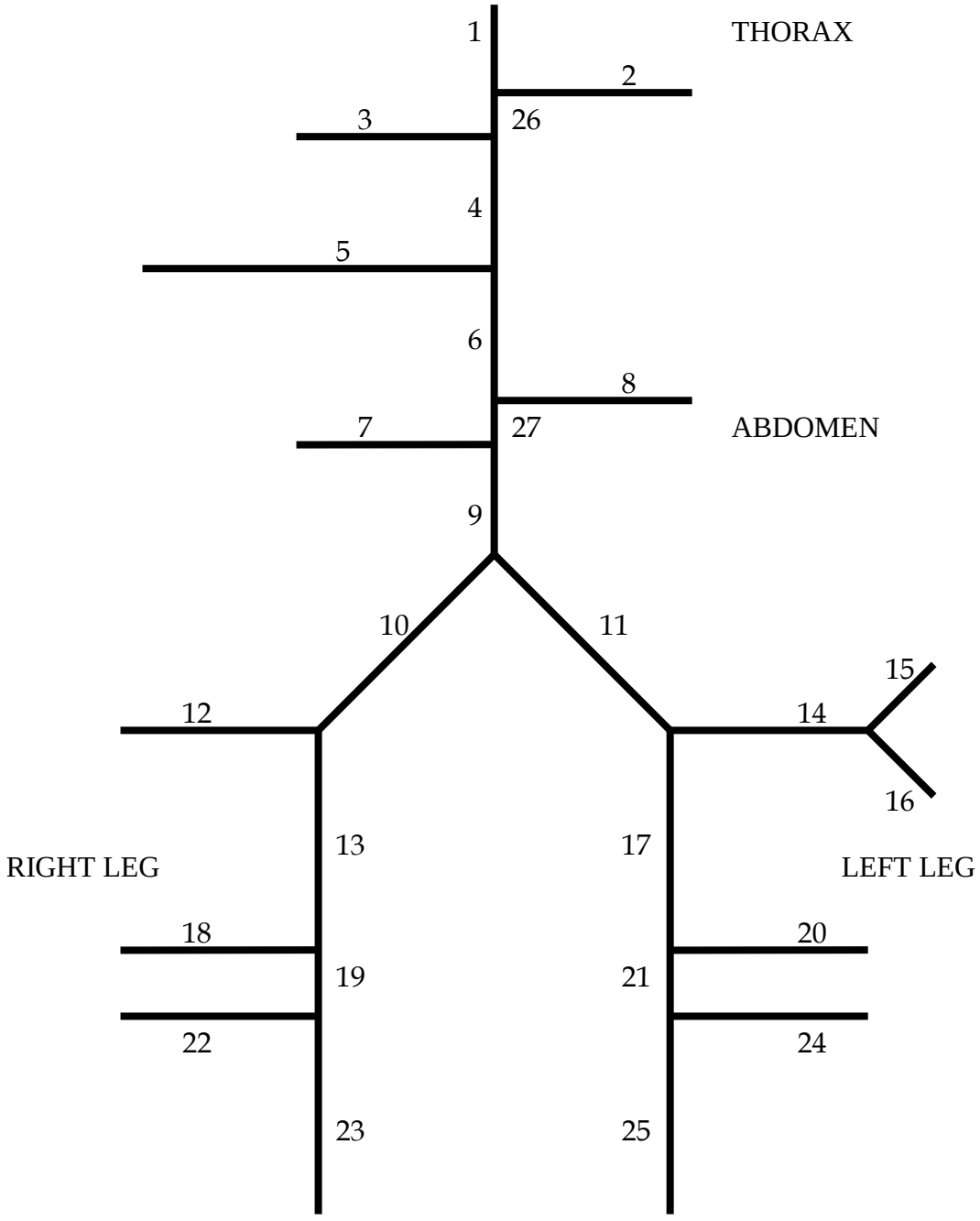

Figure 2.3.3. 1D arterial network derived from a CT scan of a patient's abdomen and lower limbs; the arteries' names and characteristics and listed in Table 2.3.1.

Table 2.3.1. List of the artery sections represented in Figure 2.3.3, with the lengths of each section, their measured cross-sectional areas, and the rigidities derived from Wang and Parker (2004). The rigidities assume a constant wave speed in each vessel that is obtained from values of Young's moduli and wall thicknesses from Westerhof et al (1969).

N°	Name	Length (mm)	Cross-Sectional Area (mm^2) Range		Rigidity (kN/m^2)
			Minimum	Maximum	
1	Thoracic Aorta	127.9	463.3	519.4	19.2
2	Splenic A	54	14.5	32.4	28.8
3	Hepatic A	61.1	41.3	61.1	22
4	Abdominal Aorta 1	12.1	360.6		20.1
5	Superior Mesenteric A	106.3	92.4	106.3	28.5
6	Abdominal Aorta 2	26.6	270.8	360.6	19.6
7	Right Renal A	48	25.7		31.2
8	Left Renal A	57.1	25.7	57.8	31.2
9	Abdominal Aorta 4	95.3	193.9	578.6	23.2
10	R Common Iliac A	106.4	57.8	115.7	26.3
11	L Common Iliac A	98.7	90.2	144.7	26.3
12	R Internal Iliac A	88.1	14.5	57.8	109
13	R External Iliac A	131.3	48.6	90.2	45.3
14	L Internal Iliac A	30.9	25.7		109
15	Posterior Trunk	63.7	14.5	57.8	109
16	Anterior Trunk	47.1	10	14.5	109
17	L External Iliac A	124.7	57.8	102.7	45.3
18	R External Circumflex A	33.6	14.5		54.4
19	R External Iliac A 0	9.1	78.6		45.3
20	L External Circumflex A	32.4	1.6	14.5	54.4
21	L External Iliac A 0	10.1	102.7		45.3
22	R Deep Femoral A	60.7	25.7	78.6	54.4
23	R Femoral A	114	32.4	57.8	57
24	L Deep Femoral A	95.1	10	19.6	54.4
25	L Femoral A	125	32.4	57.8	57
26	Abdominal Aorta 0	1.3	360.6		20.1
27	Abdominal Aorta 3	1.3	360.6		20.8

Abbreviations: A *Artery;* R *Right;* L *Left.*

matched bifurcation does not mean that waves travelling from one of the distal vessels will be transmitted well to the proximal and other distal vessels: typically returning pressure waves from the distal arteries will be attenuated with a transmission coefficient $E<1$. The transmission coefficient is given by Equation 2.3.1:

$$E = 1 + \frac{Y_L - Y_R - Y_{R'}}{Y_L + Y_R + Y_{R'}} \qquad \text{Equ. 2.3.1}$$

Y_L is the admittance of the end of the artery proximal to the bifurcation, Y_R and $Y_{R'}$ are the admittances of the two distal arteries. The admittances are given by the cross-sectional areas a and rigidities K at the vessel ends (Equation 2.3.2).

$$Y = \frac{a}{\rho c} \qquad \text{where } c \equiv \sqrt{\frac{K}{\rho}} \qquad \text{Equ. 2.3.2}$$

The transmission coefficient error σ_E due to the diameter measurement error σ_r can be computed using Equation 2.3.3:

$$\sigma_E = \frac{E\sqrt{(Y_R + Y_{R'})^2 \sigma_L^2 + Y_R^4 \sigma_R^2 + Y_{R'}^4 \sigma_{R'}^2}}{Y_L + Y_R + Y_{R'}} \qquad \text{Equ. 2.3.3}$$

Where the error in proximal admittance σ_L is given by Equation 2.3.4, and similarly for the distal admittances:

$$\sigma_L = \frac{2\rho c_L}{\pi r_L^3}\sigma_r \qquad \text{Equ. 2.3.4}$$

At any point in the arterial network, the transmission of a pressure wave will depend on the admittances of the vessels immediately proximally and distally from that point. If the two admittances are equal, the transmission coefficient is $E = 1$ and the pressure wave is transmitted with no reflections. If the distal vessel is smaller or stiffer, or both, than the proximal vessel, then the distal vessel has a smaller admittance and the transmission coefficient is $E > 1$: the transmitted pressure wave magnitude is increased and a reflected wave is created. If the distal vessel is larger or more compliant, or both, than the proximal vessel, then the distal vessel has a greater admittance and the transmission coefficient is $E < 1$: the transmitted pressure wave magnitude is reduced and a reflected wave is created of the opposite sign to that transmitted.

Table 2.3.2 lists the transmission coefficients E and their errors σ_E for all the junctions of the network modelled. The very short sections (N° 26 and 27 in

Table 2.3.2. Transmission coefficients E at the junctions of the arterial network computed from the vessel admittances, coefficients for trifurcations being computed as total transmission through two bifurcations.

Junction Linking Arteries N°	**Transmission Coefficient** $E \pm \sigma_E$
1; 2; 3; 4 (trifurcation)	1.2 ± 0.2
4; 5; 6	1 ± 0.1
6; 7; 8; 9 (trifurcation)	1 ± 0.2
9; 10; 11	0.9 ± 0.2
10; 12; 13	0.9 ± 0.4
11; 14; 17	1.2 ± 0.3
13; 18; 19	0.9 ± 0.3
14; 15; 16	0.5 ± 0.6
17; 20; 21	0.9 ± 0.3
19; 22; 23	0.9 ± 0.4
21; 24; 25	1.4 ± 0.3

Table 2.3.1) are used to model the trifurcations as two bifurcations for programming convenience. Their short lengths (1.3 mm) mean that effectively trifurcations are modelled. It is the total transmission coefficient through the trifurcation that is stated in Table 2.3.2. For all but one junction, the bifurcations and trifurcations are well matched with $E = 1$ within the error σ_E from measurement. The one differing bifurcation is that of the left external iliac artery splitting into the femoral and deep femoral arteries (arteries N° 21, 24 and 25). The transmission coefficient $E = 1.4 \pm 0.3$ suggests that the total distal admittance $Y_R + Y_{R'}$ is smaller than the proximal admittance Y_L and some resistance to the haemodynamic flow pulse is to be expected at that bifurcation. There, the pressure is expected to rise while the flow rate would drop. It is unclear whether this represents arterial disease at the site of the bifurcation, but these characteristics at the distal end of the left external iliac artery will affect the haemodynamics elsewhere in the network. This is not the same at the bifurcation on the other side (arteries N° 19, 22 and 23), i.e. at the distal end of the right external iliac artery, where the transmission coefficient is $E = 0.9 \pm 0.4$ and appears well matched. The transmission coefficient errors σ_E demonstrate the difficulty in assessing how well matched vessels are at bifurcations, especially for small vessels: the junction splitting the left internal iliac artery into its posterior and anterior trunks (arteries N° 14, 15 and 16) has a measured transmission coefficient $E = 0.5$ smaller than its error $\sigma_E = 0.6$.

Boundary conditions are required at the ends of arteries that are not connected to a bifurcation. Resistance boundaries are used at the distal ends of the vessels

as specified in Table 2.3.3; the resistances κ defined in the 1D method development are derived from the κ/a values published by Stergiopulos et al (1992). The admittance of a resistance boundary can be derived as $Y = a/\kappa$. A boundary condition is also required at the proximal end of the thoracic aorta. Different conditions are used depending on the numerical experiment being carried out. First, to determine the influence of the network on pressure waves, the amplitude of a pressure step change is assessed in all arteries based on a prescribed 100 Pa step in pressure as boundary condition at the top of the thoracic aorta. Second, to determine the influence of resistance in different parts of the network, the flow rates at the distal boundaries are evaluated for a constant prescribed flow of 2 L/min (3.3×10^{-5} m^3/s) in the thoracic aorta. Finally, pulsatile flow is simulated by prescribing a periodic 1.89×10^{-4} m^3/s

Table 2.3.3. Resistances at the distal boundaries of the terminal vessels derived from Stergiopulos et al (1992).

N°	Name	Resistance (kPa.s/m)
2	Splenic Artery	75
3	Hepatic Artery	71
5	Superior Mesenteric Artery	135
7	Right Renal Artery	29
8	Left Renal Artery	29
12	Right Internal Iliac Artery	115
15	Posterior Trunk	204
16	Anterior Trunk	79
18	Right External Circumflex Artery	69
20	Left External Circumflex Artery	69
22	Right Deep Femoral Artery	123
23	Right Femoral Artery	112
24	Left Deep Femoral Artery	93
25	Left Femoral Artery	75

flow rate for 150 ms followed by 0 m^3/s for 700 ms, implying a pulsatile flow with a period of 850 ms. This equates to an average flow rate of 2 L/min, an approximate value for physiological blood flow, and a pulse rate of 70 min^{-1} (1.18 s^{-1}).

The purpose of the numerical simulations is to study the effect on the haemodynamics of increasing the vessel rigidity of parts of the network. To this end, as well as simulating the base model using published values of vessel rigidity (healthy arteries) and peripheral resistance, three models of the same arterial network were built with different vascular prostheses. Also, one model was used with the vessel rigidity increased to simulate possible haemodynamic changes due to ageing. To examine the consequences of increases in rigidity on the haemodynamics, it is sufficient to compare the models with increased rigidity with the base model and it is not necessary to use specific physiological values of hardened arteries. A ten-fold increase in rigidity has been chosen as it would provide a 3.16-fold increase in wave speed, and though larger than published physiological increases in arterial rigidity, this uniform increase in rigidity between models has made it easier to make comparisons between models. A ten-fold increase in rigidity for the whole arterial network was modelled to examine the effect of hardened vessels due to ageing, so that the new rigidities ranged from 192 to 1 090 kN/m^2. The specifications of the three implants, represented in Figure 2.3.4, are stated in Table 2.3.4.

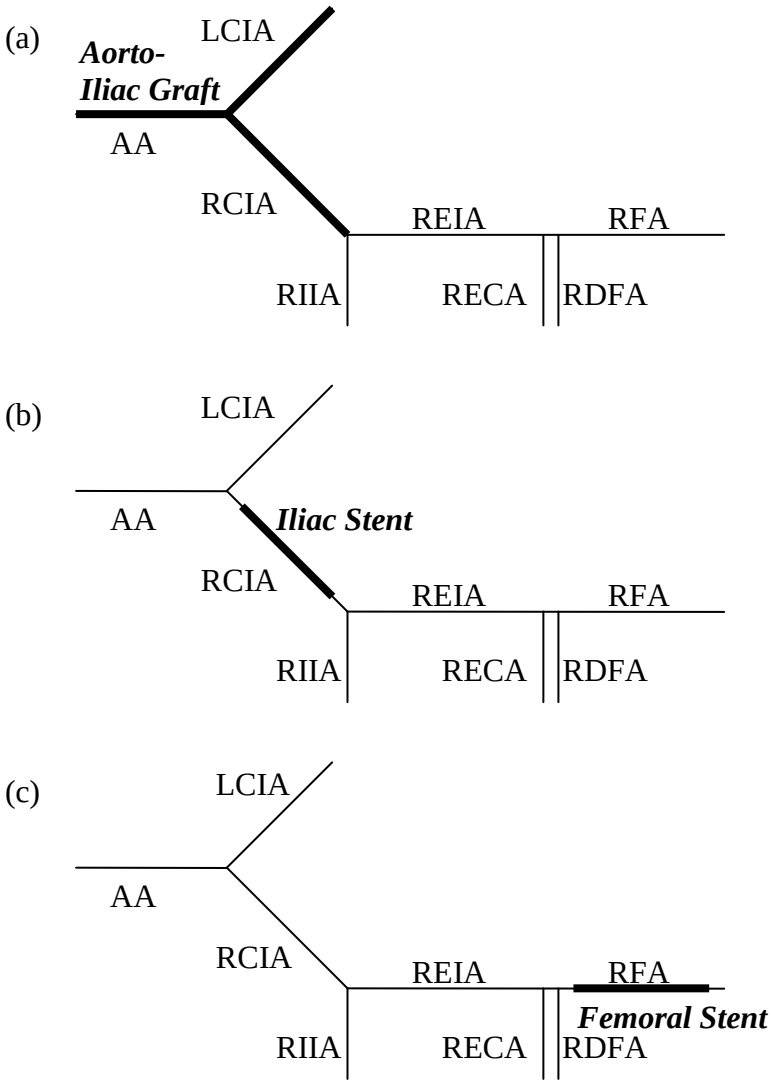

Figure 2.3.4. Schematic representation of the positions of (a) the aorto-iliac graft, (b) the iliac stent and (c) the femoral stent; a section only of the 1D arterial network (Figure 2.3.3) is represented, depicting the infra-renal Abdominal Aorta (AA), Left Common Iliac Artery (LCIA), Right Common Iliac Artery (RCIA), Right Internal Iliac Artery (RIIA), Right External Iliac Artery (REIA), Right External Circumflex Artery (RECA), Right Deep Femoral Artery (RDFA) and Right Femoral Artery (RFA).

Table 2.3.4. Vascular implant specifications for the aorto-iliac graft, the iliac stent and the femoral stent used in the numerical 1D models; properties of the implants were checked at Tayside Flow Technologies, Dundee.

Position	Length (mm)	Cross-Sectional Area (mm^2)	Rigidity (kN/m^2)
Aorto-Iliac Graft			
Abdominal Aorta 4	95.3	300	232
Right Common Iliac	106.4	150	232
Left Common Iliac	98.7	150	232
Iliac Stent			
Right Common Iliac	90	120	263
Femoral Stent			
Right Femoral	90	60	570

An aorto-iliac Y-shaped graft can be trimmed proximally and distally to allow for variations in arterial anatomy. The lengths of the aortic and iliac parts of the graft were set to be equal to the length of the patient's abdominal aorta below the renal arteries and the lengths of their common iliac arteries. The graft diameter however cannot be changed. The graft modelled was specified by a cross-sectional area of 300 mm^2 (19.5 mm diameter) for the aortic section and 150 mm^2 (13.8 mm diameter) for the iliac sections. These diameters ensure a perfect match at the aorto-iliac bifurcation with a transmission coefficient $E = 1$. The rigidity of the graft is a uniform 10 × 23.2 kN/m^2, which is ten times the rigidity of the distal section of the native abdominal aorta.

The stents modelled were both 90 mm long and were placed 10 mm below the nearest proximal bifurcation, i.e. the aorto-iliac bifurcation for the iliac stent and the bifurcation with the deep femoral artery for the femoral stent. Stents are expanded in situ to a diameter slightly greater than that of the native artery. The right common iliac artery has a maximum cross-sectional area of 115.7 mm^2

so the iliac stent is modelled with a cross-sectional area of 120 mm^2 (12.4 mm diameter). Similarly, the right femoral artery has a maximum cross-sectional area of 57.8 mm^2 so the femoral stent is modelled with a cross-sectional area of 60 mm^2 (8.7 mm diameter). The rigidities of the stents are 10×26.3 kN/m^2 and 10×57 kN/m^2, ten times the rigidities of the native right common iliac artery and right femoral artery, respectively.

The first two sets of simulations, with a prescribed 100 Pa step in pressure and with a constant prescribed flow rate of 2 L/min (3.3×10^{-5} m^3/s), are to help characterise the fluid dynamics that should be expected under simple and non-physiological flow conditions.

By specifying a 100 Pa step rise in pressure in the thoracic aorta, a wave is transmitted down the arterial network. At each bifurcation, the wave is transmitted in accordance with the transmission coefficients E estimated from the geometry (c.f. Table 2.3.2). This can be seen in Figure 2.3.5 where the incident wave of 112 Pa at the aorto-iliac bifurcation is transmitted with a coefficient of ~0.9, hence the drop to 99 Pa for the reflected and transmitted waves. By recording the pressure during the first 5 ms after the wave reaches a location (equal to ten computational time steps), the amplitudes of the pressure steps at selected positions in the network are compared between the five different models (Figure 2.3.6).

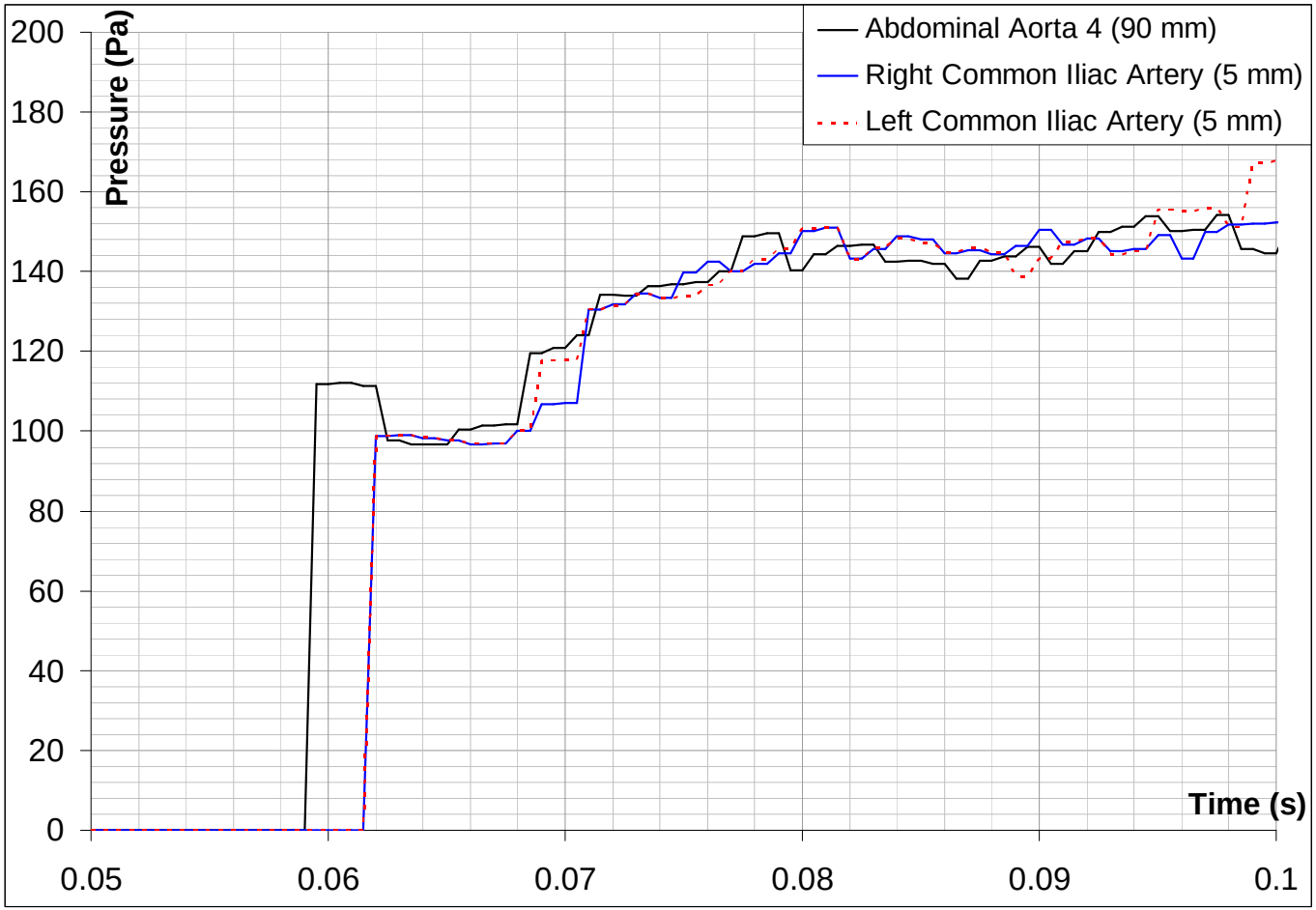

Figure 2.3.5. Pressure at the distal end of the abdominal aorta and at the proximal ends of the common iliac arteries (the figures 90 mm and 5 mm are the distances from the proximal ends of each vessel) given a 100 Pa pressure step in the thoracic aorta at time 0 s; the wave reaches the aorto-iliac bifurcation after ≈0.06 s.

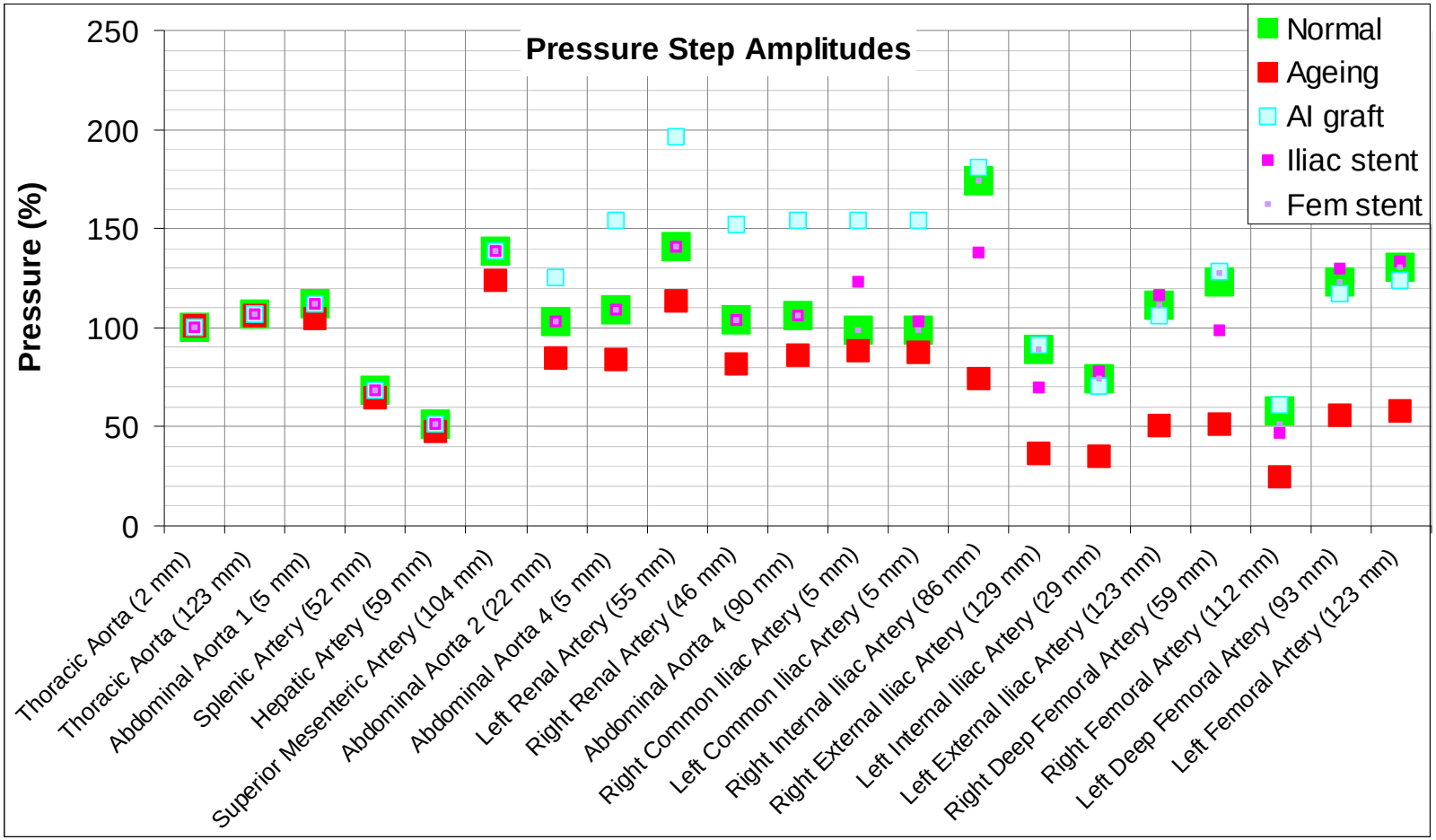

Figure 2.3.6. Amplitudes of the pressure steps as a percentage of the 100 Pa pressure step boundary condition at the thoracic aorta, for the 'normal' model (published vessel rigidities), 'ageing' (hardened arteries), the models of the AI (Aorto-Iliac) graft and the iliac and fem (femoral) stents; the figures in brackets are the distances of the recording positions from the proximal ends of the arterial sections.

The simulation of a constant 2 L/min flow rate provides another means of characterising the models. The main resistance to flow lies at the arteriolar bed which is modelled by the distal boundaries, and the network itself provides a small resistance through friction. This is shown by Figure 2.3.7 where pressures at all positions range between 54 mmHg (7.2 kPa) and 56 mmHg (7.5 kPa). The drop in pressure between the proximal end of the network and its distal ends is no more than 3%. It is worth noting that a pressure of 54 to 56 mmHg is somewhat less than the accepted physiological pressure of about 80 mmHg (11 kPa) and 120 mmHg (16 kPa) for diastolic and systolic pressures, respectively. The pressures evaluated from the pulsatile flow simulations with an average flow rate of 2 L/min are therefore underestimates of the likely physiological blood pressures. The 2 L/min average flow rate may be more suitable for the abdominal aorta below the superior mesenteric artery and so specifying a higher flow rate at the proximal end of the thoracic aorta would make the pressures closer to physiologic values. Yet, the flow rate used is of the correct order of magnitude for physiological flow in the aorta and a more precise value is not necessary for the purpose of comparing different models or arteries within models. To complete the description of this arterial network's characteristics it is useful to assess how much of the blood flow is split towards each arterial branch. It is to be expected that much of the flow will be directed towards the least resistant distal conditions, such as the renal arteries as their terminal resistances are 29 kPa.s/m (c.f. Table 2.3.3). Indeed, as is shown in

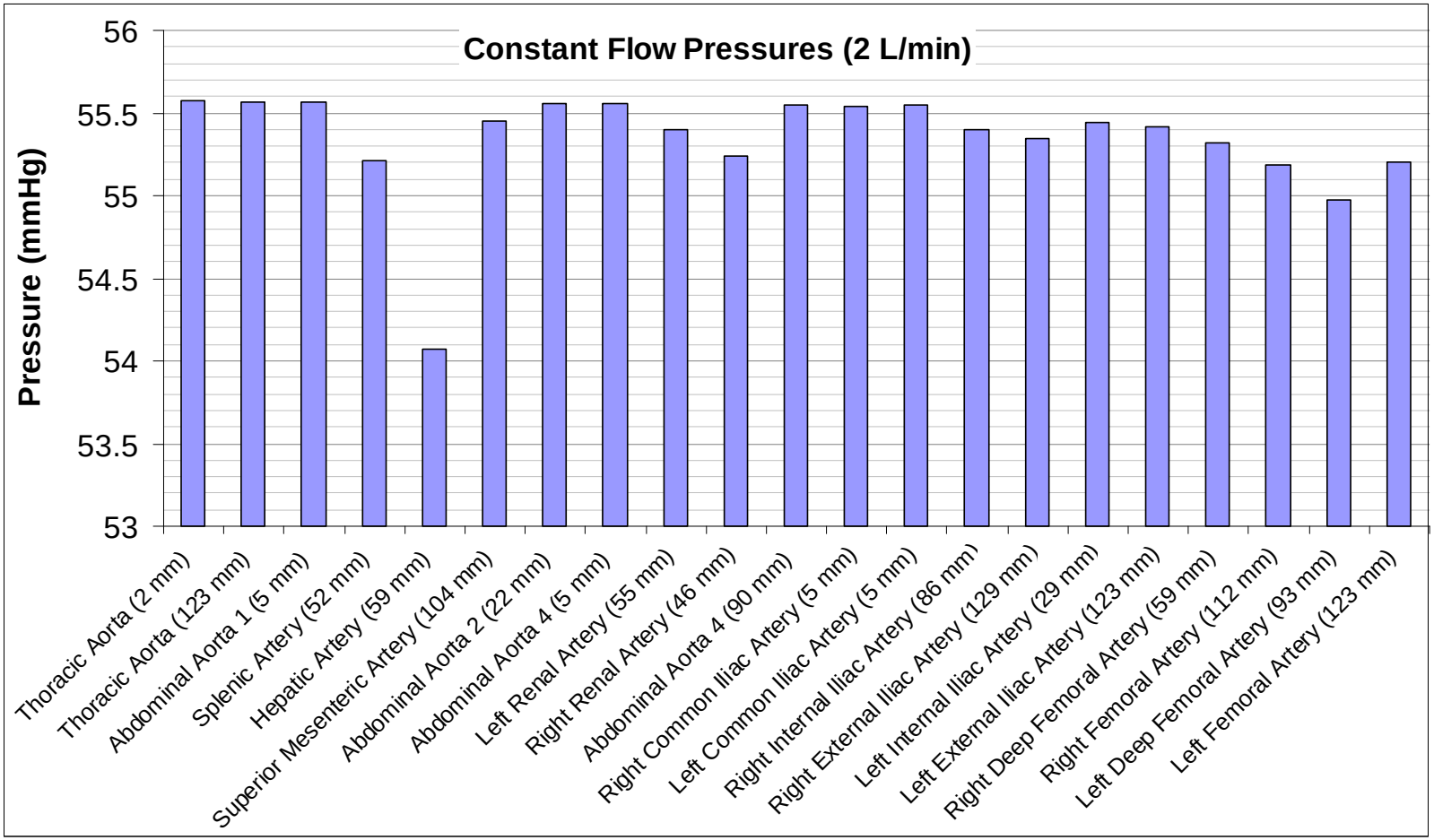

7.5 mmHg = 1 kPa

Figure 2.3.7. Haemodynamic pressures for the 'normal' model (published vessel rigidities) with a constant 2L/min flow rate boundary condition at the thoracic aorta; the figures in brackets are the distances of the recording positions from the proximal ends of the arterial sections.

Figure 2.3.8, the renal arteries take together 39% of the flow, not much less than the remaining 43% (the sum of the flow rates for the iliac arteries) that is carried by the abdominal aorta distal to the renal trifurcation.

On the one hand, the simulated transmission of pressure waves in the arterial network agrees with the transmission coefficients calculated from specified vessel characteristics and, on the other hand, the haemodynamic flow split under steady flow conditions follows what is expected from the specified resistances at the distal boundaries.

2.4 Computational Simulation Results

Elastin degradation and collagen remodelling are the processes that cause the aneurysm to grow. Infiltration of inflammatory cells into the aortic wall is thought to accelerate aneurysm growth (Sakalihasan et al 2002). Local characteristics of the infra-renal aorta such as its tortuosity can be linked to growth rate, but, as raised by MacSweeney (1999): "*Are the observed differences between individuals due to localised changes in the aneurysm wall or part of a generalised difference affecting all the arteries?*" Methodologies based on analysing patient-specific AAA such as that developed by Raghavan et al (2005) provide detailed distributions of the arterial wall pressure and shear stress, but do not explore the possible influence of clinical and geometric conditions in other parts of the arterial network. The results from the 1D arterial network simulations provide insight into the influences that vessel characteristics other than those of the abdominal aorta have on the blood flow dynamics within an AAA.

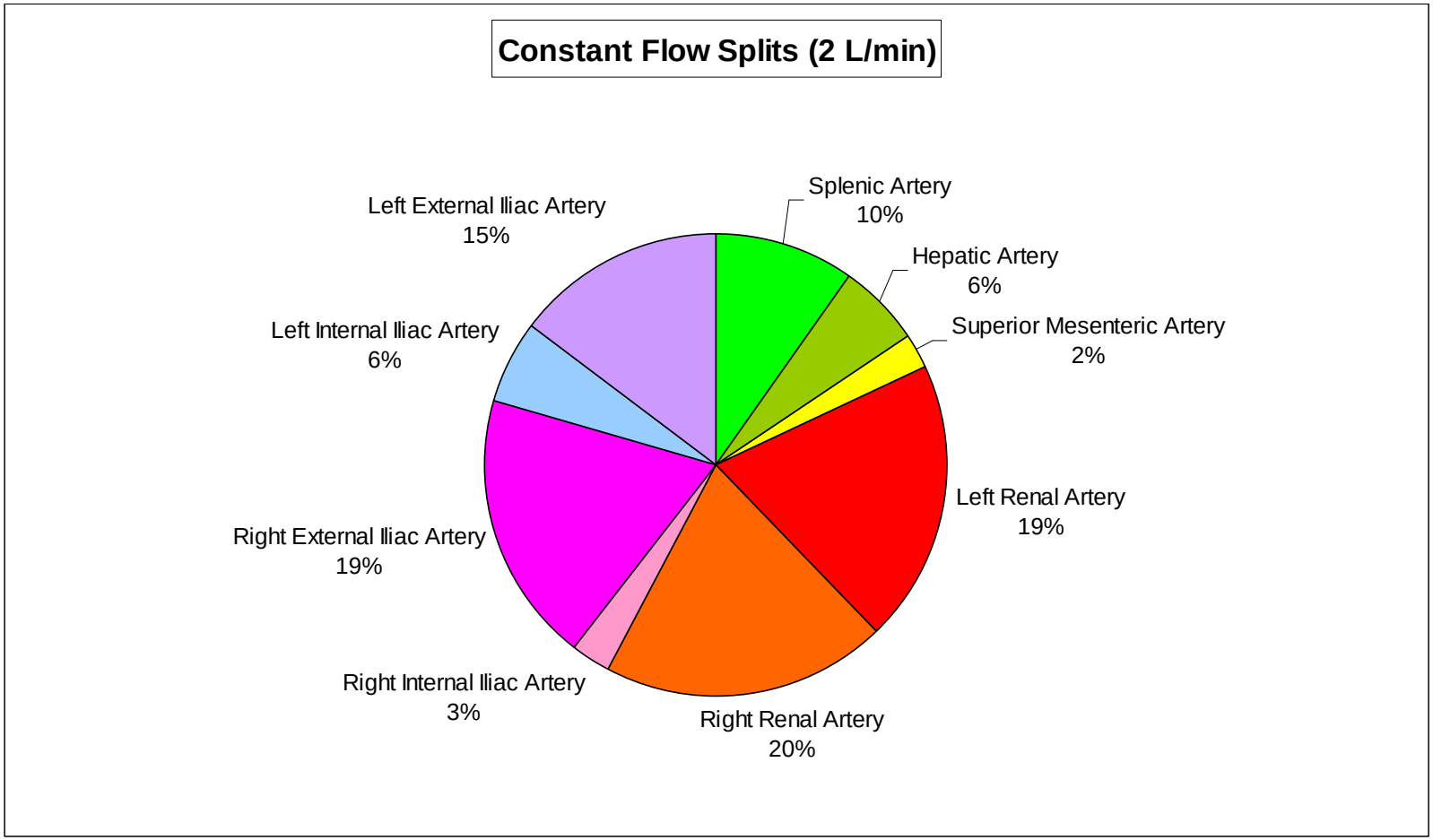

Figure 2.3.8. Flow rates as a percentage of the total flow rate of 2 L/min boundary condition at the thoracic aorta for the 'normal' model (published vessel rigidities).

A general stiffening of the arteries due to ageing reduces the step change in flow rate (from 1.09×10^{-5} m^3/s to 3.43×10^{-6} m^3/s) caused by a prescribed 100 Pa step in pressure in the thoracic aorta. Furthermore, ageing changes the increase in the rate of blood flow, relative to the blood flow rate in the thoracic aorta. The flow rate increases (relatively) more in the smaller arteries down to the infra-renal aorta (Abdominal Aorta 4 on Figure 2.4.1), including the splenic, hepatic, superior mesenteric and renal arteries. The flow rate increases (relatively) less in the infra-renal aorta, a 43% step at its proximal end (5 mm) instead of 61% in the 'normal' case. This result would suggest it requires a greater step in pressure to supply the infra-renal aorta in the older patient with the same step in flow rate as in the younger 'normal' patient. No pulsatile flow results for ageing are presented here because the program used generates the network geometry from the specified time step. This limitation of the program means that a much smaller time step needs to be specified to generate a stiffer network with a similar grid point density. At the time the 1D network simulations were carried out, the computer system used could not complete the model runs with the 5-fold increase in the number of time steps required to correctly solve the model.

Simulating the replacement of the patient's infra-renal aorta and common iliac artery by a Y-shaped aorto-iliac graft was achieved by increasing the rigidities of these vessels. Under pulsatile flow conditions, the more rigid infra-renal aorta and common iliac arteries cause a greater systolic pressure through most

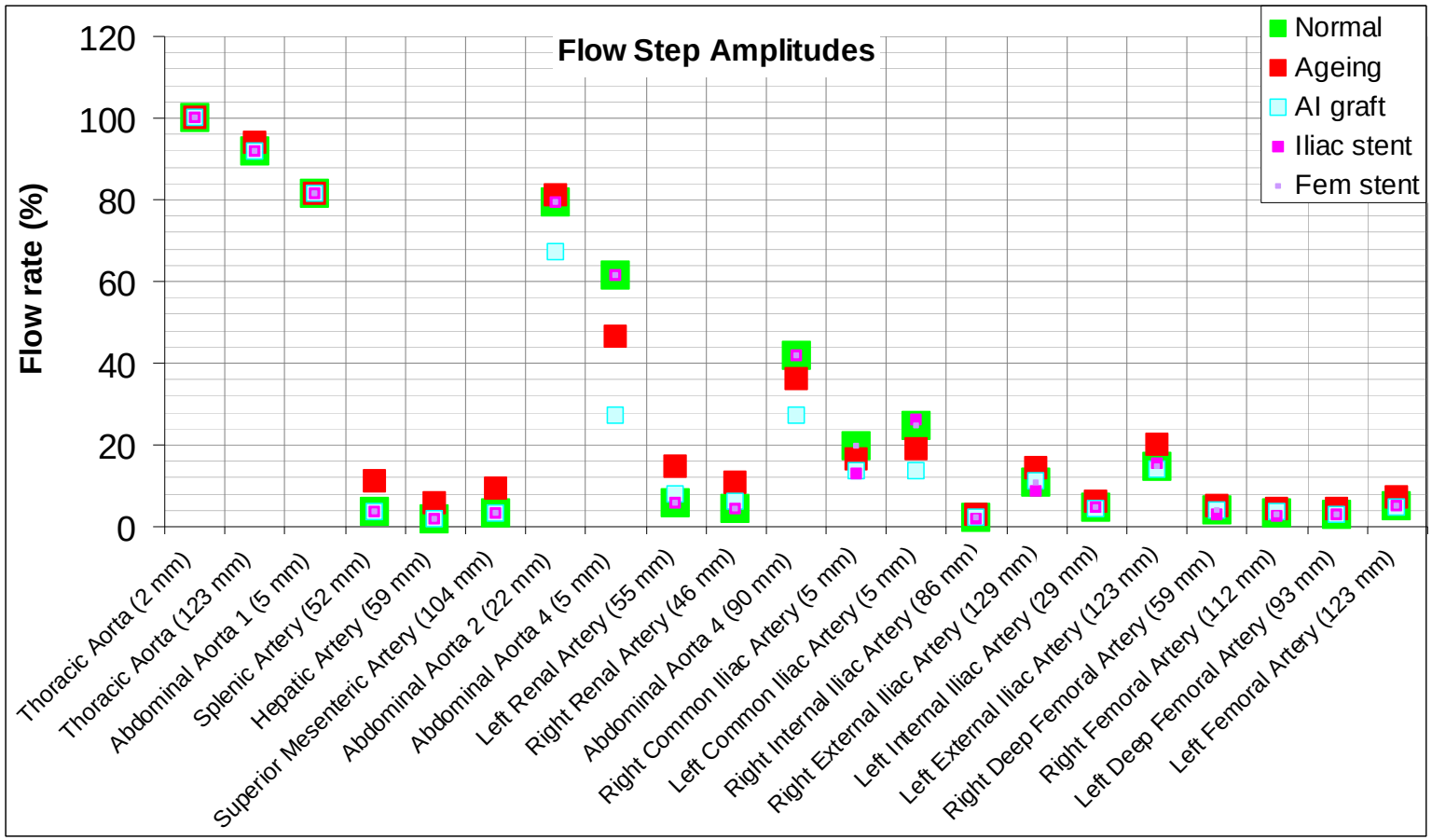

Figure 2.4.1. Amplitudes of the steps in flow rate, as a percentage of the step in flow rate of 1.09×10^{-5} m^3/s (3.43×10^{-6} m^3/s for 'ageing') at the proximal end of the thoracic aorta, as a result of a 100 Pa pressure step boundary condition at the thoracic aorta. Results of the 1D numerical simulations for the 'normal' model (published vessel rigidities), 'ageing' (hardened arteries), the models of the AI (Aorto-Iliac) graft and the iliac and fem (femoral) stents. The figures in brackets are the distances of the recording positions from the proximal ends of the arterial sections.

of the arterial network (Figure 2.4.2) and a greater systolic-diastolic pressure difference throughout the network, some 40% higher in places (Figure 2.4.3). This means that a greater systolic-diastolic pressure difference, or pulse pressure, is needed to maintain the 2 L/min (3.3×10^{-5} m^3/s) mean flow rate stipulated by the boundary condition. Even though mean flow is maintained, there are changes to the characteristics of the temporal variations in instantaneous flow rate. Compared to the 'normal' case, the peak flow rates are lower in the abdominal aorta and the distal end of the thoracic aorta (e.g. 4.2 L/min or 7×10^{-5} m^3/s instead of the 'normal' 5.4 L/min or 9×10^{-5} m^3/s at the proximal end of the infra-renal aorta) (Figure 2.4.4).

Placing a stent in the patient's right common iliac artery and right femoral artery is simulated by making a 90 mm section of these arteries more rigid. The stents cause the systolic pressure and the systolic-diastolic pressure difference to be greater in several of the arteries distal from the common iliac arteries, and a small increase in systolic-diastolic pressure difference is recorded throughout the abdominal aorta and its branches (Figure 2.4.2 and Figure 2.4.3). The stents appear to have the opposite effect to the aorto-iliac graft when it comes to flow rates. The peak flow rates are all increased in the abdominal aorta with either the more rigid common iliac artery or the more rigid femoral artery (Figure 2.4.4), up to 7.2 L/min (1.2×10^{-4} m^3/s) at the proximal end of the infra-renal aorta for the femoral stent instead of the 'normal' 5.4 L/min (9×10^{-5} m^3/s).

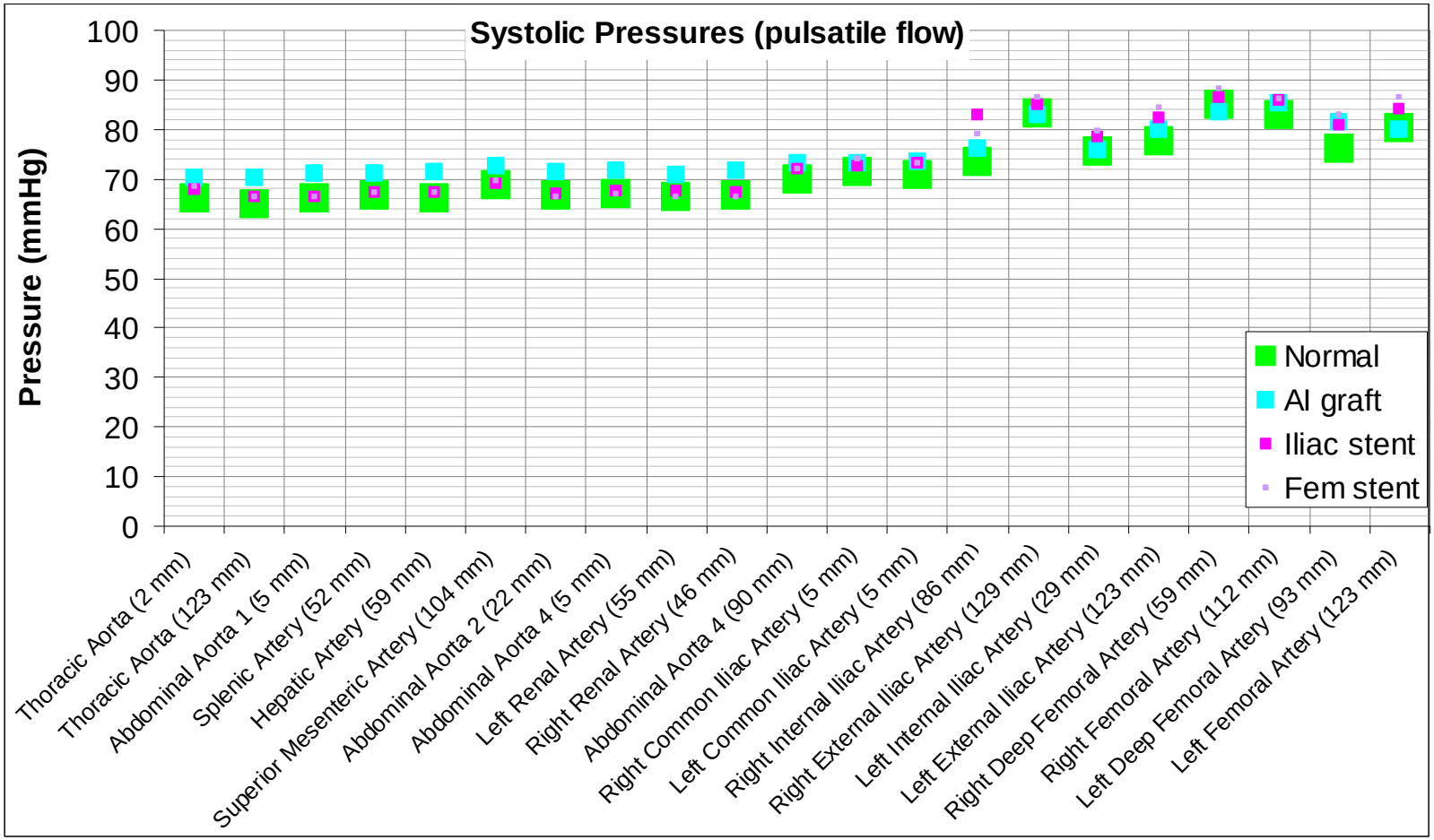

Figure 2.4.2. Systolic pressures under pulsatile flow conditions with 2 L/min mean flow rate, for the 'normal' model (published vessel rigidities) and the models of the AI (Aorto-Iliac) graft and the iliac and fem (femoral) stents. The figures in brackets are the distances of the recording positions from the proximal ends of the arterial sections.

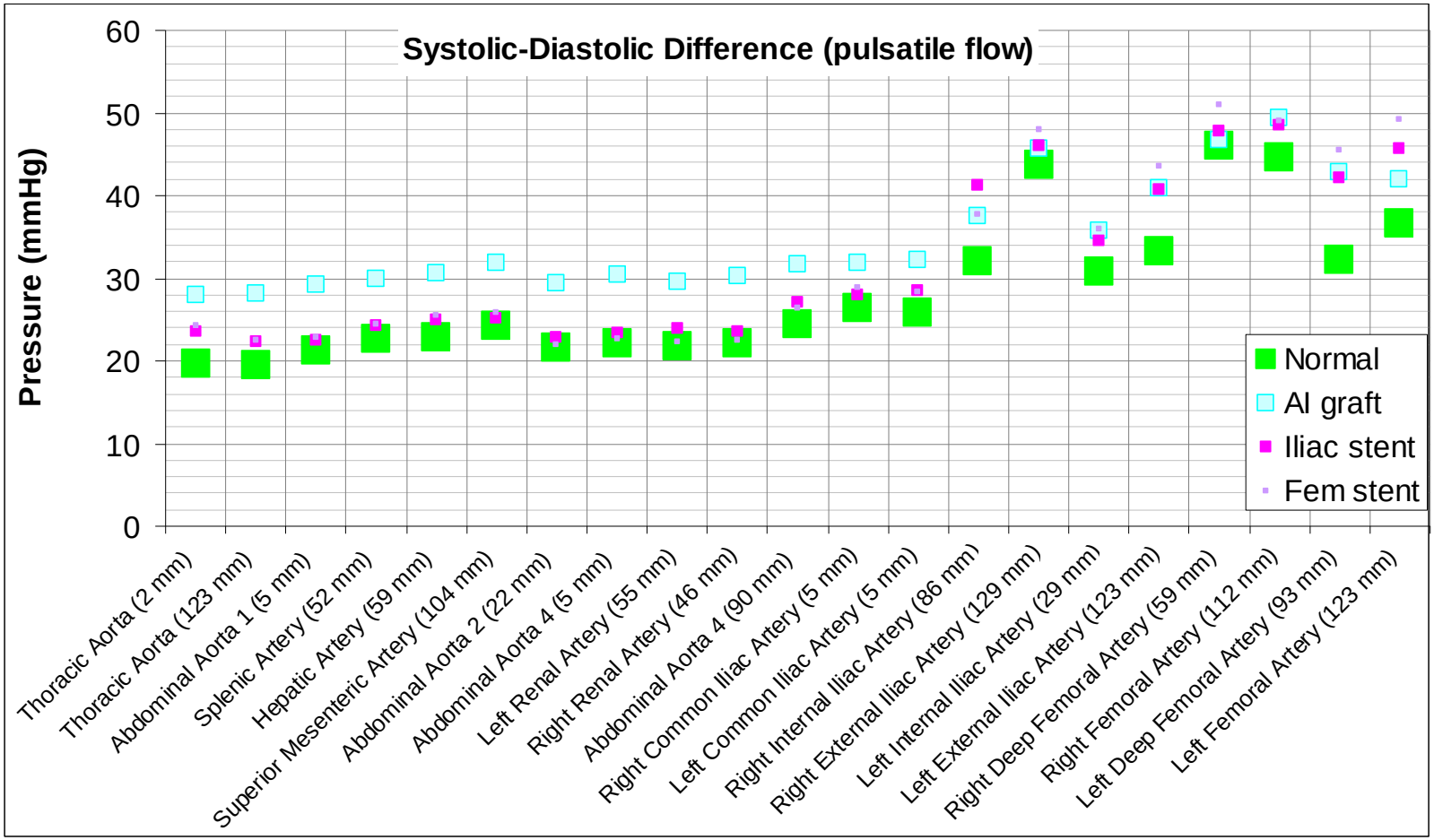

Figure 2.4.3. Systolic-diastolic pressure differences under pulsatile flow conditions with 2 L/min mean flow rate, for the 'normal' model (published vessel rigidities) and the models of the AI (Aorto-Iliac) graft and the iliac and fem (femoral) stents. The figures in brackets are the distances of the recording positions from the proximal ends of the arterial sections.

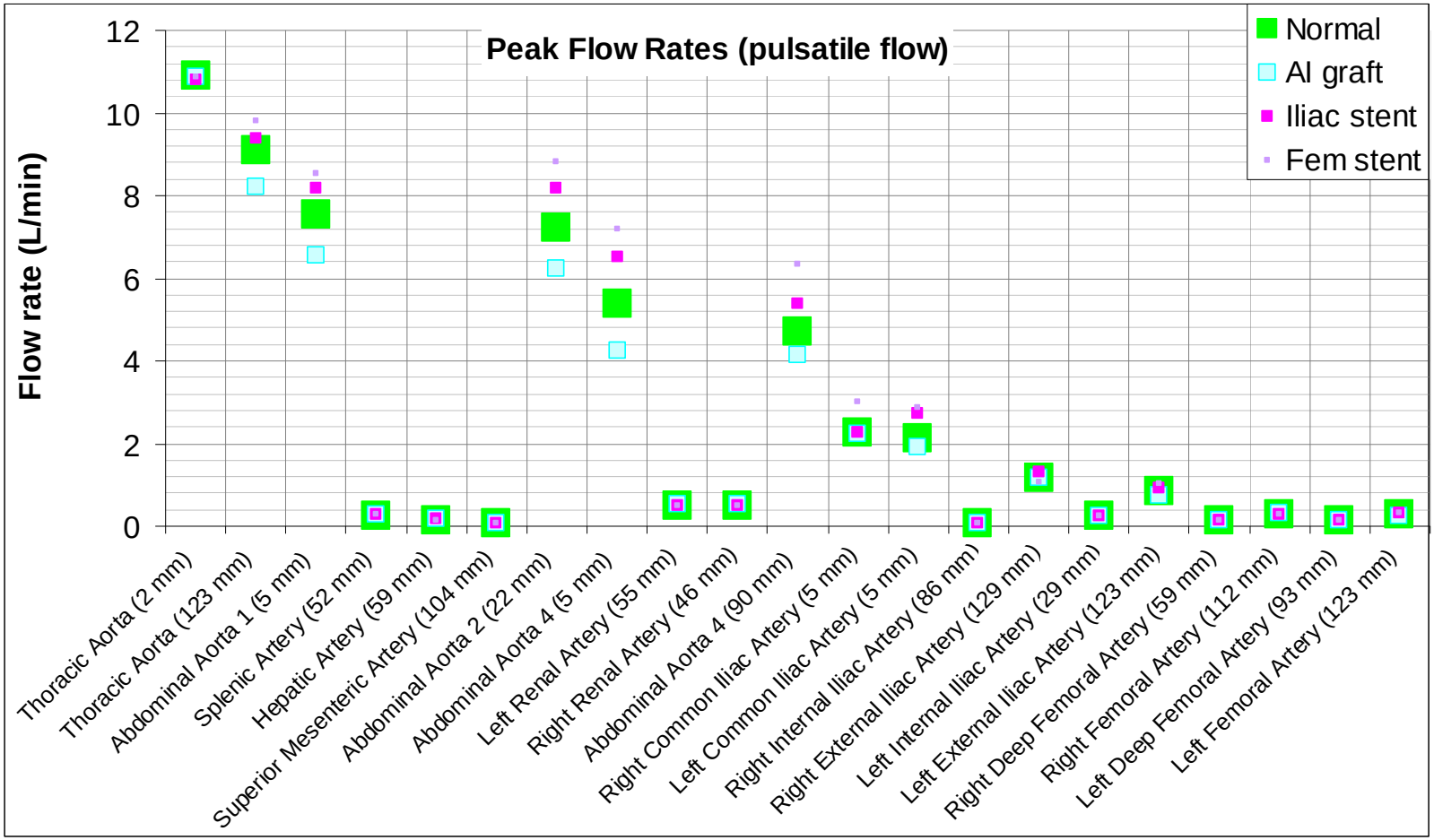

Figure 2.4.4. Peak flow rates under pulsatile flow conditions with 2 L/min mean flow rate, for the 'normal' model (published vessel rigidities) and the models of the AI (Aorto-Iliac) graft and the iliac and fem (femoral) stents. The figures in brackets are the distances of the recording positions from the proximal ends of the arterial sections.

All of the above results are based on simulations where the boundary conditions are kept the same so as to compare the haemodynamic conditions between a 'normal' model and models where arteries are more rigid. In a more complete model of the cardiovascular system it would be necessary to adjust the terminal resistance of the resistive boundaries to take into account the flow control mechanism of the arteriolar bed. The advantage of this would be to use a model that is more closely representative of flows in the cardiovascular system. The disadvantage is that it would make it more difficult to interpret the results because like-for-like comparisons would not be practicable.

This simplification is loosely analogous to the chosen use of simplified upstream boundary conditions used herein. Greatest realism is achieved with the most accurate representations of real pressure and flow histories at the upstream end of the aorta. However, the use of the various simpler boundary conditions chosen herein enhances the resulting potential to infer important underlying characteristics of the system's behaviour.

Chapter 3

Statistical Method

3.1 Methods of Statistical Investigation

Statistical study consists of first acquiring some data, then determining the relationships in the data, if any, through careful examination and application of numerical tests. The objectives of the study determine what data and tests are required; however, in medicine, obtaining data that satisfy the study objectives is often difficult, and the tests then depend on the available data.

Volunteers are required for experimental studies, where conditions are controlled and measurements regularly taken (Blanchard et al 2000). These are essential to prove the efficacy of new drugs, medical devices or procedures (Baxter et al 2002; Morosin et al 2001; Thompson and Baxter 1999). Case-control studies are normally carried out. These require considerable resources and may take several years to complete, though it is sometimes possible to carry out retrospective case-control studies (Peeters et al 2007). In contrast, observational studies do not always need volunteers and can be carried out retrospectively. One advantage with not requiring explicit consent from patients is the absence of volunteer bias. Traditional case studies such as that of Cannon et al (1963) are observational. While with prospective experimental studies the researcher controls the quality and frequency of clinical measurements, observational data obtained retrospectively is often incomplete.

Population-based studies include a specific population often limited to a region or town. For some studies the whole population is required in order to measure prevalence (Singh et al 2001) or evaluate the effect of screening (Norman et al 2004; Jamrozik et al 2000). Population-based studies also include those with a specific population limited by clinical condition, e.g. aneurysm. These have often smaller numbers of subjects and are useful for evaluating risk of a disease (Wanhainen et al 2005) or the appropriateness of a clinical procedure (Reed et al 1997). They are also used to study biological factors that appear unrelated at first, such as abdominal aortic aneurysm and bone mineral density (Jorgensen et al 2004). Martin Bland (2000) argues that "*Findings from such studies can only apply to the population from which the sample was drawn*." The study of all patients with an abdominal aortic aneurysm attending one hospital will infer conclusions the application of which to all sufferers of the condition "*depends on evidence which is not statistical and often unspecified*". It is only with the strength of a meta-analysis of similar studies that a statistical extrapolation to all patients is justifiable.

Given a population of patients at a hospital, a population-based retrospective longitudinal study is possible by examining the records of these patients. An audit of this patient information provides the material to populate a database with clinical measurements that are taken at different times of the patients' life and for various reasons. The timing of these events can be studied using the Poisson process, described by Cox and Lewis (1966). The analysis of the

magnitude of the parameters measured, with respect to other measured parameters, provides an attempt to explain causal relationships.

Statistical correlation provides a tool to measure the strength of the relationship between two parameters. Without any prior knowledge of the form of relationship between two variables, linear regression is normally used to measure that relationship, presumed linear. Chatfield (2004) suggests that "*the assumption of linearity is often made more for mathematical and computational convenience rather than because it is really believed to be true*".

The objective of such statistical studies is to reject one hypothesis in favour of another. If the initial (null) hypothesis is that risk of aneurysm rupture is dependent only on aneurysm diameter, then alternative hypotheses that could be studied could be that risk of aneurysm rupture depends on hypertension, or kidney function, or iliac artery stenosis, or cholesterol level... Hypothesis testing by linear regression is a means of determining the correlation if any between measurements, and having obtained a significance level for the regression coefficients, to keep or reject the original hypothesis.

3.2 Audit of Patient Information

The aim of this work is to find which factors are linked statistically to Abdominal Aortic Aneurysm (AAA) growth. To this end, a study has been carried out at Ninewells Hospital, Dundee, consisting of setting up a comprehensive database of clinical information for AAA patients. This has been achieved through the audit of a number of sources of information held at the

hospital. This was a population-based retrospective observational study. All AAA patients who had attended the hospital were included; only patient information that had been gathered as a result of the provision of medical care was analysed; no data were obtained prospectively from the patients and no questionnaire was used. Ethical approval was obtained for the study.

All AAA patients who had a measurement of their aneurysm size in the 6-month period from 1st March to 31st August 2005 have been included in the study. This ensured that most patients on aneurysm surveillance were included as an AAA size measurement is carried out at least once every 6 months for patients with an aneurysm size greater than 40 mm and annually for smaller aneurysms. No criterion was set for the lower limit of aneurysm size. Hence all patients recorded as having an aneurysm were included, with the smallest recorded size in the 6-month period being that of a male patient with an aortic diameter measurement of 22 mm. The inclusion of patients with very small aneurysms on the AAA surveillance programme is likely to have been due to these patients having concomitant cardiovascular risk factors. At the other end of the scale, measurements of AAA diameters up to 105 mm were recorded. These were predominantly emergency patients who present with a ruptured AAA, which included aneurysms with diameters of 105 and 100 mm in the 6-month period. Notably, the largest un-ruptured aneurysm was that of a male patient with a diameter of 97 mm, with a first recorded measurement two months earlier of 93 mm, and who survived un-ruptured for a further three

months. Figure 3.2.1 gives the distribution of AAA diameters included in the study. As the study is concerned with the natural progression of the aneurysms, patient participation ended when their aneurysm ruptured, an open or endovascular surgical intervention was carried out on their aneurysm, or in the event of death. Any clinical measurements made after any of these three events were excluded. This effectively removed from the analysis patients who presented ruptured aneurysms that had not previously been detected. Aneurysm growth is the subject of this work and it is the rate of change of aneurysm diameter that is required: at least two measurements of AAA diameter are necessary to estimate rate of change so participants with only one measurement of AAA diameter have been excluded from the analyses. 99 patients satisfied the inclusion criterion of at least one measurement of AAA size in the period 1st March to 31st August 2005, but 10 patients have been

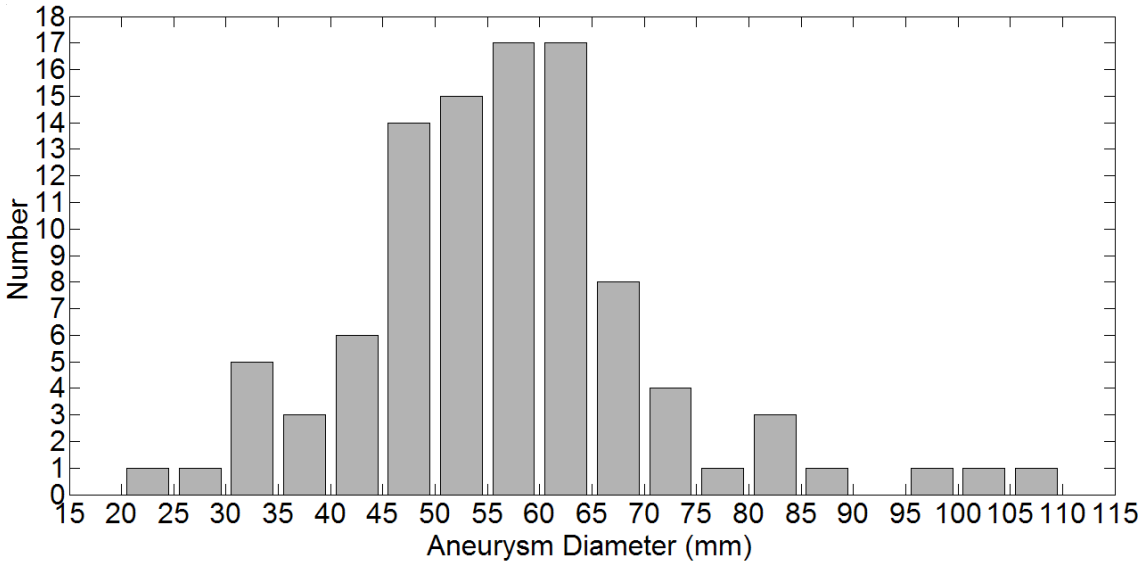

Figure 3.2.1. Distribution of abdominal aortic aneurysm diameters from the last measurement from participants of the AAA study.

excluded from the analyses because they did not have at least two measurements of aneurysm size before the end of their participation. The remaining 89 patients with AAA have been studied.

While the inclusion and exclusion criteria and the end points are clear, the onset of aneurysmal disease cannot be determined. In practice the date of the first record held by the hospital effectively defines the beginning of patient participation. Medical records are normally kept for 5 years after the last hospital attendance of the patient, after which time they are destroyed. Exceptionally, the records may be kept for longer if such is stipulated by the involvement of the patient in a clinical trial. However, patients, especially near the end of their lives, attend the hospital sufficiently frequently that the 5 year limit does not lapse until the patients' death. The first hospital attendance for one AAA patient was dated 1966 (at which time the hospital was the Dundee Royal Infirmary) and a total of 191 clinical measurement records for this patient were entered in the AAA study database, until the end of his participation in August 2005. For the 97 patients that had at least one measurement before aneurysm rupture or surgical intervention, the mean period of participation from first record was 7.8 years (Standard Deviation SD 7.3 years) with a range from 1 day to 39.0 years.

Study participants were identified by their first and last names and their Community Health Index (CHI), a 10 digit identification number which is used for health care. The CHI includes the date of birth of the patient which was also recorded in the AAA study database to provide the ages of the patients. These

personal identifiers have been anonymised by using computer generated random numbers between 1000 and 9999 to generate a unique anonymous identifier for each patient. A cross-referencing table of these 4 digit study participant numbers and the personal information of the patients is kept at the hospital. All analyses could then be carried out without risk of breach of patient confidentiality as the participant names and CHI have been removed from the data.

Information from four different sources within the hospital has been examined, namely, the Vascular Laboratory, the Clinical Radiology department, the medical records department and the laboratory for biochemical analyses.

The Vascular Laboratory manages the AAA surveillance programme. AAA patients attend the Vascular Laboratory at least every 6 or 12 months for ultrasound examination and clinical assessment. These include the measurement of the aneurysm diameter, measurements of the resting or segmental blood pressures, and a record of the patient-reported tobacco smoking status. The Ankle-Brachial Pressure Index (ABPI) is calculated from the brachial, posterior tibial and dorsalis pedis pressures and provides an indication of ischemia and the presence of arterial stenoses in the lower limbs. The Vascular Laboratory also holds a record of patients who have undergone elective and emergency aneurysm repair.

Clinical Radiology is used to obtain detailed imagery of the abdominal aorta of AAA patients. From these, aneurysm diameters are measured and reported.

Aneurysm lengths are also often reported (44 out of the 99 AAA patients), as well as the aneurysm type, fusiform or saccular (41 patients), and the presence of renal and iliac stenoses (9 patients). Whether the aneurysm extends to the iliac arteries or to the supra-renal aorta is also indicated. As well as the radiologists' reports of key aneurysm characteristics, the CT (Computed Tomography) scan images are available electronically. In this study, 47 patients had a total of 59 CT scans. These have been subsequently analysed to measure the geometric parameters describing the lumen of the AAA (c.f. thesis section 4.1). The scans have also been used to generate 3D (3-dimensional) numerical models of the AAA.

The medical records department holds a complete record of health care provided to each patient by the hospital. This includes monitoring of blood pressure, pulse rate, etc., while attending the hospital, as well as paper copies of biochemistry tests carried out, X-rays, notes of aneurysm dimensions, and concomitant clinical conditions. Normal systolic and diastolic blood pressures are reported only in the patients' medical records, and this during either a planned visit to the hospital or during an emergency attendance. Blood pressure is then often measured several times per day.

Biochemistry analyses are provides by a hospital laboratory service. In particular, patients attending the hospital either for an emergency or for elective surgery will have on average one biochemistry test carried out per day. Parameters of particular interest in relation to conditions that might affect the

circulation and aneurysm growth are levels of total cholesterol, HDL (High Density Lipoprotein) cholesterol, urea and creatinine.

Descriptive statistics of the clinical measurements obtained are listed in Table 3.2.1. A total of 3995 measurements have been analysed, consisting of an average of 40 measurements per patient (SD 31), most of which were measurements of multiple factors, such as systolic and diastolic pressures and pulse rate taken at the same time. This is essential to derive secondary information including the systolic-diastolic pressure differences, the total to HDL cholesterol ratios and the ABPI. There are 1471 measurements of urea levels, urea being an indicator of renal function and typically taken daily over the course of an AAA patient's stay in hospital. There are only two mean pressure measurements, so this parameter is not included in the statistical analyses.

The descriptive statistics highlight the difficulties associated with clinical measurements. The largest aneurysm diameter measured is 135 mm. This is a measurement taken from left to right as opposed to the standard AP (Anterior-Posterior) measurements (front to back). Aneurysms, and blood vessels in general, are not necessarily cylindrical, but have elliptical cross-sections with major and minor diameters. Anatomically, because of the hard back-bone behind the aorta, the AP diameter will often be the smallest but is the most accurate to measure by ultrasound. The highest systolic blood pressure measured is 325 mmHg (43.3 kPa). This may be surprising as the scale on a

Table 3.2.1. Arithmetic means and ranges for all patients of all primary and secondary measurement data extracted from the AAA study database for analysis. Primary data consists of raw measurements as reported. Secondary data (in italics) are clinical parameters derived from the primary data. Aneurysm diameter and length are as reported by the radiographer or clinician; measurement errors and potential outliers have been removed for all other data.

	Min.	**Mean**	**SD**	**Max.**	N
Age	30.8 yr	72.2 yr	9.0 yr	90.5 yr	3995 *
N per Patient	3	40	31	191	
Follow-up Length	1 day	7.8 yr	7.3 yr	39.0 yr	99 **
Aneurysm Diameter	20 mm	48 mm	11 mm	135 mm	836
Aneurysm Length	30 mm	80 mm	27 mm	200 mm	74
Systolic Pressure	80 mmHg 10.7 kPa	139 mmHg 18.5 kPa	35 mmHg 4.7 kPa	220 mmHg 29.3 kPa	547
Diastolic Pressure	42 mmHg 5.6 kPa	80 mmHg 10.7 kPa	20 mmHg 2.7 kPa	122 mmHg 16.3 kPa	541
Mean Pressure	98 mmHg 13.1 kPa	104 mmHg 13.9 kPa	8 mmHg 1.1 kPa	110 mmHg 14.7 kPa	2
Pulse Rate	50 min^{-1} 0.83 s^{-1}	77 min^{-1} 1.28 s^{-1}	17 min^{-1} 0.28 s^{-1}	111 min^{-1} 1.85 s^{-1}	502
Systolic-Diastolic Pressure Difference	*28 mmHg* *3.7 kPa*	*59 mmHg* *7.9 kPa*	*22 mmHg* *2.9 kPa*	*106 mmHg* *14.1 kPa*	*540*
Total Cholesterol	3.2 mmol/L	5.0 mmol/L	1.1 mmol/L	7.8 mmol/L	426
HDL Cholesterol	0.7 mmol/L	1.3 mmol/L	0.4 mmol/L	2.3 mmol/L	394
Total to HDL Cholesterol Ratio	*2.0*	*4.0*	*1.4*	*7.4*	*394*
Brachial Resting Pressure	100 mmHg 13.3 kPa	143 mmHg 19.1 kPa	24 mmHg 3.2 kPa	188 mmHg 25.1 kPa	237
Posterior Tibial Resting Pressure	52 mmHg 6.9 kPa	129 mmHg 17.2 kPa	44 mmHg 5.9 kPa	230 mmHg 30.7 kPa	235
Dorsalis Pedis Resting Pressure	58 mmHg 7.7 kPa	126 mmHg 16.8 kPa	47 mmHg 6.3 kPa	280 mmHg 37.3 kPa	234
Lower ABPI	*0.3*	*0.8*	*0.2*	*1.2*	*121*
Higher ABPI	*0.5*	*0.9*	*0.2*	*1.2*	*114*
Urea	3.0 mmol/L	7.5 mmol/L	4.0 mmol/L	17.8 mmol/L	1472
Creatinine	66 µmol/L	109 µmol/L	34 µmol/L	202 µmol/L	1467

Abbreviations: Min. *Minimum;* SD *Standard Deviation;* Max. *Maximum;* N *Number of measurements.*

* Total number of measurement times for all patients to which ages are associated.

** Total number of patients: 77 male, 20 female, 2 gender unreported.

typical sphygmomanometer ranges up to 300 mmHg (40 kPa) only, but the measurement may have been taken by an electronic pressure monitor or other device. However, it is probably an error in recording in the clinical notes and any such extreme values are not included in Table 3.2.1. The problem of haemodynamic pressures being possibly out of range of the measuring apparatus is illustrated with the maxima for the resting pressures, 300 mmHg (40.0 kPa) for both the posterior tibial and dorsalis pedis (again not listed in Table 3.2.1). In these cases the pressures represent the hardness of the artery in the lower limb, which was so rigid that it did not flex to allow a blood pressure reading. The algorithm that computes the ABPI from the resting pressures takes these into account by removing indices with values above 1.2, hence the 1.2 maxima for the ABPI. There were a total of 235 resting pressure measurements (left and right limbs), 18 of which produced ABPI greater than 1.2 and were removed. The resting pressures were supplemented with segmental pressure measurements, 18 of which produced valid ABPI, resulting in a total of 235 valid ABPI measurements. Resting and segmental pressure measurements were taken on both of the lower limbs, normally categorised as right and left, but for the purpose of this analysis the lower is named the 'lower ABPI' and the higher the 'higher ABPI'. The biochemical measurements provide indicators of concomitant diseases. Patients with total to HDL cholesterol ratios above 5 suggest hypercholesterolaemic individuals, while levels of urea and creatinine provide a measure of kidney disease. Urea and creatinine are highly correlated and can be used independently as indicators of renal function.

Much of the data are collected when the patient is under some stress, is ill or injured, in a way affecting several of the clinical parameters, for instance pulse rate with measurements up to 200 min^{-1} (3.33 s^{-1}) (not listed in Table 3.2.1), but also normal systolic and diastolic blood pressures. Some patients with renal dysfunction undergo dialysis which causes variations in urea and creatinine levels. Some adjustments to the data are possible to correct for particular patient circumstances, but each source of error is complex. For this statistical work the errors were not corrected as the corrections themselves were likely to be additional sources of error due to the complexity of each clinical case.

3.3 Data Estimate

The retrospective analysis of clinical information often involves the analysis of measurements that have been taken at different times in a patient's medical history. Typically, one parameter is not measured at the same time as another, so that if parameters change with time, these cannot be correlated with each other unless it is assumed that parameters do not change much within a certain timeframe and so may be correlated if measured within that timeframe. The statistical analysis of clinical factors that might be linked to abdominal aortic aneurysm growth, using information obtained from the patients' historical data (patients' medical records, medical imaging reports, biochemical records, records from the hospital's Vascular Laboratory, etc.) is one such database of information where measurements cannot be correlated unless an assumption is made as to the period of time over which the parameter is likely to be constant, or to have a constant-like effect on AAA growth.

Initial analyses of the data involved the use of interpolated parameters on a given date for each patient. The start of the 6 month period for patient participation, 1st March 2005, was chosen as all patients included in the study were participating at that date. Predictions were made by linear regression against time for each parameter, or log-linear for parameters with lognormal distributions, as described by Kokoska and Nevison (1989). This approach was later abandoned because it assumed that parameters changed linearly with time with constant rates of change, and in particular AAA had a constant rate of growth. Neither did it account for variations in aneurysm growth that occur over time for an individual patient.

As a consequence, it has been necessary, for the purpose of analysing the data collected for the AAA study, to develop a method of statistical analysis that may comprehensively include the patients' historical data so that, on the one hand the information may be weighted according to how correlated in time it is, and on the other hand to maximise the use of the information to strengthen the statistical significance.

The reason for developing a method to determine statistical significance from time-line data comprehensively is to have data in a form that can be examined by using regression models to determine which predictor variables might correlate with aneurysm growth. Linear regression models assume that variables follow normal distributions (Bland 2000) and transformations may be required for variables that are not normally distributed.

In particular, this is the case for aneurysm diameter. First, the shape of the distribution can be examined by plotting the histogram of diameter measurements and comparing it with different distribution functions (c.f. Figure 3.3.1). It can be seen that the lognormal distribution function provides a

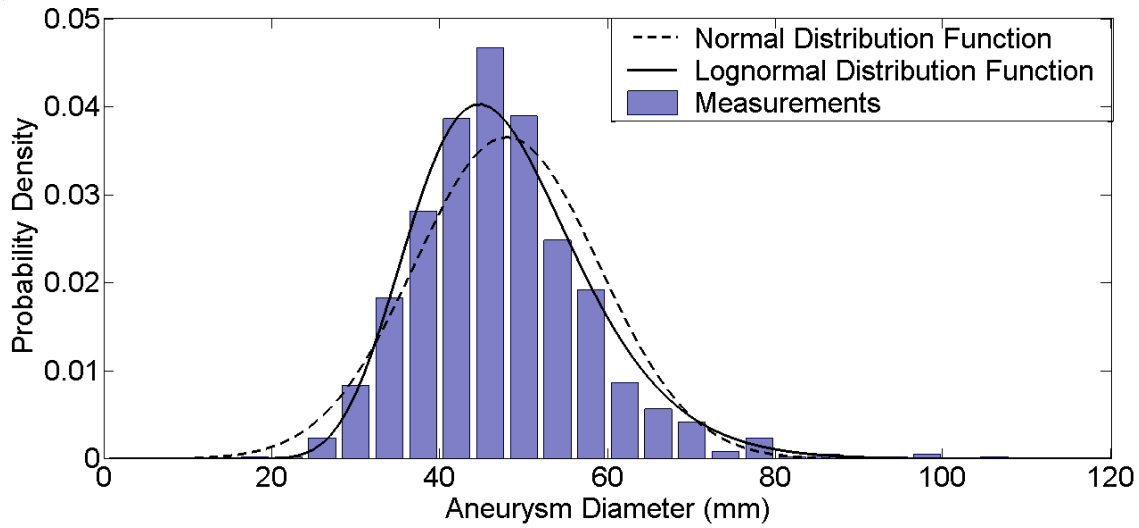

Figure 3.3.1. Normalised distribution of aneurysm diameter measurements with corresponding normal and lognormal distribution functions: the lognormal provides a better fit.

better fit than that of the normal distribution. Second, the nature of the variable provides an indication as to the distribution that is applicable. Measurements of diameter can have only positive values and their distribution will have a lower bound at 0. A distribution function with that same property such as a lognormal is likely to apply. Third, AAA growth by arterial remodelling occurs conceptually by volumetric growth or accretion as defined by Humphrey (2002). This implies that growth is proportional to the arterial circumference and hence to the aneurysm diameter. Proportionate growth is satisfied if aneurysm diameters follow a lognormal distribution, as, given a variable ξ

with a lognormal distribution, $x = \ln \xi$ is normally distributed and the derivative of x against time t is:

$$\dot{x} = \frac{d}{dt} \ln \xi = \frac{\dot{\xi}}{\xi} \qquad \text{Equ. 3.3.1}$$

$$\therefore \dot{\xi} = \xi \dot{x} \qquad \text{Equ. 3.3.2}$$

The derivative $\dot{\xi}$ of the variable with lognormal distribution, such as the rate of change of aneurysm diameter, is directly proportional to the variable ξ, the aneurysm diameter, and $\dot{x}$ is a fractional rate of change with units of inverse time. The distributions are defined by Kokoska and Nevison (1989):

Normal distribution: $$f(x) = \frac{1}{\sigma\sqrt{2\pi}} \exp\left[-\frac{(x-\mu)^2}{2\sigma^2} \right] \qquad \text{Equ. 3.3.3}$$

Lognormal distribution: $$f(\xi) = \frac{1}{\sigma\xi\sqrt{2\pi}} \exp\left[-\frac{(\ln \xi - \mu)^2}{2\sigma^2} \right] \qquad \text{Equ. 3.3.4}$$

σ and μ are the standard deviation and the mean, respectively, of the normally distributed variable x defined as $x = \ln \xi$ for the lognormal distribution. For the following derivations and analyses, the mean will always refer to the arithmetic mean as defined for a set of n measurements x_i:

$$\mu = \frac{1}{n} \sum_i x_i \qquad \text{Equ. 3.3.5}$$

For clinical parameters other than aneurysm diameter, whether a parameter is to be log-transformed is determined in the same way, by examining the

distributions of the measurements and considering the nature of the clinical measurements. Table 3.3.1 provides a list of the parameter distributions. Pressure measurements were found to be normally distributed, including the ABPI and the systolic-diastolic pressure difference. Biochemical measurements consist of concentrations which by nature cannot be negative, and examining their distributions confirmed that these tend to follow lognormal distributions. The distribution of total to HDL cholesterol ratio measurements did not warrant a log-transform, yet this parameter is the ratio of two positive cholesterol concentrations and will itself always be positive. However, in this case the data suggest a normal distribution.

Table 3.3.1. Distributions of the clinical parameters analysed with respect to aneurysm growth with their units and the units of their time-derivatives.

Parameter	Distribution	Units	Time-Derivative Units
Aneurysm Diameter	Lognormal	mm	yr^{-1}
Systolic Pressure	Normal	mmHg *or* kPa	mmHg/yr *or* kPa/yr
Diastolic Pressure	Normal	mmHg *or* kPa	mmHg/yr *or* kPa/yr
Pulse Rate	Lognormal	min^{-1} *or* s^{-1}	yr^{-1}
Systolic-Diastolic Pressure Difference	Normal	mmHg *or* kPa	mmHg/yr *or* kPa/yr
Total Cholesterol	Lognormal	mmol/L	yr^{-1}
HDL Cholesterol	Lognormal	mmol/L	yr^{-1}
Total to HDL Cholesterol Ratio	Normal	*none*	yr^{-1}
Lower ABPI	Normal	*none*	yr^{-1}
Higher ABPI	Normal	*none*	yr^{-1}
Urea	Lognormal	mmol/L	yr^{-1}
Creatinine	Lognormal	µmol/L	yr^{-1}

Being assured that as far as possible the variables are normally distributed, kernel regression smoothing (Sprent and Smeeton 2001) is a means of estimating the value the variables take at instants between measurement times.

For each measurement x_i taken at a time t_i, there is a weighting function or kernel smoother $w_i(t)$ (Hastie and Tibshirani 1990) such that the weight is greatest at the time of measurement and reduces with increasing values of $|t - t_i|$. The weighting function should also satisfy normality so that each measurement counts as one only. That is:

$$\int_{-\infty}^{+\infty} w_i(t)dt = 1 \qquad \text{Equ. 3.3.6}$$

One such weighting function, and that which is used here, is (c.f. Figure 3.3.2):

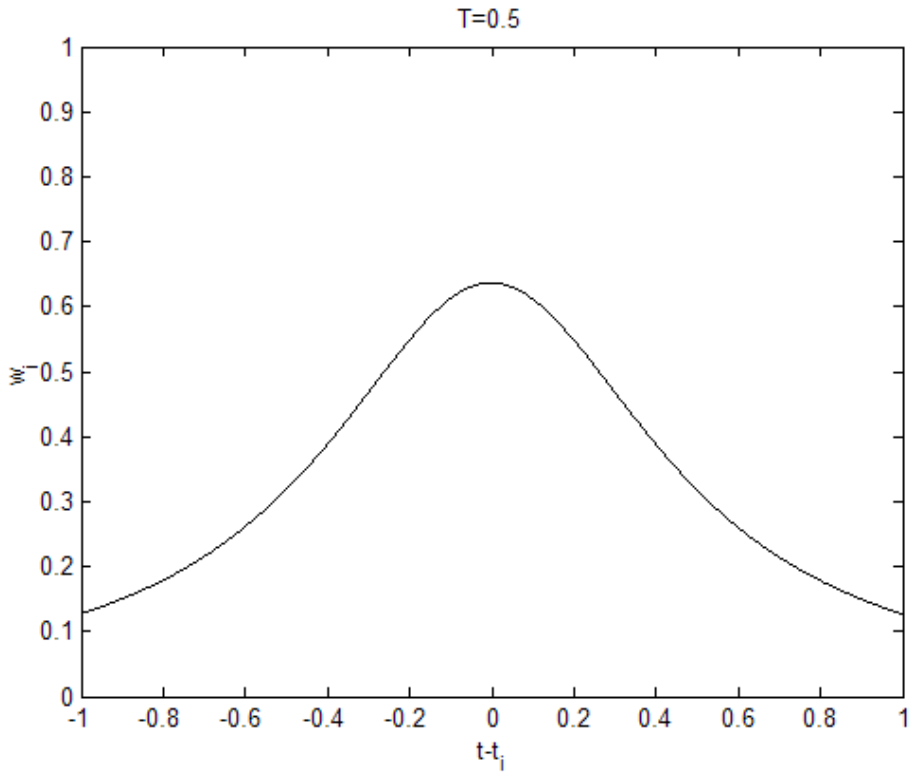

Figure 3.3.2. Weighting function $w_i(t)$ with $T = 0.5$.

$$w_i(t) = \frac{T}{\pi\left((t - t_i)^2 + T^2\right)} \qquad \text{Equ. 3.3.7}$$

T is a constant and the half-period of time over which an individual measurement is thought to be valid and applicable. For this function, the weight at a time T before or after t_i is half the maximum weight at t_i:

$$w_i(t_i \pm T) = \frac{w_i(t_i)}{2} \qquad \text{Equ. 3.3.8}$$

This form of the weighting function is somewhat empirical, but satisfies the assumption that a clinical measurement is not only valid at the time of measurement but also for a period of time before and after, and its significance drops the greater the time difference $|t - t_i|$.

The value of parameters at times between measurements can be estimated by the weighted average of the measurements x_i using the individual weighting functions $w_i(t)$:

$$x(t) = \frac{\sum_i w_i x_i}{\sum_i w_i} \qquad \text{Equ. 3.3.9}$$

This means that at a time t, the best estimate of x is the weighted mean of the measurements, weighted in function of how distant in time each measurement is. This weighted average has the property that if all the measurements are taken at the same time, then the estimate is the arithmetic mean of the n measurements:

$$x(t)=\frac{\sum_i w_i x_i}{\sum_i w_i}=\frac{w_i\sum_i x_i}{nw_i}=\frac{\sum_i x_i}{n} \qquad t_i=t_1\forall i \qquad \text{Equ. 3.3.10}$$

It is necessary to evaluate a weight associated with the parameter estimate $x(t)$, as at times close to one or several measurements the estimate is significant, while at other times away from any measurement the estimate is more unreliable. For this, each individual weighting function is first separated into different components corresponding to each interaction between measurements, then each component is further split into an independent part and an interacting part according to an interaction factor $w_{ii'}$ (Figure 3.3.3):

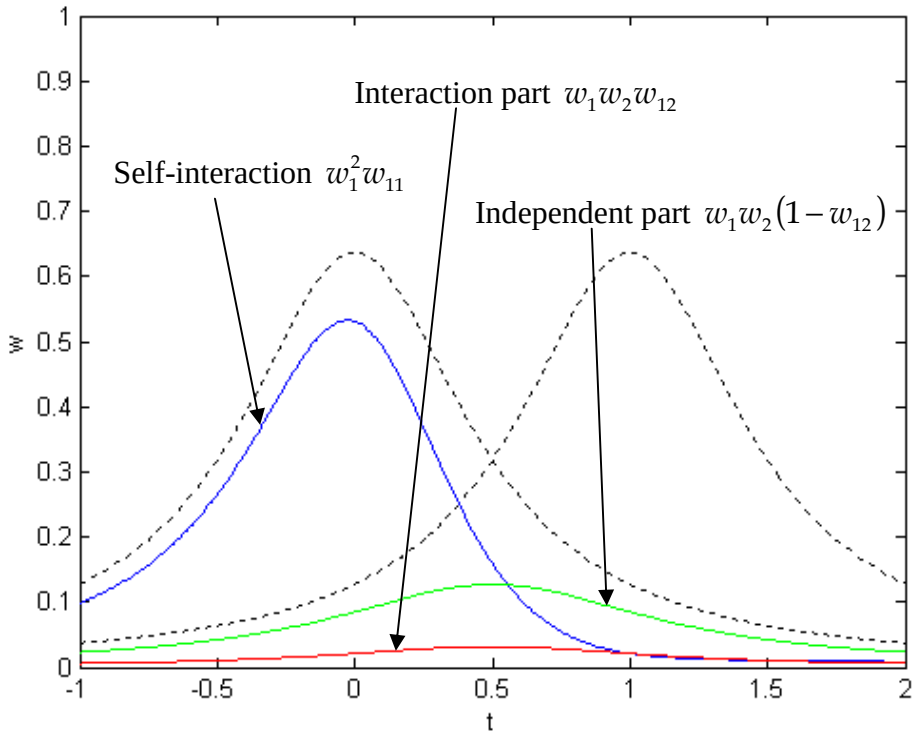

Figure 3.3.3. Independent (green), interacting (red) and self-interacting (blue) parts of the weighting function $w_1(t)$ of a measurement taken at time $t_1=0$ interacting with a measurement taken at time $t_2=1$ with $T=0.5$; individual weighting functions $w_1(t)$ and $w_2(t)$ are shown with dashed lines.

$$w_i = \frac{\sum_{i'} w_i w_{i'}}{\sum_{i'} w_{i'}} = \underbrace{\frac{\sum_{i'} w_i w_{i'}(1 - w_{ii'})}{\sum_{i'} w_{i'}}}_{\text{independent}} + \underbrace{\frac{\sum_{i'} w_i w_{i'} w_{ii'}}{\sum_{i'} w_{i'}}}_{\text{interacting}} \qquad \text{Equ. 3.3.11}$$

Two measurements will interact if they were taken close in time, and as a consequence, the product of their individual weighting functions will be greater. Their product will remain small if the measurements are not close in time and either parts (independent and interacting) remain small at all times. The interaction factor $w_{ii'}$ is not a function of time and takes values between 0, no interaction, and 1, complete interaction ($w_{ii'} \in]0;1]$). It is here given the same form as the weighting function $w_i(t)$, with the same limitations and assumptions, as there is no evidence with which to base a more complex choice, the exact shape of the kernel smoother being in this case unimportant:

$$w_{ii'} = \frac{T^2}{(t_i - t_{i'})^2 + T^2} \qquad \text{Equ. 3.3.12}$$

Having separated each interaction between measurements into independent and interacting parts, a weighting function $w(t)$ for the estimate (c.f. Figure 3.3.4 for two measurements) can be expressed as the sum of the independent parts added to the weighted average of the interacting parts:

$$w(t) = \frac{\sum_i \sum_{i'} w_i w_{i'}(1 - w_{ii'})}{\sum_i w_i} + \frac{\sum_i \sum_{i'} w_i^2 w_{i'} w_{ii'}}{\left(\sum_i w_i\right)^2} \qquad \text{Equ. 3.3.13}$$

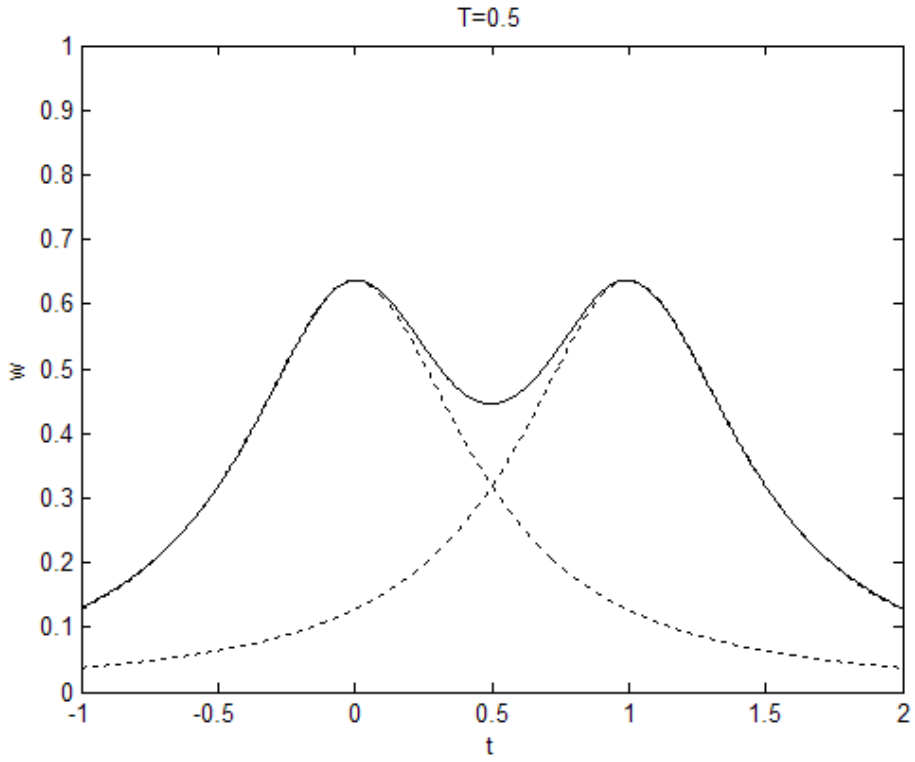

Figure 3.3.4. Weighting function $w(t)$ (solid line) for the parameter estimate from two measurements taken at times $t_1 = 0$ and $t_2 = 1$ with $T = 0.5$; individual weighting functions $w_1(t)$ and $w_2(t)$ are shown with dashed lines.

Note that when considering the interaction of a measurement with itself ($i = i'$), the interaction factor is $w_{ii} = 1$, so that it has no independent part and is fully interacting with itself. Also, if all the measurements were taken at the same time, then the weighting function of the estimate would reduce to:

$$w(t) = \frac{\sum_i \sum_{i'} w_i^2 w_{i'}}{\left(\sum_i w_i\right)^2} = \frac{n^2 w_i^3}{n^2 w_i^2} = w_i \qquad t_i = t_1 \forall i \qquad \text{Equ. 3.3.14}$$

The integral of $w(t)$ over all t represents the equivalent number of independent measurements, and it can be shown that:

$$1 \leq \int_{-\infty}^{+\infty} w(t)dt < n \qquad \text{Equ. 3.3.15}$$

If a parameter is known to have a constant rate of change a, then the best estimate of that rate of change would be the coefficient obtained from the linear regression (Barford 1985; Sprent 1969) of the parameter measurements against time. This would consist of fitting a line of equation $x = at + b$ where a and b are the coefficients of regression (Kokoska and Nevison 1989). In general, it cannot be assumed that clinical parameters change at a constant rate. Several of the parameters studied do not change linearly with time, such as blood pressure and pulse rate. There may also be sudden changes in some parameters, for example ABPI that could change because of injury, or a sudden increase in urea level due to kidney dysfunction. It is possible to estimate locally the rate of change at any time t by carrying out weighted linear regressions of the measurement points, where those measurements closer to t take more importance and those further less. The same individual weighting functions $w_i(t)$ as those for the parameter estimate (Equation 3.3.7) are used here. A weighted linear regression consists of minimising the residuals $\varepsilon_i = x_i - at_i - b$ where $a(t)$ is the rate of change and differential (locally estimated) of the parameter:

$$\begin{cases} \dfrac{\partial}{\partial a}\sum_i w_i \varepsilon_i^2 = 0 \\ \dfrac{\partial}{\partial b}\sum_i w_i \varepsilon_i^2 = 0 \end{cases} \qquad \text{Equ. 3.3.16a}$$

$$\begin{pmatrix} \sum_i w_i t_i^2 & \sum_i w_i t_i \\ \sum_i w_i t_i & \sum_i w_i \end{pmatrix} \begin{pmatrix} a \\ b \end{pmatrix} = \begin{pmatrix} \sum_i w_i x_i t_i \\ \sum_i w_i x_i \end{pmatrix} \qquad \text{Equ. 3.3.16b}$$

$$\therefore a(t) = \frac{\sum_i w_i x_i t_i \sum_i w_i - \sum_i w_i x_i \sum_i w_i t_i}{\sum_i w_i t_i^2 \sum_i w_i - \left(\sum_i w_i t_i \right)^2} \qquad \text{Equ. 3.3.17}$$

The differential estimate $a(t)$ obtained is not constant with t as it is a function of the individual weighting functions $w_i(t)$ which are themselves functions of time t. It is the best estimate for the rate of change at each particular moment in time given the relative importance of the measurements.

As with the parameter estimate $x(t)$, it is necessary to evaluate a weight associated with the differential estimate $a(t)$. To estimate the differential, the measurements need to be independent while taken sufficiently close in time to interact. On the one hand, if two measurements are taken at an interval much greater than T, then the rate of change estimated will be averaging out any changes in $a(t)$ that might have occurred; on the other hand, if two measurements are taken at an interval much smaller than T, then the estimated differential will be unreliable (the estimate being dominated by the division by a small time interval). The sum of the independent parts of the interaction components of the individual weighting functions provides a suitable expression for the weighting function $w'(t)$ to be associated with the differential estimate $a(t)$ (Figure 3.3.5):

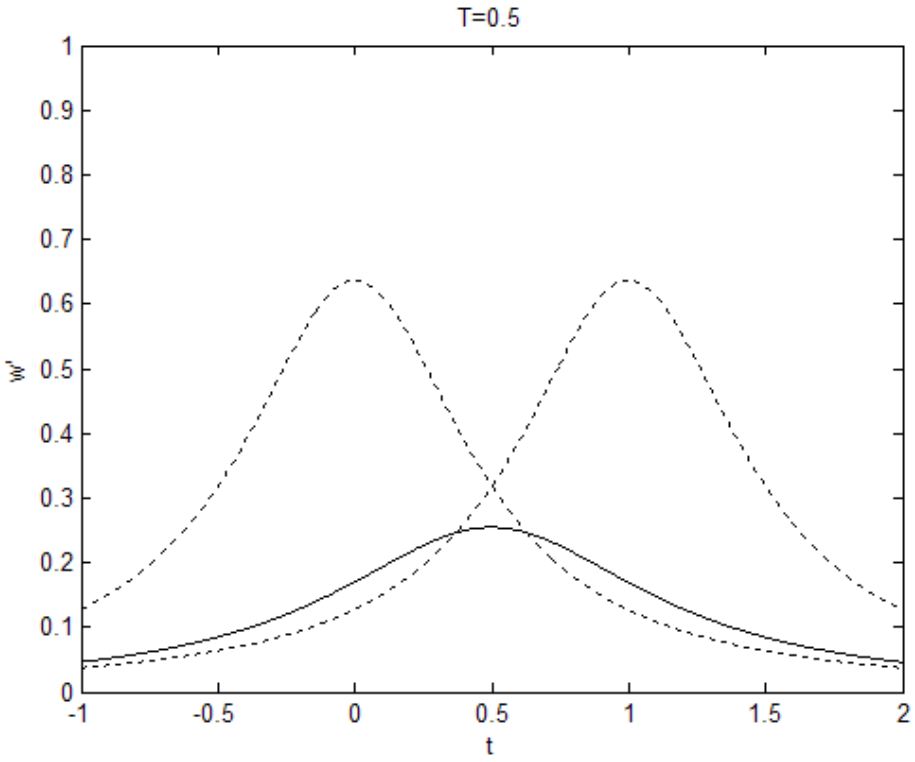

Figure 3.3.5. Weighting function $w'(t)$ (solid line) for the differential estimate from two measurements taken at times $t_1 = 0$ and $t_2 = 1$ with $T = 0.5$; individual weighting functions $w_1(t)$ and $w_2(t)$ are shown with dashed lines.

$$w'(t) = \frac{\sum_i \sum_{i'} w_i w_{i'} (1 - w_{ii'})}{\sum_i w_i} \qquad \text{Equ. 3.3.18}$$

If all the measurements were taken at the same time, $w_{ii'} = 1 \forall (i; i')$ and so $w'(t) = 0$: no differential can be estimated. The integral of $w'(t)$ over all t represents the equivalent number of independent estimates of the differential. $w'(t)$ is smaller than $w(t)$ which reflects the degrees of freedom used in the weighted linear regression used to obtain $a(t)$:

$$0 \le \int_{-\infty}^{+\infty} w'(t)dt < \int_{-\infty}^{+\infty} w(t)dt \qquad \text{Equ. 3.3.19}$$

Matlab version 6.1.0.450 release 12.1 (Mathworks Inc., Natick) was used to compute all parameter and differential estimates with their associated weighting functions for all patients (c.f. population.m and its associated function rddat.m, and wfunc.m in the Appendix).

In a controlled experiment, the various parameters being studied would be measured or set under specific conditions. With each set of measurements being independent, the relationship between parameters can be studied using linear regressions. A regression for discrete measurements results in obtaining the coefficients β_k by solving:

$$\frac{\partial}{\partial \beta_k} \sum_i \varepsilon_i^2 = 0 \forall k \qquad \text{Equ. 3.3.20}$$

Regressions consist in minimising the sum of squared residuals ε_i^2, so by extension, given continuous parametric expressions rather than discrete measurements, it is possible to obtain coefficients of regressions by solving:

$$\frac{\partial}{\partial \beta_k} \int_{-\infty}^{+\infty} \varepsilon^2(t) dt = 0 \forall k \qquad \text{Equ. 3.3.21}$$

Furthermore, given a number of sets of continuous parametric expressions, the coefficients result from solving:

$$\frac{\partial}{\partial \beta_k} \sum_j \int_{-\infty}^{+\infty} \varepsilon_j^2(t) dt = 0 \forall k \qquad \text{Equ. 3.3.22}$$

The summation and integral essentially serve the same adding function, the summation being of discrete values, the integral being of continuous values.

They are commutative. In the case of estimates from measurements of different clinical parameters against time, a set of continuous parametric expressions is the set of clinical parameter estimates for each patient j. (The index j is used to denote a patient or set of measurements and it is different from the index i that denotes individual measurements.) Also, the clinical parameter estimates have weight functions associated with them, so that, given sets of weighted continuous parametric expressions, a complete weighted linear regression consists in solving:

$$\frac{\partial}{\partial \beta_k} \sum_j \int_{-\infty}^{+\infty} W_j(t) \varepsilon_j^2(t) dt = 0 \forall k \qquad \text{Equ. 3.3.23}$$

Given a parameter $y_j(t)$ being regressed against m parameters $x_{jk}(t)$, the combined weight $W_j(t)$ of the estimates is given by the weight function $v_j(t)$ for parameter $y_j(t)$ and the weight functions $w_{jk}(t)$ for the parameters $x_{jk}(t)$:

$$W_j(t) = (m+1)\left[\frac{1}{v_j(t)} + \sum_k \frac{1}{w_{jk}(t)}\right]^{-1} \qquad \text{Equ. 3.3.24}$$

This ensures that the regression is essentially that of parameters strongly correlated in time. Also, if $w_{jk} = v_j \forall k \neq 0$, then $W_j = v_j = w_{jk;k\neq 0}$. For the purpose of the regression equations, where $k = 0$, $x_{j0} \equiv 1$ and $w_{j0} \equiv 1$ (by definition x_{j0} is not a parameter).

For example, Figure 3.3.6 illustrates for a particular AAA patient the estimates and associated weight functions from 11 measurements of aneurysm diameter and 20 measurements of systolic and diastolic pressures. The first diameter measurement was carried out at 52 years of age, the last at about 57. The best fit line using the kernel function $w_i(t)$ suggests an increase in AAA size from 40 mm to 55 mm, confirmed by the estimated rate of growth of 1 mm/yr increasing to 6 mm/yr. Blood pressure measurements were available from 31 to 53 years, ranging from 100 mmHg (13 kPa) to 150 mmHg (20 kPa) for systolic pressure, 70 mmHg (9 kPa) to 90 mmHg (12 kPa) for diastolic pressure. The associated weight functions $w_{jk}(t)$ show the low significance of the estimates between measurements separated by long periods (e.g. the absence of recorded pressure measurements between the ages of 36 and 43). Integrating the weight functions (Equation 3.3.15 and Equation 3.3.19) provides the figures of 6.2 equivalent independent measurements for aneurysm diameter, 4.8 for its rate of change and 9.9 for blood pressure. Combining these using Equation 3.3.24 results in 3.8 equivalent independent measurements, essentially available between 50 and 55 years when both pressure and aneurysm diameter measurements were being taken.

In the regressions carried out for this thesis, a more conservative calculation of the combined weight has been used by reducing $W_j(t)$ by a factor of $\sqrt{m+1}$. This is because when considering the combined weight as a function of independent orthogonal time parameters (in a space with $m+1$ dimensions),

Figure 3.3.6. Aneurysm diameter and pressure measurements with associated estimates and weight functions for a particular AAA study patient: (a) Aneurysm diameter and rate of growth measured and estimated; (b) systolic and diastolic pressures measured and estimated; (c) weights $w_{jk}(t)$ associated to the estimates of aneurysm diameter, rate of growth and blood pressures, and combined weight $W_j(t)$ for the three parameters.

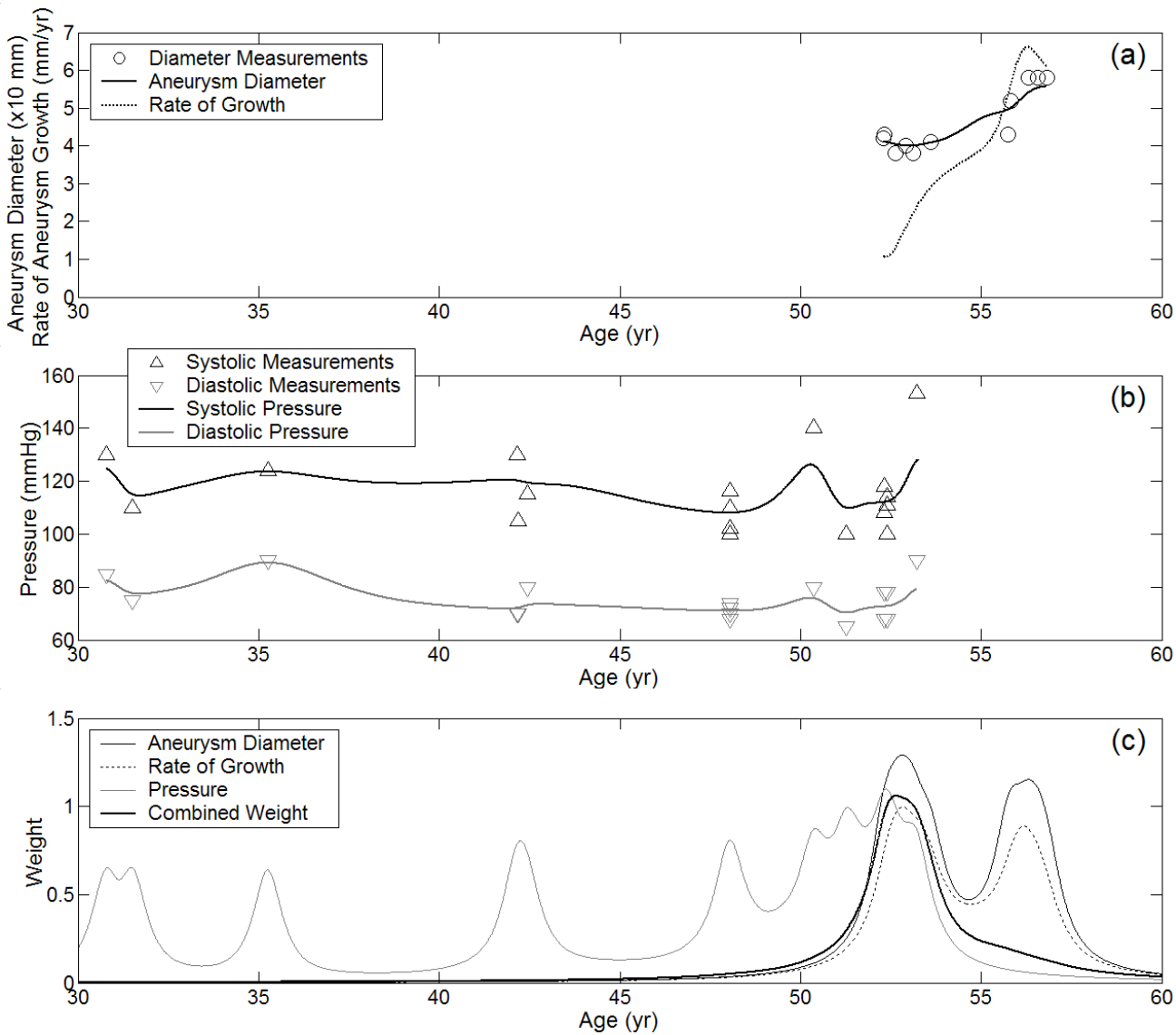

the weight when keeping all but one of the time parameters constant is inflated. To avoid this problem the combined weight is divided by the square-root of the number of dimensions, as required when collapsing a multidimensional space onto its diagonal.

To regress a parameter $y_i(t)$ against parameters $x_{jk}(t)$, the residuals are:

$$\varepsilon_j(t) = y_j - \sum_k \beta_k x_{jk} \qquad \text{Equ. 3.3.25}$$

The regression thus consists in solving the following:

$$\sum_{k'}\left(\beta_{k'} \sum_j \int_{-\infty}^{+\infty} W_j(t) x_{jk}(t) x_{jk'}(t) dt \right) = \sum_j \int_{-\infty}^{+\infty} W_j(t) x_{jk}(t) y_j(t) dt \forall k \Leftrightarrow \mathbf{X}\boldsymbol{\beta} = \mathbf{Y}$$

Equ. 3.3.26

The elements of matrix $\mathbf{X}$ are: $\sum_j \int_{-\infty}^{+\infty} W_j(t) x_{jk}(t) x_{jk'}(t) dt$ Equ. 3.3.27a

The elements of matrix $\mathbf{Y}$ are: $\sum_j \int_{-\infty}^{+\infty} W_j(t) x_{jk}(t) y_j(t) dt$ Equ. 3.3.27b

The coefficients of regression β_k are the elements of matrix $\boldsymbol{\beta}$. The total number of degrees of freedom $q-1$ available for the regression is provided by the sum of the combined weights, and the first element ($k = k' = 0$) of $\mathbf{X}$:

$$q = \sum_j \int_{-\infty}^{+\infty} W_j(t) dt \qquad \text{Equ. 3.3.28}$$

Given m degrees of freedom used by the regression, there remain $q-m-1$ residual degrees of freedom due to error. Similar implications can be derived

when calculating the sum of squares, etc., used in determining confidence intervals and probabilities of errors (Kokoska and Nevison 1989) when regressing sets of weighted continuous parameter estimates. The code in Matlab for this weighted regression method can be found as cwreg.m in the Appendix.

3.4 Multiple Linear Regression

Multiple linear regression techniques provide a means of evaluating key statistics concerning possible relationships between aneurysm growth and measured parameters. The aim of this section is to test the hypothesis that aneurysm growth is independent of the measured parameters, and, by rejecting this hypothesis, to argue that there is a link between growth and some clinical parameters.

The ratio of the sum of squares due to regression S_R and the total sum of squares S_T is the coefficient of determination $R^2 = S_R/S_T$ (equivalent to the correlation coefficient squared, but applicable to multiple regressions). R^2 provides a measure of the proportion of the data scatter accounted for by the regression, so that a coefficient of determination $R^2 = 0.10$ means that the regression accounts for 10% of the variability in scatter.

Solving Equation 3.3.26 results in coefficients of regression β_k which are statistics describing how aneurysm growth is related to the clinical parameters. The sign of β_k determines whether growth is increased or reduced.

For β_k to be significant it is necessary for its magnitude to be greater than $t\sigma\sqrt{c_{kk}}$ (Kokoska and Nevison 1989). t is Student's t-statistic dependent on the remaining degrees of freedom $q-m-1$ and the significance level p of the test. σ is the standard deviation of the residuals. c_{kk} are the diagonal elements of the matrix $(\mathbf{X}'\mathbf{X})^{-1}$. To have a 95% confidence ($p \le 0.05$) in the significance of a coefficient β_k, the t-statistic takes on the values $t = 12.71$ if there is only 1 remaining degree of freedom, $t = 2.23$ if 10 remaining degrees of freedom, and $\lim_{q\to\infty} t = 1.96$ for large numbers of degrees of freedom (typically $q-m > 150$). Hence, for few degrees of freedom, the magnitude of the β_k regression coefficient needs to be very large for it to be significant. Conversely, a t-statistic can be calculated from a coefficient β_k given σ and c_{kk}:

$$t = \frac{|\beta_k|}{\sigma\sqrt{c_{kk}}} \qquad \text{Equ. 3.4.1}$$

The p-value is the probability that the coefficient β_k is not significant. p is computed from the t-distribution function $f(x)$ and the t-statistic obtained from Equation 3.4.1:

$$p = \int_t^{+\infty} f(x)dx \qquad \text{Equ. 3.4.2}$$

While the p-value is the probability of wrongly rejecting the null hypothesis $h_0 : \beta_k = 0$, critical values of p are required as thresholds to determine the significance of regression coefficients. In particular different critical values of p

are necessary as criteria for stepwise selection methods of parameters. These thresholds need to be acceptable to the study to which they are applied (Bland 2000).

It is important to report the number of patients and measurements included in regression analyses. Even if significant with a low p-value, a coefficient β_k may be valid only under specific conditions. If it is computed from a small subset of measurements, the selection of the measurements may be biased. For example, analyses including both blood pressure and cholesterol level measurements may be biased towards conditions at the times when these measurements are coincident. In the case of the AAA study, approximately 180 cholesterol level and 160 blood pressure equivalent number of measurements (i.e. number of measurements after kernel smoothing using the weighting function described in thesis section 3.2) were available, less than half (≈70) of which were coincident. The number n of patients included in the analysis provides an assessment of the scope. The number q of equivalent measurements included is a measure of the degrees of freedom $q-1$ available to the regression. The degrees of freedom m used by a regression should be small compared to the available degrees of freedom.

It is not possible to test every possible combination of parameters, not because it is computationally intensive, but because the more combinations tested the more likely a significant regression will be found in error. If the desired confidence is 95% then 1 in 20 combinations tested may be wrongly found significant, and testing all combinations of just 12 clinical parameters would

result in several hundred errors. Hence an appropriate selection technique has to be chosen. The stepwise multiple linear regression selection method is the recommended means of selecting a subset of variables for a regression model. This method "*must be treated with care*" and is qualified as potentially "*very misleading*" (Bland 2000) as it does not remove the chance of finding a wrongly significant regression. Typically $p < 0.1$ and $p > 0.3$ are used as inclusion and exclusion criteria, respectively.

Table 3.4.1 lists the p-values for individual linear regressions of all 12 factors. Simple linear regressions were carried out against each factor individually to determine the significant factors. Aneurysm diameter was selected with $p = 0.07$ as the only significant factor for aneurysm growth rate. The next significant factor is HDL cholesterol with $p = 0.21$ ($p = 0.29$ once adjusted for aneurysm diameter).

Table 3.4.1. Individual linear regressions of aneurysm growth against all factors including aneurysm diameter, p is the probability of wrongly rejecting the null hypothesis $h_0 : \beta_k = 0$ where β_k is the regression coefficient.

	p
Systolic Pressure	0.83
Diastolic Pressure	0.91
Systolic-Diastolic Pressure Difference	0.88
Pulse Rate	0.65
Lower ABPI	0.48
Higher ABPI	0.83
Urea	0.59
Creatinine	0.60
Total Cholesterol	0.41
HDL Cholesterol	0.21
Total to HDL Cholesterol Ratio	0.48
Aneurysm Diameter	0.07

Some parameters are strongly correlated with each other. For instance, systolic and diastolic pressure are related (correlation coefficient $r = 0.82$) because the former cannot be lower than the latter. Similarly, for the lower and higher ABPI, $r = 0.84$. Table 3.4.2 and Table 3.4.3 highlight all the couples of factors that have a significant correlation coefficient r with $p < 0.05$. From 12 clinical factors a total of 19 significant correlations were found.

3.5 Clinical Factors

The linear regression models applied to the clinical factors measured from patients with AAA at Ninewells Hospital, Dundee, resulted in the selection of aneurysm diameter as a significant predictor of the rate of aneurysm growth. None of the other factors have been found to be statistically linked to AAA growth, either because the variability of the data meant that the factors could not be selected with sufficient confidence, or simply because these factors are not predictors of aneurysm growth rate.

The most significant predictor of AAA growth rate is the log-transformed AAA diameter. (If the log-transformed diameter is significant in a linear model, then the untransformed diameter is also significant in an exponential model; hence the term 'log-transformed' need not be used when reporting significance.) The regression coefficient of growth rate against diameter is $\beta_k = 0.05 \pm 0.03\ \mathrm{yr}^{-1}/\ln(\mathrm{mm})$ 95% Confidence Interval (CI) [0;0.1] $\mathrm{yr}^{-1}/\ln(\mathrm{mm})$ with $p = 0.07$ (Table 3.5.1). With HDL cholesterol in the regression model, the

Table 3.4.2. Number of patients n (upper value) with equivalent number of independent measurements q (lower value) for the correlation analyses of couples of factors; highlighted in bold are significant correlation coefficients r (listed in Table 3.4.3) with $p < 0.05$ where p is the probability of wrongly rejecting the null hypothesis $h_0 : r = 0$.

	(1)	(2)	(3)	(4)	(5)	(6)	(7)	(8)	(9)	(10)	(11)
Systolic Pressure (1)	63 164.2	$= n$ $= q$									
Diastolic Pressure (2)	**61** **162.6**	61 162.4									
Systolic-Diastolic Pressure Difference (3)	**61** **162.6**	**61** **162.3**	61 162.3								
Lower ABPI (4)	44 37.2	43 36.5	43 36.4	68 71.5							
Higher ABPI (5)	42 35.5	41 34.7	41 34.7	**64** **67.5**	64 67.2						
Urea (6)	60 128.8	58 126.2	58 126.2	65 84.0	61 78.6	93 465.4					
Creatinine (7)	**93** **464.2**	58 124.2	**58** **124.2**	65 84.1	61 78.6	**93** **464.2**	93 464.5				
Total Cholesterol (8)	55 82.4	53 80.8	53 80.8	62 63.7	58 59.9	**82** **215.7**	**82** **216.0**	84 193.0			
HDL Cholesterol (9)	54 69.0	52 67.4	**52** **67.4**	61 61.2	57 57.3	**82** **210.6**	**82** **210.9**	**83** **181.4**	83 179.4		
Total to HDL Cholesterol Ratio (10)	54 69.0	52 67.4	**52** **67.4**	61 61.2	57 57.3	82 210.6	82 210.9	**83** **181.4**	**83** **179.4**	83 179.4	
Aneurysm Diameter (11)	**61** **94.5**	**59** **92.5**	59 92.5	68 95.2	64 89.4	92 285.4	92 285.7	83 181.5	82 176.4	**82** **176.4**	95 368.4

Table 3.4.3. Coefficients of correlation r (upper value) with probability p (lower value) of wrongly rejecting the null hypothesis $h_0 : r = 0$ for the correlation analyses of couples of factors; highlighted in bold are significant correlation coefficients with $p < 0.05$, number of patients n and equivalent number of independent measurements q are listed in Table 3.4.2.

	(1)	(2)	(3)	(4)	(5)	(6)	(7)	(8)	(9)	(10)	(11)
Systolic Pressure (1)	1 0	$= r$ $= p$									
Diastolic Pressure (2)	**0.82** **<0.001**	1 0									
Systolic-Diastolic Pressure Difference (3)	**0.90** **<0.001**	**0.49** **<0.001**	1 0								
Lower ABPI (4)	-0.20 0.2	-0.01 1.0	-0.22 0.2	1 0							
Higher ABPI (5)	-0.21 0.2	0.03 0.8	-0.26 0.1	**0.84** **<0.001**	1 0						
Urea (6)	-0.03 0.7	-0.03 0.8	-0.06 0.5	-0.09 0.4	-0.14 0.2	1 0					
Creatinine (7)	**-0.18** **0.04**	-0.02 0.8	**-0.27** **0.002**	-0.09 0.4	-0.01 0.9	**0.79** **<0.001**	1 0				
Total Cholesterol (8)	0.14 0.2	0.21 0.06	0.08 0.5	-0.12 0.3	-0.09 0.5	**-0.21** **0.001**	**-0.36** **<0.001**	1 0			
HDL Cholesterol (9)	0.22 0.07	0.04 0.7	**0.28** **0.02**	-0.08 0.5	-0.11 0.4	**-0.16** **0.02**	**-0.30** **<0.001**	**0.36** **<0.001**	1 0		
Total to HDL Cholesterol Ratio (10)	-0.15 0.2	0.07 0.6	**-0.24** **0.04**	-0.01 0.9	0.02 0.9	0.02 0.8	0.06 0.4	**0.30** **<0.001**	**-0.78** **<0.001**	1 0	
Aneurysm Diameter (11)	**-0.26** **0.01**	**-0.33** **0.001**	-0.15 0.2	0.17 0.1	0.13 0.2	0.11 0.07	0.00 0.9	-0.06 0.4	0.13 0.09	**-0.18** **0.01**	1 0

Table 3.5.1. Coefficients of regression β_k for the linear regression of aneurysm growth rate against aneurysm diameter, with probability p of wrongly rejecting the null hypothesis $h_0 : \beta_k = 0$, with 89 patients and 312.8 degrees of freedom.

	Regression Coefficient β_k	**Standard Error**	**95% Confidence Interval**	**Units**	**Probability p**
Unit ($x_{j0} \equiv 1$)	0.056	±0.004	[0.045;0.065]	yr^{-1}	<0.001
Aneurysm Diameter	0.05	±0.03	[0.00;0.10]	yr^{-1}	0.07

regression coefficient becomes 0.08 ± 0.04 yr^{-1}/ln(mm) 95% CI [0;0.17] yr^{-1}/ln(mm) (Table 3.5.2). The unit yr^{-1}/ln(mm) for the regression coefficients of proportionate growth rate against log-transformed diameter is used here to distinguish it from (mm/yr)/mm applicable to the coefficients for absolute rate of growth against untransformed diameter.

Table 3.5.2. Coefficients of regression β_k for the linear regression of aneurysm growth rate against aneurysm diameter and HDL cholesterol, with probability p of wrongly rejecting the null hypothesis $h_0 : \beta_k = 0$, with 78 patients and 137.8 degrees of freedom.

	Regression Coefficient β_k	**Standard Error**	**95% Confidence Interval**	**Units**	**Probability p**
Unit ($x_{j0} \equiv 1$)	0.053	±0.007	[0.039;0.068]	yr^{-1}	<0.001
Aneurysm Diameter	0.08	±0.04	[0.00;0.17]	yr^{-1}	0.05
HDL Cholesterol	0.03	±0.03	[-0.02;0.08]	yr^{-1}	0.3

Having accounted for the proportionality between absolute rate of growth and aneurysm diameter by taking the logarithm of diameter and regressing the proportionate rate of growth, the log-transformed aneurysm diameter has remained an important predictor of proportionate growth. The coefficient of 0.05 yr^{-1}/ln(mm) means that for each doubling in diameter the proportionate

rate of growth increases by 0.035 yr^{-1}: e.g. compared to a 30 mm diameter AAA, a 60 mm diameter AAA is predicted to grow at an extra 2 mm/yr over and above the doubling in growth rate due to the doubling in diameter. This regression of AAA rate of growth against AAA diameter may account for some of the variance in rates illustrated by the expansion patterns of 98 aortic aneurysms reported by Bengtsson et al (1993).

The next most significant independent predictor of AAA growth rate is HDL cholesterol. The regression coefficient of growth rate against HDL cholesterol is $\beta_k = 0.03 \pm 0.02\ yr^{-1}$ 95% CI [-0.02;0.08] yr^{-1} with $p = 0.2$ (Table 3.5.3). With the logarithm of aneurysm diameter in the regression model, the regression coefficient becomes 0.03 ± 0.03 yr^{-1} 95% CI [-0.02;0.08] yr^{-1} (Table 3.5.2).

Table 3.5.3. Coefficients of regression β_k for the linear regression of aneurysm growth rate against HDL cholesterol, with probability p of wrongly rejecting the null hypothesis $h_0 : \beta_k = 0$, with 78 patients and 149.5 degrees of freedom.

	Regression Coefficient β_k	**Standard Error**	**95% Confidence Interval**	**Units**	**Probability p**
Unit ($x_{j0} \equiv 1$)	0.054	±0.007	[0.041;0.067]	yr^{-1}	<0.001
HDL Cholesterol	0.03	±0.02	[-0.02;0.08]	yr^{-1}	0.2

For the linear regression of AAA growth on aneurysm diameter, Bengtsson et al (1993) report a regression coefficient of 0.11 (mm/yr)/mm with $p < 0.001$ and a coefficient of determination $R^2 = 0.11$. Lindholt et al (1998) report 0.22 (mm/yr)/mm and Brady et al (2004) 0.129 (mm/yr)/mm, both with strong significance. However, none of these studies transformed their aneurysm diameter measurements to ensure that they followed normal distributions,

despite the histogram of the distribution of 155 aortic diameters plotted by Bengtsson et al (1993) showing a log-normal distribution. Brady et al (2004) found however that exponential growth models, equivalent to log-transforming the diameters, did not fit their data well. These apparently strongly significant results reported in the literature are due to having regressed the absolute rate of growth without taking the logarithm of the diameter.

In a study with 199 patients, Schewe et al (1994) found that both rate of AAA growth and AAA diameter were possible predictors of aneurysm rupture ($p \leq 0.036$), suggesting that rate of growth and diameter are linked. The study by Wilson et al (1999) of 60 patients including some from Ninewells Hospital, Dundee, used Spearman's rank correlation analysis and found a significant correlation between aortic diameter and growth rate ($p < 0.001$). Figure 3.5.1 compares the regression line for the simple linear regression of growth rate against diameter (as reported in Table 3.5.1) with measurements of mean growth rates at different AAA diameters reported by Brown et al (1996) with error bars representing the standard deviations, and by Schewe et al (1994). The model is clearly consistent with measurements reported in the literature, though the large standard deviations warrant caution.

For the linear regression of AAA growth on HDL cholesterol, Brady et al (2004) measured a regression coefficient of 0.35 mm/yr/(mmol/L) 95% CI [-0.13;0.85] mm/yr/(mmol/L), which while not statistically significant ($p > 0.05$) would tend to indicate a positive regression of AAA growth rate

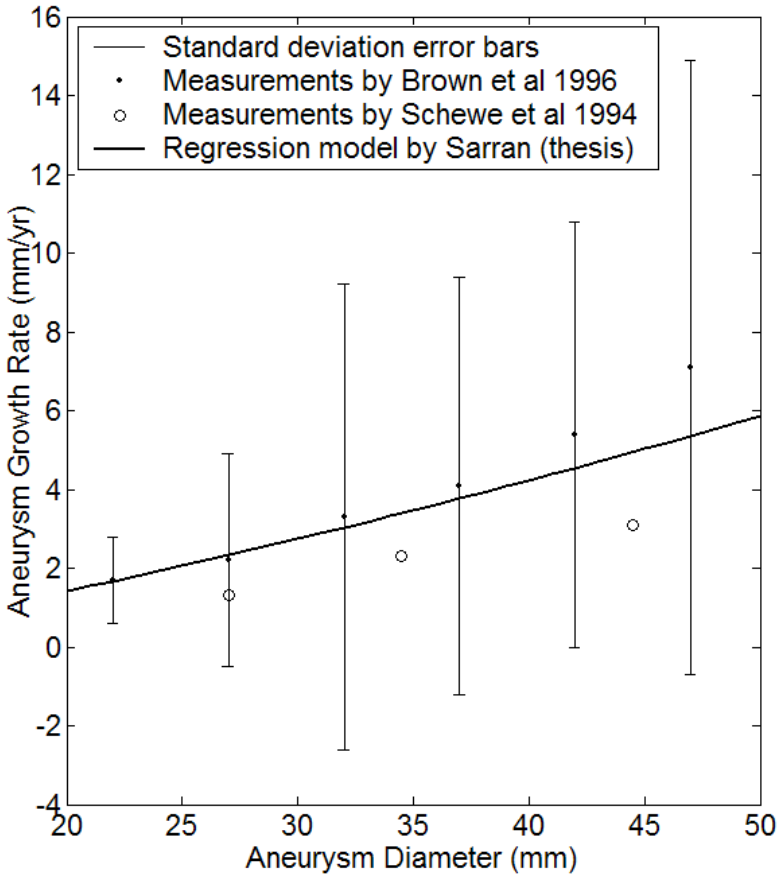

Figure 3.5.1. Plot of the regression line for the simple linear regression of aneurysm growth rate on aneurysm diameter (model presented in this thesis), compared with measurements of growth rate taken by Brown et al (1996) with error bars representing standard deviation, and by Schewe et al (1994).

against HDL cholesterol similar to that measured here. Brady et al (2004) also measured the coefficient of regression against total cholesterol as 0.017 mm/y/(mmol/L) 95% CI [-0.092;0.133] mm/y/(mmol/L), again not strictly significant but tending towards a positive regression. Chang et al (1997) did not find hypercholesterolaemia linked to growth rate ($p > 0.1$). In common with other atherosclerotic diseases, abdominal aortic aneurysms result from the degradation of elastin, a product of which is elastin-derived peptides. Concentrations of serum elastin-derived peptides were found to be significantly

higher in patients with AAA by Petersen et al (2002) who also mention that elastin-derived peptides have the potential to induce cholesterol production. Hence, while total cholesterol may not be a causal factor of aneurysm growth, it may be itself a by-product of the elastin degradation present in aneurysms. Serum elastin peptides however were not associated with aneurysm growth rate by Lindholt et al (2001), but higher levels of serum elastin peptides were linked to a greater risk of aneurysm rupture. While HDL cholesterol was selected by the stepwise method as a possible predictor of aneurysm growth rate, the associated p-value remains high with $p \geq 0.2$. This means that there is a greater than 1 in 5 chance that the association of HDL cholesterol with aneurysm growth is due to random scatter in the data and not due to a biochemical phenomenon. No explanation for the association of HDL cholesterol with aneurysm growth was found in literature.

None of the haemodynamic factors such as blood pressure, pulse rate or ABPI, have been found significant by the linear regression method. While Chang et al (1997) found that age, severe cardiac disease, stroke and smoking were linked to increased AAA growth rate ($p < 0.05$), he did not find hypertension significant ($p = 0.1$). Indeed, regression of AAA growth rate on systolic pressure results in a coefficient with 95% CI [-0.0011;0.0013] mm/yr/mmHg ([-0.008;0.01] mm/yr/kPa) with $p = 0.8$. Similarly, Brady et al (2004) did not find systolic pressure to be significant with 95% CI [-0.006;0.003] mm/yr/mmHg and [-0.007;0.003] mm/yr/mmHg. Regression of AAA growth rate on diastolic pressure results in a coefficient with 95% CI [-0.003;0.002]

mm/yr/mmHg ([-0.02;0.02] mm/yr/kPa) with $p = 0.9$. Lindholt et al (1998) did not find diastolic pressure to be a significant predictor of growth with 95% CI [-0.02;0.03] mm/yr/mmHg. The regression coefficient for the systolic-diastolic pressure difference was also computed, with 95% CI [-0.0017;0.002] mm/yr/mmHg ([-0.013;0.015] mm/yr/kPa) with $p = 0.9$. The study by Wilson et al (1999) attempted to predict growth rates from measurements of the elastic modulus, a function of the systolic-diastolic pressure difference, and the stiffness, a function of the difference between the logarithms of systolic and diastolic pressures. Along with the mean arterial pressure, neither elastic modulus nor stiffness were found to be significant predictors of AAA growth rate ($p \geq 0.15$) using Spearman's rank correlation method. The lack of significance of the haemodynamic factors with respect to AAA growth has also been found with risk of AAA rupture. Schewe et al (1994) found that neither systolic pressure nor diastolic pressure nor the systolic-diastolic pressure difference were predictors of rupture ($p > 0.13$). This is supported by the results of Lederle et al (2002) who evaluated risk ratios for rupture with 95% CI [0.98;1.01] $mmHg^{-1}$ and [0.98;1.04] $mmHg^{-1}$ for systolic and diastolic pressure, respectively. The regression of growth rate against lower and higher ABPI resulted in 95% CI [-0.08;0.16] mm/yr ($p = 0.5$) and [-0.13;0.16] mm/yr ($p = 0.8$), neither being significant. This is a different result from that suggested by Diehm et al (2005), namely that "*AAA growth is significantly slower in patients with low ankle-brachial index*", with coefficients of regression of 1.0 mm/yr 95% CI [0.4;1.7] mm/yr and 1.1 mm/yr 95% CI [0.5;1.7] mm/yr (Brady et al 2004)

calculated from measurements from 1743 patients. This number of patients is vastly superior to the 66 patients in the AAA study with valid ABPI measurements that were used here. That and the fact that coefficients of ~1 mm/yr per ABPI are particularly small and possibly not clinically relevant would suggest that ABPI is not a predictor of clinically significant growth rates and therefore would not return a statistically significant regression coefficient with the number of measurements analysed here.

Chapter 4

Analysis of Aortic Geometry

4.1 Shape Analysis

Instead of analysing proxies of haemodynamics, or indeed in conjunction with these analyses, the rate of aneurysm growth has been analysed against the geometry of the infra-renal abdominal aorta. In particular, the stepwise multiple linear regression analyses of parameters strongly support the selection of abdominal aortic diameter as being a significant predictor of exponential growth. Nevertheless, studies of geometrical parameters in relation to risk of aneurysm rupture have highlighted the unreliability of simple diameter as a criterion (Giannoglou et al 2006). The tortuosity (or centreline asymmetry) of the AAA (Abdominal Aortic Aneurysm) has been linked to elevated wall stress in AAA by Doyle et al (2009) and to high wall shear stress in the superficial femoral artery by Wood et al (2006). Measures of radii of curvature have been linked to the locations of high stresses on the aortic wall, but do not predict stress magnitude (Hua and Mower 2001); this would be supported by earlier autopsy measurements by Darling et al (1977) who found varying sites of rupture with most being retroperitoneal. This raises the question of whether there are other geometric characteristics of the aortic lumen that can predict risk of aneurysm growth.

To determine the possible statistical links between AAA geometry and AAA growth, factors describing the shape of the arterial lumen have been measured

from medical imaging. For 47 patients there were a total of 59 CT (Computed Tomography) abdominal scans referenced on the study database. These CT scans consisted of the imaging of consecutive cross-section slices of the abdomen. In all but the most unusual of cases, the abdominal aorta lies essentially parallel to the axis of the abdomen and each abdominal CT image represents a cross-section of the aorta.

Figure 4.1.1 illustrates measurements of an aortic lumen taken on a typical CT image. A vertical measuring scale available on the CT imaging system can be used as an axis with origin O and directed towards S (two arbitrary fixed points specific to the CT scanner). First, the position of the centre at O' of the aortic lumen, defined as the mid-point of the shortest diameter $[BB']$ (i.e. $O'B = O'B'$), is measured using the vertical scaling tool $[OS)$ as an axis of reference defining a cylindrical CT coordinate system $(r;\theta;z)$. The measurements of the distance OO' and the angle $\left(\overrightarrow{OS};\overrightarrow{OO'}\right)$ provide the first two coordinates for the centre O':

$$r = OO' \qquad \text{Equ. 4.1.1a}$$

$$\theta = \left(\overrightarrow{OS};\overrightarrow{OO'}\right) \qquad \text{Equ. 4.1.1b}$$

The origin of the z-axis is defined as the trifurcation of the renal arteries with the abdominal aorta (as depicted by Figure 4.1.2). The CT images have numbers I such that if I_0 is the number of the image with the proximal ends of the renal arteries, the z-coordinate of the lumen cross-section is:

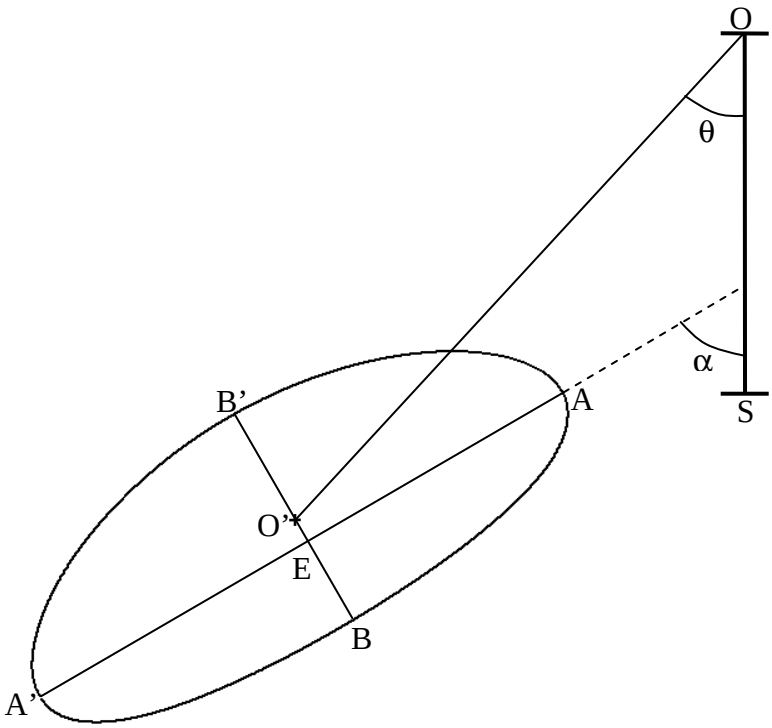

Figure 4.1.1. Graphical representation of the lumen shape at the proximal end of the infra-renal abdominal aorta of a patient (2-dimensional, see Figure 4.1.2 for a 3-dimensional representation of the CT imaging with the coordinate systems). In this example the measurements were $AA' = 33\,\text{mm}$, $BB' = 25\,\text{mm}$, $BE = 11\,\text{mm}$ and $\alpha = 67°$ which result in a lumen shape with a maximum radius $a = 16.5\,\text{mm}$, an ellipsity $b = 0.758$, a parabolic distortion $\varepsilon = 0.091$ and an orientation $\phi = -148.6°$ (the orientation of the proximal ends of the renal arteries is $\phi_0 = -8.4°$).

$$z = (I - I_0)\frac{t_{CT}}{2} \qquad \text{Equ. 4.1.2}$$

t_{CT} is the CT slice thickness and the CT system typically produces two images per slice. To standardise the dimensions of the infra-renal aorta between patients, it has been necessary to transform the coordinates linked to the CT machine to coordinates linked to the aorta itself. The z-axis is therefore defined as the straight line that runs from the trifurcation with the renal arteries to the aorto-iliac bifurcation. With $(r_0; \theta_0)$ the cylindrical CT coordinates of the lumen

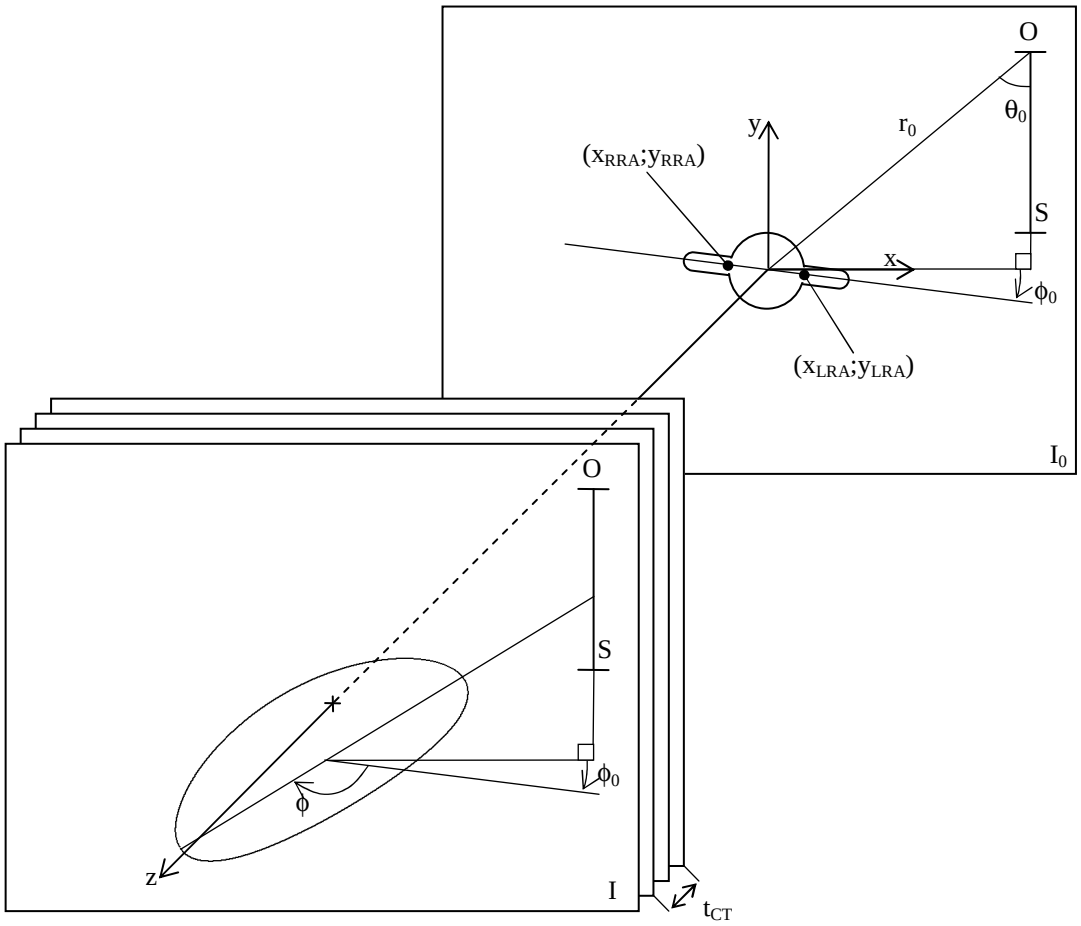

Figure 4.1.2. Diagram representing the stack of CT images with CT slice thickness t_{CT}, with the image I_0 that of the trifurcation of the renal arteries with the abdominal aorta and the image I that of the aortic lumen drawn in Figure 4.1.1. The scaling tool $[OS)$ of the CT imaging system that defines the cylindrical CT coordinate system $(r;\theta;z)$ is shown on both images, and the axes of the Cartesian coordinate system $(x;y;z)$ that originate at the trifurcation are also shown. On image I_0, the orientation ϕ_0 of the renal arteries is given by the coordinates $(x_{LRA};y_{LRA})$ and $(x_{RRA};y_{RRA})$ of the proximal ends of the left and right renal arteries, respectively; on image I, the orientation ϕ of the lumen shape is relative to the orientation ϕ_0 of the renal arteries.

centre at the trifurcation, the $(x;y)$ Cartesian coordinates of the lumen centre on a line running through the trifurcation point (but still aligned with the CT system) are given by:

$$\begin{cases} x = r_0 \sin\theta_0 - r\sin\theta \\ y = r_0 \cos\theta_0 - r\cos\theta \end{cases} \qquad \text{Equ. 4.1.3}$$

A sequential computation of rotations of the $(x;y)$ coordinates around the three orthogonal axes adjusts the coordinates to the alignment with the z-axis passing through the aorto-iliac bifurcation. The actual total correction being quite small, the adjustment has negligible effect on the z-coordinate values. This also holds true for the lumen shape parameters described next. Unlike the AAA asymmetry study of Doyle et al (2009) that only included asymmetry in the anterior-posterior plane, the centreline definition that has been used here includes both x and y coordinates; furthermore, in addition to the measurement of the lumen centre, parameters measured from the shape of the lumen cross-section have also been analysed.

On a CT image (c.f. the diagram of Figure 4.1.1), the measurements of the maximum diameter $[AA']$ and the minimum diameter $[BB']$ provide an assessment of the axial distortion, or compression, of the shape of the lumen, quantified as the ellipsity b (Equation 4.1.4b). The offset segment $[O'E]$ between the centre O' of the lumen and the intersect $E \in (AA') \cap (BB')$ of the two diameters (c.f. Figure 4.1.1) provides a measure of a secondary distortion which can be included in the lumen function (thereafter) as a quadratic term and

hence quantified by the parabolic distortion ε (Equation 4.1.4c). $O'E$ being usually small, it is best obtained by measuring $[BE]$. Finally, the orientation ϕ (Equation 4.1.4d) is the angle that the maximum diameter makes with respect to the orientation ϕ_0 of the renal arteries. It is obtained from the measurement of angle $\alpha = \left(\overrightarrow{OS}; \overrightarrow{AA'}\right)$ between the axis of reference $[OS)$ and the maximum diameter $[AA']$ (c.f. Figure 4.1.1). The major, or maximum, radius a (Equation 4.1.4a) is half of diameter $[AA']$.

$$a = \frac{AA'}{2} \qquad \text{Equ. 4.1.4a}$$

$$b = \frac{BB'}{AA'} \qquad \text{Equ. 4.1.4b}$$

$$\varepsilon = \frac{2O'E}{AA'} = b - \frac{BE}{a} \qquad \text{Equ. 4.1.4c}$$

$$\phi = -\alpha - \frac{\pi}{2} - \phi_0 \pmod{2\pi} \qquad \text{Equ. 4.1.4d}$$

By determining from measurement the Cartesian coordinates $\left(x_{LRA}; y_{LRA}\right)$ and $\left(x_{RRA}; y_{RRA}\right)$ of the proximal ends of the left and right renal arteries, respectively, the orientation ϕ_0 of the renal arteries is defined by Equation 4.1.5 (c.f. Figure 4.1.2).

$$\tan\phi_0 = \frac{y_{LRA} - y_{RRA}}{x_{LRA} - x_{RRA}} \qquad \text{Equ. 4.1.5}$$

From the parameters derived from the measurements of a cross-section of aortic lumen, the lumen function $\Lambda(\theta')$ is a complex function of angle parameter θ' that describes numerically the shape of the lumen edge. For a

lumen with a circular cross-section of radius a, the lumen function $\Lambda(\theta')$ is given by Equation 4.1.6.

$$\Lambda(\theta') = ae^{i\theta'} \qquad \text{Equ. 4.1.6}$$

For a lumen with an elliptical cross-section of maximum radius a and ellipsity b, the lumen function $\Lambda(\theta') = S(\theta')e^{i\theta'}$ has to satisfy Equation 4.1.7, where $S(\theta')$ is a scaling factor dependent on angle θ':

$$\begin{cases} \Lambda(\theta' = 0) = a \\ \Lambda(\theta' = \frac{\pi}{2}) = iba \end{cases} \qquad \text{Equ. 4.1.7}$$

The solution for $S(\theta')$ that satisfies Equation 4.1.7 is:

$$S(\theta') = \sqrt{\frac{\cos^2\theta'}{a^2} + \frac{\sin^2\theta'}{b^2a^2}}^{-1} \qquad \text{Equ. 4.1.8}$$

For a distorted lumen with a measurement ε of parabolic distortion (c.f. Equation 4.1.4c), the imaginary part of $e^{i\theta'}$ has an additional term $\frac{S(\theta')}{a}\varepsilon\cos^2\theta'$ which is a function of the square of the real part of $e^{i\theta'}$ with the parabolic distortion factor ε appropriately scaled by $\frac{S(\theta')}{a}$. Equation 4.1.9 defines an elliptical lumen function with parabolic distortion ε.

$$\Lambda(\theta') = S(\theta')\left[e^{i\theta'} + i\frac{S(\theta')}{a}\varepsilon\cos^2\theta'\right] \qquad \text{Equ. 4.1.9}$$

The lumen function can be rotated by its orientation ϕ and translated by its centre coordinate $x + iy$, such that the full lumen function $\Lambda(\theta')$, substituting for $S(\theta')$, is given by Equation 4.1.10:

$$\Lambda(\theta') = \frac{e^{i\theta'} + \frac{i\varepsilon}{a}\cos^2\theta' \Big/ \sqrt{\frac{\cos^2\theta'}{a^2} + \frac{\sin^2\theta'}{b^2a^2}}}{\sqrt{\frac{\cos^2\theta'}{a^2} + \frac{\sin^2\theta'}{b^2a^2}}} e^{i\phi} + x + iy \qquad \text{Equ. 4.1.10}$$

The lumen function is used here first to illustrate the influence of the measured parameters x, y, a, b, ε and ϕ on the shape of the lumen (e.g. Figure 4.1.3) and second to reconstruct the 3-dimensional shape of the aorta by layering

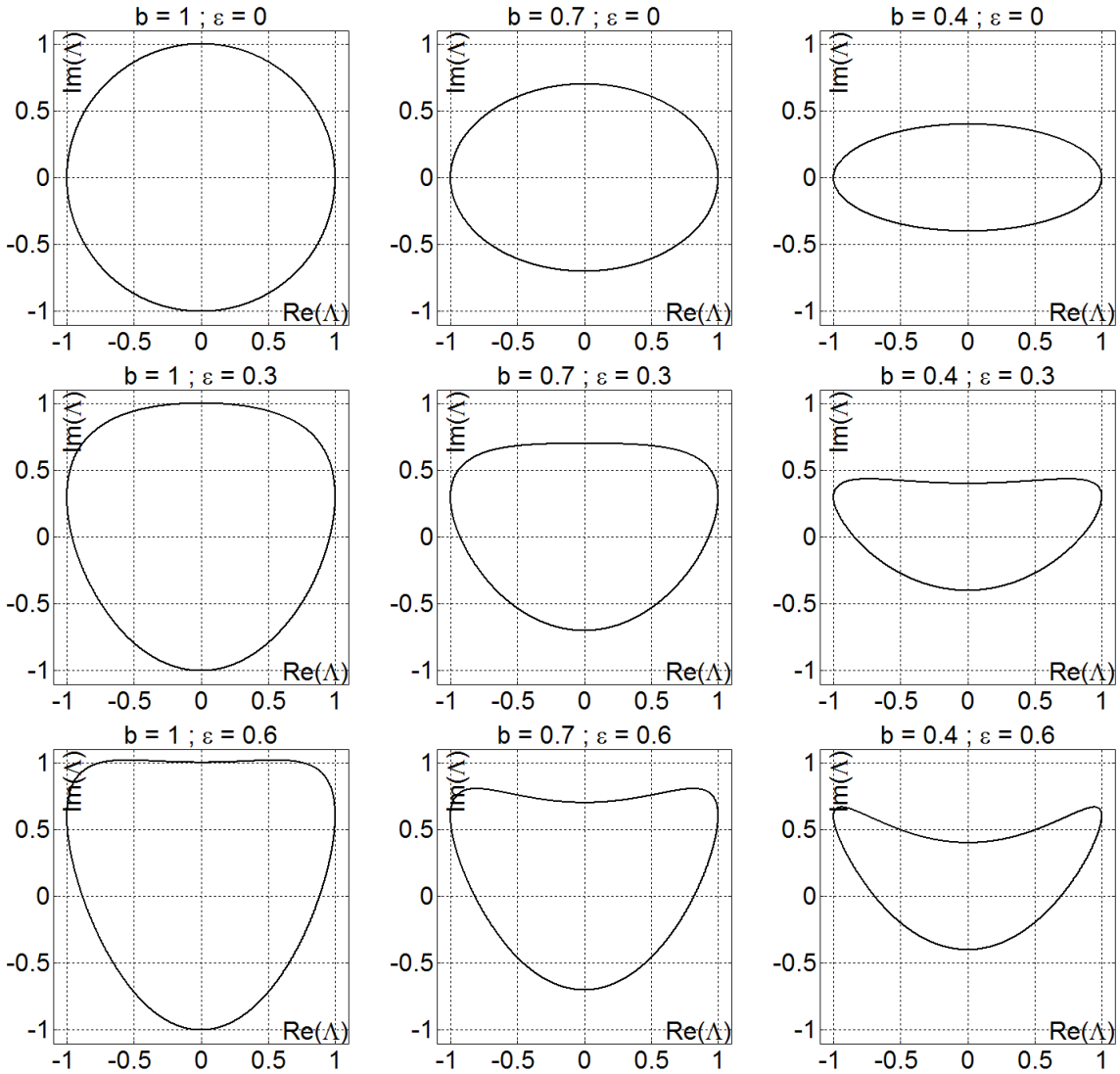

Figure 4.1.3. Plots of the parametric lumen function $\Lambda(\theta')$ with radius $a = 1$ for ellipsities $b \in \{0.4;0.7;1\}$ and parabolic distortions $\varepsilon \in \{0;0.3;0.6\}$.

cross-sectional lines defined by the lumen function (e.g. Figure 4.1.4). Figure 4.1.3 illustrates the influence of ellipsity and parabolic distortion on the shape of the lumen.

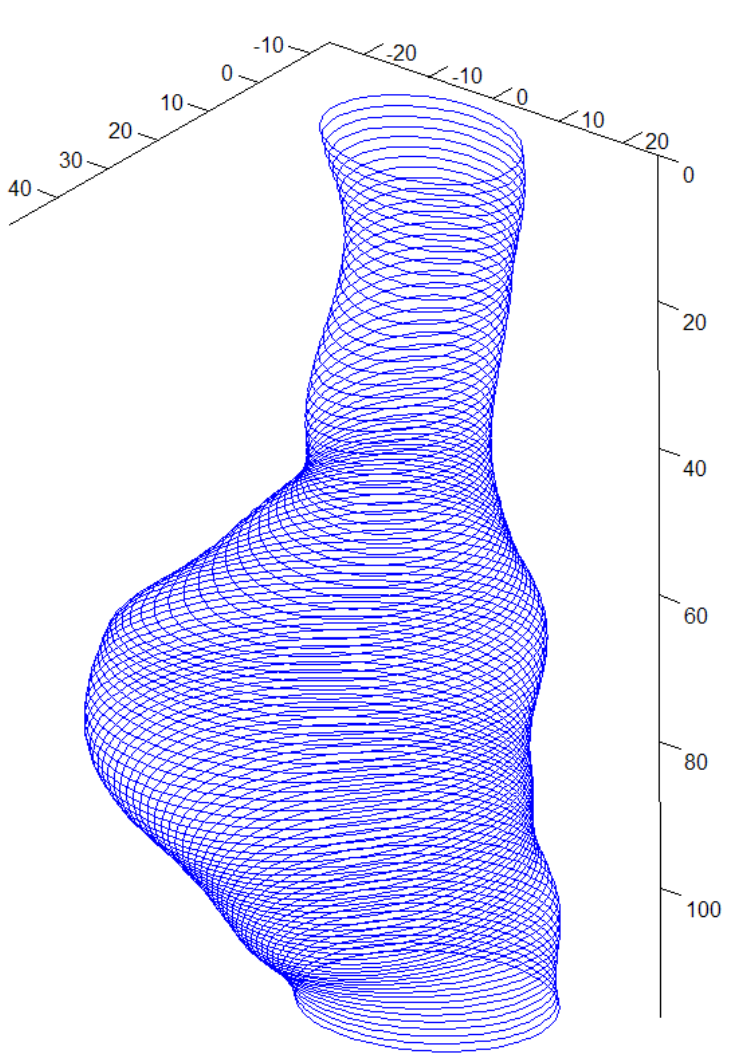

Figure 4.1.4. Infra-renal aorta surface of a patient, defined by individual lumen cross-sectional lines reconstructed from Fourier coefficients of the shape parameters.

The parameters x, y, a, b, ε and ϕ have been chosen in such a way as to avoid their interdependence: the ellipsity b provides no information on the radius a; the parabolic distortion ε no information on the radius a or the

ellipsity b, etc. As these parameters vary along the length of the abdominal aorta, it is possible to use the properties of Fourier series (Jordan and Smith 1994) to obtain independent components of the parameters by computing Fourier coefficients. As the parameters are not strictly periodic, the analysis has been adapted so that the coefficients for $a(z)$, $b(z)$, $\varepsilon(z)$ and $\phi(z)$ are given by Equation 4.1.11a, while because the aortic centreline must pass through the centres of the trifurcation and of the aorto-iliac bifurcation, the functions $x(z)$ and $y(z)$ are bound at the ends of the infra-renal aorta, $z=0$ and $z=L$, and their coefficients are therefore given by Equation 4.1.11b. Being measures of length, the parameters $x(z)$, $y(z)$ and $a(z)$ are normalised by using L as a reduction factor.

$$\begin{cases} a_\nu = \dfrac{2}{L}\int_0^L a(z)\cos\dfrac{\nu\pi z}{L}dz \\ a_0 = \dfrac{1}{L}\int_0^L a(z)dz \end{cases} \qquad \text{Equ. 4.1.11a}$$

$$x_\nu = \frac{2}{L}\int_0^L x(z)\sin\frac{\nu\pi z}{L}dz \qquad \text{Equ. 4.1.11b}$$

In the case of the AAA patient already taken as an example for Figure 4.1.1, coefficients $x_1 = 0.06$ and $y_1 = 0.12$ indicate that the aorta centreline deviates some 6% and 12% of the infra-renal aorta length L, along the x and y axes, respectively, the other coefficients being much smaller (c.f. Figure 4.1.5). The mean maximum radius is given as a function of length by $a_0 L = 0.16L$, the negative first coefficient $a_1 = -0.04$ indicating that the aorta is wider at its distal

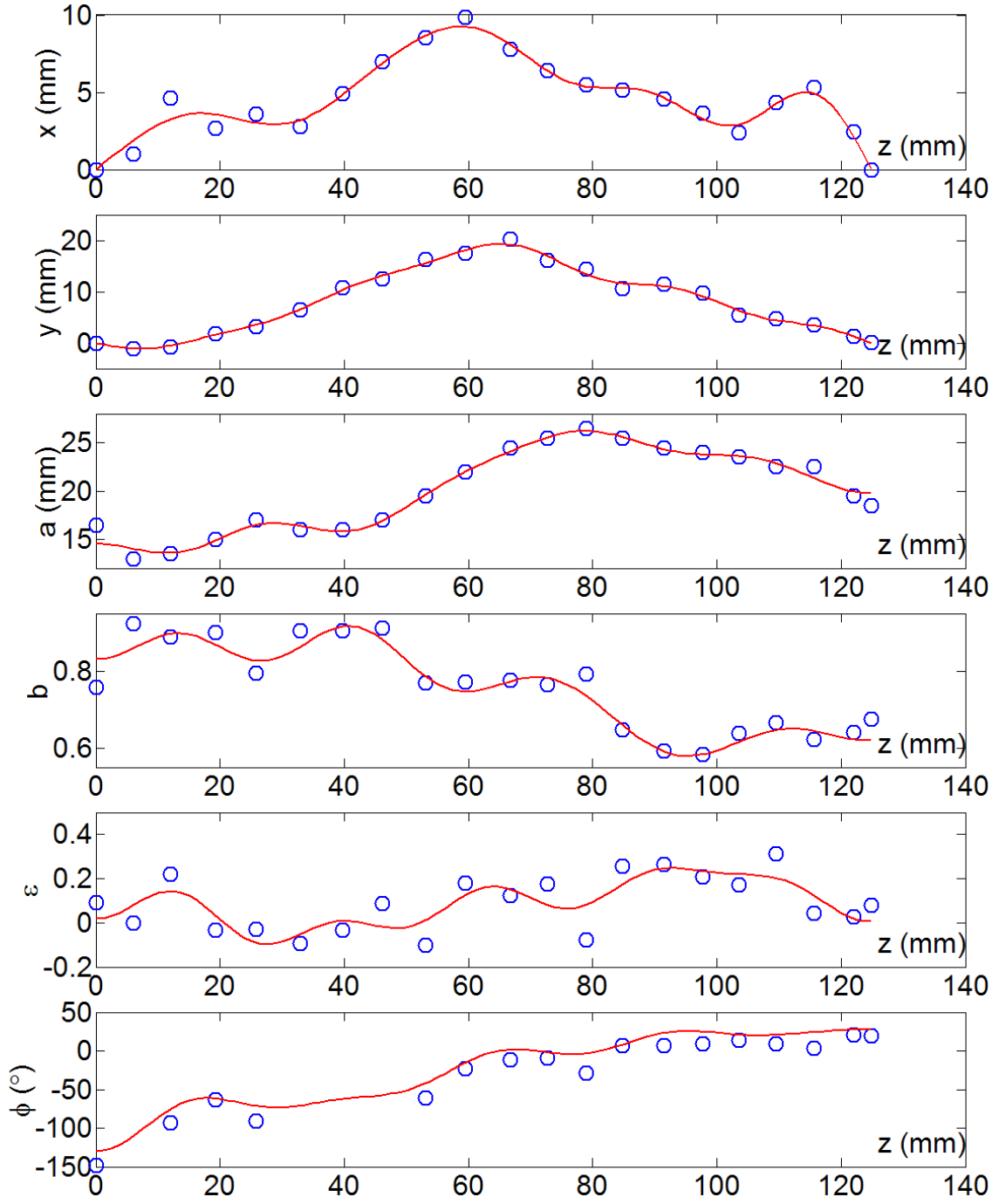

Figure 4.1.5. Plots of the estimates (circles) at regular intervals from CT of the coordinates x and y, the maximum radius a, the ellipsity b, the parabolic distortion ε and the orientation ϕ, and of their functions (lines) as reconstituted from the first 10 Fourier coefficients, of the infra-renal abdominal aorta of the patient.

section than proximally, but the actual distal end narrows ($a_2 = -0.02$), which is often typical of abdominal aortic aneurysms. The mean ellipsity is $b_0 = 0.76$ with $b_1 = 0.14$, indicating that the proximal section is more circular and the distal section takes the shape of a narrower ellipse.

In general, the aorta shape is described by the first 2 to 5 coefficients of each parameter with the higher frequencies (higher ν) being small. The coefficients ε_ν for parabolic distortion tend to remain small for all ν which means that most of the lumen shape is described by x_ν, y_ν, a_ν and b_ν. While important for the reconstruction of the lumen shape, the orientation ϕ measured from images where the cross-sectional shape is quasi circular ($b > 0.9$ and $\varepsilon < 0.1$) is irrelevant and is removed from the Fourier analysis.

Despite the relatively small number of patients with CT scans, it has been possible to carry out simple linear regression analyses of the rate of aneurysm growth on the Fourier coefficients. For this, the aneurysm growth rate is estimated for the time at which the CT scan was carried out, as there is usually no more than one CT scan per patient. Using Equation 3.3.17 provides a suitable estimate of growth. The p-values for the linear regressions of aneurysm growth are listed in Table 4.1.1 for each Fourier coefficient separately. Aneurysm growth regresses against the mean maximum radius a_0 with $p = 0.06$. Only two other coefficients appear more significant: b_3 with $p = 0.05$ and x_4 with $p = 0.02$. To some extent, b_3 has a reasonable geometric interpretation: a

Table 4.1.1. Probabilities p for the regressions of aneurysm growth estimated at time of CT scan against each Fourier coefficient of lumen shape up to $\nu = 4$, individually.

ν	0	1	2	3	4
x_ν		0.1	0.3	0.2	0.02
y_ν		0.6	0.1	0.2	0.5
a_ν	0.06	0.7	0.1	0.4	0.9
b_ν	0.1	0.2	0.3	0.05	0.2
ε_ν	0.3	0.8	0.2	0.8	1
ϕ_ν	0.7	0.5	0.09	0.8	0.6

positive b_3 means a more circular lumen cross-section at the trifurcation and in the distal section of the infra-renal aorta, and a more elliptical cross-section in the proximal section and at the aorto-iliac bifurcation. A positive x_4 means that the infra-renal aorta first bears left, then right, then left again, then right again, before joining the bifurcation. While this may describe a particularly tortuous aorta, the regression is linear indicating that first bearing to the left has the opposite effect on aortic growth from first bearing to the right. This illustrates how the use of the geometric coefficients in regression analyses makes the results difficult to interpret clinically.

While multiple linear regressions could be carried out, the stepwise selection method is inappropriate for this geometric data because there are too many coefficients relative to the number of patients.

The full shape of the lumen can be reconstructed using the Fourier coefficients computed for the six different parameters. A dense layering of lumen cross-sectional lines obtained from the coefficients provides the final shape of the

infra-renal aorta (Figure 4.1.4) in a way analogous to the methods described by Raghavan et al (2000) and Venkatasubramaniam et al (2004). The lumen surface is meshed using Star-CD (CD Adapco, London) by defining a regular cylinder, which is then dilated into the shape specified by the lumen function Λ (Hammer et al 2009; Wolters et al 2005; Leung et al 2006). The dilated cylinder surface is then used by the Star-CD automatic meshing program to produce a meshed 3D (3-dimensional) fluid domain using polyhedral cells (Figure 4.1.6).

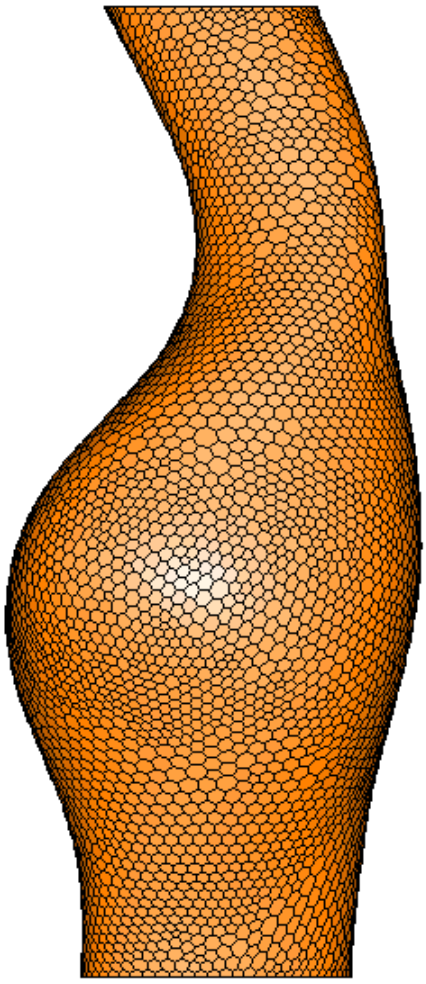

Figure 4.1.6. 3D numerical model of the fluid domain defined by the lumen of the infra-renal aorta of the patient, generated by the automatic meshing capability of Star-CD (CD Adapco, London) with polyhedral cells.

Throughout the analysis of the geometric characteristics of AAA, a thrombus in the artery is regarded as part of the aortic wall. While a thrombus is not a fluid, the possible action it has on the aortic wall has been considered a risk for rupture and for AAA growth, although what exactly the risks are has been a matter of some controversy (Shurink et al 2000; Mower and Quinones 2001). Consequently, for the purpose of this analysis, the aortic lumen is deemed to be the open fluid lumen excluding the areas of thrombus. For completeness, geometric measurements of the lumen defined by the actual arterial wall on the CT images and including thrombosed areas have been taken at the same time as the measurements of the open lumen so that these are available for analysis (given appropriate methods).

Simple geometric measurements from CT scans provide sufficient information to build numerical 3D models of the infra-renal aorta with AAA. The automatic meshing program provides good quality polyhedral meshes that can be used in subsequent CFD (Computational Fluid Dynamics) analyses (Di Martino et al 2001; Li and Kleinstreuer 2006) to compute maximum local wall stresses. The importance of carrying out the full 3D CFD numerical analyses is highlighted by Fillinger et al (2002); only peak wall stress obtained from 3D reconstruction was found to be significant in relation to AAA rupture (or symptomatic AAA) and not indices of geometric shape. CFD analyses were not carried out on the numerical AAA models built at Ninewells Hospital, Dundee, however. The development of the methods required for this is outside the scope of the work presented here.

4.2 Geometric Factors

While some studies have used CT scans to link risk of AAA rupture to geometric factors such as aneurysm diameter itself (e.g. Siegel et al 1994), few have broken down the geometry of the AAA into independent separate components such as have been described earlier with radii a_v, ellipsity b_v, aorta centreline coordinates x_v and y_v, etc. Doyle et al (2009) examined the variation in y (vessel asymmetry) and $2a$ (diameter) against aortic wall stress but not rate of AAA growth. Vorp (2007) is critical of the perceived clinical importance of maximum AAA diameter towards risk of rupture, and states that "*the "maximum criterion diameter" is not reliable*". It therefore becomes important not only to analyse diameter with respect to aneurysm growth rate but also to analyse other geometric components derived from CT scans.

Similarly to finding a statistical link between AAA diameter and aneurysm growth when aneurysm diameter is included as a clinical factor, the linear regression of the rate of aneurysm growth on the mean maximum radius a_0 of the infra-renal aorta results in a regression coefficient (with standard error) of 1.0 ± 0.5 yr^{-1} with $p = 0.06$. Figure 4.2.1 is a scatter plot of the a_0 factors obtained from CT versus the estimated rate of growth at the time of the scan. With more statistical significance than the mean maximum radius, the rate of aneurysm growth was found to regress against the geometric factor b_3 with $p = 0.05$ and a regression coefficient of -0.6 ± 0.3 yr^{-1} (Figure 4.2.2). When

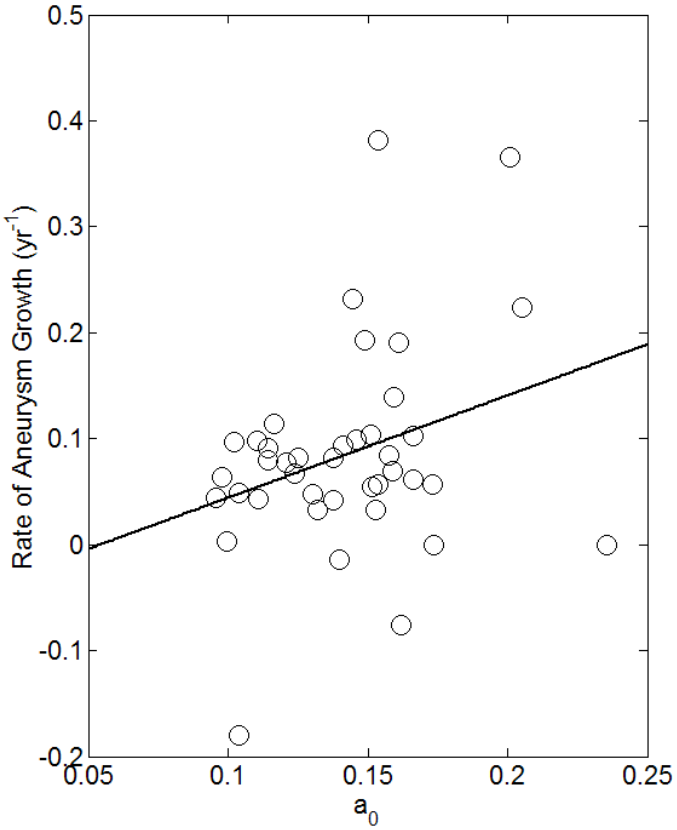

Figure 4.2.1. Scatter plot with regression line of aneurysm growth rate against a_0 (mean maximum radius) with $n = 40$ measurements; regression accounts for 9% of the variability in scatter and probability of type I error is $p = 0.06$.

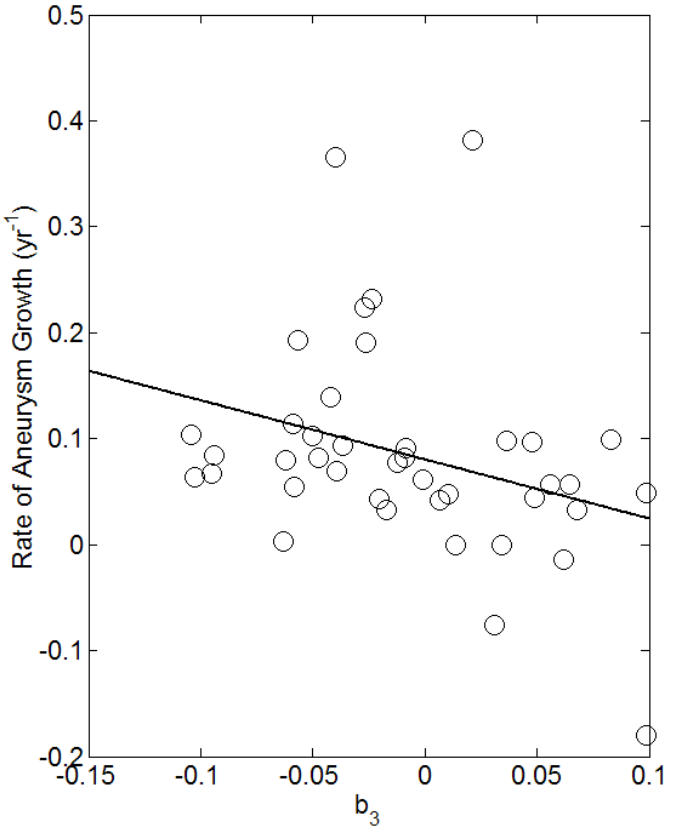

Figure 4.2.2. Scatter plot with regression line of aneurysm growth rate against b_3 with $n = 40$ measurements; regression accounts for 10% of the variability in scatter and probability of type I error is $p = 0.05$.

regressing against each of the geometric factors up to $\nu = 4$ (the first 4 or 5 components of the Fourier series) the most significant factor was x_4 with $p = 0.02$ and a regression coefficient of 2.3 ± 1.0 yr^{-1} (Figure 4.2.3).

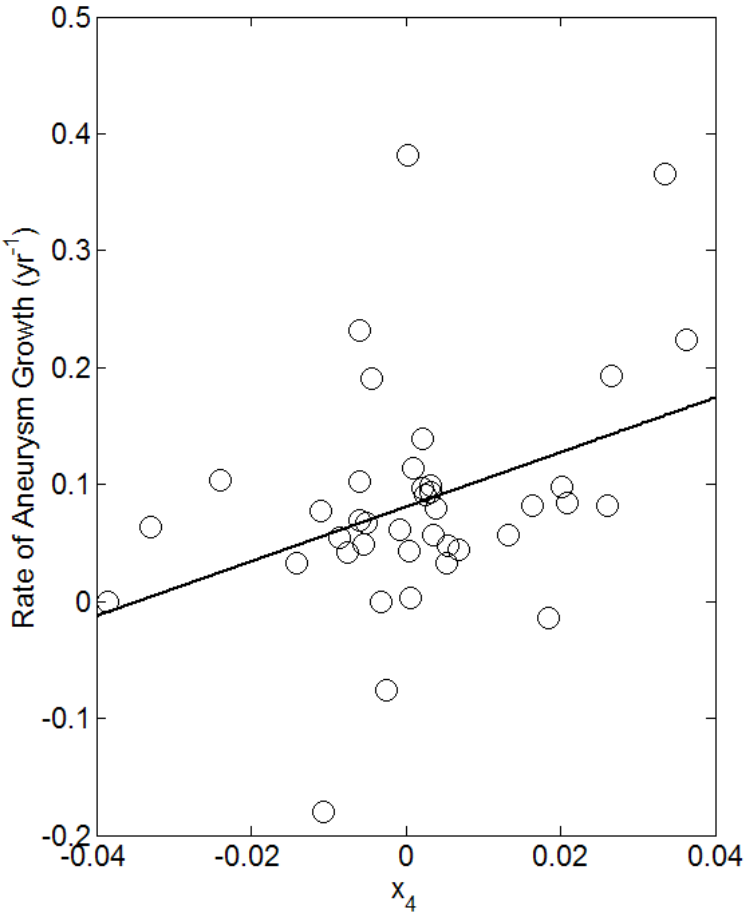

Figure 4.2.3. Scatter plot with regression line of aneurysm growth rate against x_4 with $n = 40$ measurements; regression accounts for 13% of the variability in scatter and probability of type I error is $p = 0.02$.

a_0 represents the larger radius of an elliptical lumen and hence $2a_0$ the larger diameter which Fillinger (2007) suggests may provide a better indication of rupture risk, but also considers that the larger diameter may be overestimated due to the tortuosity of the vessel. This was already considered when taking measurements from the CT images; infra-renal abdominal aortas that displayed

particularly unusual morphologies were not included in the analysis. Geometric factors based on arterial diameter, such as "*the ratio of the aneurysm diameter to the supraceliac aortic diameter*" (Ouriel et al 1992), have been studied in relation to aneurysm rupture. Fillinger et al (2004) found a number of different arterial geometry measurements and indices including the maximum aneurysm diameter itself and the supraceliac and infrarenal aortic diameters to be significantly greater in ruptured cases. The supraceliac and infrarenal diameters remained significant after matching AAA by diameter. This would suggest that lower negative a_2 values, corresponding to an aortic shape whereby the radius is small at the ends of the infra-renal abdominal aorta and large in the middle, are less of a risk for rupture. Regression of rate of growth against a_2 results in a regression coefficient of -1.3 ± 0.9 yr^{-1} and a coefficient of determination $R^2 = 0.06$. The probability of error remains somewhat large with $p = 0.1$, but the result suggests that greater growth rates occur in AAA with low a_2, i.e. AAA more saccular and less fusiform in shape.

Greater rates of growth are linked with lower (negative) b_3. Perhaps the negative b_3 corresponds to aneurysms that lie in the distal half of the infra-renal aorta, the proximal half of circular cross-section with a more elliptical lumen at the trifurcation, the distal half of more elliptical cross-section with a more circular lumen at the bifurcation. Fillinger et al (2004) measured the ellipsity of the aneurysm in terms of its maximum diameter less its minimum diameter. They found a greater risk of rupture for the more elliptical AAA ($p = 0.02$). The regression of rate of growth on mean ellipsity b_0 of the infra-renal aorta results

in a regression coefficient of -0.4 ± 0.2 yr^{-1} with $p = 0.1$ (Figure 4.2.4) which may suggest that the more elliptical aortas experience a greater rate of growth as well as risk of rupture.

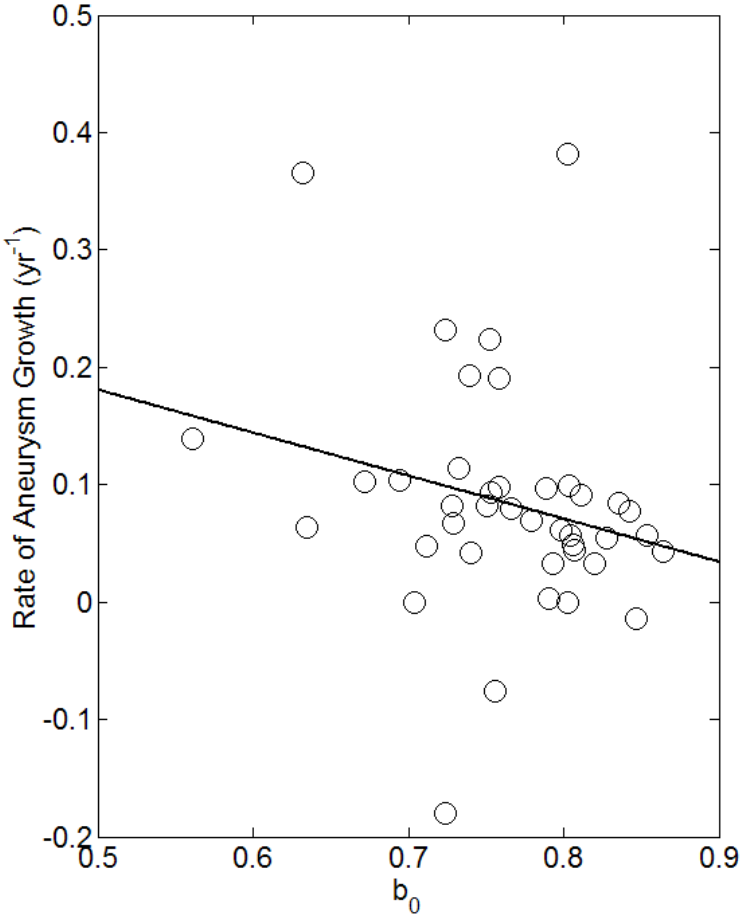

Figure 4.2.4. Scatter plot with regression line of aneurysm growth rate against b_0 (mean ellipsity) with $n = 40$ measurements; regression accounts for 6% of the variability in scatter and probability of type I error is $p = 0.1$.

The x_4 component may be taken as a measure of left-right tortuosity (or horizontal tortuosity when supine), but a measure of tortuosity with a direction, positive values meaning the aorta first bears left after the trifurcation, negative values meaning the aorta first bears right. While tortuosity was weakly associated with risk of rupture (Fillinger et al 2004) with lower tortuosity linked

to greater rupture risk, Sacks et al (1999) argues that the greater the tortuosity the greater the number of high curvature areas of the aortic wall that may correspond to high wall tension and stress. This association between tortuosity and wall stress has also been shown by Doyle et al (2009). It is also suggested that as the spatial distribution of these focal areas of curvature is not uniform, the rate of growth of the aortic wall and the risk of its rupture may not be uniform either. Furthermore, for the x_4 component, it is not simply the degree of tortuosity that appears important, but also its direction. Studies of the rupture sites of AAA (Golledge et al 1999) have found that the risk of rupture appears to be one-sided. Perhaps the rate of AAA growth is also dependent on the direction of the tortuous path the infra-renal aorta takes.

The statistical analysis of the geometric components evaluated for this study remains empirical. The complex geometric nature of the problem that is presented by a tortuous and elliptical aneurysm with varying shape and size (Sacks et al 1999) suggests that the rate of aneurysm growth is not spatially uniform and so the limitations of predicting rates of aneurysm growth are not surprising. The statistical analyses, by being empirical, have been criticised as not having "*a physically sound theoretical basis*" (Vorp 2007). However, the lack of any strong relationship between the geometric factors evaluated here and the rate of aneurysm growth could reside in part in the low number of patients with CT scans included in the analysis; the approach that was taken here to analyse a set of independent geometric components that fully describe the aneurysm remains original. The set of geometric factors also enables the

construction of 3D numerical models with which computational fluid dynamic simulations can be carried out. Computations of the wall shear stress and pressure by Papaharilaou et al (2007) with numerical models of AAA found an increased pressure loading throughout most of the aneurysm and in particular at the distal end of the AAA (pressure some 15% higher than the peak systolic pressure). The geometric factors would help in examining the influence of varying each in turn on the simulated aortic wall shear stress and pressure.

Chapter 5

Discussion and Conclusion

5.1 Discussion

It has been described how Abdominal Aortic Aneurysm (AAA) growth is linked to changes to the principal constituents of the arterial wall, elastin degradation and collagen remodelling (Chapter 1). A method to simulate 1D models of the arterial network has been developed. Using this 1D method it has been found that more rigid abdominal aorta and iliac arteries together cause a greater systolic-diastolic pressure difference throughout the network modelled and a smaller variation in flow rate in the aorta. In contrast, a more rigid iliac or femoral artery has much less of an effect on the systolic-diastolic pressure difference and causes a greater variation in flow rate in the aorta. However, the 1D model used is limited in that it makes certain assumptions, in particular concerning the flow-control mechanism. A statistical method has been developed and used to analyse the AAA patient data available at Ninewells Hospital, Dundee. This small, but careful statistical study was undertaken with the objective of reducing uncertainty about the causes of AAA growth. The regression analysis of clinical factors yields that aneurysm diameter is linked to aneurysm growth and HDL cholesterol may also be linked to growth. None of the haemodynamic clinical factors such as blood pressure or ABPI have been found statistically significant with respect to aneurysm growth rate. From the regression analysis of geometric factors of the infra-renal abdominal aorta, it

has been found that aneurysm growth is linked to the mean maximum radius, the mean ellipsity and its variation along the length of the aorta, and variations of one of the centreline coordinates that has been associated with tortuosity. The reliability of some of these conclusions is questionable because of the sample size and attention has been drawn to this limitation when applicable. While these analyses have linked some of the clinical and geometric factors to aneurysm growth, they have not provided an answer to the causes of aneurysm growth.

The experimental study carried out by Peattie et al (2004) demonstrates that important shear stresses occur at the proximal and distal ends of the AAA. High shear stress is thought to damage the endothelium and generate thrombus. As suggested by the 1D simulations of stents, hardening of arteries in the lower limbs, e.g. through peripheral vascular disease, increases the instantaneous peak flow rates in the abdominal aorta, hence contributing further to shear stress. In this way, damage to the intima and then the media would cause the aneurysm to grow. Interestingly, the comparison of aneurysm models of different sizes yielded the greatest shear stress occurring in the model equivalent to a 43 mm diameter aneurysm, with lower maximum shear stresses for smaller and larger aneurysms. This is explained by the vortex that is formed in aneurysms during flow deceleration. However, wall pressure was measured several orders of magnitude greater than wall shear stresses (Peattie et al 2004).

The computational fluid dynamics modelling of a 60 mm diameter AAA before endovascular repair, and of the same AAA with an endovascular graft,

provided by Li and Kleinstreuer (2005) is a useful demonstration of the main haemodynamic characteristics. Their results clearly show the vortices at the proximal end of the AAA during flow deceleration, which are linked to higher wall shear stress, as shown in their article where areas of high wall stress are noted at the proximal and distal ends of the aneurysm. The vessel specifications used in the models indicate that while the implant of an aorto-iliac graft removes the bulge of the aneurysm, it also further increases the rigidity of the vessel from an already rigid aneurysm. If aneurysm growth is caused by wall shear stress, then the implant would inhibit shear stress and growth, the implant effectively shielding the arterial wall (Li and Kleinstreuer 2005).

Thrombus also shields the arterial wall from further possible damage caused by high shear stress. It has already been mentioned that research into the role of thrombus in aneurysms has returned contradictory results. Indeed, thrombus sac pressure appears not to be linked to AAA size or thrombus volume (Hans et al 2003). What the study of the effect of clamping the smaller arterial branches of the infra-renal aorta did show, however, is that even these smaller vessels play a role in the pressures present in the AAA lumen and thrombus. The vessels, namely the lumbar and inferior mesenteric arteries, were too small for the CT imagery that was used for the 1D model and were assumed to be small enough to be negligible. It would be possible to develop the 1D model to add permeability to the characteristics of vessels, which would avoid explicitly specifying additional arterial sections for small arteries to the 1D network. Even

these smaller vessels may have an influence on the haemodynamics in abdominal aortic aneurysms.

The deformation of collagen over time is the primary mechanism in AAA growth. Every unit area of arterial wall will grow due to collagen remodelling. Because of this it is expected that the rate of AAA growth will be proportional to aneurysm diameter. Collagen remodelling and proportionate growth may also account for the increasing tortuosity displayed by aortic aneurysms. It is the proportionate rate of growth that must be analysed and not the absolute growth rate. The requirement to consider the proportionate growth rate because of the mechanism of collagen remodelling is backed up by the shape of the statistical distribution of AAA diameters. Aneurysm diameter follows a lognormal distribution which means that the diameters must be log-transformed so that a normally distributed diameter is analysed. In this way, the AAA growth rate is the rate of change of the logarithm of aneurysm diameter which is a rate of proportionate growth. No reference has been found in the literature of analysing proportionate growth instead of absolute growth, and the results thereof reported here are new.

It is not obvious whether biochemical processes are a cause of aneurysm growth or simply a consequence thereof. If collagen remodelling was the sole mechanism of AAA growth then the aneurysm diameter would not be a predictor of proportionate growth rate. In larger aneurysms the rate of collagen remodelling is accelerated because there is none of the load bearing elastin left, while in smaller aneurysms the rate of expansion of the arterial wall is slower

because of remaining elastin. Therefore, the increase in proportionate rate of growth with aneurysm diameter may be explained by elastin degradation.

A number of geometric factors of the infra-renal aorta were found statistically significant in relation to AAA growth rate. In particular, the mean maximum radius is related to the aneurysm diameter, and both are predictors of AAA growth rate. The geometric factors provide a complex description of each aneurysm. The derivation of the terms of the lumen function, and using Fourier transforms, made each geometric factor as far as possible mathematically independent. Yet, upon further examination of each factor one by one with each other, a multitude of correlations have been found. This is not surprising as the morphology of the aneurysmal infra-renal aorta constitutes a subset of all possible combinations of the geometric factors. Computing up to the 4^{th} Fourier component provides 18 geometric factors for radius, ellipsity and centreline coordinates, and a further 10 for parabolic distortion and orientation. From these 28 factors, there are 60 significant correlations, or 26 if analysing radius, ellipsity and centreline only.

Besides the mean maximum radius, the statistical analysis of the geometric factors suggests that the ellipsity and tortuosity of the infra-renal aorta are linked to the aneurysm growth rate. Both ellipsity and tortuosity are linked to high curvature parts of the aorta, which not only have been associated with elevated aortic wall stress (Doyle et al 2009) but also affect the local blood flow dynamics. While it has been shown that risk of aneurysm rupture may be predicted by computing the AAA mechanical wall stress distribution (Doyle et

al 2011), if AAA growth rate is affected by wall shear stress, then the local haemodynamics may become significant. This may explain the additional risk factors included in the model by Helderman et al (2010) such as ischemic heart disease and peripheral arterial disease. Geometry affects the haemodynamics such that to determine the causal effect of geometry on the haemodynamics it is necessary to analyse 3D models of the infra-renal aorta and the blood flow within them. The geometric factors obtained from the abdominal scans provide the information required to create suitable 3D numerical models of AAA (Hammer et al 2009); changes in the haemodynamics due to variations in any of the geometric factors can then be examined.

While it has been shown that the geometric factors, that affect the haemodynamics of the AAA, are linked to aneurysm growth rate, none of the clinical haemodynamic factors such as blood pressure, pulse rate or Ankle-Brachial Pressure Index (ABPI) are statistically linked to AAA growth rate. This is surprising insofar as a more rigid infra-renal aorta is shown to increase the systolic-diastolic pressure difference. The vascular wall of an aneurysm, depleted of elastin, has certainly greater rigidity than a healthy abdominal aorta. The 1D haemodynamics, including the systolic-diastolic pressure difference, are a result of the summed effect of pressure and flow rate wave reflections caused by variations of vascular characteristics in the arterial network. These reflections are governed by the admittance of each vessel section. It is possible for the admittance of the abdominal aorta to remain the same if the cross-sectional area of the vessel grows with the square-root of

rigidity: indeed an aneurysm is not only a more rigid vessel it also has an increased diameter and cross-sectional area. In this way the admittance and the systolic-diastolic pressure difference remain unaffected by aneurysm growth.

The overall blood flow dynamics in the abdominal aorta does not appear to be affected by AAA growth. The significant links between geometric factors and rate of aneurysm growth suggest that it is the detail of the geometry of the AAA that affects arterial wall stress (Helderman et al 2008); this in turn may cause increased collagen remodelling, elastin degradation and aneurysm growth.

It has been suggested that high shear stress damages the vascular wall and causes aneurysm growth. The vessel characteristics at parts of the arterial network other than the infra-renal aorta affect the blood flow in the AAA and will influence the local haemodynamics, such as shear stress, close to the aneurysm wall. This supports a possible link between ABPI, an indicator of peripheral vascular disease, and AAA growth rate and could be an additional risk factor for the multi factorial prediction model suggested by Helderman et al (2008). Therefore, while the precise haemodynamic cause of aneurysm growth depends on the detail of the AAA geometry, vessel characteristics at other parts of the arterial network will influence the haemodynamics local to the AAA.

The 1D method used for simulating the blood flow in the arterial network provides a useful tool to evaluate the overall haemodynamics in different sections of arteries. The 1D program could be further used to assess other

vascular conditions that may affect the blood flow characteristics in the abdominal aorta, such as arterial stenoses, renal disease, cardiac function, etc. The 1D method may be particularly useful to specify boundary conditions to detailed 3D models of AAA, especially as the 1D program used here does not need to iterate to reach a solution at each time step.

In an attempt to strengthen the statistical analyses by making better use of the data available for each AAA patient, the development of an extension to the method of multiple linear regression is presented in this thesis. The method enables the inclusion of all measurements of a parameter taken at different times by estimating a continuous expression for the parameter with an associated weight function. A combined weight function is then derived and included in the multiple linear regression models, which translates into appropriate degrees of freedom for the regressions. In this work, the combined weight and degrees of freedom have been underestimated and further work is required to provide a suitable method for combining the weight functions of the individual parameters. Underestimating the degrees of freedom still provides robust statistical analyses by overestimating the chance for error, while taking the risk of overestimating the number of degrees of freedom would have meant risking obtaining erroneous results. One advantage of the method is to include the natural history of each AAA as estimated from the measurements rather than just the characteristics of each AAA at a single moment in time.

Vorp (2007) describes the "*fallacy*" of using AAA diameter to assess risk of rupture. In his review of AAA biomechanics, he explains the dependency of

rupture risk on AAA wall stress and strength. In particular, risk of aneurysm rupture is influenced by the precise geometry of the abdominal aorta and arterial wall stress depends on the haemodynamics close to the vascular wall. Similarly, the rate of AAA growth depends on the local detail of the haemodynamics which will be influenced by the 3D geometry. However, it is suggested that the haemodynamic conditions connected to the rate of AAA growth are different to those linked to rupture risk. Peaks in intra-luminal blood pressure will directly influence vascular wall stress and an AAA will rupture when this exceeds its strength. For AAA growth rate, it remains unclear which of shear stress or wall pressure is the cause. High shear stress has been suggested to damage the intima and generate thrombus which in turn has been linked to arterial wall weakening by hypoxia (Vorp and Vande Geest 2005); high wall pressure has also been suggested to play a role through macrophage-mediated arterial wall weakening. It is probable that both shear stress and wall pressure are causes of AAA growth.

5.2 Conclusion

The aim of this thesis is to determine what, in terms of blood flow dynamics, causes abdominal aortic aneurysms to grow.

The 1D simulations (Chapter 2) have shown that changes in characteristics of the arterial network outside the abdominal aorta affect the haemodynamics within. This however needs to be confirmed by further work on the 1D model

to better simulate all of the physiological processes involved in the vascular system.

The statistical analysis of AAA growth rate in relation to clinical factors including aneurysm diameter itself (Chapter 3) has shown that aneurysm diameter remains a significant predictor of AAA growth. Independently, the analysis also suggests that HDL cholesterol may also be linked to AAA growth. By analysing the logarithm of aneurysm diameter, the exponential growth of aneurysms is implicit in the statistical model. Despite this, the proportionate growth rate has been found to increase with increasing aneurysm diameter, i.e. over and above the rate of arterial remodelling that would be expected from the arterial wall surface area only. None of the haemodynamic factors such as blood pressure or ABPI have been linked to AAA growth.

The statistical analysis of AAA growth rate in relation to geometric factors (Chapter 4) has shown that the mean maximum radius, the mean ellipsity and the longitudinal variations of the abdominal aorta's ellipsity and centreline are linked to AAA growth.

In summary, the conlusions are, (i) aneurysm diameter is strongly predictive of aneurysm growth rate, (ii) there are significant statistical links between several geometric characteristics of the abdominal aorta and the rate of AAA growth.

In relation to the aim of the thesis, it has been found that there is insufficient evidence to show that there are haemodynamic causes to AAA growth, either

because it is the detailed blood flow dynamics within the aorta that is important, or because there have been too few patients included in the statistical analysis of the clinical and haemodynamic factors, or that indeed there are no haemodynamic causes of AAA growth.

5.3 Future Studies

Abdominal aortic aneurysm is associated with aortic wall inflammation which affects the structure of the arterial wall and consequently the vessel size (Libby 2002). Hypertension is associated with atherosclerosis, yet the causal link remains unresolved (Libby et al 2011). While the study by Leung et al (2006) demonstrates that the interaction of the AAA structure with the fluid dynamics within has little effect on arterial wall stress, progression of disease that might influence AAA growth may require estimation of wall shear stress through simulation of the haemodynamics with fluid-structure interaction (Fraser et al 2009). Diseases of the cardio-vascular system affecting the haemodynamics are still significant factors in predicting AAA growth rate even with a static structural wall stress model (Helderman et al 2010).

Given that it is the detailed fluid dynamics local to aortic aneurysms rather than the overall blood flow characteristics (e.g. flow rate, blood pressure) of the aorta that are likely to be haemodynamically linked to AAA growth, to determine what characteristics of the aortic fluid dynamics may be causes of growth it is necessary to solve 3D models of aneurysms. The flow in standardised models of aneurysms have been studied (e.g. Khanafer et al 2007;

Ekaterinaris et al 2006; Peattie et al 2004; Finol et al 2003; Finol and Amon 2001) as well as flows in patient-specific models of aneurysms directly reproduced as true geometries from medical imaging (e.g. Yamamoto et al 2006; Yeung et al 2006; Finol and Amon 2003). In each case, small numbers of geometric configurations or patient cases have been studied. Considering recent advances in computer technology, it is proposed that numerical solutions of the fluid dynamics within abdominal aortic aneurysms are obtained by varying each geometric factor in turn. In this way, starting from a standard geometry, it would be possible to simulate the haemodynamics over a range of different aneurysmal geometries. The results of these Computational Fluid Dynamics (CFD) simulations, and in particular the conditions at the vascular wall, could then be catalogued. The catalogue of CFD results could then be used to retrieve haemodynamic conditions such as shear stress and wall pressure given an AAA patient with specific aorta geometry.

This approach presents a number of foreseeable difficulties. The range of geometric parameters needs to be informed by descriptive statistics of measurements taken from medical imaging of AAA patients. The parameters that have been used for the statistical analysis of AAA growth rate against the infra-renal aorta geometry are one such set of geometric parameters measured from medical imaging. Automatic meshing of 3D models is now possible with CFD software and provides a means of rapidly creating the model to be solved from the geometric specifications (Raghavan et al 2005). To investigate the automatic meshing capability of Star-CD (CD Adapco, London), numerical

models of AAA were built (Figure 5.3.1) using the geometric parameters of 39 of the 40 AAA which geometries were analysed statistically. The CFD software has inbuilt mesh quality checks which rejected 1 of the 40 models. A further complication may be the need to model some of the biochemical processes themselves by considering the characteristics and composition of the arterial lumen wall, for example the diffusion of oxygen through thrombus (Vande Geest et al 2006; Vorp et al 1998). It has already been described how thrombus geometry can be measured in the same way as the lumen.

The systematic solving of CFD models of AAA over a range of geometries and boundary conditions could form the basis of an empirical formula that can be used to predict the rate of aneurysm growth, in a similar way as that developed by Li and Kleinstreuer (2005) for risk of rupture. Such a formula would be directly useful to the clinician for evaluating a patient's prognosis. The CFD results would indicate which geometric and haemodynamic features are linked to aneurysm growth. Furthermore, by determining the biochemistry processes that are sensitive to the haemodynamic processes linked to growth, the haemodynamic causes of AAA growth may be found.

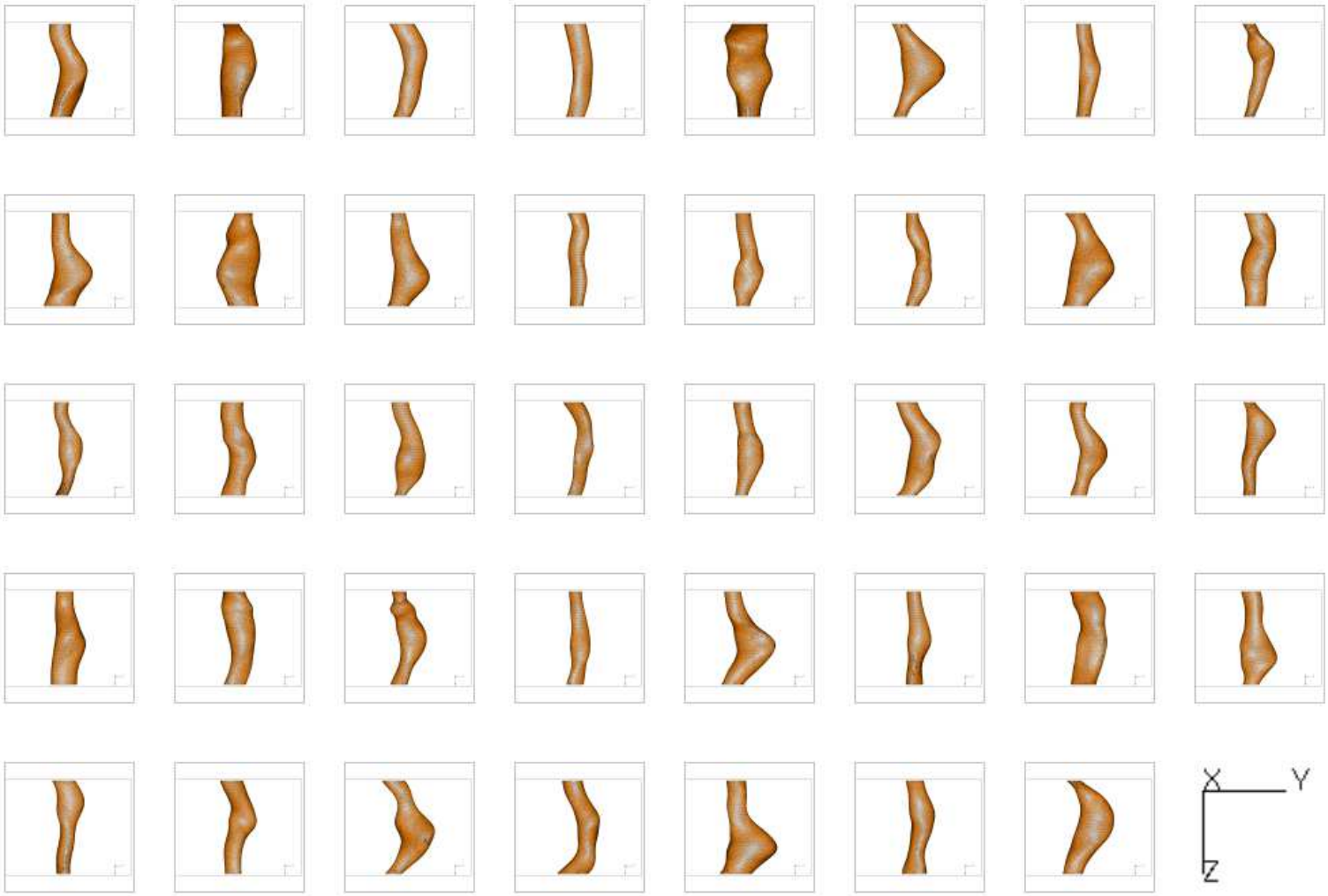

Figure 5.3.1. Numerical models of abdominal aortic aneurysm lumens of 39 AAA study patients at Ninewells Hospital, Dundee, using the automatic meshing capability of Star-CD (CD Adapco, London).

References:

Anliker (M.), Rockwell (R.L.) and Ogden (E.). Nonlinear analysis of flow pulses and shock waves in arteries; part I: derivation and properties of mathematical model. *Zeitschrift fur Angewandte Mathematik und Physik* **22** 217-246, 1971. [*§1.3, 2.1*]

Aikawa (M.), Sugiyama (S.), Hill (C.C.), Voglic (S.J.), Rabkin (E.), Fukumoto (Y.), Schoen (F.J.), Witztum (J.L.) and Libby (P.). Lipid lowering reduces oxidative stress and endothelial cell activation in rabbit atheroma. *Circulation* **106** 1390-1396, 2002. [*§1.2*]

Atabek (H.B.). Wave propagation through a viscous fluid contained in a tethered, initially stressed, orthotropic elastic tube. *Biophysical Journal* **8** 626-649, 1968. [*§2.1*]

Atabek (H.B.) and Lew (H.S.). Wave propagation through a viscous incompressible fluid contained in an initially stressed elastic tube. *Biophysical Journal* **6** 481-503, 1966. [*§2.1*]

Augst (A.D.), Ariff (B.), Thom (S.A.G.M.), Xu (X.Y.) and Hughes (A.D.). Analysis of complex flow and the relationship between blood pressure, wall shear stress, and intima-media thickness in the human carotid artery. *American Journal of Physiology Heart and Circulation Physiology* **293** H1031-H1037, 2007. [*§1.2*]

Avolio (A.P.). Multi-branched model of the human arterial system. *Medical and Biological Engineering and Computing* **18** 709-718, 1980. [*§2.1*]

Barford (N.C.). *Experimental Measurements: Precision, Error and Truth* 2nd ed. ch. 3 pp. 60-84. Wiley (Chichester) 1985. [*§3.3*]

Batchelor (G.K.). *An Introduction to Fluid Dynamics*. Cambridge University Press 1967. [*§2.2*]

Baxter (B.T.). Regarding "Use of doxycycline to decrease the growth rate of abdominal aortic aneurysms: a randomized, double-blind, placebo-controlled pilot study". *Journal of Vascular Surgery* **34** 757-758, 2001. [*§1.2*]

Baxter (B.T.), Pearce (W.H.), Waltke (E.A.), Littooy (F.N.), Hallett (J.W.), Kent (K.C.), Upchurch (G.R.), Chaikof (E.L.), Mills (J.L.), Fleckten (B.), Longo (G.M.), Lee (J.K.) and Thompson (R.W.). Prolonged administration of doxycycline in patients with small asymptomatic abdominal aortic aneurysms: report of a prospective (phase II) multicenter study. *Journal of Vascular Surgery* **36**(1) 1-12, 2002. [*§1.2, 3.1*]

Belardinelli (E.) and Cavalcanti (S.). Theoretical analysis of pressure pulse propagation in arterial vessels. *Journal of Biomechanics* **25**(11) 1337-1349, 1992. [*§2.1*]

Bengtsson (H.), Bergqvist (D.), Ekberg (O.) and Ranstam (J.). Expansion pattern and risk of rupture of abdominal aortic aneurysms that were not operated on. *European Journal of Surgery* **159**(9) 461-467, 1993. [*§3.5*]

Bergel (D.H.). The dynamic elastic properties of the arterial wall. *Journal of Physiology* **156** 458-469, 1961. [*§2.1*]

Berger (D.S.), Li (J.K.-J.), Laskey (W.K.) and Noordergraaf (A.). Repeated reflection of waves in the systemic arterial system. *American Journal of Physiology* **264**(1) H269-H281, 1993. [*§2.1*]

Berger (D.S.), Li (J.K.-J.) and Noordergraaf (A.). Arterial wave propagation phenomena, ventricular work, and power dissipation. *Annals of Biomedical Engineering* **23** 804-811, 1995. [*§2.1*]

Blanchard (J.F.). Epidemiology of abdominal aortic aneurysms. *Epidemiologic Reviews* **21**(2) 207-221, 1999. [*§1.1*]

Blanchard (J.F.), Armenian (H.K.) and Poulter Friesen (P.). Risk factors for abdominal aortic aneurysm: results of a case-control study. *American Journal of Epidemiology* **151**(6) 575-583, 2000. [*§3.1*]

Bland (M.). *An Introduction to Medical Statistics* 3rd ed. Oxford University Press 2000. [*§3.3, 3.4*]

Boerrigter (B.), Mauritz (G.-J.), Marcus (J.T.), Helderman (F.), Postmus (P.E.), Westerhof (N.) and Vonk-Noordegraaf (A.). Progressive dilatation of the main pulmonary artery is a characteristic of pulmonary arterial hypertension and is not related to changes in pressure. *Chest* **138**(6) 1395-1401, 2010. [*§1.2*]

Brady (A.R.), Brown (L.C.), Fowkes (F.G.R.), Greenhalgh (R.M.), Powell (J.T.), Ruckley (C.V.) and Thompson (S.G.). Long-term outcomes of immediate repair compared with surveillance of small abdominal aortic aneurysms. *New England Journal of Medicine* **346**(19) 1445-1452, 2002. [*§1.1*]

Brady (A.R.), Thompson (S.G.), Fowkes (F.G.R.), Greenhalgh (R.M.) and Powell (J.T.). Abdominal aortic aneurysm expansion. *Circulation* **110** 16-21, 2004. [*§1.1, 1.2, 3.5*]

Brewster (D.C.), Cronenwett (J.L.), Hallett (J.W.), Johnston (K.W.), Krupski (W.C.) and Matsumura (J.S.). Guidelines for the treatment of abdominal aortic aneurysms. *Journal of Vascular Surgery* **37**(5) 1106-1117, 2003. [*§1.1*]

Brown (L.C.) and Powell (J.T.). Risk factors for aneurysm rupture in patients kept under ultrasound surveillance. *Annals of Surgery* **230**(3) 289-297, 1999. [*§1.1*]

Brown (P.M.), Pattenden (R.), Vernooy (C.), Zelt (D.T.) and Gutelius (J.R.). Selective management of abdominal aortic aneurysms in a prospective measurement program. *Journal of Vascular Surgery* **23**(2) 213-222, 1996. [*§3.5*]

Burnette (R.R.). Computer simulation of human blood flow and vascular resistance. *Computers in Biology and Medicine* **26**(5) 363-369, 1996. [*§2.1*]

Cannon (J.A.), Van De Water (J.) and Barker (W.F.). Experience with the surgical management of 100 consecutive cases of abdominal aortic aneurysm. *American Journal of Surgery* **106** 128-143, 1963. [*§1.1, 3.1*]

Cannon Albright (L.A.), Camp (N.J.), Farnham (J.M.), MacDonald (J.), Abtin (K.) and Rowe (K.G.). A genealogical assessment of heritable predisposition to aneurysms. *Journal of Neurosurgery* **99** 637-643, 2003. [*§1.1*]

Caro (C.G.), Pedley (T.J.), Schroter (R.C.) and Seed (W.A.). *The Mechanics of the Circulation* ch. 7 pp. 86-105. Oxford University 1978. [*§1.1*]

Caro (C.G.), Pedley (T.J.), Schroter (R.C.) and Seed (W.A.). *The Mechanics of the Circulation* ch. 12 pp. 243-349. Oxford University 1978. [*§1.3*]

Chang (J.B.), Stein (T.A.), Liu (J.P.) and Dunn (M.E.). Risk factors associated with rapid growth of small abdominal aortic aneurysms. *Surgery* **121**(2) 117-122, 1997. [*§1.2, 3.5*]

Chatfield (C.). *The Analysis of Time Series* 6th ed. ch. 11 pp. 217-240. Chapman and Hall (London) 2004. [*§3.1*]

Chaudhuri (A.), Ansdell (L.E.), Grass (A.J.) and Adiseshiah (M.). Aneurysmal hypertension and its relationship to sac thrombus: a semi-qualitative analysis by experimental fluid mechanics. *European Journal of Vascular and Endovascular Surgery* **27** 305-310, 2004. [*§2.1*]

Chung (T.J.). *Computational Fluid Dynamics*. Cambridge University 2002. [*§2.1*]

Collin (J.), Araujo (L.), Walton (J.) and Lindsell (D.). Oxford screening programme for abdominal aortic aneurysm in men aged 65 to 74 years. *Lancet* **2** 613-615, 1988. [*§1.1*]

Cooney (D.O.). The dynamics of the circulatory system. *Biomedical Engineering Principles* ch. 4 pp. 69-92. Dekker (New York) 1976. [*§2.1*]

Cox (D.R.) and Lewis (P.A.W.). *The Statistical Analysis of Series of Events*. Methuen (London) 1966. [*§3.1*]

Cox (R.H.). Comparison of linearized wave propagation models for arterial blood flow analysis. *Journal of Biomechanics* **2** 251-265, 1969. [*§2.1*]

Crawford (C.M.), Hurtgen-Grace (K.), Talarico (E.) and Marley (J.). Abdominal aortic aneurysm: an illustrated narrative review. *Journal of Manipulative and Physiological Therapeutics* **26**(3) 184-195, 2003. [*§1.1*]

Darling (R.C.), Messina (C.R.), Brewster (D.C.) and Ottinger (L.W.). Autopsy study of unoperated abdominal aortic aneurysms. *Cardiovascular Surgery* **56**(3) II 161-164, 1977. [*§4.1*]

Dawson (J.), Cockerill (G.W.), Choke (E.), Belli (A.-M.), Loftus (I.) and Thompson (M.M.). Aortic aneurysms secrete interleukin-6 into the circulation. *Journal of Vascular Surgery* **45**(2) 350-356, 2007. [*§1.2*]

Deters (O.J.), Bargeron (C.B.), Mark (F.F.) and Friedman (M.H.). Measurement of wall motion and wall shear in a compliant arterial cast. *Journal of Biomechanical Engineering* **108** 355-358, 1986. [*§2.1*]

Di Martino (E.S.), Guadagni (G.), Fumero (A.), Ballerini (G.), Spirito (R.), Biglioli (P.) and Redaelli (A.). Fluid-structure interaction within realistic three-dimensional models of the aneurysmatic aorta as a guidance to assess the risk of rupture of the aneurysm. *Medical Engineering and Physics* **23**(9) 647-655, 2001. [*§2.1, 4.1*]

Diehm (N.), Schmidli (J.), Dai-Do (D.) and Baumgartner (I.). Current evidence and prospects for medical treatment of abdominal aortic aneurysms. *Vasa* **34**(4) 217-223, 2005. [*§3.5*]

Dollar (A.L.). Anatomy of the aorta. in Lindsay (J.). *Diseases of the Aorta* ch. 1 pp. 1-5. Lea and Febiger (Malvern) 1994. [*§1.1*]

Doorly (D.J.), Sherwin (S.J.), Franke (P.T.) and Peiro (J.). Vortical flow structure indentification and flow transport in arteries. *Computer Methods in Biomechanics and Biomedical Engineering* **5**(3) 261-275, 2002. [*§2.1*]

Douglas (J.F.), Gasiorek (J.M.) and Swaffield (J.A.). *Fluid Mechanics* 4th ed. ch. 21 pp. 658-707. Prentice Hall (Harlow) 2001. [*§2.2*]

Doyle (B.J.), Hoskins (P.R.) and McGloughlin (T.M.). Computational rupture predictions of AAAs: what needs to be done next? *Journal of Endovascular Therapy* **18**(2) 226-229, 2011. [*§1.2, 5.1*]

Doyle (B.J.), Callanan (A.), Burke (P.E.), Grace (P.A.), Walsh (M.T.), Vorp (D.A.) and McGloughlin (T.M.). Vessel asymmetry as an additional diagnostic tool in the assessment of abdominal aortic aneurysms. *Journal of Vascular Surgery* **49**(2) 443-454, 2009. [*§4.1, 4.2, 5.1*]

Dubost (C.), Allary (M.) and Oeconomos (N.). Resection of an aneurysm of the abdominal aorta. *Archives of Surgery* **64** 405-408, 1952. [*§1.1*]

Duclaux (V.), Gallaire (F.) and Clanet (C.). A fluid mechanical view on abdominal aortic aneurysms. *Journal of Fluid Mechanics* **664** 5-32, 2010. [*§1.2*]

Egelhoff (C.J.), Budwig (R.S.), Elger (D.F.), Khraishi (T.A.) and Johansen (K.H.). Model studies of the flow in abdominal aortic aneurysms during resting and exercise conditions. *Journal of Biomechanics* **32** 1319-1329, 1999. [*§2.1*]

Ekaterinaris (J.A.), Ioannou (C.V.) and Katsamouris (A.N.). Flow dynamics in expansions characterizing abdominal aorta aneurysms. *Annals of Vascular Surgery* **20**(3) 351-359, 2006. [*§2.1, 5.3*]

Faxon (D.P.), Fuster (V.), Libby (P.), Beckman (J.A.), Hiatt (W.R.), Thompson (R.W.), Topper (J.N.), Annex (B.H.), Rundback (J.H.), Fabunmi (R.P.), Robertson (R.M.) and Loscalzo (J.). Atherosclerotic vascular disease conference: writing group III: pathophysiology. American Heart Association Conference Proceedings. *Circulation* **109** 2617-2625, 2004. [*§1.1*]

Fillinger (M.). Who should we operate on and how do we decide: predicting rupture and survival in patients with aortic aneurysm. *Seminars in Vascular Surgery* **20**(2) 121-127, 2007. [*§4.2*]

Fillinger (M.F.), Racusin (J.), Baker (R.K.), Cronenwett (J.L.), Teutelink (A.), Schermerhorn (M.L.), Zwolak (R.M.), Powell (R.J.), Walsh (D.B.) and Rzucidlo (E.M.). Anatomic characteristics of ruptured abdominal aortic aneurysm on conventional CT scans: implications for rupture risk. *Journal of Vascular Surgery* **39**(6) 1243-1252, 2004. [*§4.2*]

Fillinger (M.F.), Raghavan (M.L.), Marra (S.P.), Cronenwett (J.L.) and Kennedy (F.E.). In vivo analysis of mechanical wall stress and abdominal aortic aneurysm rupture risk. *Journal of Vascular Surgery* **36**(3) 589-597, 2002. [*§4.1*]

Finol (E.A.) and Amon (C.H.). Blood flow in abdominal aortic aneurysms: pulsatile flow hemodynamics. *Journal of Biomechanical Engineering* **123**(5) 474-484, 2001. [*§2.1, 5.3*]

Finol (E.A.) and Amon (C.H.). Flow dynamics in anatomical models of abdominal aortic aneurysms: computational analysis of pulsatile flow. *Acta Cientifica Venezolana* **54**(1) 43-49, 2003. [*§2.1, 5.3*]

Finol (E.A.), Keyhani (K.) and Amon (C.H.). The effect of asymmetry in abdominal aortic aneurysms under physiologically realistic pulsatile flow conditions. *Journal of Biomechanical Engineering* **125**(2) 207-217, 2003. [*§2.1, 5.3*]

Fraser (K.H.), Li (M.-X.), Lee (W.T.), Easson (W.J.) and Hoskins (P.R.). Fluid-structure interaction in axially symmetric models of abdominal aortic aneurysms. *Proceedings of the Institution of Mechanical Engineers* Part H, *Journal of Engineering in Medicine* **223** 195-209, 2009. [*§5.3*]

Freestone (T.), Turner (R.J.), Coady (A.), Higman (D.J.), Greenhalgh (R.M.) and Powell (J.T.). Inflammation and matrix metalloproteinases in the enlarging abdominal aortic aneurysm. *Arteriosclerosis, Thrombosis, and Vascular Biology* **15** 1145-1151, 1995. [*§1.2*]

Fridez (P.), Rachev (A.), Meister (J.-J.), Hayashi (K.) and Stergiopulos (N.). Model of geometrical and smooth muscle tone adaptation of carotid artery subject to step change in pressure. *American Journal of Physiology Heart and Circulatory Physiology* **280** H2752-H2760, 2001. [*§1.2*]

Gadowski (G.R.), Pilcher (D.B.) and Ricci (M.A.). Abdominal aortic aneurysm expansion rate: effect of size and beta-adrenergic blockade. *Journal of Vascular Surgery* **19**(4) 727-731, 1994. [*§1.2*]

Gerrard (J.H.). An experimental test of the theory of waves in fluid-filled deformable tubes. *Journal of Fluid Mechanics* **156** 321-347, 1985. [*§2.1*]

Ghiassy (F.). A non-linear study of the systemic circulatory system. MSc Bio-Medical Engineering Science. University of Dundee 1982. [*§2.2*]

Giannoglou (G.), Giannakoulas (G.), Soulis (J.), Chatzizisis (Y.), Perdikides (T.), Melas (N.), Parcharidis (G.) and Louridas (G.). Predicting the risk of rupture of abdominal aortic aneurysms by utilizing various geometrical parameters: revisiting the diameter criterion. *Angiology* **57**(4) 487-494, 2006. [*§4.1*]

Gibson (G.A.). *Disease of the Heart and Aorta* ch. XVI pp. 828-885. Pentland (Edinburgh) 1898. [*§1.1*]

Golledge (J.), Abrokwah (J.), Shenoy (K.N.) and Armour (R.H.). Morphology of ruptured abdominal aortic aneurysms. *European Journal of Vascular and Endovascular Surgery* **18** 96-104, 1999. [*§4.2*]

Golledge (J.), Muller (J.), Shephard (N.), Clancy (P.), Smallwood (L.), Moran (C.), Dear (A.E.), Palmer (L.J.) and Norman (P.E.). Association between osteopontin and human abdominal aortic aneurysm. *Arteriosclerosis, Thrombosis and Vascular Biology* **27** 655-660, 2007. [*§1.2*]

Groen (H.C.), Gijsen (F.J.H.), van der Lugt (A.), Ferguson (M.S.), Hatsukami (T.S.), van der Steen (A.F.W.), Yuan (C.) and Wentzel (J.J.). Plaque rupture in the carotid artery is localized at the high shear stress region. *Stroke* **38** 2379-2381, 2007. [*§1.2*]

Halazun (K.J.), Bofkin (K.A.), Asthana (S.), Evans (C.), Henderson (M.) and Spark (J.I.). Hyperhomocysteinaemia is associated with the rate of abdominal aortic aneurysm expansion. *European Journal of Vascular and Endovascular Surgery* **33**(4) 391-394, 2007. [*§1.2*]

Hallett (J.W.). Management of abdominal aortic aneurysms. *Mayo Clinic Proceedings* **75**(4) 395-399, 2000. [*§1.1*]

Hammer (S.), Jeays (A.), Allan (P.L.), Hose (R.), Barber (D.), Easson (W.J.) and Hoskins (P.R.). Acquisition of 3-D arterial geometries and integration with computational fluid dynamics. *Ultrasound in Medicine and Biology* **35**(12) 2069-2083, 2009. [*§2.1, 4.1, 5.1*]

Hans (S.S.), Jareunpoon (O.), Huang (R.), Hans (B.), Bove (P.) and Zelenock (G.B.). Relationship of residual intraluminal to intrathrombotic pressure in a closed aneurysmal sac. *Journal of Vascular Surgery* **37**(5) 949-953, 2003. [*§5.1*]

Hastie (T.J.) and Tibshirani (R.J.). *Generalized Additive Models* ch. 2 pp. 9-38. Chapman and Hall (London) 1990. [*§3.3*]

Helderman (F.), Manoch (I.J.), Breeuwer (M.), Kose (U.), Schouten (O.), van Sambeek (M.R.M.), Poldermans (D.), Pattynama (P.T.M.), Wisselink (W.), van

der Steen (A.F.W.) and Krams (R.). A numerical model to predict abdominal aortic aneurysm expansion based on local wall stress and stiffness. *Medical and Biological Engineering and Computing* **46** 1121-1127, 2008. [*§1.2*]

Helderman (F.), Manoch (I.J.), Breeuwer (M.), Kose (U.), Boersma (H.), van Sambeek (M.R.H.M.), Pattynama (P.M.T.), Schouten (O.), Poldermans (D.), Wisselink (W.), van der Steen (A.F.W.) and Krams (R.). Predicting patient-specific expansion of abdominal aortic aneurysms. *European Journal of Vascular and Endovascular Surgery* **40** 47-53, 2010. [*§1.2, 5.1, 5.3*]

Henney (A.M.), Adiseshiah (M.), Poulter (N.), MacSweeney (S.T.R.), Greenhalgh (R.M.) and Powell (J.T.). Abdominal aortic aneurysm. *Lancet* **341**(8839) 215-220, 1993. [*§1.1*]

Holdsworth (J.D.). Screening for abdominal aortic aneurysm in Northumberland. *British Journal of Surgery* **81** 710-712, 1994. [*§1.1*]

Horsten (J.N.A.M.), Van Steenhoven (A.A.) and Van Dongen (M.E.H.). Linear propagation of pulsatile waves in viscoelastic tubes. *Journal of Biomechanics* **22**(5) 477-484, 1989. [*§2.1*]

Hoshina (K.), Miyata (T.), Hatakeyama (T.), Shigematsu (H.) and Nagawa (H.). Hemodynamic influence of peripheral vascular occlusive disease on abdominal aortic aneurysms. *International Angiology* **23**(4) 373-378, 2004. [*§1.3*]

Hoskins (P.R.). Physical properties of tissues relevant to arterial ultrasound imaging and blood velocity measurement. *Ultrasound in Medicine and Biology* **33**(10) 1527-1539, 2007. [*§2.1, 2.3*]

Hoskins (P.R.) and Hardman (D.). Three-dimensional imaging and computational modelling for estimation of wall stresses in arteries. *British Journal of Radiology* **82** S3-S17, 2009. [*§1.2*]

Hua (J.) and Mower (W.R.). Simple geometric characteristics fail to reliably predict abdominal aortic aneurysm wall stresses. *Journal of Vascular Surgery* **34**(2) 308-315, 2001. [*§4.1*]

Humphrey (J.D.). *Cardiovascular Solid Mechanics* 7.1.2 pp. 254-259. Springer (New York) 2002. [*§1.1*]

Humphrey (J.D.). *Cardiovascular Solid Mechanics* 9.1.2 pp. 505-511. Springer (New York) 2002. [*§3.3*]

Jamrozik (K.), Norman (P.E.), Spencer (C.A.), Parsons (R.W.), Tuohy (R.), Lawrence-Brown (M.M.) and Dickinson (J.A.). Screening for abdominal aortic aneurysm: lessons from a population-based study. *Medical Journal of Australia* **173** 345-350, 2000. [*§1.1, 3.1*]

Jones (H.J.S.), Ibrahim (A.E.K.), Hoskins (C.) and Derodra (J.K.). Aortic aneurysm screening in general practice. *Lancet* **348** 1320, 1996. [*§1.1*]

Jones (T.E.). Computer modelling of the cardiovascular system. A thesis submitted in part fulfilment of the requirements of the degree of MSc in Biomedical Engineering Science. University of Dundee 1985. [*§2.2*]

Jordan (D.W.) and Smith (P.). *Mathematical Techniques* ch. 24 pp. 409-426. Oxford University Press 1994. [*§4.1*]

Jorgensen (L.), Singh (K.), Rosvold Bernsten (G.K.) and Jacobsen (B.K.). A population-based study of the prevalence of abdominal aortic aneurysms in relation to bone mineral density. *American Journal of Epidemiology* **159**(10) 945-949, 2004. [*§1.1*]

Kanai (H.), Hasegawa (H.), Ichiki (M.), Tezuka (F.) and Koiwa (Y.). Elasticity imaging of atheroma with transcutaneous ultrasound. *Circulation* **107** 3018-3021, 2003. [*§2.1*]

Karamanoglu (M.), Gallagher (D.E.), Avolio (A.P.) and O'Rourke (M.F.). Functional origin of reflected pressure waves in a multibranched model of the human arterial system. *American Journal of Physiology* **267** H1681-H1688, 1994. [*§2.1*]

Kato (K.), Ishiguchi (T.), Maruyama (K.), Naganawa (S.) and Ishigaki (T.). Accuracy of plastic replica of aortic aneurysm using 3D-CT data for transluminal stent-grafting: experimental and clinical evaluation. *Journal of Computer Assisted Tomography* **25**(2) 300-304, 2001. [*§2.1*]

Katz (D.A.), Littenberg (B.) and Cronenwett (J.L.). Management of small abdominal aortic aneurysms. *Journal of the American Medical Association* **268**(19) 2678-2686, 1992. [*§1.1*]

Kent (K.C.) and Boyce (S.W.). Aneurysms of the aorta. in Lindsay (J.). *Diseases of the Aorta* ch. 8 pp. 109-125. Lea and Febiger (Malvern) 1994. [*§1.1*]

Kent (K.C.), Boyce (S.W.) and Skillman (J.J.). Surgical principles for operative treatment of aortic aneurysms. in Lindsay (J.). *Diseases of the Aorta* ch. 16 pp. 285-297. Lea and Febiger (Malvern) 1994b. [*§1.1*]

Khanafer (K.M.), Bull (J.L.), Upchurch (G.R.) and Berguer (R.). Turbulence significantly increases pressure and fluid shear stress in an aortic aneurysm model under resting and exercise flow conditions. *Annals of Vascular Surgery* **21**(1) 67-74, 2007. [*§5.3*]

Kinlay (S.), Libby (P.) and Ganz (P.). Endothelial function and coronary artery disease. *Current Opinion in Lipidology* **12** 383-389, 2001. [*§1.2*]

Kleinstreuer (C.) and Li (Z.). Analysis and computer program for rupture-risk prediction of abdominal aortic aneurysms. *Biomedical Engineering Online* **5** 19, 2006. [*§1.1*]

Kokoska (S.) and Nevison (C.). *Statistical Tables and Formulae*. Springer-Verlag (New York) 1989. [*§3.3, 3.4*]

Kornet (L.), Lambregts (J.), Hoeks (A.P.G.) and Reneman (R.S.). Differences in near-wall shear rate in the carotid artery within subjects are associated with

different intima-media thicknesses. *Arteriosclerosis, Thrombosis, and Vascular Biology* **18** 1877-1884, 1998. [*§1.2*]

Kornet (L.), Hoeks (A.P.G.), Lambregts (J.) and Reneman (R.S.). In the femoral artery bifurcation, differences in mean wall shear stress within subjects are associated with different intima-media thicknesses. *Arteriosclerosis, Thrombosis, and Vascular Biology* **19** 2933-2939, 1999. [*§1.2*]

Krohn (C.D.), Kullmann (G.), Kvernebo (K.), Rosen (L.) and Kroese (A.). Ultrasonographic screening for abdominal aortic aneurysm. *European Journal of Surgery* **158** 527-530, 1992. [*§1.1*]

Ku (D.N.). Blood flow in arteries. *Annual Review of Fluid Mechanics* **29** 399-434, 1997. [*§2.1*]

Kuivaniemi (H.), Kyo (Y.), Lenk (G.) and Tromp (G.). Genome-wide approach to finding abdominal aortic aneurysm susceptibility genes in humans. *Annals of the New York Academy of Sciences* **1085** 270-281, 2006. [*§1.1*]

Kuivaniemi (H.), Shibamura (H.), Arthur (C.), Berguer (R.), Cole (C.W.), Juvonen (T.), Kline (R.A.), Limet (R.), MacKean (G.), Norrgard (O.), Pals (G.), Powell (J.T.), Rainio (P.), Sakalihasan (N.), van Vlijmen-van Keulen (C.), Verloes (A.) and Tromp (G.). Familial abdominal aortic aneurysms: collection of 233 multiplex families. *Journal of Vascular Surgery* **37**(2) 340-345, 2003. [*§1.1*]

Lasheras (J.C.). Haemodynamic stresses and the onset and progression of vascular diseases. *Journal of Fluid Mechanics* **664** 1-4, 2010. [*§1.2*]

Lederle (F.A.), Johnson (G.R.), Wilson (S.E.), Ballard (D.J.), Jordan (W.D.), Blebea (J.), Littooy (F.N.), Freischlag (J.A.), Bandyk (D.), Rapp (J.H.) and Salam (A.A.). Rupture rate of large abdominal aortic aneurysms in patients refusing or unfit for elective repair. *Journal of the American Medical Association* **287**(22) 2968-2972, 2002. [*§1.1, 3.5*]

Lermusiaux (P.), Leroux (C.), Tasse (J.C.), Castellani (L.) and Martinez (R.). Aortic aneurysm: construction of a life-size model by rapid prototyping. *Annals of Vascular Surgery* **15**(2) 131-135, 2001. [*§2.1*]

Leung (J.H.), Wright (A.R.), Cheshire (N.), Crane (J.), Thom (S.A.), Hughes (A.D.) and Xu (Y.). Fluid structure interaction of patient specific abdominal aortic aneurysms: a comparison with solid stress models. *Biomedical Engineering Online* **5** 33, 2006. [*§2.1, 4.1, 5.3*]

Leuprecht (A.) and Perktold (K.). Computer simulation of non-Newtonian effects on blood flow in large arteries. *Computer Methods in Biomechanics and Biomedical Engineering* **4** 149-163, 2001. [*§2.1*]

Li (Z.) and Kleinstreuer (C.). A new wall stress equation for aneurysm-rupture prediction. *Annals of Biomedical Engineering* **33**(2) 209-213, 2005. [*§5.3*]

Li (Z.) and Kleinstreuer (C.). Blood flow and structure interactions in a stented abdominal aortic aneurysm model. *Medical Engineering and Physics* **27** 369-382, 2005. [*§5.1*]

Li (Z.) and Kleinstreuer (C.). Effect of blood flow and vessel geometry on wall stress and rupture risk of abdominal aortic aneurysms. *Journal of Medical Engineering and Technology* **30**(2) 283-297, 2006. [*§4.1*]

Libby (P.), Aikawa (M.), Kinlay (S.), Selwyn (A.) and Ganz (P.). Lipid lowering improves endothelial functions. *International Journal of Cardiology* **74** S3-S10, 2000. [*§1.2*]

Libby (P.). Inflammation in atherosclerosis. *Nature* **420** 868-874, 2002. [*§1.2, 5.3*]

Libby (P.), Ridker (P.M.) and Hansson (G.K.). Progress and challenges in translating the biology of atherosclerosis. *Nature* **473** 317-325, 2011. [*§1.2, 5.3*]

Liepsch (D.) and Moravec (S.). Pulsatile flow of non-Newtonian fluid in distensible models of human arteries. *Biorheology* **21** 571-586, 1984. [*§2.1*]

Lindholt (J.S.), Ashton (H.A.), Heickendorff (L.) and Scott (R.A.P.). Serum elastin peptides in the preoperative evaluation of abdominal aortic aneurysms. *European Journal of Vascular and Endovascular Surgery* **22** 546-550, 2001. [*§3.5*]

Lindholt (J.S.), Heegaard (N.H.H.), Vammen (S.), Fasting (H.), Henneberg (E.W.) and Heickendorff (L.). Smoking, but not lipids, lipoprotein (a) and antibodies against oxidised LDL, is correlated to the expansion of abdominal aortic aneurysms. *European Journal of Vascular and Endovascular Surgery* **21** 52-56, 2001. [*§1.2*]

Lindholt (J.S.), Heickendorff (L.), Antonsen (S.), Fasting (H.) and Henneberg (E.W.). Natural history of abdominal aortic aneurysm with and without coexisting chronic obstructive pulmonary disease. *Journal of Vascular Surgery* **28**(2) 226-233, 1998. [*§1.2, 3.5*]

Lindholt (J.S.), Jorgensen (B.), Klitgaard (N.A.) and Henneberg (E.W.). Systemic levels of cotinine and elastase, but not pulmonary function, are associated with the progression of small abdominal aortic aneurysms. *European Journal of Vascular and Endovascular Surgery* **26** 418-422, 2003. [*§1.2*]

Lindholt (J.S.), Juul (S.), Fasting (H.) and Henneberg (E.W.). Preliminary ten year results from a randomised single centre mass screening trial for abdominal aortic aneurysm. *European Journal of Vascular and Endovascular Surgery* **32** 608-614, 2006. [*§1.1*]

Ling (S.C.) and Atabek (H.B.). A nonlinear analysis of pulsatile flow in arteries. *Journal of Fluid Mechanics* **55**(3) 493-511, 1972. [*§2.1*]

Loh (C.S.), Stevenson (I.M.), Wu (A.V.O.) and Eyes (B.). Ultrasound scan screening for abdominal aortic aneurysm. *British Journal of Surgery* **76** 417, 1989. [*§1.1*]

Lou (Z.) and Yang (W.-J.). Biofluid dynamics at arterial bifurcations. *Critical Reviews in Biomedical Engineering* **19**(6) 455-493, 1992. [*§2.1*]

MacSweeney (S.T.R.). Mechanical properties of abdominal aortic aneurysm and prediction of risk of rupture. *Cardiovascular Surgery* **7**(2) 158-159, 1999. [*§2.4*]

MacSweeney (S.T.R.), Powell (J.T.) and Greenhalgh (R.M.). Pathogenesis of abdominal aortic aneurysm. *British Journal of Surgery* **81** 935-941, 1994. [*§1.1*]

Marques (P.F.), Oliveira (M.E.C.), Franca (A.S.) and Pinotti (M.). Modeling and simulation of pulsatile blood flow with a physiologic wave pattern. *Artificial Organs* **27**(5) 478-485, 2003. [*§2.1*]

Masuda (H.), Zhuang (Y.-J.), Singh (T.M.), Kawamura (K.), Murakami (M.), Zarins (C.K.) and Glagov (S.). Adaptive remodeling of internal elastic lamina and endothelial lining during flow-induced arterial enlargement. *Arteriosclerosis, Thrombosis, and Vascular Biology* **19** 2298-2307, 1999. [*§1.2*]

McCleary (A.J.) and Mahomed (A.). *Lancet* **353**(9150) 408, 1999. [*§1.1*]

Mirsky (I.). Wave propagation in a viscous fluid contained in an orthotropic elastic tube. *Biophysical Journal* **7** 165-186, 1967. [*§2.1*]

Mosorin (M.), Juvonen (J.), Biancari (F.), Satta (J.), Surcel (H.-M.), Leinonen (M.), Saikku (P.) and Juvonen (T.). Use of doxycycline to decrease the growth rate of abdominal aortic aneurysms: a randomized, double-blind, placebo-controlled pilot study. *Journal of Vascular Surgery* **34**(4) 606-610, 2001. [*§1.2, 3.1*]

Mower (W.R.) and Quinones (W.J.). Regarding "Thrombus within an aortic aneurysm does not reduce pressure on the aneurysm wall". *Journal of Vascular Surgery* **33**(3) 660-661, 2001. [*§4.1*]

Nassiet (F.), Perrinauld (J.-C.) and Rivoallan (L.). *Mathematiques Term S. Dimatheme* ch. 1 p. 8. Didier (Paris) 1994. [*§2.2*]

Newman (A.B.), Arnold (A.M.), Burke (G.L.), O'Leary (D.H.) and Manolio (T.A.). Cardiovascular disease and mortality in older adults with small abdominal aortic aneurysms detected by ultrasonography: the cardiovascular health study. *Annals of Internal Medicine* **134**(3) 182-190, 2001. [*§1.1*]

Nicholls (S.C.), Gardner (J.B.), Meissner (M.H.) and Johansen (K.H.). Rupture in small abdominal aortic aneurysms. *Journal of Vascular Surgery* **28**(5) 884-888, 1998. [*§1.1*]

Norman (P.E.), Jamrozik (K.), Lawrence-Brown (M.M.), Le (M.T.Q.), Spencer (C.A.), Tuohy (R.J.), Parsons (R.W.) and Dickinson (J.A.). Population based randomised controlled trial on impact of screening on mortality from abdominal aortic aneurysm. *British Medical Journal* **329** 1259, 2004. [*§3.1*]

Ogata (T.), Shibamura (H.), Tromp (G.), Sinha (M.), Goddard (K.A.B.), Sakalihasan (N.), Limet (R.), MacKlean (G.L.), Arthur (C.), Sueda (T.), Land (S.) and Kuivaniemi (H.). Genetic analysis of polymorphisms in biologically relevant candidate genes in patients with abdominal aortic aneurysms. *Journal of Vascular Surgery* **41**(6) 1036-1042, 2005. [*§1.1*]

Ouriel (K.), Green (R.M.), Donayre (C.), Shortell (C.K.), Elliott (J.) and DeWeese (J.A.). An evaluation of new methods of expressing aortic aneurysm size: relationship to rupture. *Journal of Vascular Surgery* **15**(1) 12-20, 1992. [*§1.1, 4.2*]

Pan (J.-H.), Lindholt (J.S.), Sukhova (G.K.), Baugh (J.A.), Henneberg (E.W.), Bucala (R.), Donnelly (S.C.), Libby (P.), Metz (C.) and Shi (G.-P.). Macrophage

migration inhibitory factor is associated with aneurysmal expansion. *Journal of Vascular Surgery* **37**(3) 628-635, 2003. [*§1.2*]

Papaharilaou (Y.), Ekaterinaris (J.A.), Manousaki (E.) and Katsamouris (A.N.). A decoupled fluid structure approach for estimating wall stress in abdominal aortic aneurysms. *Journal of Biomechanics* **40** 367-377, 2007. [*§2.1, 4.2*]

Parker (K.H.) and Jones (C.J.H.). Forward and backward running waves in the arteries: analysis using the method of characteristics. J*ournal of Biomechanical Engineering* **112** 322-326, 1990. [*§2.1*]

Peattie (R.A.), Riehle (T.J.) and Bluth (E.I.). Pulsatile flow in fusiform models of abdominal aortic aneurysms: flow fields, velocity patterns and flow-induced wall stresses. *Journal of Biomechanical Engineering* **126**(4) 438-446, 2004. [*§2.1, 5.1, 5.3*]

Pedrizzetti (G.), Domenichini (F.), Tortoriello (A.) and Zovatto (L.). Pulsatile flow inside moderately elastic arteries, its modelling and effects of elasticity. *Computer Methods in Biomechanics and Biomedical Engineering* **5**(3) 219-231, 2002. [*§2.1*]

Peeters (A.C.), van Landeghem (B.A.), Graafsma (S.J.), Kranendonk (S.E.), Hermus (A.R.), Blom (H.J.) and den Heijer (M.). Low vitamin B6, and not plasma homocysteine concentration, as risk factor for abdominal aortic aneurysm: a retrospective case-control study. *Journal of Vascular Surgery* **45**(4) 701-705, 2007. [*§3.1*]

Petersen (E.), Wagberg (F.) and Angquist (K.-A.). Serum concentrations of elastin-derived peptides in patients with specific manifestations of atherosclerotic disease. *European Journal of Vascular and Endovascular Surgery* **24** 440-444, 2002. [*§3.5*]

Pleumeekers (H.J.C.M.), Hoes (A.W.), van der Does (E.), van Urk (H.), Hofman (A.), de Jong (P.T.V.M.) and Grobbee (D.E.). Aneurysms of the abdominal aorta in older adults. *American Journal of Epidemiology* **142** 1291-1299, 1995. [*§1.1*]

Powell (J.T.). Early surgery did not reduce 6-year mortality in patients with small abdominal aortic aneurysms. *American College of Physicians Journal Club* **130**(3) 73, 1999. [*§1.1*]

Powell (J.T.) et al. Mortality results for randomised controlled trial of early elective surgery or ultrasonographic surveillance for small abdominal aortic aneurysms. *Lancet* **352**(9141) 1649-1655, 1998. [*§1.1*]

Pretre (R.) and Turina (M.I.). Facts, at last, on management of small infrarenal aortic aneurysms. *Lancet* **352**(9141) 1642-1643, 1998. [*§1.1*]

Raghavan (M.L.), Fillinger (M.F.), Marra (S.P.), Naegelein (B.P.) and Kennedy (F.E.). Automated methodology for determination of stress distribution in human abdominal aortic aneurysm. *Journal of Biomechanical Engineering* **127**(5) 868-871, 2005. [*§2.4, 5.3*]

Raghavan (M.L.), Vorp (D.A.), Federle (M.P.), Makaroun (M.S.) and Webster (M.W.). Wall stress distribution on three-dimensionally reconstructed models of human aortic aneurysms. *Journal of Vascular Surgery* **31**(4) 760-769, 2000. [*§4.1*]

Reed (W.W.), Hallett (J.W.), Damiano (M.A.) and Ballard (D.J.). Learning from the last ultrasound. *Archives of Internal Medicine* **157**(18) 2064-2068, 1997. [*§3.1*]

Rutten (M.C.M.). Fluid-solid interaction in large arteries ch. 2 pp. 9-24. Proefschrift ter verkrijging van de graad van doctor. Technische Universiteit Eindhoven 1998. [*§1.1*]

Sacks (M.S.), Vorp (D.A.), Raghavan (M.L.), Federle (M.P.) and Webster (M.W.). In vivo three-dimensional surface geometry of abdominal aortic aneurysms. *Annals of Biomedical Engineering* **27**(4) 469-479, 1999. [*§4.2*]

Sakalihasan (N.), Van Damme (H.), Gomez (P.), Rigo (P.), Lapiere (C.M.), Nusgens (B.) and Limet (R.). Positron Emission Tomography (PET) evaluation of Abdominal Aortic Aneurysm (AAA). *European Journal of Vascular and Endovascular Surgery* **23** 431-436, 2002. [*§2.4*]

Salo (J.A.), Soisalon-Soininen (S.), Bondestam (S.) and Mattila (P.S.). Familial occurrence of abdominal aortic aneurysm. *Annals of Internal Medicine* **130**(8) 637-342, 1999. [*§1.1*]

Sandford (R.M.), Brown (M.J.), London (N.J.) and Sayers (R.D.). The genetic basis of abdominal aortic aneurysms: a review. *European Journal of Vascular and Endovascular Surgery* **33** 381-390, 2007. [*§1.1*]

Satoh (K.), Tsukamoto (M.), Shindoh (M.), Totsuka (Y.), Oda (T.) and Matsumoto (K.-I.). Increased expression of tenascin-X in thoracic and abdominal aortic aneurysm tissues. *Biological and Pharmaceutical Bulletin* **33**(11) 1898-1902, 2010. [*§1.2*]

Satta (J.), Juvonen (T.), Haukipuro (K.), Juvonen (M.) and Kairaluoma (M.I.). Increased turnover of collagen in abdominal aortic aneurysms, demonstrated by measuring the concentration of the aminoterminal propeptide of type III procollagen in peripheral and aortal blood samples. *Journal of Vascular Surgery* **22**(2) 155-160, 1995. [*§1.2*]

Schewe (C.K.), Schweikart (H.P.), Hammel (G.), Spengel (F.A.), Zollner (N.) and Zoller (W.G.). Influence of selective management on the prognosis and the risk of rupture of abdominal aortic aneurysms. *Clinical Investigator* **72**(8) 585-591, 1994. [*§1.1, 3.5*]

Schulz (S.), Bauernschmitt (R.), Albers (J.), Riesenberg (A.), Schwarzhaupt (A.), Vahl (C.F.) and Kiencke (U.). A mathematical high time resolution model of the arterial system under extracorporeal circulation. *Biomedical Sciences Instrumentation* **33** 406-411, 1997. [*§2.1*]

Schurink (G.W.H.), van Baalen (J.M.), Visser (M.J.T.) and van Bockel (J.H.). Thrombus within an aortic aneurysm does not reduce pressure on the aneurysm wall. *Journal of Vascular Surgery* **31**(3) 501-506, 2000. [*§4.1*]

Scott (R.A.P.). The Multicentre Aneurysm Screening Study (MASS) into the effect of abdominal aortic aneurysm screening on mortality in men: a randomised controlled trial. *Lancet* **360** 1531-1539, 2002. [*§1.1*]

Scott (R.A.P.), Wilson (N.M.), Ashton (H.A.) and Kay (D.N.). Influence of screening on the incidence of ruptured abdominal aortic aneurysm: 5-year results of a randomized controlled study. *British Journal of Surgery* **82** 1066-1070, 1995. [*§1.1*]

Scotti (C.M.), Shkolnik (A.D.), Muluk (S.C.) and Finol (E.A.). Fluid-structure interaction in abdominal aortic aneurysms: effects of asymmetry and wall thickness. *Biomedical Engineering Online* **4** 64, 2005. [*§2.1*]

Segers (D.), Helderman (F.), Cheng (C.), van Damme (L.C.A.), Tempel (D.), Boersma (E.), Serruys (P.W.), de Crom (R.), van der Steen (A.F.W.), Holvoet (P.) and Krams (R.). Gelatinolytic activity in atherosclerotic plaques is highly localized and is associated with both macrophages and smooth muscle cells in vivo. *Circulation* **115** 609-616, 2007. [*§1.2*]

Shapiro (A.H.). *The Dynamics and Thermodynamics of Compressible Fluid Flow* vol. 1 app. A pp. 595-609. Wiley (United States of America) 1953. [*§2.1*]

Sherwin (S.J.), Franke (V.), Peiro (J.) and Parker (K.). One dimensional modelling of a vascular network in space-time variables. *Journal of Engineering Mathematics* **47** 217-250, 2003. [*§2.1, 2.2*]

Siegel (C.L.), Cohan (R.H.), Korobkin (M.), Alpern (M.B.), Courneya (D.L.) and Leder (R.A.). Abdominal aortic aneurysm morphology. *A.J.R.* **163** 1123-1129, 1994. [*§4.2*]

Singh (K.), Bonaa (K.H.), Jacobsen (B.K.), Bjork (L.) and Solberg (S.). Prevalence of and risk factors for abdominal aortic aneurysms in a population-based study. *American Journal of Epidemiology* **154**(3) 236-244, 2001. [*§1.1, 3.1*]

Skalak (R.). Synthesis of a complete circulation. in Bergel (ed.) *Cardiovascular Fluid Dynamics* vol. 2 ch. 19 pp. 341-376. Academic Press (London) 1972. [*§2.1*]

Skalak (R.), Ozkaya, (N.) and Skalak (T.C.). Biofluid mechanics. *Annual Review of Fluid Mechanics* **21** 167-204, 1989. [*§2.1*]

Smith (F.C.T.), Grimshaw (G.M.), Paterson (I.S.), Shearman (C.P.) and Hamer (J.D.). Ultrasonographic screening for abdominal aortic aneurysm in an urban community. *British Journal of Surgery* **80**(11) 1406-1409, 1993. [*§1.1*]

Sprent (P.). *Models in Regression*. Methuen (London) 1969. [*§3.3*]

Sprent (P.) and Smeeton (N.C.). *Applied Nonparametric Statistical Methods* ch. 8 pp. 274-309. Chapman and Hall (Boca Raton) 2001. [*§3.3*]

Steinman (D.A.), Milner (J.S.), Norley (C.J.), Lownie (S.P.) and Holdsworth (D.W.). Image-based computational simulation of flow dynamics in a giant

intracranial aneurysm. *American Journal of Neuroradiology* **24** 559-566, 2003. [*§2.1*]

Steinman (D.A.), Vorp (D.A.) and Ethier (C.R.). Computational modeling of arterial biomechanics: insights into pathogenesis and treatment of vascular disease. *Journal of Vascular Surgery* **37**(5) 1118-1128, 2003. [*§2.1*]

Stergiopulos (N.), Young (D.F.) and Rogge (T.R.). Numerical study of pressure and flow propagation in arteries. *Biomedical Sciences Instrumentation* **27** 93-104, 1991. [*§2.1*]

Stergiopulos (N.), Young (D.F.) and Rogge (T.R.). Computer simulation of arterial flow with applications to arterial and aortic stenoses. *Journal of Biomechanics* **25**(12) 1477-1488, 1992. [*§2.3*]

Stroev (P.V.), Hoskins (P.R.) and Easson (W.J.). Distribution of wall shear rate throughout the arterial tree: a case study. *Atherosclerosis* **191** 276-280, 2007. [*§1.2*]

Suda (M.), Eder (O.J.), Kunsch (B.), Magometschnigg (D.) and Magometschnigg (H.). Preoperative assessment and prediction of postoperative results in an artificial arterial network using computer simulation. *Computer Methods and Programs in Biomedicine* **41** 77-87, 1993. [*§2.1*]

Swedenborg (J.) and Eriksson (P.). The intraluminal thrombus as a source of proteolytic activity. *Annals of the New York Academy of Sciences* **1085** 133-138, 2006. [*§1.2*]

Thompson (R.W.) and Baxter (B.T.). MMP inhibition in abdominal aortic aneurysms. *Annals of the New York Academy of Science* **878** 159-178, 1999. [*§3.1*]

Thompson (R.W.), Geraghty (P.J.) and Lee (J.K.). Abdominal aortic aneurysms: basic mechanisms and clinical implications. *Current Problems in Surgery* **39**(2) 110-230, 2002. [*§1.1*]

Tilson (M.D.) and Ro (C.Y.). The candidate gene approach to susceptibility for abdominal aortic aneurysm. *Annals of the New York Academy of Sciences* **1085** 282-290, 2006. [*§1.1*]

Treska (V.), Wenham (P.W.), Valenta (J.), Topolcan (O.) and Pecen (L.). Plasma endothelin levels in patients with abdominal aortic aneurysms. *European Journal of Vascular and Endovascular Surgery* **17** 424-428, 1999. [*§1.2*]

Vande Geest (J.P.), Simon (B.R.) and Mortazavi (A.). Toward a model for local drug delivery in abdominal aortic aneurysms. *Annals of the New York Academy of Sciences* **1085** 396-399, 2006. [*§5.3*]

Vardulaki (K.A.), Prevost (T.C.), Walker (N.M.), Day (N.E.), Wilmink (A.B.M.), Quick (C.R.G.), Ashton (H.A.) and Scott (R.A.P.). Growth rates and risk of rupture of abdominal aortic aneurysms. *British Journal of Surgery* **85** 1674-1680, 1998. [*§1.1*]

Vardy (A.). *Fluid Principles* ch. 7 pp. 179-214. McGraw-Hill (Maidenhead) 1990. [*§2.2*]

Vazquez (C.), Sakalihasan (N.), D'Harcour (J.-B.) and Limet (R.). Routine ultrasound screening for abdominal aortic aneurysm among 65- and 75-year-old men in a city of 200,000 inhabitants. *Annals of Vascular Surgery* **12**(6) 544-549, 1998. [*§1.1*]

Vega de Ceniga (M.), Gomez (R.), Estallo (L.), Rodriguez (L.), Baquer (M.) and Barba (A.). Growth rate and associated factors in small abdominal aortic aneurysms. *European Journal of Vascular and Endovascular Surgery* **31**(3) 231-236, 2006. [*§1.2*]

Venkatasubramaniam (A.K.), Fagan (M.J.), Mehta (T.), Mylankal (K.J.), Ray (B.), Kuhan (G.), Chetter (I.C.) and McCollum (P.T.). A comparative study of aortic wall stress using finite element analysis for ruptured and non-ruptured abdominal aortic aneurysms. *European Journal of Vascular and Endovascular Surgery* **28**(2) 168-176, 2004. [*§4.1*]

Versteeg (H.K.) and Malalasekera (W.). *An Introduction to Computational Fluid Dynamics - The Finite Volume Method* ch. 2 pp. 10-40. Prentice Hall (Harlow) 1995. [*§2.1*]

Vorp (D.A.). Biomechanics of abdominal aortic aneurysm. *Journal of Biomechanics* **40** 1887-1902, 2007. [*§4.2, 5.1*]

Vorp (D.A.) and Vande Geest (J.P.). Biomechanical determinants of abdominal aortic aneurysm rupture. *Arteriosclerosis, Thrombosis, and Vascular Biology* **25** 1558-1566, 2005. [*§5.1*]

Vorp (D.A.), Wang (D.H.J.), Webster (M.W.) and Federspiel (W.J.). Effect of intraluminal thrombus thickness and bulge diameter on the oxygen diffusion in abdominal aortic aneurysm. *Journal of Biomechanical Engineering* **120**(5) 579-583, 1998. [*§5.3*]

Wang (J.J.) and Parker (K.H.). Wave propagation in a model of the arterial circulation. *Journal of Biomechanics* **37** 457-470, 2004. [*§2.1, 2.3*]

Wanhainen (A.), Bergqvist (D.), Boman (K.), Nilsson (T.K.), Rutegard (J.) and Bjorck (M.). Risk factors associated with abdominal aortic aneurysm: a population-based study with historical and current data. *Journal of Vascular Surgery* **41**(3) 390-396, 2005. [*§3.1*]

Wanhainen (A.), Bjorck (M.), Boman (K.), Rutegard (J.) and Bergqvist (D.). Influence of diagnostic criteria on the prevalence of abdominal aortic aneurysm. *Journal of Vascular Surgery* **34**(2) 229-235, 2001. [*§1.1*]

Watson (G.N.). *A Treatise on the Theory of Bessel Functions* 2nd ed. Cambridge University Press 1944. [*§2.1*]

Westerhof (N.), Bosman (F.), De Vries (C.J.) and Noordergraaf (A.). Analog studies of the human systemic arterial tree. *Journal of Biomechanics* **2** 121-143, 1969. [*§2.3*].

Wilmink (A.B.M.) and Quick (C.R.G.). Epidemiology and potential for prevention of abdominal aortic aneurysm. *British Journal of Surgery* **85** 155-162, 1998. [*§1.1*]

Wilmink (T.B.M.), Quick (C.R.G.) and Day (N.E.). The association between cigarette smoking and abdominal aortic aneurysms. *Journal of Vascular Surgery* **30**(6) 1099-1105, 1999. [*§1.2*]

Wilson (K.), Whyman (M.), Hoskins (P.), Lee (A.J.), Bradbury (A.W.), Fowkes (F.G.R.) and Ruckley (C.V.). The relationship between abdominal aortic aneurysm wall compliance, maximum diameter and growth rate. *Cardiovascular Surgery* **7**(2) 208-213, 1999. [*§1.2, 3.5*]

Witzig (K.). Uber erzwungene Wellenbewegungen zaher, inkompressibler Flussigkeiten in elastischen Rohren. Inaugural-Dissertation der hohen philosophischen Fakultat der Universitat Bern zur Erlangung der Doktorwurde. Universitat Bern 1914. [*§2.1*]

Wolinsky (H.) and Glagov (S.). A lamellar unit of aortic medial structure and function in mammals. *Circulation Research* **20** 99-111, 1967. [*§1.1*]

Wolters (B.J.B.M.), Rutten (M.C.M.), Schurink (G.W.H.), Kose (U.), de Hart (J.) and van de Vosse (F.N.). A patient-specific computational model of fluid-structure interaction in abdominal aortic aneurysms. *Medical Engineering and Physics* **27**(10) 871-883, 2005. [*§2.1, 4.1*]

Womersley (J.R.). An elastic tube theory of pulse transmission and oscillatory flow in mammalian arteries. Wright Air Development Center technical report TR 56-614. United States Air Force (Wright-Patterson Air Force Base) 1957. [*§2.1*]

Wood (N.B.), Zhao (S.Z.), Zambanini (A.), Jackson (M.), Gedroyc (W.), Thom (S.A.), Hughes (A.D.) and Xu (X.Y.). Curvature and tortuosity of the superficial femoral artery: a possible risk factor for peripheral arterial disease. *Journal of Applied Physiology* **101** 1412-1418, 2006. [*§4.1*]

Yamamoto (S.), Maruyama (S.), Nakahara (Y.), Yoneyama (S.), Tanifuji (S.), Wada (S.), Hamada (S.), Komizu (M.), Johkoh (T.), Doi (M.) and Yamaguchi (T.). Computational flow dynamics in abdominal aortic aneurysm using multislice computed tomography. *Nippon Hoshasen Gijutsu Gakkai Zasshi* **62**(1) 115-121, 2006. [*§2.1, 5.3*]

Yeung (J.J.), Kim (H.J.), Abbruzzese (T.A.), Vignon-Clementel (I.E.), Draney-Blomme (M.T.), Yeung (K.K.), Perkash (I.), Herfkens (R.J.), Taylor (C.A.) and Dalman (R.L.). Aortoiliac hemodynamic and morphologic adaptation to chronic spinal cord injury. *Journal of Vascular Sugery* **44**(6) 1254-1265, 2006. [*§5.3*]

Young (H.D.). *University Physics* 8th ed. ch. 11 pp. 287-314. Addison-Wesley (Reading) 1992. [*§2.2*]

Appendix

Programs and Functions

geogen.m

```
function geogen(dt,gr)
% Program GeoGen version 3.0c
% C.E. SARRAN 2004-2007 (c.e.sarran@dundee.ac.uk)
% (c) University of Dundee 2004-2007
% (c) NHS Tayside 2007
% (c) Tayside Flow Technologies Limited 2004
%
% The program Geogen is used to generate the geometry file
% required for use by the program Art.
% Geogen requires the following Matlab data file:
%  fn.mat  : contains the ordered list of file names as a
%            10 by n character array of the vessel
%            specifications (n is the number of vessels)
% Geogen requires the ASCII data files listed in fn.mat
% containing the vessel characteristics as defined by the
% data file format specified below (S).
% Geogen writes a Matlab data file geo.mat that contains
% the following variables:
%  para  : cell array containing the parameters describing
%          each vessel
%  szp   : numeric array of the number of grid points for
%          each vessel
%
% The following variables are required to run Geogen:
%
% dt    : time step size
% gr    : density
%
% data file format:
% S(1,:)    : distance L up to which vessel parameters
%             apply
% S(2,:)    : cross-sectional area a
% S(3,:)    : compliance factor C
% S(4,:)    : friction factor f
%
% file names for vessel specifications should be generated
% here
% e.g. fn(:,1)='aorta.dat'; % branch 1 is given by the
%                             aorta data file

% File names are specified in fn.mat
```

```
%%%%%%%%%%%%%%%%%%%%%%%%%%%%%%%%%%%%%%%%%%%%%%%%%%%%%%%%%%%%%%%%%%%%%%%
% file names for vessel specifications should be generated
% here
% e.g. fn(:,1)='aorta.dat'; % branch 1 is given by the
%                             aorta data file

% fn(:,1)='pi.dat';
load fn;

%%%%%%%%%%%%%%%%%%%%%%%%%%%%%%%%%%%%%%%%%%%%%%%%%%%%%%%%%%%%%%%%%%%%%%%

% Display progress - "computing geometry"
disp(' computing geometry')

% Repeat for each vessel data file
for h=1:size(fn,2)

 % Checks that the file exists by attempting to open it
 % checks that a file exists
 fid=fopen(fn(:,h));

 % If successfully opened, close the file then load the
 % vessel specifications and create the vessel grid
 if fid>0
  fclose(fid);

  % loads data file

  % Delete the vessel specifications variable S,
  % then load the vessel specifications from file
  clear S;
  S(:,:)=load(fn(:,h));

  % Determine the number of vessel sections with different
  % specifications
  sz=size(S,2);

  % S(1,:)    : distance L up to which vessel parameters
  %             apply
  % S(2,:)    : cross-sectional area a
  % S(3,:)    : compliance factor C
  % S(4,:)    : friction factor f

  % Initialise the grid point coordinate and number
  % variables z and m
  z=0;  % grid point coordinate at start of section
  m=0;  % last grid point number before start of section

  % computes geometry parameters

  % Repeat for each different vessel section
```

```
  for i=1:sz

   % Compute wave velocity c from compliance factor and
   % density
   c=sqrt(S(3,i)/gr);

   % Compute number of grid points that fall within this
   % section given length of section, time step duration
   % and wave velocity
   n=round((S(1,i)-z)/dt/c);

   % Assign vessel characteristics to identified n grid
   % points falling within this vessel section
   for j=m+1:m+n
    para{h}(1,j)=S(2,i);        % cross-sectional area a
    para{h}(2,j)=c;             % wavespeed c
    para{h}(3,j)=S(3,i);        % compliance factor C
    para{h}(4,j)=S(4,i);        % friction factor f
    para{h}(5,j)=z+(j-m)*dt*c;  % grid point coordinate z
   end

   % Increment grid point coordinate and number given n
   % grid points
   z=z+n*dt*c;
   m=m+n;
  end

  % Save number of grid points for the vessel in szp array
  szp(h)=m;  % number of grid points for the vessel

 end

 %h
end

% saves geometry file

% Display progress - "saving geometry"
disp(' saving geometry')

% Save variables para and szp to Matlab data file geo.mat
save geo para szp;
```

bcgen.m

```
function bcgen(dt)
% Program BCGen version 2.3c
% C.E. SARRAN 2004-2007 (c.e.sarran@dundee.ac.uk)
```

```
% (c) University of Dundee 2004-2007
% (c) NHS Tayside 2007
% (c) Tayside Flow Technologies Limited 2004
%
% The program Bcgen is used to generate the boundary
% conditions file required for use by the program Art.
% Bcgen requires the following Matlab data file:
%  bfn.mat  : contains the ordered list of file names as a
%             10 by n character array of the vessel
%             specifications (n is the number of vessels)
% Bcgen requires the ASCII data files listed in bfn.mat
% containing the boundary conditions as defined by the data
% file format specified below (S).
% Bcgen writes a Matlab data file bc.mat that contains the
% following variables:
%  bc  : m by 3 by n numeric array containing the
%        parameters describing each boundary condition (m
%        is the number of time steps and n is the number of
%        vessels)
%  T   : boundary conditions period
%
% The following variables are required to run Bcgen:
%
% dt    : time step size
%
% data file format:
% S(1,:)    : time up to which boundary condition
%             parameters apply
% S(2,:)    : boundary type
% S(3,:)    : boundary condition at start of period
%             specified
% S(4,:)    : boundary condition at end of period specified
%
% file names for boundary condition specifications should
% be generated here
% e.g. fn(:,1)='lhsbc.dat'; % boundary of branch 1 is given
%                             by the lhsbc data file
%
% note: the vessel with the highest number in the network
%       should have a specified boundary condition

% File names are specified in bfn.mat
%%%%%%%%%%%%%%%%%%%%%%%%%%%%%%%%%%%%%%%%%%%%%%%%%%%%%%%%%%%%%%%%%%%%%%%%%%%%%%%
% file names for boundary condition specifications should
% be generated here
% e.g. fn(:,1)='lhsbc.dat'; % boundary of branch 1 is given
%                             by the lhsbc data file

% file names must be 6 characters long before the extension

%fn(:,1)='lbc.dat';  % lhs branch end
```

```
%fn(:,4)='rbc.dat';  % rhs branch end
load bfn;

%%%%%%%%%%%%%%%%%%%%%%%%%%%%%%%%%%%%%%%%%%%%%%%%%%%%%%%%%%%%%%%%%%%%%%%

% Display progress - "computing boundary conditions"
disp(' computing boundary conditions')

% Initialising the boundary conditions period
T=0;  % grid time at end of period specified by boundary
      % condition data file

% Repeat for each boundary condition data file
for h=1:size(fn,2)

 % Checks that the file exists by attempting to open it
 % checks that a file exists
 fid=fopen(fn(:,h));

 % If successfully opened, close the file then load the
 % specifications and create boundary conditions for each
 % time step
 if fid>0
  fclose(fid);

  % loads data file

  % Delete the boundary condition specifications variable
  % S, then load the boundary condition specifications from
  % file
  clear S;
  S(:,:)=load(fn(:,h));

  % Determine the number of periods of time with different
  % specifications
  sz=size(S,1);

  % S(1,:)    : time up to which boundary condition
  %             parameters apply
  % S(2,:)    : boundary type
  % S(3,:)    : boundary condition at start of period
  %             specified
  % S(4,:)    : boundary condition at end of period
  %             specified

  % Initialise time t, grid time tn and grid time number m
  t=0;   % time at start of period specified by boundary
         % condition data file
  tn=0;  % grid time at start of period specified by
         % boundary condition data file
  m=1;   % first grid time number at start of period
```

```
        % specified by boundary condition data file

  % computes boundary conditions

  % Repeat for each period of time with different
  % specifications
  for i=1:sz

   % Compute number of time steps that fall within the time
   % period with specified boundary conditions given time
   % period duration and time step duration
   n=round((S(i,1)-tn)/dt);

   % Assign boundary condition parameters to identified n
   % time steps falling within the specified time period
   for j=m:m-1+n
    bc(j,1,h)=S(i,2);                  % boundary type
    bc(j,2,h)=S(i,3)+(S(i,4)-S(i,3))/(S(i,1)-t)*(j*dt-t);
                                       % boundary condition
    bc(j,3,h)=j*dt;                    % grid time
   end

   % Increment time t, grid time tn and grid time number m
   t=S(i,1);
   tn=tn+n*dt;
   m=m+n;
  end

 end

 % Adjust boundary conditions period to latest grid time
 if T<tn
  T=tn;
 end

end

% saves boundary conditions file

% Display progress - "saving boundary conditions"
disp(' saving boundary conditions')

% Save variables bc and T to Matlab data file bc.mat
save bc bc T;
```

art2.m

```
function art2(dt,ts,n)
% Program Art version 3.0c
% C.E. SARRAN 2004-2007 (c.e.sarran@dundee.ac.uk)
% (c) University of Dundee 2004-2007
% (c) NHS Tayside 2007
% (c) Tayside Flow Technologies Limited 2004
%
% The program Art (Art 2) solves the characteristic
% equations for pressure and flow rate in a network of
% flexible vessels.
% It can be used, for example, to simulate the flow of
% blood in 1D models of the arterial network.
% Art 2 requires the following Matlab function files:
%  test.m   : tests the vessel network for errors
%  lhsb.m   : solves for pressure and flow rate at a left
%             hand-side boundary
%  rhsb.m   : solves for pressure and flow rate at a right
%             hand-side boundary
%  bif.m    : solves for pressure and flow rates at a
%             bifurcation with two vessels 'downstream'
%  bifb.m   : solves for pressure and flow rates at a
%             bifurcation with two vessels 'upstream'
%  point.m  : solves for pressure and flow rate at all
%             other grid points
% Art 2 requires the following Matlab data files:
%  geo.mat  : geometry file generated by the function
%             geogen.m containing the variables para and
%             szp (see below)
%  bc.mat   : boundary conditions file generated by the
%             function bcgen.m containing the variables bc
%             and T (see below)
% Art 2 requires the following ASCII data file:
%  net.dat  : n records of 3 integers corresponding to the
%             vessel identification numbers, positive for
%             'downstream' vessel ends and negative for
%             'upstream' vessel ends (n is the number of
%             bifurcations)
% Art 2 writes a Matlab data file grid.mat that contains
% the following variables:
%  v     : m by 2 cell array of 2 by x numeric arrays
%          containing the p (pressure) and q (flow rate)
%          values at the last time step of the computation
%          and at the second-last time step (m is the
%          number of vessels and x is the number of grid
%          points for each vessel)
%  pq    : m by k cell array of 2 by x numeric arrays
%          containing the p (pressure) and q (flow rate)
```

```
%          values at each time step saved at regular
%          intervals specified by ts (m is the number of
%          vessels, k is the number of saved time steps and
%          x is the number of grid points for each vessel)
%  tt    : numeric array of the times at which p and q
%          values were saved in the pq array
%  para  : cell array containing the parameters describing
%          each vessel (from geo.mat)
%  szp   : numeric array of the number of grid points for
%          each vessel (from geo.mat)
%  bc    : m by 3 by x numeric array containing the
%          parameters describing each boundary condition (m
%          is the number of time steps and x is the number
%          of vessels) (from bc.mat)
%  T     : boundary condition period (from bc.mat)
%  net   : m by 3 numeric array of vessel identification
%          numbers describing the bifurcations of the
%          network, positive values for 'downstream' vessel
%          ends and negative for 'upstream' (m is the
%          number of bifurcations)
%  dt    : time step size
%  ts    : time between saved solutions
%  n     : number of periods
%  gr    : density
%  gm    : molecular viscosity
%
% The following variables are required to run Art 2:
%
% dt    : time step size
% ts    : time between saved solutions
% n     : number of periods

% Define values for the density and molecular viscosity of
% blood
gr=1050;    % density
gm=.00368;  % molecular viscosity

% Display progress - "testing network"
disp('testing network')

% Tests the vessel network for errors, returning the number
% tst of errors and b identifying the vessel ends with
% missing boundary conditions
[tst,b]=test;  % tests network

% If the test fails displays the number of errors and ends
if tst>0
 disp([num2str(tst) ' errors'])
                                % displays number of errors
else
```

```
% Display progress - "loading geometry"
disp('loading geometry')

% Loads the geometry file generated by geogen.m
load geo;  % loads geometry file

% Display progress - "loading boundary conditions"
disp('loading boundary conditions')

% Loads the boundary conditions file generated by bcgen.m
load bc;  % loads boundary conditions file

% Display progress - "loading network data"
disp('loading network data')

% Loads the network configuration from the network data
% file
load net.dat;  % loads network data file

% Display progress - "initialising model"
disp('initialising model')

% Create a grid v for the vessels specified by the
% geometry file geo.mat with two time steps so as to
% compute the solutions for pressure and flow rate and
% initialise both pressure and flow rate to zero
for h=1:size(para,2)
 v{h,1}(1:2,1:size(para{h},2)+1)=zeros;
 v{h,2}=v{h,1};
end
%v(1:2,1:size(para,2)+1,1:size(para,3),1:2)=zeros;
                                        % initialises model

% Initialise a counter j to save solutions at regular
% intervals
j=1;

% Initialise the number of saved time steps per period
nts=0;

% Initialise the sums of squared residuals for plotting
smr=[0 0;0 0];

% Display progress - "sorting network information"
disp('sorting network information')

% Sort network information for each bifurcation into
% vessel number order including sign (negative for
% 'upstream' ends, positive for 'downstream' ends)
net=sort(net,2);  % sorts network information
```

```
% Set up display of residuals using a log-scale on the
% vertical axis with red used for pressure P and blue for
% flow rate Q
semilogy(T,1,'r.',T,1,'b.')
legend('P','Q',3)

% 'hold on' is required to prevent display refresh
hold on

% A pause is required to reduce diplay flicker
pause(.00001)

% Repeat computation for the number of periods specified
for m=1:n  % steps through number of periods

 % Display progress - "starting period" with period number
 disp(['starting period ' num2str(m) '...'])

 % Repeat computation for each time step
 for t=1:size(bc,1)  % steps through number of time steps

  % Solves for pressure and flow rate at all the
  % boundaries
  % solves boundaries
  for h=1:size(b,1)

   % Uses lhsb.m if it is a left-hand-side boundary
   if b(h,1)==1
    [v{h,2}(1,1),v{h,2}(2,1)]=lhsb(bc(t,1,h),bc(t,2, ...
     h),v{h,1}(1,2),v{h,1}(2,2),para{h}(1,1), ...
     para{h}(2,1),para{h}(4,1),gr,dt);
   end

   % Uses rhsb.m if it is a right-hand-side boundary
   if b(h,2)==1
    [v{h,2}(1,szp(h)+1),v{h,2}(2,szp(h)+1)]=rhsb(bc(t, ...
     1,h),bc(t,2,h),v{h,1}(1,szp(h)),v{h,1}(2,szp(h)), ...
     para{h}(1,szp(h)),para{h}(2,szp(h)),para{h}(4, ...
     szp(h)),gr,dt);
   end

  end

  % If the model consists of a single vessel with
  % specified boundary conditions required at both ends,
  % use rhsb.m for the righ-hand-side boundary (this is
  % because the second vessel end will have been missed by
  % the selection above)
  % solves right-hand-side boundary if single vessel model
  if sum(b(1,:))==2
   [v{1,2}(1,szp(1)+1),v{1,2}(2,szp(1)+1)]=rhsb(bc(t, ...
```

```
  1,2),bc(t,2,2),v{1,1}(1,szp(1)),v{1,1}(2,szp(1)), ...
  para{1}(1,szp(1)),para{1}(2,szp(1)),para{1}(4, ...
  szp(1)),gr,dt);
end

% Solves for pressure and flow rates at all the
% bifurcations
% solves bifurcations
for i=1:size(net,1)

 % Uses bif.m if it is a bifurcation with two vessels
 % 'downstream'
 if prod(net(i,:))>0
  [v{abs(net(i,3)),2}(1,szp(abs(net(i,3)))+1), ...
   v{abs(net(i,1)),2}(2,1),v{abs(net(i,2)),2}(2,1)]= ...
   bif(v{abs(net(i,3)),1}(1,szp(abs(net(i,3)))), ...
   v{abs(net(i,3)),1}(2,szp(abs(net(i,3)))), ...
   para{abs(net(i,3))}(1,szp(abs(net(i,3)))), ...
   para{abs(net(i,3))}(2,szp(abs(net(i,3)))), ...
   para{abs(net(i,3))}(4,szp(abs(net(i,3)))), ...
   v{abs(net(i,1)),1}(1,2),v{abs(net(i,1)),1}(2,2), ...
   para{abs(net(i,1))}(1,1),para{abs(net(i, ...
   1))}(2,1),para{abs(net(i,1))}(4,1),v{abs(net(i, ...
   2)),1}(1,2),v{abs(net(i,2)),1}(2,2), ...
   para{abs(net(i,2))}(1,1),para{abs(net(i,2))}(2, ...
   1),para{abs(net(i,2))}(4,1),gr,dt);

  % Pressure is equal in all three vessels at the
  % bifurcation
  v{abs(net(i,1)),2}(1,1)=v{abs(net(i,3)),2}(1, ...
   szp(abs(net(i,3)))+1);
  v{abs(net(i,2)),2}(1,1)=v{abs(net(i,3)), ...
   2}(1,szp(abs(net(i,3)))+1);

  % Flow rate in the 'upstream' vessel is the sum of the
  % flow rates in the 'downstream' vessels at the
  % bifurcation
  v{abs(net(i,3)),2}(2,szp(abs(net(i,3)))+1)= ...
   v{abs(net(i,1)),2}(2,1)+v{abs(net(i,2)),2}(2,1);

 % Uses bifb.m if it is a bifurcation with two vessels
 % 'upstream'
 elseif prod(net(i,:))<0
  [v{abs(net(i,1)),2}(1,1),v{abs(net(i,2)),2}(2, ...
   szp(abs(net(i,2)))+1),v{abs(net(i,3)),2}(2, ...
   szp(abs(net(i,3)))+1)]=bifb(v{abs(net(i,2)),1}(1, ...
   szp(abs(net(i,2)))),v{abs(net(i,2)),1}(2, ...
   szp(abs(net(i,2)))),para{abs(net(i,2))}(1, ...
   szp(abs(net(i,2)))),para{abs(net(i,2))}(2, ...
   szp(abs(net(i,2)))),para{abs(net(i,2))}(4, ...
   szp(abs(net(i,2)))),v{abs(net(i,3)),1}(1, ...
```

```
   szp(abs(net(i,3)))),v{abs(net(i,3)),1}(2, ...
   szp(abs(net(i,3)))),para{abs(net(i,3))}(1, ...
   szp(abs(net(i,3)))),para{abs(net(i,3))}(2, ...
   szp(abs(net(i,3)))),para{abs(net(i,3))}(4, ...
   szp(abs(net(i,3)))),v{abs(net(i,1)),1}(1,2), ...
   v{abs(net(i,1)),1}(2,2),para{abs(net(i,1))}(1,1), ...
   para{abs(net(i,1))}(2,1),para{abs(net(i,1))}(4, ...
   1),gr,dt);

  % Pressure is equal in all three vessels at the
  % bifurcation
  v{abs(net(i,2)),2}(1,szp(abs(net(i,2)))+1)= ...
   v{abs(net(i,1)),2}(1,1);
  v{abs(net(i,3)),2}(1,szp(abs(net(i,3)))+1)= ...
   v{abs(net(i,1)),2}(1,1);

  % Flow rate in the 'downstream' vessel is the sum of
  % the flow rates in the 'upstream' vessels at the
  % bifurcation
  v{abs(net(i,1)),2}(2,1)=v{abs(net(i,2)),2}(2, ...
   szp(abs(net(i,2)))+1)+v{abs(net(i,3)),2}(2, ...
   szp(abs(net(i,3)))+1);
 end
end

% Solves for pressure and flow rate at all the other
% grid points of all the vessels using point.m
% solves all other grid points
for h=1:size(para,2)
 for i=2:szp(h)
  [v{h,2}(1,i),v{h,2}(2,i)]=point(v{h,1}(1,i-1),v{h, ...
   1}(2,i-1),para{h}(1,i-1),para{h}(2,i-1), ...
   para{h}(4,i-1),v{h,1}(1,i+1),v{h,1}(2,i+1), ...
   para{h}(1,i),para{h}(2,i),para{h}(4,i),gr,dt);
 end
end

% Saves the solution and plots the residuals statistics
% if the time interval between saved solutions has
% lapsed
% saves results
if (m-1)*T+t*dt>j*ts

 % Saves the solution for each vessel
 for h=1:size(para,2)
  pq{h,j}=v{h,2};
 end

 % Computes and saves the time for the solution
 tt(j)=(m-1)*T+t*dt;
```

```
% Add the sum of squared residuals for pressure and
% flow rate for each vessel to the current sum of
% squared residuals
for h=1:size(para,2)
 smr(1,2)=smr(1,2)+sum(pq{h,j}(1,:).^2,2);
 smr(2,2)=smr(2,2)+sum(pq{h,j}(2,:).^2,2);

 % If first period fully computed, then adjust the sums
 % of squared residuals
 if tt(j)>T

  % Calculate once the number of saved time steps per
  % period
  if nts==0
   nts=j-1;
  end

  % Remove the sum of squared residuals for the
  % previous period from the current sum of squared
  % residuals
  smr(1,2)=smr(1,2)-sum(pq{h,j-nts}(1,:).^2,2);
  smr(2,2)=smr(2,2)-sum(pq{h,j-nts}(2,:).^2,2);

  % Add the sum of squared residuals for the previous
  % period to the sum of squared residuals of one
  % period ago
  smr(1,1)=smr(1,1)+sum(pq{h,j-nts}(1,:).^2,2);
  smr(2,1)=smr(2,1)+sum(pq{h,j-nts}(2,:).^2,2);

  % If second period fully computed, then remove the
  % sum of squared residuals for the period two periods
  % ago from the sum of squared residuals of one period
  % ago
  if j>2*nts
   smr(1,1)=smr(1,1)-sum(pq{h,j-2*nts}(1,:).^2,2);
   smr(2,1)=smr(2,1)-sum(pq{h,j-2*nts}(2,:).^2,2);
  end
 end
end

% If first period fully computed, plot the residuals
% statistics; these are the relative change in sum of
% squared residuals from the previous period
% Note: because of the way these statistics are
% computed, they are dependent on the time step size
if tt(j)>T
 semilogy(tt(j),abs(smr(1,2)-smr(1,1))/smr(1,2), ...
  'r.',tt(j),abs(smr(2,2)-smr(2,1))/smr(2,2),'b.')
 pause(.00001)

% For the first period, only indicate progress of
```

```
    % computation on the plot
    else
     semilogy(tt(j),1,'r-',tt(j),1,'b-')
     pause(.00001)
    end

    % Increment counter of saved solutions
    j=j+1;
   end

   % At the end of each time step, copy the solution for
   % each vessel to be used as starting conditions for the
   % next time step
   for h=1:size(para,2)
    v{h,1}=v{h,2};
   end
  end

  % Display progress - "period completed" with period
  % number
  disp(['period ' num2str(m) ' completed.'])
 end

 % saves solution file

 % Display progress - "saving solution"
 disp('saving solution')

 % Save variables v, pq, tt, para, szp, bc, T, net, dt, ts,
 % n, gr and gm to Matlab data file grid.mat
 save grid v pq tt para szp bc T net dt ts n gr gm;

 % 'hold off' is required to allow display refresh again
 hold off

end
```

test.m

```
function [tst,b]=test
% Program Test version 3.0c
% C.E. SARRAN 2004-2007 (c.e.sarran@dundee.ac.uk)
% (c) University of Dundee 2004-2007
% (c) NHS Tayside 2007
% (c) Tayside Flow Technologies Limited 2004
%
% The Test program tests for errors in a vessel network
% with its boundary conditions.
```

```
% The tests ensure that each vessel has one and only one
% 'upstream' and 'downstream' end, that each vessel has at
% least one grid point and boundary conditions are
% specified to vessel ends that are not connected to any
% other vessel.
% The function Test is required by the program Art 2.
% Test requires the following Matlab data files:
%  geo.mat  : geometry file generated by the function
%             geogen.m containing the variables para and
%             szp
%  bc.mat   : boundary conditions file generated by the
%             function bcgen.m containing the variables bc
%             and T
% Test requires the following ASCII data file:
%  net.dat  : n records of 3 integers corresponding to the
%             vessel identification numbers, positive for
%             'downstream' vessel ends and negative for
%             'upstream' vessel ends (n is the number of
%             bifurcations)
% Test returns the following variables:
%  tst  : number of errors
%  b    : numeric array of identifiers of vessel ends that
%         require boundary conditions (i.e. that are not
%         connected to other vessels)

% Display progress - "loading geometry"
disp(' loading geometry')

% Loads the geometry file generated by geogen.m
load geo;

% Display progress - "loading boundary conditions"
disp(' loading boundary conditions')

% Loads the boundary conditions file generated by bcgen.m
load bc;

% Display progress - "loading network data"
disp(' loading network data')

% Loads the network configuration from the network data
% file
load net.dat;

% Initialise the number of errors variable tst
tst=0;  % number of errors

% Initialise the vessel ends requiring boundary conditions
% array b according to the size of the network
b(1:size(szp,2),1:2)=ones;
             % vessel ends that require boundary conditions
```

```
% Display progress - "checking"
disp(' checking...')

% Repeat for each vessel end specified by the network
% configuration
for i=1:size(net,1)
 for j=1:size(net,2)

  % checks that each vessel end is not repeated

  % Check that there are several vessels in the network as
  % a vessel 0 is only specified if the network is a single
  % vessel
  if net(i,j)~=0

   % Check that this vessel end is not already specified; b
   % is 0 if the vessel end has already been specified, 1
   % if it has not
   if b(abs(net(i,j)),round(sign(net(i,j))/2+1.5))==0

    % Increment the number of errors
    tst=tst+1;

    % Display error - "test error: repeated vessel end"
    disp('test error: repeated vessel end')
   end

   % Identify with b that the vessel end is specified
   b(abs(net(i,j)),round(sign(net(i,j))/2+1.5))=0;
  end

  % checks that each vessel has at least one grid point

  % Check that the network consists of a single vessel
  if net(i,j)==0

   % Check that the single vessel has at least 1 grid point
   if szp(1)<1

    % Increment the number of errors
    tst=tst+1;

    % Display error - "test error: vessel has no grid
    % point"
    disp('test error: vessel has no grid point')
   end

   % In the case that the network consists of multiple
   % vessels check that each vessel has at least 1 grid
   % point
```

```
  elseif szp(abs(net(i,j)))<1

   % Increment the number of errors
   tst=tst+1;

   % Display error - "test error: vessel has no grid point"
   disp('test error: vessel has no grid point')
  end

 end
end

% checks that boundary conditions are specified

% Boundary conditions are required at both ends of the
% first vessel in the case of a single vessel network
if sum(b(1,:))==2

 % Check that a boundary condition has been specified at
 % both ends of the vessel
 for j=1:2
  if bc(1,1,j)==0

   % Increment the number of errors
   tst=tst+1;

   % Display error - "test error: boundary condition is not
   % specified"
   disp('test error: boundary condition is not specified')
  end
 end

% Check boundary conditions for a network of multiple
% vessels
else

 % Repeat for each vessel
 for i=1:size(para,2)

  % Check if a vessel end needs a boundary condition
  % specified
  if sum(b(i,:))>0

   % Check that a boundary condition has indeed been
   % specified
   if bc(1,1,i)==0

    % Increment the number of errors
    tst=tst+1;

    % Display error - "test error: boundary condition is
```

```
    % not specified"
    disp('test error: boundary condition is not specified')
   end
  end
 end
end

% Display progress - "checks completed"
disp(' checks completed.')
```

lhsb.m

```
function [pv,qv]=lhsb(lhs,bc,p,q,a,c,f,gr,dt)
% LHSB function version 2.1c
% C.E. SARRAN 2004 (c.e.sarran@dundee.ac.uk)
% (c) University of Dundee 2004
% (c) Tayside Flow Technologies Limited 2004
%
% The LHSB function solves the characteristic equation for
% pressure and flow rate at a 'left-hand-side' boundary.
% The LHSB function is required by the program Art 2.
%
% The following variables are required to run the LHSB
% function:
%
% lhs   : boundary type
% bc    : boundary condition
% p     : right-hand-side pressure at previous time step
% q     : right-hand-side flow rate at previous time step
% a     : right-hand-side cross-sectional area
% c     : right-hand-side wavespeed
% f     : right-hand-side friction factor
% gr    : density
% dt    : time step size
%
% The following variables are returned by the LHSB
% function:
%
% pv    : pressure at boundary characteristic point
% qv    : flow rate at boundary characteristic point

% If pressure is defined at the boundary compute flow rate
if lhs==1  % pressure boundary
 pv=bc;
 qv=(bc-p+(gr*c/a-c*f*dt/a^2)*q)/(gr*c/a+c*f*dt/a^2);

% If flow rate is defined at the boundary compute pressure
elseif lhs==2  % flow rate boundary
```

```
 qv=bc;
 pv=p+gr*c/a*(bc-q)+c*f*dt/a^2*(bc+q);

% If a resistance is defined at the boundary compute
% pressure and flow rate
elseif lhs==3  % resistance boundary
 A1=[1 bc/a;1 -gr*c/a-c*f*dt/a^2];
 A3=[0;p-(gr*c/a-c*f*dt/a^2)*q];
 A2=A1\A3;
 pv=A2(1);
 qv=A2(2);

% If the boundary is defined to reflect incoming pressure
% waves compute pressure and flow rate with change in
% pressure as a proportion of the incoming pressure wave
else  % reflection boundary
 A1=[1 0;1 -gr*c/a+c*f*dt/a^2];
 A3=[(1-bc)*p;p-(gr*c/a-c*f*dt/a^2)*q];
 A2=A1\A3;
 pv=A2(1);
 qv=A2(2);
end
```

rhsb.m

```
function [pv,qv]=rhsb(rhs,bc,p,q,a,c,f,gr,dt)
% RHSB function version 2.1c
% C.E. SARRAN 2004 (c.e.sarran@dundee.ac.uk)
% (c) University of Dundee 2004
% (c) Tayside Flow Technologies Limited 2004
%
% The RHSB function solves the characteristic equations for
% pressure and flow rate at a 'right-hand-side' boundary.
% The RHSB function is required by the program Art 2.
%
% The following variables are required to run the RHSB
% function:
%
% rhs   : boundary type
% bc    : boundary condition
% p     : left-hand-side pressure at previous time step
% q     : left-hand-side flow rate at previous time step
% a     : left-hand-side cross-sectional area
% c     : left-hand-side wavespeed
% f     : left-hand-side friction factor
% gr    : density
% dt    : time step size
%
```

```
% The following variables are returned by the RHSB
% function:
%
% pv    : pressure at boundary characteristic point
% qv    : flow rate at boundary characteristic point

% If pressure is defined at the boundary compute flow rate
if rhs==1  % pressure boundary
 pv=bc;
 qv=(p-bc+(gr*c/a-c*f*dt/a^2)*q)/(gr*c/a+c*f*dt/a^2);

% If flow rate is defined at the boundary compute pressure
elseif rhs==2  % flow rate boundary
 qv=bc;
 pv=p-gr*c/a*(bc-q)-c*f*dt/a^2*(bc+q);

% If a resistance is defined at the boundary compute
% pressure and flow rate
elseif rhs==3  % resistance boundary
 A1=[1 gr*c/a+c*f*dt/a^2;1 -bc/a];
 A3=[p+(gr*c/a-c*f*dt/a^2)*q;0];
 A2=A1\A3;
 pv=A2(1);
 qv=A2(2);

% If the boundary is defined to reflect incoming pressure
% waves compute pressure and flow rate with change in
% pressure as a proportion of the incoming pressure wave
else  % reflection boundary
 A1=[1 gr*c/a+c*f*dt/a^2;1 0];
 A3=[p+(gr*c/a-c*f*dt/a^2)*q;(1-bc)*p];
 A2=A1\A3;
 pv=A2(1);
 qv=A2(2);
end
```

bif.m

```
function [pv,qv1,qv2]=bif(pl,ql,al,cl,fl,pr1,qr1,ar1, ...
 cr1,fr1,pr2,qr2,ar2,cr2,fr2,gr,dt)
% Bif function version 2.0c
% C.E. SARRAN 2004 (c.e.sarran@dundee.ac.uk)
% (c) University of Dundee 2004
% (c) Tayside Flow Technologies Limited 2004
%
% The Bif function solves the characteristic equations for
% pressure and flow rate at a bifurcation with two 'right-
% hand-side' vessels.
```

```
% The Bif function is required by the program Art 2.
%
% The following variables are required to run the Bif
% function:
%
% pl    : left-hand-side pressure at previous time step
% pr1   : pressure in first right-hand-side branch at
%         previous time step
% pr2   : pressure in second right-hand-side branch at
%         previous time step
% ql    : left-hand-side flow rate at previous time step
% qr1   : flow rate in first right-hand-side branch at
%         previous time step
% qr2   : flow rate in second right-hand-side branch at
%         previous time step
% al    : left-hand-side cross-sectional area
% ar1   : cross-sectional area of first right-hand-side
%         branch
% ar2   : cross-sectional area of second right-hand-side
%         branch
% cl    : left-hand-side wavespeed
% cr1   : wavespeed in first right-hand-side branch
% cr2   : wavespeed in second right-hand-side branch
% fl    : left-hand-side friction factor
% fr1   : friction factor in first right-hand-side branch
% fr2   : friction factor in second right-hand-side branch
% gr    : density
% dt    : time step size
%
% The following variables are returned by the Bif function:
%
% pv    : pressure at bifurcation characteristic point
% qv1   : flow rate in first right-hand-side branch at
%         bifurcation characteristic point
% qv2   : flow rate in second right-hand-side branch at
%         bifurcation characteristic point

% Compute pressure at the bifurcation and the flow rates at
% the bifurcation in each of the two 'right-hand-side'
% vessels
A1=[1 gr*cl/al+cl*fl*dt/al^2 gr*cl/al+cl*fl*dt/al^2;1 ...
 -gr*cr1/ar1-cr1*fr1*dt/ar1^2 0;1 0 -gr*cr2/ar2-cr2* ...
 fr2*dt/ar2^2];
A3=[pl+(gr*cl/al-cl*fl*dt/al^2)*ql;pr1-(gr*cr1/ar1-cr1* ...
 fr1*dt/ar1^2)*qr1;pr2-(gr*cr2/ar2-cr2*fr2*dt/ar2^2)*qr2];
A2=A1\A3;
pv=A2(1);
qv1=A2(2);
qv2=A2(3);
```

bifb.m

```
function [pv,qv1,qv2]=bifb(pl1,ql1,al1,cl1,fl1,pl2,ql2, ...
 al2,cl2,fl2,pr,qr,ar,cr,fr,gr,dt)
% BifB function version 2.0c
% C.E. SARRAN 2004 (c.e.sarran@dundee.ac.uk)
% (c) University of Dundee 2004
% (c) Tayside Flow Technologies Limited 2004
%
% The Bifb function solves the characteristic equations for
% pressure and flow rate at a bifurcation with two 'left-
% hand-side' vessels.
% The Bifb function is required by the program Art 2.
%
% The following variables are required by the Bifb
% function:
%
% pl1   : pressure in first left-hand-side branch at
%         previous time step
% pl2   : pressure in second left-hand-side branch at
%         previous time step
% pr    : right-hand-side pressure at previous time step
% ql1   : flow rate in first left-hand-side branch at
%         previous time step
% ql2   : flow rate in second left-hand-side branch at
%         previous time step
% qr    : right-hand-side flow rate at previous time step
% al1   : cross-sectional area of first left-hand-side
%         branch
% al2   : cross-sectional area of second left-hand-side
%         branch
% ar    : right-hand-side cross-sectional area
% cl1   : wavespeed in first left-hand-side branch
% cl2   : wavespeed in second left-hand-side branch
% cr    : right-hand-side wavespeed
% fl1   : friction factor in first left-hand-side branch
% fl2   : friction factor in second left-hand-side branch
% fr    : right-hand-side friction factor
% gr    : density
% dt    : time step size
%
% The following variables are returned by the Bifb
% function:
%
% pv    : pressure at bifurcation characteristic point
% qv1   : flow rate in first left-hand-side branch at
%         bifurcation characteristic point
% qv2   : flow rate in second left-hand-side branch at
%         bifurcation characteristic point
```

```
% Compute pressure at the bifurcation and the flow rates at
% the bifurcation in each of the two 'left-hand-side'
% vessels
A1=[1 gr*cl1/al1+cl1*fl1*dt/al1^2 0;1 0 gr*cl2/al2+cl2* ...
 fl2*dt/al2^2;1 -gr*cr/ar-cr*fr*dt/ar^2 -gr*cr/ar-cr* ...
 fr*dt/ar^2];
A3=[pl1+(gr*cl1/al1-cl1*fl1*dt/al1^2)*ql1;pl2+(gr*cl2/ ...
 al2-cl2*fl2*dt/al2^2)*ql2;pr-(gr*cr/ar-cr*fr*dt/ar^2)*qr];
A2=A1\A3;
pv=A2(1);
qv1=A2(2);
qv2=A2(3);
```

point.m

```
function [pv,qv]=point(pl,ql,al,cl,fl,pr,qr,ar,cr,fr,gr,dt)
% Point function version 2.0c
% C.E. SARRAN 2004 (c.e.sarran@dundee.ac.uk)
% (c) University of Dundee 2004
% (c) Tayside Flow Technologies Limited 2004
%
% The Point function solves the characteristic equations
% for pressure and flow rate at a point in a vessel.
% The Point function is required by the program Art 2.
%
% The following variables are required to run the Point
% function:
%
% pl    : left-hand-side pressure at previous time step
% pr    : right-hand-side pressure at previous time step
% ql    : left-hand-side flow rate at previous time step
% qr    : right-hand-side flow rate at previous time step
% al    : left-hand-side cross-sectional area
% ar    : right-hand-side cross-sectional area
% cl    : left-hand-side wavespeed
% cr    : right-hand-side wavespeed
% fl    : left-hand-side friction factor
% fr    : right-hand-side friction factor
% gr    : density
% dt    : time step size
%
% The following variables are returned by the Point
% function:
%
% pv    : pressure at characteristic point
% qv    : flow rate at characteristic point

% Compute pressure and flow rate
```

```
A1=[1 gr*cl/al+cl*fl*dt/al^2;1 -gr*cr/ar-cr*fr*dt/ar^2];
A3=[pl+(gr*cl/al-cl*fl*dt/al^2)*ql;pr-(gr*cr/ar-cr*fr* ...
 dt/ar^2)*qr];
A2=A1\A3;
pv=A2(1);
qv=A2(2);
```

population.m

```
function population
% POPULATION version 1.1c - reads and computes data from
% the AAA Study database
% (c) University of Dundee 2005-2007
% (c) NHS Tayside 2005-2007
% C.E. SARRAN 2006-2007 (c.e.sarran@dundee.ac.uk)
%
% The program Population reads the anonymised extracts from
% the AAA Study database and computes primary and secondary
% data for each of the AAA Study participants.
% Population requires the following Matlab function file:
%  rddat.m  : computes time series against age for every
%             patient for a given parameter
% Population requires the following comma-separated ASCII
% data files:
%  part.csv  : study participants data
%  meas.csv  : main clinical measurements data
%  sten.csv  : stenoses data
%  csd.csv   : cardiac stress data
%  rp.csv    : resting pressure data
%  sp.csv    : segmental pressure data
%  pep.csv   : post-exercise pressure data
%  ct.csv    : CT imaging cross-referencing data between
%              the AAA Study measurement number and the CT
%              scan number
% Each of the comma-separated ASCII data files contains the
% variables listed as follows:
%
% requires: part.csv    -   SN      dob     gender  dor
%                           ed
%           meas.csv    -   MN      SN      d       ad
%                           al      at      sp      dp
%                           mp      pr      cho     hdl
%                           u       c       cig     diab
%                           renal
%           sten.csv    -   MN      STp     STs     STa
%           csd.csv     -   MN      CSDlpr  CSDhpr  CSDlsp
%                           CSDhsp  CSDldp  CSDhdp
%           rp.csv      -   MN      RPrb    RPlb    RPrpt
```

```
%                           RPlpt   RPrdp   RPldp
%           sp.csv      -   MN      SPrb    SPlb    SPrt
%                           SPlt    SPrc    SPlc    SPra
%                           SPla
%           pep.csv     -   MN      PEPrb   PEPlb   PEPra
%                           PEPla
%
% The variables of the AAA Study database extracts are:
%  SN       : participant study number
%  dob      : date of birth
%  gender   : gender
%  dor      : date of aneurysm rupture
%  ed       : participation end date
%  MN       : measurement number
%  d        : measurement date
%  ad       : aneurysm diameter
%  al       : aneurysm length
%  at       : aneurysm type
%  sp       : systolic pressure
%  dp       : diastolic pressure
%  mp       : mean pressure
%  pr       : pulse rate
%  cho      : total cholesterol level
%  hdl      : HDL cholesterol level
%  u        : urea level
%  c        : creatinine level
%  cig      : number of cigarettes smoked
%  diab     : diabetes
%  renal    : renal disease
%  STp      : stenosis position
%  STs      : stenosis side
%  STa      : stenosis amount
%  CSDlpr   : cardiac stress data lower pulse rate
%  CSDhpr   : cardiac stress data higher pulse rate
%  CSDlsp   : cardiac stress data lower systolic pressure
%  CSDhsp   : cardiac stress data higher systolic pressure
%  CSDldp   : cardiac stress data lower diastolic pressure
%  CSDhdp   : cardiac stress data higher diastolic pressure
%  RPrb     : right brachial resting pressure
%  RPlb     : left brachial resting pressure
%  RPrpt    : right posterior tibial resting pressure
%  RPlpt    : left posterior tibial resting pressure
%  RPrdp    : right dorsalis pedis resting pressure
%  RPldp    : left dorsalis pedis resting pressure
%  SPrb     : right brachial segmental pressure
%  SPlb     : left brachial segmental pressure
%  SPrt     : right thigh segmental pressure
%  SPlt     : left thigh segmental pressure
%  SPrc     : right calf segmental pressure
%  SPlc     : left calf segmental pressure
%  SPra     : right ankle segmental pressure
```

```
%  SPla    : left ankle segmental pressure
%  PEPrb   : right brachial post-exercise pressure
%  PEPlb   : left brachial post-exercise pressure
%  PEPra   : right ankle post-exercise pressure
%  PEPla   : left ankle post-exercise pressure
% Population writes a Matlab data file dat.mat that
% contains the following variables:
%  dat   : cell array containing the time series for every
%          patient for each parameter
%  datR  : cell array containing the time series for
%          patients with a ruptured aneurysm
%  g     : numeric array containing the time series of CT
%          scan numbers for every patient
%  gR    : numeric array containing the time series of CT
%          scan numbers for patients with a ruptured
%          aneurysm

%READ PARTICIPANT AND MEASUREMENT DATA

% Load participant and measurement data and display
% progress - "loading participant data..." "loading
% measurement data..."
disp('loading participant data...'), load part.csv,
 disp('loading measurement data...'), load meas.csv

% Display progress - "reading measurement data..."
disp('reading measurement data...')

% Compute time series of aneurysm diameters (1) and
% aneurysm lengths (2)
for d=1:2, [dat{d},datR{d}]=rddat(part,meas,meas,d+3,-.5);
 end

% Compute time series of aneurysm types (3)
[dat{3},datR{3}]=rddat(part,meas,meas,6,.5);

% Compute time series of systolic pressures (4), diastolic
% pressures (5), mean pressures (6) and pulse rates (7)
for d=4:7, [dat{d},datR{d}]=rddat(part,meas,meas,d+3,-.5);
 end

% Compute time series of total cholesterol levels (9) and
% HDL cholesterol levels (10)
for d=9:10, [dat{d},datR{d}]=rddat(part,meas,meas,d+2,-.5);
 end

% Compute time series of urea levels (12)
[dat{12},datR{12}]=rddat(part,meas,meas,13,-.5);

% Compute time series of diabetes (13) and renal diseases
% (14)
```

```
for d=13:14, [dat{d},datR{d}]=rddat(part,meas,meas,d+3,.5);
 end

% Compute time series of urea levels (63) and creatinine
% levels (64)
for d=63:64,
 [dat{d},datR{d}]=rddat(part,meas,meas,d-50,-.5); end

%OBTAIN SECONDARY MEASUREMENT DATA

% Display progress - "computing secondary measurement
% data..."
disp('computing secondary measurement data...')

% Calculate the systolic-diastolic pressure difference from
% the systolic and diastolic pressures
for i=1:size(meas,1)
 if (meas(i,7)>-.5)&(meas(i,8)>-.5),
  spdp0(i,:)=[meas(i,1) meas(i,7)-meas(i,8)]; else,
  spdp0(i,:)=[meas(i,1) -1]; end
end

% Compute time series of systolic-diastolic pressure
% differences (8)
[dat{8},datR{8}]=rddat(part,meas,spdp0,2,-.5);

% Calculate the total to HDL cholesterol level ratio from
% the total and HDL cholesterol levels
for i=1:size(meas,1)
 if (meas(i,11)>-.5)&(meas(i,12)>-.5),
  chohdl0(i,:)=[meas(i,1) meas(i,11)/meas(i,12)]; else,
  chohdl0(i,:)=[meas(i,1) -1]; end
end

% Compute time series of total to HDL cholesterol level
% ratios (11)
[dat{11},datR{11}]=rddat(part,meas,chohdl0,2,-.5);

%READ STENOSIS DATA

% Load stenosis data and display progress - "loading
% stenosis data..."
disp('loading stenosis data...'), load sten.csv

% Display progress - "reading stenosis data..."
disp('reading stenosis data...')

% Compute time series of stenosis positions (60) and
% stenosis sides (61)
for d=60:61,
 [dat{d},datR{d}]=rddat(part,meas,sten,d-58,.5); end
```

```
% Compute time series of stenosis amounts (62)
[dat{62},datR{62}]=rddat(part,meas,sten,4,-.5);

%READ CARDIAC STRESS DATA

% Load cardiac stress data and display progress - "loading
% cardiac stress data..."
disp('loading cardiac stress data...'), load csd.csv

% Display progress - "reading cardiac stress data..."
disp('reading cardiac stress data...')

% Compute time series of lower pulse rates (15) and higher
% pulse rates (16)
for d=15:16,
 [dat{d},datR{d}]=rddat(part,meas,csd,d-13,-.5); end

% Compute time series of lower systolic pressures (18) and
% higher systolic pressures (19)
for d=18:19,
 [dat{d},datR{d}]=rddat(part,meas,csd,d-14,-.5); end

% Compute time series of lower diastolic pressures (21) and
% higher diastolic pressures (22)
for d=21:22,
 [dat{d},datR{d}]=rddat(part,meas,csd,d-15,-.5); end

%OBTAIN SECONDARY CARDIAC STRESS DATA

% Display progress - "computing secondary cardiac stress
% data..."
disp('computing secondary cardiac stress data...')

% Calculate the average pulse rate, systolic and diastolic
% pressures from the lower and higher pulse rates, systolic
% and diastolic pressures
for i=1:size(csd,1)
 if csd(i,2)<-.5, csd(i,2)=csd(i,3); end
 if csd(i,3)<-.5, csd(i,3)=csd(i,2); end
 if csd(i,4)<-.5, csd(i,4)=csd(i,5); end
 if csd(i,5)<-.5, csd(i,5)=csd(i,4); end
 if csd(i,6)<-.5, csd(i,6)=csd(i,7); end
 if csd(i,7)<-.5, csd(i,7)=csd(i,6); end
 if sum(csd(i,2:3))>-.5,
  CSDapr0(i,:)=[csd(i,1) mean(csd(i,2:3))]; else,
  CSDapr0(i,:)=[csd(i,1) -1]; end
 if sum(csd(i,4:5))>-.5,
  CSDasp0(i,:)=[csd(i,1) mean(csd(i,4:5))]; else,
  CSDasp0(i,:)=[csd(i,1) -1]; end
 if sum(csd(i,6:7))>-.5,
```

```
  CSDadp0(i,:)=[csd(i,1) mean(csd(i,6:7))]; else,
  CSDadp0(i,:)=[csd(i,1) -1]; end
end

% Compute time series of average pulse rates (17), average
% systolic pressures (20) and average diastolic pressures
% (23)
[dat{17},datR{17}]=rddat(part,meas,CSDapr0,2,-.5);
 [dat{20},datR{20}]=rddat(part,meas,CSDasp0,2,-.5);
[dat{23},datR{23}]=rddat(part,meas,CSDadp0,2,-.5);

%READ RESTING PRESSURE DATA

% Load resting pressure data and display progress -
% "loading resting pressure data..."
disp('loading resting pressure data...'), load rp.csv

% Display progress - "reading resting pressure data..."
disp('reading resting pressure data...')

% Compute time series of right brachial pressures (24),
% left brachial pressures (25), right posterior tibial
% pressures (26), left posterior tibial pressures (27),
% right dorsalis pedis pressures (28) and left dorsalis
% pedis pressures (29)
for d=24:29, [dat{d},datR{d}]=rddat(part,meas,rp,d-22,-.5);
 end

%READ SEGMENTAL PRESSURE DATA

% Load segmental pressure data and display progress -
% "loading segmental pressure data..."
disp('loading segmental pressure data...'), load sp.csv

% Display progress - "reading segmental pressure data..."
disp('reading segmental pressure data...')

% Compute time series of right brachial pressures (30),
% left brachial pressures (31), right thigh pressures (32),
% left thigh pressures (33), right calf pressures (34),
% left calf pressures (35), right ankle pressures (36) and
% left ankle pressures (37)
for d=30:37, [dat{d},datR{d}]=rddat(part,meas,sp,d-28,-.5);
 end

%OBTAIN SECONDARY SEGMENTAL PRESSURE DATA

% Display progress - "computing secondary segmental
% pressure data..."
disp('computing secondary segmental pressure data...')
```

```
% Calculate the right and left brachial-thigh, thigh-calf
% and calf-ankle pressure differences from the right and
% left brachial, thigh, calf and ankle pressures
for i=1:size(sp,1)
 if (sum(sp(i,2:3))>-1.5)&(sp(i,4)>-.5),
  SPrbtpd0(i,:)=[sp(i,1) max(sp(i,2:3))-sp(i,4)]; else,
  SPrbtpd0(i,:)=[sp(i,1) -1]; end
 if (sum(sp(i,2:3))>-1.5)&(sp(i,5)>-.5),
  SPlbtpd0(i,:)=[sp(i,1) max(sp(i,2:3))-sp(i,5)]; else,
  SPlbtpd0(i,:)=[sp(i,1) -1]; end
 if (sp(i,4)>-.5)&(sp(i,6)>-.5),
  SPrtcpd0(i,:)=[sp(i,1) sp(i,4)-sp(i,6)]; else,
  SPrtcpd0(i,:)=[sp(i,1) -1]; end
 if (sp(i,5)>-.5)&(sp(i,7)>-.5),
  SPltcpd0(i,:)=[sp(i,1) sp(i,5)-sp(i,7)]; else,
  SPltcpd0(i,:)=[sp(i,1) -1]; end
 if (sp(i,6)>-.5)&(sp(i,8)>-.5),
  SPrcapd0(i,:)=[sp(i,1) sp(i,6)-sp(i,8)]; else,
  SPrcapd0(i,:)=[sp(i,1) -1]; end
 if (sp(i,7)>-.5)&(sp(i,9)>-.5),
  SPlcapd0(i,:)=[sp(i,1) sp(i,7)-sp(i,9)]; else,
  SPlcapd0(i,:)=[sp(i,1) -1]; end
end

% Compute time series of right brachial-thigh pressure
% differences (38), left brachial-thigh pressure
% differences (39), right thigh-calf pressure differences
% (40), left thigh-calf pressure differences (41), right
% calf-ankle pressure differences (42) and left calf-ankle
% pressures differences (43)
[dat{38},datR{38}]=rddat(part,meas,SPrbtpd0,2,-.5);
 [dat{39},datR{39}]=rddat(part,meas,SPlbtpd0,2,-.5);
[dat{40},datR{40}]=rddat(part,meas,SPrtcpd0,2,-.5);
 [dat{41},datR{41}]=rddat(part,meas,SPltcpd0,2,-.5);
[dat{42},datR{42}]=rddat(part,meas,SPrcapd0,2,-.5);
 [dat{43},datR{43}]=rddat(part,meas,SPlcapd0,2,-.5);

%OBTAIN SECONDARY RESTING AND SEGMENTAL PRESSURE DATA

% Display progress - "computing secondary resting and
% segmental pressure data..."
disp(['computing secondary resting and segmental' ...
 ' pressure data...'])

% Calculate the right and left ankle-brachial pressure
% indices from the right and left brachial, posterior
% tibial and dorsalis pedis resting pressures
for i=1:size(rp,1)
 if (sum(rp(i,2:3))>-1.5)&(sum(rp(i,[4 6]))>-1.5),
  rabpi0(i,:)=[rp(i,1) max(rp(i,[4 6]))/max(rp(i,2:3))];
  if rabpi0(i,2)>1.2, rabpi0(i,2)=-1; end
```

```
 else, rabpi0(i,:)=[rp(i,1) -1]; end
 if (sum(rp(i,2:3))>-1.5)&(sum(rp(i,[5 7]))>-1.5),
  labpi0(i,:)=[rp(i,1) max(rp(i,[5 7]))/max(rp(i,2:3))];
  if labpi0(i,2)>1.2, labpi0(i,2)=-1; end
 else, labpi0(i,:)=[rp(i,1) -1]; end
end

% Calculate the right and left ankle-brachial pressure
% indices from the right and left brachial and ankle
% segmental pressures
for i=1:size(sp,1)
 if (sum(sp(i,2:3))>-1.5)&(sp(i,8)>-.5),
  rabpi0(size(rp,1)+i,:)=[sp(i,1) sp(i,8)/max(sp(i,2:3))];
  if rabpi0(size(rp,1)+i,2)>1.2, rabpi0(size(rp,1)+i,2)=-1;
   end
 else, rabpi0(size(rp,1)+i,:)=[sp(i,1) -1]; end
 if (sum(sp(i,2:3))>-1.5)&(sp(i,9)>-.5),
  labpi0(size(rp,1)+i,:)=[sp(i,1) sp(i,9)/max(sp(i,2:3))];
  if labpi0(size(rp,1)+i,2)>1.2, labpi0(size(rp,1)+i,2)=-1;
   end
 else, labpi0(size(rp,1)+i,:)=[sp(i,1) -1]; end
end

% Compute time series of right ankle-brachial pressure
% indices (65) and left ankle-brachial pressure indices
% (66)
[dat{65},datR{65}]=rddat(part,meas,rabpi0,2,-.5);
 [dat{66},datR{66}]=rddat(part,meas,labpi0,2,-.5);

% Calculate the lower and higher ankle-brachial pressure
% indices from the right and left ankle-brachial pressure
% indices
for i=1:size(rabpi0,1)
 if rabpi0(i,2)*labpi0(i,2)>0
  habpi1(i,:)=[rabpi0(i,1) max([rabpi0(i,2) labpi0(i,2)])];
   labpi1(i,:)=[rabpi0(i,1) min([rabpi0(i,2) ...
   labpi0(i,2)])];
 else, habpi1(i,:)=[rabpi0(i,1) -1];
  labpi1(i,:)=[rabpi0(i,1) max([rabpi0(i,2) labpi0(i,2)])];
  end
end

% Compute time series of lower ankle-brachial pressure
% indices (47) and higher ankle-brachial pressure indices
% (48)
[dat{47},datR{47}]=rddat(part,meas,labpi1,2,-.5);
 [dat{48},datR{48}]=rddat(part,meas,habpi1,2,-.5);

% Calculate the right and left brachial-ankle pressure
% differences from the right and left brachial, posterior
% tibial and dorsalis pedis resting pressures
```

```
for i=1:size(rp,1)
 if (sum(rp(i,2:3))>-1.5)&(sum(rp(i,[4 6]))>-1.5),
  rbapd0(i,:)=[rp(i,1) max(rp(i,2:3))-max(rp(i,[4 6]))];
 else, rbapd0(i,:)=[rp(i,1) -1]; end
 if (sum(rp(i,2:3))>-1.5)&(sum(rp(i,[5 7]))>-1.5),
  lbapd0(i,:)=[rp(i,1) max(rp(i,2:3))-max(rp(i,[5 7]))];
 else, lbapd0(i,:)=[rp(i,1) -1]; end
end

% Calculate the right and left brachial-ankle pressure
% differences from the right and left brachial and ankle
% segmental pressures
for i=1:size(sp,1)
 if (sum(sp(i,2:3))>-1.5)&(sp(i,8)>-.5),
  rbapd0(size(rp,1)+i,:)=[sp(i,1) max(sp(i,2:3))-sp(i,8)];
 else, rbapd0(size(rp,1)+i,:)=[sp(i,1) -1]; end
 if (sum(sp(i,2:3))>-1.5)&(sp(i,9)>-.5),
  lbapd0(size(rp,1)+i,:)=[sp(i,1) max(sp(i,2:3))-sp(i,9)];
 else, lbapd0(size(rp,1)+i,:)=[sp(i,1) -1]; end
end

% Compute time series of right brachial-ankle pressure
% differences (49) and left brachial-ankle pressure
% differences (50)
[dat{49},datR{49}]=rddat(part,meas,rbapd0,2,-.5);
 [dat{50},datR{50}]=rddat(part,meas,lbapd0,2,-.5);

% Calculate the brachial and right and left ankle pressures
% from the right and left brachial, posterior tibial and
% dorsalis pedis resting pressures
for i=1:size(rp,1)
 if sum(rp(i,2:3))>-1.5,
  abp0(i,:)=[rp(i,1) max(rp(i,2:3))]; else,
  abp0(i,:)=[rp(i,1) -1]; end
 if sum(rp(i,[4 6]))>-1.5,
  arap0(i,:)=[rp(i,1) max(rp(i,[4 6]))]; else,
  arap0(i,:)=[rp(i,1) -1]; end
 if sum(rp(i,[5 7]))>-1.5,
  alap0(i,:)=[rp(i,1) max(rp(i,[5 7]))]; else,
  alap0(i,:)=[rp(i,1) -1]; end
end

% Calculate the brachial and right and left ankle pressures
% from the right and left brachial and ankle segmental
% pressures
for i=1:size(sp,1)
 if sum(sp(i,2:3))>-1.5,
  abp0(size(rp,1)+i,:)=[sp(i,1) max(sp(i,2:3))]; else,
  abp0(size(rp,1)+i,:)=[sp(i,1) -1]; end
 arap0(size(rp,1)+i,:)=[sp(i,1) sp(i,8)];
  alap0(size(rp,1)+i,:)=[sp(i,1) sp(i,9)];
```

```
end

% Compute time series of brachial pressures (44), right
% ankle pressures (45) and left ankle pressures (46)
[dat{44},datR{44}]=rddat(part,meas,abp0,2,-.5);
 [dat{45},datR{45}]=rddat(part,meas,arap0,2,-.5);
[dat{46},datR{46}]=rddat(part,meas,alap0,2,-.5);

%READ POST-EXERCISE PRESSURE DATA

% Load post-exercise pressure data and display progress -
% "loading post-exercise pressure data..."
disp('loading post-exercise pressure data...'),
 load pep.csv

% Display progress - "reading post-exercise pressure
% data..."
disp('reading post-exercise pressure data...')

% Compute time series of right brachial pressures (51) and
% left brachial pressures (52)
for d=51:52,
 [dat{d},datR{d}]=rddat(part,meas,pep,d-49,-.5); end

% Compute time series of right ankle pressures (54) and
% left ankle pressures (55)
for d=54:55,
 [dat{d},datR{d}]=rddat(part,meas,pep,d-50,-.5); end

%OBTAIN SECONDARY POST-EXERCISE PRESSURE DATA

% Display progress - "computing secondary post-exercise
% pressure data..."
disp('computing secondary post-exercise pressure data...')

% Calculate the right and left ankle-brachial pressure
% indices from the right and left brachial and ankle
% pressures
for i=1:size(pep,1)
 if (sum(pep(i,2:3))>-1.5)&(pep(i,4)>-.5),
  PEPrabpi0(i,:)=[pep(i,1) pep(i,4)/max(pep(i,2:3))];
  if PEPrabpi0(i,2)>1.2, PEPrabpi0(i,2)=-1; end
 else, PEPrabpi0(i,:)=[pep(i,1) -1]; end
 if (sum(pep(i,2:3))>-1.5)&(pep(i,5)>-.5),
  PEPlabpi0(i,:)=[pep(i,1) pep(i,5)/max(pep(i,2:3))];
  if PEPlabpi0(i,2)>1.2, PEPlabpi0(i,2)=-1; end
 else, PEPlabpi0(i,:)=[pep(i,1) -1]; end
end

% Compute time series of right ankle-brachial pressure
% indices (56) and left ankle-brachial pressure indices
```

```
% (57)
[dat{56},datR{56}]=rddat(part,meas,PEPrabpi0,2,-.5);
 [dat{57},datR{57}]=rddat(part,meas,PEPlabpi0,2,-.5);

% Calculate the right and left brachial-ankle pressure
% differences from the right and left brachial and ankle
% pressures
for i=1:size(pep,1)
 if (sum(pep(i,2:3))>-1.5)&(pep(i,4)>-.5),
  PEPrbapd0(i,:)=[pep(i,1) max(pep(i,2:3))-pep(i,4)];
 else, PEPrbapd0(i,:)=[pep(i,1) -1]; end
 if (sum(pep(i,2:3))>-1.5)&(pep(i,5)>-.5),
  PEPlbapd0(i,:)=[pep(i,1) max(pep(i,2:3))-pep(i,5)];
 else, PEPlbapd0(i,:)=[pep(i,1) -1]; end
end

% Compute time series of right brachial-ankle pressure
% differences (58) and left brachial-ankle pressure
% differences (59)
[dat{58},datR{58}]=rddat(part,meas,PEPrbapd0,2,-.5);
 [dat{59},datR{59}]=rddat(part,meas,PEPlbapd0,2,-.5);

% Calculate the brachial pressure from the right and left
% brachial pressures
for i=1:size(pep,1), if sum(pep(i,2:3))>-1.5,
 PEPabp0(i,:)=[pep(i,1) max(pep(i,2:3))]; else,
 PEPabp0(i,:)=[pep(i,1) -1]; end, end

% Compute time series of brachial pressures (53)
[dat{53},datR{53}]=rddat(part,meas,PEPabp0,2,-.5);

%READ CT GEOMETRY INDEX

% Load the CT geometry index and display progress -
% "loading CT geometry index..."
disp('loading CT geometry index...'), load ct.csv

% Compute time series of the CT geometry index and display
% progress - "reading CT geometry index..."
disp('reading CT geometry index...'),
[g,gR]=rddat(part,meas,ct,2,.5);

% Save variables dat, datR, g and gR to Matlab data file
% dat.mat
disp('saving data...'), save dat dat datR g gR
```

rddat.m

```
function [d,dR]=rddat(part,meas,v,c,t)
% RDDAT version 1.0c - reads data from AAA csv file
% (c) University of Dundee 2005-2006
% (c) NHS Tayside 2005-2006
% C.E. SARRAN 2005-2006 (c.e.sarran@dundee.ac.uk)
%
% The Rddat function takes data from the AAA Study database
% comma-separated ASCII files to compute time series
% information for every patient for a given parameter.
% The Rddat function is required by the program Population.
% The following variables are required to run the Rddat
% function:
%  part  : study participants data
%  meas  : main clinical measurements data
%  v     : numeric array with the measurement number in the
%          first column containing the parameter specified
%          by c
%  c     : column of v containing the parameter
%  t     : type of parameter (-0.5 for numerical; +0.5 for
%          categorical)
% The following variables are returned by the Rddat
% function:
%  d   : n by 3 numeric array with n the number of
%        measurements and containing the participant
%        number, the age at the time of measurement and the
%        measurement itself
%  dR  : n by 4 numeric array with n the number of
%        measurements and containing the participant
%        number, the age at the time of measurement, the
%        measurement itself and the time before rupture for
%        patients with a ruptured aneurysm

% Initialise variables and counters
d=0; dR=0; m=1; n=1;

% For each measurement from each participant, compute the
% participant age and where applicable the time before
% rupture
for i=1:size(v,1), if v(i,c)>t, for j=1:size(meas,1),
 if v(i,1)==meas(j,1)
    for k=1:size(part,1), if meas(j,2)==part(k,1)
      if ~((part(k,5)>0)&(meas(j,3)>part(k,5)))
       d(m,1)=part(k,1);
        d(m,2)=(meas(j,3)-part(k,2))/365.25; d(m,3)=v(i,c);
       if part(k,4)>0
        dR(n,1)=d(m,1); dR(n,2)=d(m,2); dR(n,3)=d(m,3);
         dR(n,4)=(part(k,4)-meas(j,3))/365.25; n=n+1;
```

```
       end
       m=m+1;
      end
      break;
     end, end
    break;
   end, end, end, end

% Sort the data by participant number and by age
if size(d,2)>1, d=sortrows(sortrows(d,2),1); end
if size(dR,2)>1, dR=sortrows(sortrows(dR,2),1); end
```

wfunc.m

```
function wfunc(t)
% Program WFUNC version 4.1c - computes parameter and
% differential estimates and associated weight functions
% (c) University of Dundee 2007
% (c) NHS Tayside 2007
% C.E. SARRAN 2007 (c.e.sarran@dundee.ac.uk)
%
% The Wfunc program takes the data generated by the program
% Population and the anonymised extract of participant data
% from the AAA Study database to compute parameter and
% parameter differential estimates and their associated
% weight functions for each parameter and patient.
% Wfunc requires the following Matlab data file:
%  dat.mat  : data derived from the extracts of the AAA
%             Study database and computed by the program
%             Population
% Wfunc requires the following comma-separated ASCII data
% file:
%  part.csv  : study participants data
% part.csv contains the following variables:
%  SN      : participant study number
%  dob     : date of birth
%  gender  : gender
%  dor     : date of aneurysm rupture
%  ed      : participation end date
% Wfunc writes a Matlab data file mn.mat that contains the
% following variables:
%  ddat  : cell array of n by 5 numeric arrays containing
%          the participant study number, the parameter
%          estimate, its associated weight, the
%          differential estimate and its associated weight
%          for the date specified at the start of the
%          program
%  par   : numeric array of the m parameter indices
```

```
%          referencing the parameter means mx and sum of
%          weights mw
%  mx    : m by 2 numeric array containing the means of the
%          parameter estimates and of the differential
%          estimates
%  mw    : m by 2 numeric array containing the sum of
%          weights of the parameter estimates and of the
%          differential estimates
% Wfunc writes one Matlab data file per study participant,
% with a filename of the format wf0000.mat where the 4
% digits are the participant study number, that contains
% where applicable the following transformed variables, the
% digits in the variable names identifying as detailed
% below the parameter to which they relate:
%  pwf1 to pwf64  : 30001 by 2 numeric arrays of parameter
%                   estimates with associated weights at
%                   0.01 y intervals from -100 y to 200 y
%  dwf1 to dwf64  : 30001 by 2 numeric arrays of
%                   differential estimates with associated
%                   weights at 0.01 y intervals from -100 y
%                   to 200 y
%  tx1  to tx64   : n by 2 numeric arrays of the n
%                   transformed parameter measurements with
%                   age at measurement in the 1st column
% List of parameter indices:
%  1   : aneurysm diameter
%  4   : systolic pressure
%  5   : diastolic pressure
%  7   : pulse rate
%  8   : systolic-diastolic pressure difference
%  9   : total cholesterol level
%  10  : HDL cholesterol level
%  11  : total to HDL cholesterol level ratio
%  47  : lower ankle-brachial pressure index
%  48  : higher ankle-brachial pressure index
%  63  : urea level
%  64  : creatinine level
% The following variable is required to run Wfunc:
%
% t -   time period for measurement significance (y)
%
% A date can be specified to return the parameter and
% differential estimates; here d=38142 corresponds to 1
% March 2005.
%
% date =    1-3-2005    [d=38412]

% Set date and load derived data and participant data
d=38412; load dat, load part.csv

% Set list of parameters to be included and initialise
```

```
% variables mx and mw
para=[1 4 5 7 8 9 10 11 47 48 63 64];
 mx=zeros(size(para,2),2); mw=mx;

% Compute estimates and weight functions for each parameter
for h=1:size(para,2)

 % Initialise list of valid participant study numbers and
 % counter
 clear id; id0=[dat{para(h)}(1,1) 0]; m=1;

 % Repeat for each measurement record
 for i=1:size(dat{para(h)},1)

  % Add participant study number to list if not already
  % included
  if id0(m,1)~=dat{para(h)}(i,1), m=m+1;
   id0(m,:)=[dat{para(h)}(i,1) 0]; end

  % Check with the participant data that there is no
  % participation end date or that the measurement was
  % taken before the participation end date; increment the
  % number of measurements where required
  for j=1:size(part,1), if part(j,1)==id0(m,1),
   if (part(j,5)<-.5)|(dat{para(h)}(i,2)*365.25+part(j, ...
    2)<part(j,5)-.5)
     id0(m,2)=id0(m,2)+1; end, end, end, end

 % Initialise counter and compile list of valid participant
 % study numbers from the temporary list
 m=1;
 for i=1:size(id0,1), if id0(i,2)>.5, id(m)=id0(i,1);
  m=m+1; end, end

 % Display progress in terms of the number of patients
 % identified with measurements for each parameter
 disp(['parameter ' num2str(para(h)) ' : ...
  'num2str(size(id,2)) ' patients identified'])

 % Compute estimates and weight functions for each patient
 for g=1:size(id,2)

  % Display progress in terms of the number of patients
  % processed for each parameter
  disp(['parameter ' num2str(para(h)) ...
   ' : processing patient no. ' num2str(id(g)) ' (' ...
   num2str(g) '/' num2str(size(id,2)) ')'])

  % Find date of birth of patient
  for j=1:size(part,1), if part(j,1)==id(g), db=part(j,2);
   end, end
```

```
% Initialise index in terms of specified date and date of
% birth, transformed measurements variable and counter
di=round(((d-db)/365.25+100)*100)+1; clear tx; m=1;

% Extract ages and measurements from derived data for
% given parameter and patient, ensuring that there is no
% participation end date or that the measurement was
% taken before the participation end date
for i=1:size(dat{para(h)},1),
 if dat{para(h)}(i,1)==id(g), for j=1:size(part,1),
 if part(j,1)==id(g)
    if (part(j,5)<.5)|(dat{para(h)}(i,2)*365.25+ ...
     part(j,2)<part(j,5)-.5)
     tx(m,:)=dat{para(h)}(i,2:3); m=m+1; end, end, end,
      end, end

% Log-transform the measurements if of a parameter that
% follows a log-distribution
if (para(h)==1)|(para(h)==7)|((para(h)>=9)&(para(h)<= ...
 11))|(para(h)==63)|(para(h)==64),
 tx(:,2)=log(tx(:,2)); end

% Initialise the variables for the comprehensive analysis
% of time-line data
sw=zeros(size([-100:.01:200]',1),1); swx=sw; swxt=sw;
 swt=sw; swt2=sw; ss1=sw; ss2=sw;

% Repeat for each measurement
for i=1:size(tx,1)

 % Compute the weighting function, the sum of weighted
 % measurements and the sum of weights
 wi=t/pi./(([-100:.01:200]'-tx(i,1)).^2+t^2);
  swx=swx+wi*tx(i,2); sw=sw+wi;

 % Repeat again for each measurement to include the
 % interactions between measurements
 for j=1:size(tx,1)

  % Compute the second weighting function, the
  % interaction factor and the independent and
  % interacting parts of the weighting function
  wj=t/pi./(([-100:.01:200]'-tx(j,1)).^2+t^2);
   wij=t^2/((tx(i,1)-tx(j,1))^2+t^2);
   ss1=ss1+wi.*wj*(1-wij);
  ss2=ss2+wi.^2.*wj*wij; end

 % If there are 2 or more measurements, compute the terms
 % of the locally estimated differential
 if size(tx,1)>1.5, swxt=swxt+wi*tx(i,2)*tx(i,1);
```

```
  swt=swt+wi*tx(i,1); swt2=swt2+wi*tx(i,1)^2; end, end

% Compute the parameter estimate with its associated
% weight function and update the means and sum of weights
% of the parameter estimates
pwf=[swx./sw ss1./sw+ss2./sw.^2];
 mx(h,1)=mx(h,1)+sum(prod(pwf,2));
 mw(h,1)=mw(h,1)+sum(pwf(:,2));

% Repeat over the given range of time
for l=1:size(sw,1)

 % Compute by weighted linear regression the differential
 % estimate where the denominator is none-zero
 if swt2(l,1)*sw(l,1)-swt(l,1)^2>1e-8,
  dwf(l,1)=(swxt(l,1)*sw(l,1)-swx(l,1)*swt(l,1))/ ...
   (swt2(l,1)*sw(l,1)-swt(l,1)^2);

 % Assume a differential estimate of zero where the
 % denominator is zero
 else, dwf(l,1)=0; end, end

% Compute the weight function associated with the
% differential estimate, update the means and sum of
% weights of the differential estimates and record both
% parameter and differential estimates and their
% associated weights with the participant study number
dwf(:,2)=ss1./sw; mx(h,2)=mx(h,2)+sum(prod(dwf,2));
 mw(h,2)=mw(h,2)+sum(dwf(:,2));
 ddat{para(h)}(g,:)=[id(g) pwf(di,:) dwf(di,:)];

% Display the measurements (pink) and parameter estimate
% (blue) on the top plot labelled P, the differential
% estimate (red) on the middle plot labelled D and both
% associated weight functions (parameter in blue,
% differential in red) on the bottom plot labelled W,
% with the set date indicated by a green vertical line
tl=[-100:.01:200]'; subplot(311),
 plot(tx(:,1),tx(:,2),'mo',tl,pwf(:,1),'b-'), xs=axis;
 hold on, plot([d-db d-db]/365.25,xs(3:4),'g-'), hold off
axis([min(tx(:,1))-1 max(tx(:,1))+1 xs(3:4)]),
 ylabel('P')
title(['parameter ' num2str(para(h)) ...
 ' : patient no. ' num2str(id(g)) ' (' num2str(g) '/' ...
 num2str(size(id,2)) ')'])
subplot(312), plot(tl,dwf(:,1),'r-'), xs=axis; hold on,
 plot([d-db d-db]/365.25,xs(3:4),'g-'), hold off
if abs(xs(4)-xs(3))<1e-7, xs(3)=xs(3)-1; xs(4)=xs(4)+1;
 end
axis([min(tx(:,1))-1 max(tx(:,1))+1 xs(3:4)]),
 ylabel('D'), subplot(313),
```

```
   plot(tl,pwf(:,2),'b:',tl,dwf(:,2),'r:'), xs=axis;
   hold on
  plot([d-db d-db]/365.25,xs(3:4),'g-'), hold off,
   axis([min(tx(:,1))-1 max(tx(:,1))+1 xs(3:4)]),
   ylabel('W')
  xlabel(['P: ' num2str(fix(sum(pwf(:,2))*.1)*.1) ...
   '; D: ' num2str(fix(sum(dwf(:,2))*.1)*.1)]),
   pause(.001)

  % Change variables' names to indicate the parameter
  % analysed and, either append to file if the file already
  % exists, or save to a new file, with the filename
  % including the participant study number
  eval(['pwf' num2str(para(h)) '=single(pwf); dwf' ...
   num2str(para(h)) '=single(dwf); tx' num2str(para(h)) ...
   '=single(tx); ' 'if exist(''wf' num2str(id(g)) ...
   '.mat'')==2, ' 'save wf' num2str(id(g)) ' pwf' ...
   num2str(para(h)) ' dwf' num2str(para(h)) ' tx' ...
   num2str(para(h)) ' -append, ' 'else, save wf' ...
   num2str(id(g)) ' pwf' num2str(para(h)) ' dwf' ...
   num2str(para(h)) ' tx' num2str(para(h)) ', end']);

 end, end

% Compute the means of the parameter and differential
% estimates, save variables ddat, par, mx and mw to Matlab
% data file mn.mat and close the plot
mx=mx./mw; par=para; save mn ddat par mx mw, close
```

cwreg.m

```
function cwreg(para,parap,parai,a)
% Program CWREG version 3.1c - carries out a complete
% weighted multiple linear regression of AAA Study
% parameters
% (c) University of Dundee 2007
% (c) NHS Tayside 2007
% C.E. SARRAN 2007 (c.e.sarran@dundee.ac.uk)
%
% The Cwreg program takes the data generated by the
% programs Population and Wfunc and the anonymised extract
% of participant data from the AAA Study database to carry
% out a complete weighted multiple linear regression and
% produce a comprehensive set of regression statistics.
% Cwreg requires the following Matlab data files:
%  dat.mat  : data derived from the extracts of the AAA
%             Study database and computed by the program
%             Population
```

```
%  mn.mat   : summary data including means and sums of
%             weights of parameters and parameter
%             differentials computed by the program Wfunc
% Cwreg requires one Matlab data file per study
% participant, if required by the regression analysis, with
% a filename of the format wf0000.mat where the 4 digits
% are the participant study number, that contains where
% applicable the parameter and differential estimates and
% their associated weights.
% Cwreg requires the following comma-separated ASCII data
% file:
%  part.csv  : study participant data
% part.csv contains the following variables:
%  SN      : participant study number
%  dob     : date of birth
%  gender  : gender
%  dor     : date of aneurysm rupture
%  ed      : participation end date
% Cwreg writes a Matlab data file d.mat that contains the
% following variables:
%  par   : parameter indices referencing the parameter
%          means
%  mx    : means of the parameter and differential
%          estimates
%  xx    : X matrix
%  xy    : Y matrix
%  b     : regression coefficients
%  sb    : standard errors of regression coefficients
%  id    : list of patient study numbers
%  SST   : total sum of squares
%  SSR   : sum of squares due to regression
%  SSE   : sum of squares due to error
%  MSR   : mean sum of squares due to regression
%  MSE   : mean sum of squares due to error
%  ci    : regression coefficients confidence intervals
%  pb    : probability of type I error for a single
%          regression coefficient
%  pF    : probability of type I error for all regression
%          coefficients
%  v     : analysis of variance table
%  T     : T-statistic
%  s     : standard error for mean response and prediction
%          interval
%  ddat  : parameter and differential estimates and their
%          associated weights for all the patients at the
%          date set in the Wfunc program
%  yw    : predicted parameter estimate and associated
%          weight
%  xw    : predictor parameter estimates and associated
%          weights
%  wi    : combined weight
```

```
%  pr1   : a probability of type I error for a correlation
%          coefficient between predicted and predictor
%          parameters
%  pr2   : a probability of type I error for a correlation
%          coefficient between two predictor parameters
% The following variables are required to run Cwreg:
%
% para  -   predicted parameter
% parap -   predictor parameters
% parai -   predictor interactions
% a     -   confidence interval (%)
%
% para should be at least and only one parameter index,
% parap should be a list of parameter indices, parai should
% be a list of couples of parameter indices (e.g. [4 5; 5
% 7; 9 10]); '.5' indicates a parameter differential (e.g.
% 1.5 for aneurysm diameter rate of change), from the
% following list.
% List of parameter indices:
%  1   : aneurysm diameter
%  4   : systolic pressure
%  5   : diastolic pressure
%  7   : pulse rate
%  8   : systolic-diastolic pressure difference
%  9   : total cholesterol level
%  10  : HDL cholesterol level
%  11  : total to HDL cholesterol level ratio
%  47  : lower ankle-brachial pressure index
%  48  : higher ankle-brachial pressure index
%  63  : urea level
%  64  : creatinine level

%*********************************************************

% Load derived data and participant data
load dat       % load data generated by program Population
load part.csv  % load patient details

% FIND PATIENTS WITH VALID PREDICTED PARAMETER MEASUREMENTS
% *********************************************************

% Initialise patient list, patient counter and post-
% processing array
id0=[dat{fix(para)}(1,1) 0];  % initialise patient list
m=1;                          % initialise patient counter
yxe=zeros(0,1+size(parap,2)+size(parai,1));
                        % initialise post-processing array

% Add a patient to the list if a measurement of the
% predicted parameter is found
for i=1:size(dat{fix(para)},1)
```

```
      % search through measurements of predicted parameter

 if id0(m,1)~=dat{fix(para)}(i,1)    %
  m=m+1;                             % add patient to list
  id0(m,:)=[dat{fix(para)}(i,1) 0];  %
 end                                 %

 % Check that the measurements were made during the
 % participating period and increment the count if valid
 for j=1:size(part,1)                                      %
  if part(j,1)==id0(m,1)                                   %
   if (part(j,5)<-.5)|(dat{fix(para)}(i,2)*365.25+ ...  %
    part(j,2)<part(j,5)-.5)                                %
    id0(m,2)=id0(m,2)+1;                                   %
   end                                                     %
  end              % check that measurement was made during
 end               % participating period

end

% Initialise a patient counter
m=1;  % initialise patient counter

% Only keep in the patient list those patients with at
% least 1 valid measurement where the predicted parameter
% is a primitive parameter or those with at least 2 valid
% measurements where the predicted parameter is a
% differential and derivative parameter
if para-fix(para)<.2  %
                      %
 for i=1:size(id0,1)  %
  if id0(i,2)>.5      %
   id(m)=id0(i,1);    %
   m=m+1;             %
  end     % list patients with at least 1 measurement where
 end      % predicted parameter is a primitive

else                  %
                      %
 for i=1:size(id0,1)  %
  if id0(i,2)>1.5     %
   id(m)=id0(i,1);    %
   m=m+1;             %
  end    % list patients with at least 2 measurements where
 end     % predicted parameter is a derivative

end

% FIND PATIENTS WITH VALID PREDICTOR PARAMETER MEASUREMENTS
% ********************************************************
```

```
% Check for each predictor parameter in turn
for h=1:size(parap,2)  % check each predictor parameter

 % Initialise patient lists and patient counter
 id1=id;                              %
 clear id;                            % initialise patient
 id0=[dat{fix(parap(h))}(1,1) 0];  % lists
 m=1;                              % initialise patient counter

 % Add a patient to the list if a measurement of the
 % predictor parameter is found
 for i=1:size(dat{fix(parap(h))},1)
       % search through measurements of predictor parameter

  if id0(m,1)~=dat{fix(parap(h))}(i,1)    %
   m=m+1;                                 %
   id0(m,:)=[dat{fix(parap(h))}(i,1) 0];  %
  end                                      % add patient to list

  % Check that the measurements were made during the
  % participating period and increment the count if valid
  for j=1:size(part,1)                                    %
   if part(j,1)==id0(m,1)                                 %
    if (part(j,5)<-.5)|(dat{fix(parap(h))}(i,2)* ...  %
     365.25+part(j,2)<part(j,5)-.5)                       %
     id0(m,2)=id0(m,2)+1;                                 %
    end                                                   %
   end             % check that measurement was made during
  end              % participating period

 end

 % Initialise a patient counter
 m=1;  % initialise patient counter

 % Only keep in the patient list those patients with at
 % least 1 valid measurement where the predictor parameter
 % is a primitive parameter or those with at least 2
 % measurements where the predictor parameter is a
 % differential and derivative parameter
 if parap(h)-fix(parap(h))<.2            %
                                         %
  for i=1:size(id0,1)                    %
   for j=1:size(id1,2)                   %
    if (id0(i,1)==id1(j))&(id0(i,2)>.5)  %
     id(m)=id0(i,1);                     %
     m=m+1;                              %
    end  % list patients already with valid data and with
   end   % at least 1 measurement where predictor parameter
  end    % is a primitive
```

```
 else                                          %
                                               %
  for i=1:size(id0,1)                          %
   for j=1:size(id1,2)                         %
    if (id0(i,1)==id1(j))&(id0(i,2)>1.5)       %
     id(m)=id0(i,1);                           %
     m=m+1;                                    %
    end    % list patients already with valid data and with
   end     % at least 2 measurements where predictor
  end      % parameter is a derivative

 end

end

% FIND PATIENTS WITH VALID INTERACTION PARAMETER
% MEASUREMENTS ****************************************

% Check for each interaction parameter in turn
for h=1:size(parai,1)  % check each interaction parameter
 for g=1:2             %

  % Initialise patient lists and patient counter
  id1=id;                                  %
  clear id;                                % initialise patient
  id0=[dat{fix(parai(h,g))}(1,1) 0];  % lists
  m=1;                           % initialise patient counter

  % Add a patient to the list if a measurement of the
  % interaction parameter is found
  for i=1:size(dat{fix(parai(h,g))},1)
     % search through measurements of interaction parameter

   if id0(m,1)~=dat{fix(parai(h,g))}(i,1)    %
    m=m+1;                                   %
    id0(m,:)=[dat{fix(parai(h,g))}(i,1) 0];  %
   end                                       % add patient to list

   % Check that the measurements were made during the
   % participating period and increment the count if valid
   for j=1:size(part,1)                                      %
    if part(j,1)==id0(m,1)                                   %
     if (part(j,5)<-.5)|(dat{fix(parai(h,g))}(i,2)* ...  %
      365.25+part(j,2)<part(j,5)-.5)                         %
      id0(m,2)=id0(m,2)+1;                                   %
     end                                                     %
    end            % check that measurement was made during
   end             % participating period

  end
```

```
  % Initialise a patient counter
  m=1;  % initialise patient counter

  % Only keep in the patient list those patients with at
  % least 1 valid measurement where the interaction
  % parameter is a primitive parameter or those with at
  % least 2 measurements where the interaction parameter is
  % a differential and derivative parameter
  if parai(h,g)-fix(parai(h,g))<.2        %
                                          %
   for i=1:size(id0,1)                    %
    for j=1:size(id1,2)                   %
     if (id0(i,1)==id1(j))&(id0(i,2)>.5)  %
      id(m)=id0(i,1);                     %
      m=m+1;                              %
     end   % list patients already with valid data and with
    end    % at least 1 measurement where interaction
   end     % parameter is a primitive

  else                                     %
                                           %
   for i=1:size(id0,1)                     %
    for j=1:size(id1,2)                    %
     if (id0(i,1)==id1(j))&(id0(i,2)>1.5)  %
      id(m)=id0(i,1);                      %
      m=m+1;                               %
     end   % list patients already with valid data and with
    end    % at least 2 measurements where interaction
   end     % parameter is a derivative

  end

 end

end

%*********************************************************

% Display progress in terms of the number of patients
% identified
disp([num2str(size(id,2)) ' patients identified'])
       % display number of patients with valid measurements

%*********************************************************

% Initialise the X and Y matrices and the sum of y-squares
xx=zeros(1+size(parap,2)+size(parai,1));
                                    % initialise X matrix
xy=zeros(1+size(parap,2)+size(parai,1),1);
                                    % initialise Y matrix
Sy2=0;  % initialise sum of y-squares
```

```
% Load the means and sum of weights of parameters and
% parameter differentials
load mn  % load data estimates and descriptive statistics
         % generated by program WFunc

% Repeat the following computation for each patient in the
% list
for g=1:size(id,2)  % evaluate for each patient listed

% FIND PREDICTED PARAMETER ESTIMATES **********************

 % Display progress in terms of the number of patients
 % processed
 disp(['processing patient no. ' num2str(id(g)) ' (' ...
  num2str(g) '/' num2str(size(id,2)) ')'])

 % Load the predicted parameter (variable starting with
 % pwf) from the patient-specific data file if a primitive
 % parameter
 if para-fix(para)<.2

  eval(['load wf' num2str(id(g)) ' pwf' ...              %
   num2str(fix(para)) ' tx' num2str(fix(para)) ', ' ...  %
   'yw=double(pwf' num2str(fix(para)) '); ' ...          %
   'ty=double(tx' num2str(fix(para)) '); ' ...           %
   'clear pwf' num2str(fix(para)) ' tx' ...              %
   num2str(fix(para))]);                                 %
         % load patient weighted functions where predicted
         % parameter is a primitive

  % Remove the mean to avoid correlation with interactions
  for l=1:size(par,2)         %
   if par(l)==fix(para)       %
    yw(:,1)=yw(:,1)-mx(l,1);  %
   end          % remove mean from function where predicted
  end           % parameter is a primitive

 % Load the predicted parameter (variable starting with
 % dwf) from the patient-specific data file if a
 % differential and derivative parameter
 else

  eval(['load wf' num2str(id(g)) ' dwf' ...              %
   num2str(fix(para)) ' tx' num2str(fix(para)) ', ' ...  %
   'yw=double(dwf' num2str(fix(para)) '); ' ...          %
   'ty=double(tx' num2str(fix(para)) '); ' ...           %
   'clear dwf' num2str(fix(para)) ' tx' ...              %
   num2str(fix(para))]);                                 %
         % load patient weighted functions where predicted
         % parameter is a derivative
```

```
  % Remove the mean to avoid correlation with interactions
  for l=1:size(par,2)         %
   if par(l)==fix(para)       %
    yw(:,1)=yw(:,1)-mx(l,2);  %
   end          % remove mean from function where predicted
  end           % parameter is a derivative

 end

% FIND PREDICTOR PARAMETER ESTIMATES **********************

 % Load each predictor parameter in turn
 for i=1:size(parap,2)  % check each predictor parameter

  % Load the predictor parameter (variable starting with
  % pwf) from the patient-specific data file if a primitive
  % parameter
  if parap(i)-fix(parap(i))<.2

   eval(['load wf' num2str(id(g)) ' pwf' ...           %
    num2str(fix(parap(i))) ', ' ...                    %
    'xw(:,:,i)=double(pwf' num2str(fix(parap(i))) ...  %
    '); ' 'clear pwf' num2str(fix(parap(i)))]);        %
         % load patient weighted functions where predictor
         % parameter is a primitive

   % Remove the mean to avoid correlation with interactions
   for l=1:size(par,2)             %
    if par(l)==fix(parap(i))       %
     xw(:,1,i)=xw(:,1,i)-mx(l,1);  %
    end         % remove mean from function where predictor
   end          % parameter is a primitive

  % Load the predictor parameter (variable starting with
  % dwf) from the patient-specific data file if a
  % differential and derivative parameter
  else

   eval(['load wf' num2str(id(g)) ' dwf' ...           %
    num2str(fix(parap(i))) ', ' ...                    %
    'xw(:,:,i)=double(dwf' num2str(fix(parap(i))) ...  %
    '); ' 'clear dwf' num2str(fix(parap(i)))]);        %
         % load patient weighted functions where predictor
         % parameter is a derivative

   % Remove the mean to avoid correlation with interactions
   for l=1:size(par,2)             %
    if par(l)==fix(parap(i))       %
     xw(:,1,i)=xw(:,1,i)-mx(l,2);  %
    end         % remove mean from function where predictor
```

```
   end          % parameter is a derivative

  end
 end

% FIND INTERACTION ESTIMATES ******************************

 % Load each interaction parameter in turn
 for j=1:size(parai,1)  % evaluate for each interaction

  for k=1:2  % check each interaction parameter

   % Load the interaction parameter (variable starting with
   % pwf) from the patient-specific data file if a
   % primitive parameter
   if parai(j,k)-fix(parai(j,k))<.2

    eval(['load wf' num2str(id(g)) ' pwf' ...        %
     num2str(fix(parai(j,k))) ', ' ...               %
     'xwi(:,:,k)=double(pwf' ...                     %
     num2str(fix(parai(j,k))) '); ' 'clear pwf' ...  %
     num2str(fix(parai(j,k)))]);                     %
        % load patient weighted functions where interaction
        % parameter is a primitive

    % Remove the mean to avoid correlation with
    % interactions
    for l=1:size(par,2)              %
     if par(l)==fix(parai(j,k))      %
      xwi(:,1,k)=xwi(:,1,k)-mx(l,1);  %
     end      % remove mean from function where interaction
    end       % parameter is a primitive

   % Load the interaction parameter (variable starting with
   % dwf) from the patient-specific data file if a
   % differential and derivative parameter
   else

    eval(['load wf' num2str(id(g)) ' dwf' ...        %
     num2str(fix(parai(j,k))) ', ' ...               %
     'xwi(:,:,k)=double(dwf' ...                     %
     num2str(fix(parai(j,k))) '); ' 'clear dwf' ...  %
     num2str(fix(parai(j,k)))]);                     %
        % load patient weighted functions where interaction
        % parameter is a derivative

    % Remove the mean to avoid correlation with
    % interactions
    for l=1:size(par,2)              %
     if par(l)==fix(parai(j,k))      %
      xwi(:,1,k)=xwi(:,1,k)-mx(l,2);  %
```

```
     end      % remove mean from function where interaction
    end       % parameter is a derivative

   end
  end

  % Compute the interaction parameter and its combined
  % weight from the 2 interacting parameters
  xw(:,:,size(parap,2)+j)=[prod(xwi(:,1,:),3) ...
   sqrt(2)./sum(1./xwi(:,2,:),3)];
                      % interaction and its combined weight

 end

% ADD ESTIMATES TO X AND Y MATRICES ***********************

 % Compute the combined weight, and the weighted sum of y
 % as element 1 of the Y matrix
 wi=sqrt(1+size(parap,2)+size(parai,1))./(1./yw(:,2)+ ...
  sum(1./xw(:,2,:),3));  % combined weight
 xy(1)=xy(1)+sum(wi.*yw(:,1)*.01);  % weighted sum of y
                                    %             --> Y ` 1

 % The following instructions can be included in the
 % program to plot predicted weighted functions and
 % combined weighting function for each patient
%-------------------------------------------------------------
% tl=[-100:.01:200];                                         %
% subplot(211)                                               %
% plot(tl,yw(:,1),'b-')                                      %
% xs=axis;                                                   %
% axis([min(ty(:,1))-1 max(ty(:,1))+1 xs(3:4)])              %
% ylabel('Y')                                                %
% title(['patient no. ' num2str(id(g)) ' (' ...              %
%  num2str(g) '/' num2str(size(id,2)) ')'])                  %
% subplot(212)                                               %
% plot(tl,yw(:,2),'b:',tl,wi,'r:')                           %
% xs=axis;                                                   %
% axis([min(ty(:,1))-1 max(ty(:,1))+1 xs(3:4)])              %
% ylabel('W')                                                %
% xlabel(['Y: ' num2str(fix(sum(yw(:,2))*.1)*.1) ...         %
%  ' ; Q: ' num2str(fix(sum(wi)*.1)*.1)])                    %
% pause(.001)   % instructions to plot predicted weighted
%               % functions and combined weighting function
%               % for each patient if required
%-------------------------------------------------------------

 % Compute the sum of weights as element (1;1) of the X
 % matrix
 xx(1,1)=xx(1,1)+sum(wi*.01);  % sum of weights
                               %              --> X ` 1 1
```

```
 % Build post-processing array (not used in this version)
 we=0;                                          %
 e=zeros(1,1+size(parap,2)+size(parai,1));      %
 m=size(yxe,1)+1;                               %
                                                %
 for i=size(wi,1):-1:1                          %
                                                %
  we=we+wi(i)*.01;                              %
  e(1)=e(1)+wi(i)*yw(i,1)*.01;                  %
                                                %
  for j=1:size(parap,2)+size(parai,1)           %
   e(j+1)=e(j+1)+wi(i)*xw(i,1,j)*.01;           %
  end                                           %
                                                %
  if we>1                                       %
   we=0;                                        %
   yxe(m,:)=e;                                  %
   m=m+1;                                       %
   e=zeros(1,1+size(parap,2)+size(parai,1));    %
  end                                           %
                                                %
 end                          % build post-processing array

 % Compute the weighted sum of x.y, the weighted sum of x
 % and the weighted sum of x.x and include these in the X
 % matrix
 for i=2:size(xx,1)

  xy(i)=xy(i)+sum(wi.*xw(:,1,i-1).*yw(:,1)*.01);
    % weighted sum of x.y                          --> Y ` i
  xx(i,1)=xx(i,1)+sum(wi.*xw(:,1,i-1)*.01);
    % weighted sum of x                            --> X ` i 1
  xx(1,i)=xx(i,1);  %                             --> X ` 1 i

  for j=2:size(xx,1)
   xx(i,j)=xx(i,j)+sum(wi.*xw(:,1,i-1).*xw(:,1,j-1)*.01);
     % weighted sum of x.x                          --> X ` i j
  end

 end

 % Compute the weighted sum of y-square
 Sy2=Sy2+sum(wi.*yw(:,1).^2*.01);
                                % weighted sum of y-square

end

% COEFFICIENTS OF CORRELATION ****************************

% Set the self-correlation coefficient to 1 for the
```

```
% predicted parameter and initialise the probability of
% type I error
r2(1,1)=1;
     % self-correlation coefficient for predicted parameter
pr2=nan;

% Use the t-distribution if the degrees of freedom from the
% equivalent number of measurements are less than 100 and
% set the specific t-distribution with the sum of weights
% and using the gamma function
if xx(1,1)-2<100

 tdist=inline([num2str(gamma((xx(1,1)-1)/2)/sqrt(pi*...  %
  (xx(1,1)-2))/gamma((xx(1,1)-2)/2)) '*(1+x.^2/' ...     %
  num2str(xx(1,1)-2) ').^' num2str(-(xx(1,1)-1)/2)]);    %
       % t-distribution:
       % f(t) = G((n+1)/2) / sqrt( pi n ) / G(n/2)
       %       . ( 1 + t^2 / n )^-((n+1)/2)
       % n = sum of weights - 2  (G is the gamma function)

% Use the z-distribution if the degrees of freedom from the
% equivalent number of measurements are greater than 100
else

 tdist=inline('exp(-x.^2/2)/sqrt(2*pi)');  %
                        % normal z-distribution:
                        % f(z) = e^-(z^2/2) / sqrt( 2 pi )

end

% Display a blank line for neatness
disp(' ')

% The correlation coefficients between predicted and
% predictor parameters are first evaluated
for i=2:size(xx,1)
      % evaluate correlation coefficients between predicted
      % parameter and predictor parameters

 % By reducing the X and Y matrices to those elements
 % relevant to the parameters being considered, compute the
 % regression coefficients, the sum of squares due to
 % regression, the total sum of squares and the coefficient
 % of determination
 xxr=[xx(1,1) xx(1,i);xx(i,1) xx(i,i)];
                              % reduction of X matrix (Xr)
 xyr=[xy(1);xy(i)];           % reduction of Y matrix (Yr)
 br=xxr\xyr;
          % reduced regression coefficient ( Xr . Br = Yr )
 SSRr=br'*xyr-xyr(1)^2/xxr(1,1);
                        % sum of squares due to regression
```

```
SSTr=Sy2-xyr(1)^2/xxr(1,1);  % total sum of squares
r2(i,1)=SSRr/SSTr;  % coefficient of determination
r2(1,i)=r2(i,1);    %

% Compute the probability of type I error from the t-
% distribution or z-distribution
pr1=1-quad(tdist,0,abs(sqrt(r2(i,1)*(xx(1,1)-2)/(1- ...
 r2(i,1)))))*2;  % probability of type I error (h0:r=0)

% Display the parameter indices with the correlation
% coefficient, whose sign is obtained from the regression
% coefficient, and its associated probability of type I
% error
disp([i 1 sign(br(2))*sqrt(r2(i,1)) pr1])
  % display parameter indices, correlation coefficient and
  % p-value

% The correlation coefficients between predictor
% parameters are evaluated
for j=2:size(xx,1)
     % evaluate correlation coefficients between predictor
     % parameters themselves
 if j~=i  %

  % By reducing the X and Y matrices to those elements
  % relevant to the parameters being considered, compute
  % the regression coefficients, the sum of squares due to
  % regression, the total sum of squares and the
  % coefficient of determination
  xxr=[xx(1,1) xx(1,i);xx(i,1) xx(i,i)];
                              % reduction of X matrix (Xr)
  xyr=[xx(1,j);xx(i,j)];      % reduction of Y matric (Yr)
  br=xxr\xyr;
        % reduced regression coefficient ( Xr . Br = Yr )
  SSRr=br'*xyr-xyr(1)^2/xxr(1,1);
                         % sum of squares due to regression
  SSTr=xx(j,j)-xyr(1)^2/xxr(1,1);  % total sum of squares
  r2(i,j)=SSRr/SSTr;  % coefficient of determination

  % Compute the probability of type I error from the t-
  % distribution or z-distribution and for one side only
  % of the correlation coefficients table
  if j>i  % one side only of diagonal of correlation
          % coefficients table
   pr2=1-quad(tdist,0,abs(sqrt(r2(i,j)*(xx(1,1)-2)/(1- ...
    r2(i,j)))))*2;  % probability of type I error (h0:r=0)

   % Display the parameter indices with the correlation
   % coefficient, whose sign is obtained from the
   % regression coefficient, and its associated
   % probability of type I error
```

```
    disp([i j sign(br(2))*sqrt(r2(i,j)) pr2])
       % display parameter indices, correlation coefficient
       % and p-value
   end

  % The correlation coefficient is 1 for parameters that
  % are identical
  else

   r2(i,j)=1;  % self-correlation coefficient for predictor
               % parameters

  end
 end

end

% Display the coefficients of determination (r2)
disp('r2 :')       % display coefficients of determination
disp(num2str(r2))  %

% COEFFICIENTS OF REGRESSION AND COEFFICIENT OF MULTIPLE
% DETERMINATION ******************************************

% Compute the regression coefficients, the total sum of
% squares, the sum of squares due to regression, the sum of
% squares due to error, the standard errors of the
% regression coefficients, the coefficient of multiple
% determination and the adjusted coefficient of multiple
% determination
b=xx\xy;  % regression coefficient ( X . B = Y )
SST=Sy2-xy(1)^2/xx(1,1);  % total sum of squares
SSR=b'*xy-xy(1)^2/xx(1,1);
                          % sum of squares due to regression
SSE=SST-SSR;              % sum of squares due to error
MSR=SSR/(size(parap,2)+size(parai,1));
                     % mean sum of squares due to regression
MSE=SSE/(xx(1,1)-size(parap,2)-size(parai,1)-1);
                          % mean sum of squares due to error
sb=sqrt(SSE*diag(inv(xx))/(xx(1,1)-size(parap,2)- ...
 size(parai,1)-1));
                  % standard error of regression coefficient
R2=SSR/SST;       % coefficient of multiple determination
Ra2=1-(xx(1,1)-1)/(xx(1,1)-size(parap,2)-size(parai,1)- ...
 1)*SSE/SST;
           % adjusted coefficient of multiple determination

% Use the t-distribution if the degrees of freedom from the
% equivalent number of measurements and the number of
% parameters are less than 100 and set the specific t-
% distribution with the sum of weights and number of
```

```
% parameters and using the gamma function
if xx(1,1)-size(para,2)-1<100

 tdist=inline([num2str(gamma((xx(1,1)-size(parap,2)-...  %
  size(parai,1))/2)/sqrt(pi*(xx(1,1)-size(parap,2)-...   %
  size(parai,1)-1))/gamma((xx(1,1)-size(parap,2)-...     %
  size(parai,1)-1)/2)) '*(1+x.^2/' ...                   %
  num2str(xx(1,1)-size(parap,2)-size(parai,1)-1) ...     %
  ').^' ...                                              %
  num2str(-(xx(1,1)-size(parap,2)-size(parai,1))/2)]);   %
                % t-distribution:
                % f(t) = G((n+1)/2) / sqrt( pi n ) / G(n/2)
                %       . ( 1 + t^2 / n )^-((n+1)/2)
                % n = sum of weights - number of parameters
                % (G is the gamma function)

% Use the z-distribution if the degrees of freedom from the
% equivalent number of measurements and the number of
% parameters are greater than 100
else

 tdist=inline('exp(-x.^2/2)/sqrt(2*pi)');  %
                         % normal z-distribution
                         % f(z) = e^-(z^2/2) / sqrt( 2 pi )

end

% Compute the probability of type I error from the t-
% distribution or z-distribution
pr=1-quad(tdist,0,abs(sqrt(R2*(size(id,2)-2)/(1-R2))))*2;
                    % probability of type I error (h0:r=0)

% Display the number of patients (n), the coefficient of
% multiple determination (R2), the adjusted coefficient of
% multiple determination (Ra2) and the probability of type
% I error (p)
disp(' '), disp('n         R2        Ra2       p')  %
disp(num2str([size(id,2) R2 Ra2 pr],10))            %
      % display number of patients, coefficient of multiple
      % determination, adjusted coefficient of multiple
      % determination and p-value

% COEFFICIENTS OF REGRESSION CONFIDENCE INTERVALS *********

% Only carry out the following iterative procedure if there
% are sufficient degrees of freedom from the equivalent
% number of measurements and the number of predictor and
% interaction parameters
if xx(1,1)-size(parap,2)-size(parai,1)>0
       % check that there are sufficient degrees of freedom
```

```
 % The following iterative procedure determines the t-
 % statistic from the t-distribution or the z-statistic
 % from the z-distribution for the confidence interval
 % specified
%-------------------------------------------------------
 for i=.0001:10000                                    %
  T=i;                                                %
  if quad(tdist,0,T)>a/200                            %
   for j=1:10                                         %
    T=i-1+j/10;                                       %
    if quad(tdist,0,T)>a/200                          %
     for k=1:10                                       %
      T=i-1+(j-1)/10+k/100;                           %
      if quad(tdist,0,T)>a/200                        %
       for l=1:10                                     %
        T=i-1+(j-1)/10+(k-1)/100+l/1e3;               %
        if quad(tdist,0,T)>a/200                      %
         T=i-1+(j-1)/10+(k-1)/100+(l-1)/1e3;          %
         break                                        %
        end                                           %
       end                                            %
       break                                          %
      end                                             %
     end                                              %
     break                                            %
    end                                               %
   end                                                %
   break                                              %
  end                                                 %
 end                                                  %
     % recursive instructions to find a value t from the t-
     % distribution or a value z from the normal z-
     % distribution that satisfies the required confidence
     % interval
%-------------------------------------------------------

% Default to 0 if there are insufficient degrees of freedom
else   %
       % insufficient degrees of freedom
 T=0;  %

end

% Compute the confidence intervals of the regression
% coefficients
ci=[b-sb*T b+sb*T];
             % regression coefficients confidence intervals

%*******************************************************

% Compute the probability of type I error for each
```

```
% regression coefficient
for i=1:size(b,1)                              %
 pb(i,1)=1-quad(tdist,0,abs(b(i)/sb(i)))*2;  %
end                 % probability of type I error (h0:b=0)

% Display the regression coefficients (b), their standard
% errors (sb), their confidence intervals' lower (CI-) and
% upper (CI+) bounds and their probabilities of type I
% error
disp(' ')                                          %
disp('b         sb        CI-       CI+       p')  %
disp(num2str([b sb ci pb],10))                     %
  % display regression coefficients, their standard errors,
  % their confidence intervals and p-values

% ANALYSIS OF VARIANCE ************************************

% Use the F-distribution to compute the probability of type
% I error for multiple regression if the degrees of freedom
% from the equivalent number of measurements and the number
% of parameters are less than 100 and set the specific F-
% distribution with the sum of weights and number of
% parameters and using the gamma function
if xx(1,1)-size(parap,2)-size(parai,1)-1<100

 pF=1-quad([num2str(gamma((xx(1,1)-1)/2)*(size(parap,...  %
  2)+size(parai,1))^((size(parap,2)+size(parai,1))/...    %
  2)*(xx(1,1)-size(parap,2)-size(parai,1)-1)^((xx(1,...   %
  1)-size(parap,2)-size(parai,1)-1)/2)/...                %
  gamma((size(parap,2)+size(parai,1))/2)/gamma((xx(1,...  %
  1)-size(parap,2)-size(parai,1)-1)/2)) '*x.^' ...        %
  num2str((size(parap,2)+size(parai,1))/2-1) '.*(' ...    %
  num2str(xx(1,1)-size(parap,2)-size(parai,1)-1) '+' ...  %
  num2str(size(parap,2)+size(parai,1)) '*x).^' ...        %
  num2str(-(xx(1,1)-1)/2)],0,MSR/MSE);                    %
    % probability of type I error (h0:b=0 for all
    % coefficients b)
    %
    % F-distribution:
    % f(F) = G((n1+n2)/2) n1^(n1/2) n2^(n2/2) / G(n1/2)
    %     / G(n2/2) . F^(n1/2-1) ( n2 + n1 F )^-((n1+n2)/2)
    % n1 = number of parameters - 1
    % n2 = sum of weights - number of parameters
    % (G is the gamma function)

% Use the chi-square distribution to compute the
% probability of type I error for multiple regression if
% the degrees of freedom from the equivalent number of
% measurements and the number of parameters are greater
% than 100 and set the specific chi-square distribution
% with the number of parameters and using the gamma
```

```
% function
else                                                          %
                                                              %
 pF=1-quad(['exp(-x/2).*x.^' ...                              %
  num2str((size(parap,2)+size(parai,1))/2-1) '/' ...          %
  num2str(2^((size(parap,2)+size(parai,1))/2)*...             %
  gamma((size(parap,2)+size(parai,1))/2))],0,MSR/MSE);  %
             % probability of type I error (h0:b=0 for all
             % coefficients b)
             %
             % CHI-square distribution:
             % f(CHI^2) = e^-(CHI^2/2) (CHI^2)^(n/2-1)
             %           / 2^(n/2) / G(n/2)
             % n = number of parameters - 1
             % (G is the gamma function)
end

% Save the total degrees of freedom, the total sum of
% squares, the degrees of freedom for the regression, the
% sum of squares due to regression, the mean sum of squares
% due to regession, the F-statistic and the probability of
% type I error for multiple regression in the first two
% lines of the analysis of variance table
v(1:2,:)=[xx(1,1)-1 SST nan nan nan;size(parap,2)+ ...
 size(parai,1) SSR MSR MSR/MSE pF];
                        % start analysis of variance table

% Display the degrees of freedom (dof), the sums of squares
% (SS), the mean sums of squares (MS) the F-statistics (F)
% and the probabilities of type I error (p) from the
% analysis of variance table, as well as the coefficient of
% determination displayed as a percentage
disp(' '),                                                    %
 disp('dof       SS        MS        F         p')           %
disp(num2str([xx(1,1)-1 SST],10))                             %
disp([num2str([size(parap,2)+size(parai,1) SSR MSR ...  %
 MSR/MSE pF fix(SSR/SST*100)],10) '%'])                       %
                    % display start of analysis of variance

% Use the F-distribution if the degrees of freedom from the
% equivalent number of measurements and the number of
% parameters are less than 100 and set the specific F-
% distribution with the sum of weights and using the gamma
% function
if xx(1,1)-size(parap,2)-size(parai,1)-1<100
                                                             %
 fdist=inline([num2str(gamma((xx(1,1)-1)/2)*(xx(1,1)-...  %
  2)^((xx(1,1)-2)/2)/gamma(1/2)/gamma((xx(1,1)-2)/...     %
  2)) '*x.^-(1/2).*(' num2str(xx(1,1)-2) '+x).^' ...      %
  num2str(-(xx(1,1)-1)/2)]);                              %
             % F-distribution:
```

```
                % f(F) = G((n+1)/2) n^(n/2) / G(1/2) / G(n/2)
                %       . F^-(1/2) ( n + F )^-((n+1)/2)
                % n = sum of weights - 2
                % (G is the gamma function)

% Use a set chi-square distribution if the degrees of
% freedom from the equivalent number of measurements and
% the number of parameters are greater than 100 and using
% the gamma function
else
                                                        %
 fdist= ...                                             %
  inline('exp(-x/2).*x.^-(1/2)/2^(1/2)/gamma(1/2)');  %
                  % CHI-square distribution:
                  % f(CHI^2) = e^-(CHI^2/2) (CHI^2)^-(1/2)
                  %           / sqrt(2) / G(1/2)
                  % (G is the gamma function)
end

% For each predictor and interaction parameter, by reducing
% the X and Y matrices to those elements relevant to the
% parameters being considered, compute the regression
% coefficients, the sum of squares due to regression and
% the mean sum of squares given all other parameters
for i=1:size(parap,2)+size(parai,1)
      % analyse variance for each predictor and interaction
      % parameter
 xxv=xx([1:i i+2:size(xx,1)],[1:i i+2:size(xx,2)]);
                                % reduction of X matrix (Xr)
 xyv=xy([1:i i+2:size(xy,1)],1);
                                % reduction of Y matrix (Yr)
 bv=xxv\xyv;
          % reduced regression coefficient ( Xr . Br = Yr )
 SSRv=bv'*xyv-xy(1)^2/xx(1,1);
                           % sum of squares due to regression
 MSRv=SSR-SSRv;  % mean sum of squares due to regression
                 % given all other parameters

 % Compute the probability of type I error for the
 % parameter given all other parameters from the F-
 % distribution or chi-square distribution
 pFv=1-quad(fdist,0,MSRv/MSE);
      % probability of type I error (h0:b=0 given all other
      % parameters)

 % Save the degree of freedom for the regression, the sum
 % of squares and mean sum of squares due to regession, the
 % F-statistic and the probability of type I error into the
 % analysis of variance table
 v(i+2,:)=[1 MSRv MSRv MSRv/MSE pFv];
                           % write analysis of variance table
```

```
 % Display the degree of freedom, the sum of squares, the
 % mean sum of squares, the F-statistic and the probability
 % of type I error from the analysis of variance table, as
 % well as the coefficient of determination displayed as a
 % percentage
 disp([num2str([1 MSRv MSRv MSRv/MSE pFv fix(MSRv/SST* ...
  100)],10) '%'])  % display analysis of variance
end

% Save the residual degrees of freedom, the sum of squares
% due to error and the mean sum of squares due to error in
% the last line of the analysis of variance table
v(size(parap,2)+size(parai,1)+3,:)=[xx(1,1)-size(parap, ...
 2)-size(parai,1)-1 SSE MSE nan nan];
                        % finish analysis of variance table

% Compute the standard error for the mean response and
% prediction interval
s=sqrt(SSE/(xx(1,1)-size(parap,2)-size(parai,1)-1));
          % standard error for mean response and prediction
          % interval

% Display the residual degrees of freedom, the sum of
% squares due to error and the mean sum of squares due to
% error
disp(num2str([xx(1,1)-size(parap,2)-size(parai,1)-1 SSE ...
 MSE],10))  % display end of analysis of variance

%*********************************************************

% Save variables par, mx, xx, xy, b, sb, id, SST, SSR, SSE,
% MSR, MSE, ci, pb, pF, v, T, s, ddat, yw, xw, wi, pr1 and
% pr2 to Matlab data file d.mat and close the plot if
% required
save d par mx xx xy b sb id SST SSR SSE MSR MSE ci pb ...
 pF v T s ddat yw xw wi pr1 pr2
                                % save regression statistics

%close  % close figure plot if required
```